PENSOFT

MUSEUM FÜR
NATURKUNDE
BERLIN

für Natur

In Focus

The cover picture shows habitus of female paratype *Euclimacia radioquaesentis* sp. nov. dorsal view.

See paper of **Ehlers S, Li H, Kirschey L, Ohl M** A new species of the mantidfly genus *Euclimacia* from Vietnam (Neuroptera, Mantispidae)

Cover design
Pensoft

Deutsche Entomologische Zeitschrift
An International Journal of Systematic Entomology

Content of volume **71** (**2**) 2024

Abstract & Indexing Information

Phylogeny of the Chinese species groups of the subgenus *Homoneura* Wulp, 1891 (Diptera, Lauxaniidae, Homoneurinae) based on morphological characters

Yao Yao[1], Chaoyang Kong[1], Pu Miao[2], Shengjuan Zhao[3], Wenliang Li[1]

1   *College of Horticulture and Plant Protection, Henan University of Science and Technology, Luoyang 471023, China*

2   *Henan Tobacco Company Luoyang company, Luoyang 471000, China*

3   *College of Food & Bioengineering, Henan University of Science and Technology, Luoyang 471023, China*

https://zoobank.org/243FCE92-70C3-431B-93F8-BF82B2A9823E

Corresponding author: Wenliang Li (wenliangli@haust.edu.cn)

Abstract

The subgenus *Homoneura* Wulp, 1891 (Diptera, Lauxaniidae, Homoneurinae) is highly diverse with more than 220 species known from China, representing more than 80% of the Chinese genus *Homoneura* Wulp, 1891. These species were assigned into 21 species groups in studies mainly focusing on the classification and description of species. The phylogenetic relationships of each subgenus of *Homoneura* and the phylogenetic relationship of the species groups are still not well understood. We investigated the male morphology to provide the basis to further revise the species groups of this subgenus. In this survey, 230 species were examined and 117 morphological characters obtained, a phylogenetic analysis was conducted using the maximum parsimony analysis with TNT and WinClada. The analyses yielded 45 most parsimonious trees and one strict consensus tree. A phylogenetic hypothesis is proposed dividing the subgenus *Homoneura* into 12 species groups: *H. (H.) nigrifacies*, *H. (H.) pallida*, *H. (H.) patella*, *H. (H.) beckeri*, *H. (H.) formosae*, *H. (H.) henanensis*, *H. (H.) nigra*, *H. (H.) notostigma*, *H. (H.) ornatifrons*, and *H. (H.) trispina*, *H. (H.) laticosta*, and *H. (H.) quinquenotata*. This research provides valuable contributions towards a better understanding of the phylogenetic relationships within the subgenus *Homoneura*. However, the monophyly of the genus and subgenus was not supported.

Key Words

Introduction

The genus *Homoneura* Wulp, 1891 (Diptera, Lauxaniidae, Homoneurinae) comprises more than 750 described species in eight known subgenera distributed worldwide (Chen 2022). *Homoneura* is widely distributed in all major zoogeographical regions except for the Neotropical region and plays a very important role in the ecological system (Shi et al. 2017). The subgenus *Homoneura* Wulp, 1891 comprises more than 700 described species and has the highest species richness of Lauxaniidae (You et al. 2023). When the classification of this group entered the second stage of prosperity and development, the number of

described species increased markedly, significantly reducing the efficiency of comparative morphological studies. Therefore, some scholars began to study species groups among the subgenera of *Homoneura* based on characters such as wing spots and male genitalia. Miller (1977a, 1977b) made a comprehensive revision of 50 species, nine groups and four subgenera of *Homoneura* distributed in the Nearctic region in his monograph "Taxonomy and Biology of *Homoneura* in the Nearctic region". In particular, the establishment of species groups was an important contribution to the systematic study of *Homoneura* (Miller 1977a, 1977b). Later, Papp proposed two species groups from the Palaearctic region and four species groups from

the Oriental region (Papp 1978; Papp et al. 2006). Sasakawa (1992) proposed a new species group from the Oriental region. Kim (1994) distributed the Australian species of *Homoneura* into 15 species groups, and established 20 species groups of the global subgenera of *Homoneura*. Shi and Yang (2014) divided the Chinese species of the *Homoneura* subgenus into 21 species groups, but some of the species could not be classified into species groups. Up to now, only five scholars have made a morphological classification of species groups, because of the loss or destruction of type specimens. The descriptions were too simple to study carefully. The accuracy and availability of a species group system is doubtful, and the phylogenetic relationships of existing species groups have not been comprehensively tested.

The phylogenetical approach is an important way to reveal the relationships between taxa; however, relationships within *Homoneura* are relatively behind. Stuckenberg (1971) hypothesized the relationships among 19 genera of Homoneurinae based on morphological characters, and divided the 19 genera into three generic groups, with *Homoneura* in the first group; Sasakawa (1992) hypothesized the phylogenetic relationships among five subgenera of *Homoneura* based on six morphological characters, with the subgenera distributed into two clades, one containing the subgenera *Chaetohomoneura* Malloch, 1927 and *Neohomoneura* Malloch, 1927, and the other comprising three subgenera with *Euhomoneura* Malloch, 1927 and *Homoneura* presented as sister groups, and the subgenus *Minettioides* Malloch, 1929 closely related to these (Sasakawa 1992). In the only existing molecular phylogenetic study on the generic relationships of *Homoneura*, Shi et al. (2017) explored the relationships based on two mitochondrial and two nuclear genetic markers, and the hypothesis of subgeneric monophyly was not corroborated. Kong et al. (2022) presented the first morphological phylogeny of *Homoneura*, and the hypothetical monophyly of the genus and subgenus was also not supported. Furthermore, the phylogenetic relationships among other subgenera of *Homoneura* were also discussed. The evolutionary relationships among the *Homoneura* subgenera are not completely clear, and phylogenetic relationships of some species groups have not been studied yet, making systematic classification studies in this genus difficult. At present, no phylogenetic studies of the *Homoneura* subgenera have been published using morphological evidence. Despite its high diversity and ecological significance, the phylogenetic relationships in *Homoneura* and its subgenera remain to be studied.

Methods

All the specimens are deposited in College of Horticulture and Plant Protection, Henan University of Science and Technology, Henan, China (Suppl. material 1).

Morphological study and terminology

General terminology follows Cumming and Wood (2017), and Gaimari and Miller (2021). The specimens

were observed with a Motic SMZ-168 stereomicroscope and the external morphological characters were examined. Genitalia preparations were made by removing and macerating the apical portion of the abdomen in cold saturated NaOH for six hours, then rinsing and neutralizing them with glacial acetic acid for dissection and study. After examination in glycerine, they were transferred to fresh glycerine and stored in a microvial pinned below the specimen or moved to an ethanol tube together with the wet specimens. Most characters were illustrated using photographs and line drawings. Photographs were taken using a Canon EOS6D microscope (Canon, Tokyo, Japan) and stacked using Helicon Focus v7.0.2.0 (Helicon Soft, Kharkiv, Ukraine). Line drawings were drawn with Adobe Illustrator 2021 v25.2.1 (Adobe, San Jose, USA).

Specimen morphological characters

The morphological characters were numerically coded (Suppl. material 2). Ninety-eight characters are binary and 25 are multistate. Plesiomorphic states were coded with (0), and apomorphic with (1,2,3), missing character states were coded with (?), and inapplicable states were scored as (–).

List of characters used in the cladistic analysis

The partial characters and all pictures were adapted from Kong et al. (2022) and revised accordingly for the purposes of deeper research.

Head:

1. Size of head, height of head/width of head in frontal view and the eyes are included: (0) ≤ 4/5 (Fig. 1A); (1) > 4/5 (Fig. 1J).
2. Color of ocellar triangle: (0) black (Fig. 1A); (1) brown to yellow (Fig. 1E).
3. Number of ocellar seta: (0) 2; (1) 3.
4. Length of ocellar seta/length of anterior fronto-orbital seta: (0) ≥ 1 (Fig. 1F); (1) < 1 and ≥ 1/2;(2) < 1/2 (Fig. 1E).
5. Length of anterior fronto-orbital seta/length of posterior fronto-orbital seta: (0) < 1 (Fig. 1B); (1) ≥ 1 (Fig. 1M).
6. Length between anterior fronto-orbital seta and posterior fronto-orbital seta/length between posterior fronto-orbital seta and inner vertical bristles: (0) > 1/2 (Fig. 1G); (1) ≤ 1/2.
7. Frons: (0) flat (Fig. 1F); (1) distinct uplifted; (2) distinct concave (Fig. 1J).
8. Length of frons/width of frons: (0) ≤ 1 (Fig. 1A); (1) > 1 (Fig. 1E).
9. Middle of frons: (0) without spot or stripe (Fig. 1L); (1) with a dark median longitudinal stripe extending from anterior margin to the ocellar triangle or the top of the head (Fig. 1C).

10. Between the middle of frons and fronto-orbital seta: (0) with two longitudinal stripes extending to both sides of the ocellar triangle (Fig. 1A); (1) without stripe (Fig. 1B).

11. The area around the fronto-orbital setae and the outer vertical bristles: (0) without spot or stripe (Fig. 1H); (1) with spot (Fig. 1A); (2) with stripe along the bases (Fig. 1D).

12. Presence of a spot at the costal margin of frons: (0) absent (Fig. 1I); (1) present.

13. Facial angle of frons: (0) approach straight angle; (1) approach right angle.

14. Color of face: (0) black (Fig. 1L); (1) brown to yellow (Fig. 1D).

15. Spot on face: (0) absent (Fig. 1I); (1) irregular; (2) round (Fig. 1M).

16. Middle of face: (0) flat (Fig. 1I); (1) distinct uplifted (Fig. 1K).

17. Ventral margin of face: (0) strumaes on both sides (Fig. L); (1) lamellar processes in the middle (Fig. 1J); (2) flat (Fig. 1D).

18. Width of ventral margin of face/height of gena: (0) ≥ 3 (Fig. 1I); (1) < 3 (Fig. 1J).

19. Spot on gena: (0) absent (Fig. 1N); (1) present (Fig. 1O).

20. Below eye on gena: (0) without strong seta (Fig. 1M); (1) with strong seta (Fig. 1H).

21. Length of gena/length of eye: (0) <1/3 (Fig. 1N); (1) ≥ 1/3 (Fig. 1J).

22. Face and gena: (0) do not extend (Fig. 1L); (1) distinct extend ventrally (Fig. 1J).

23. Color of pedicel: (0) black (Fig. 1H); (1) brown to yellow (Fig. 1G).

24. Number of scape long bristle that is not shorter than the length of the first flagellomere: (0) 0 (Fig. 1G); (1) 2 (Fig. 1J).
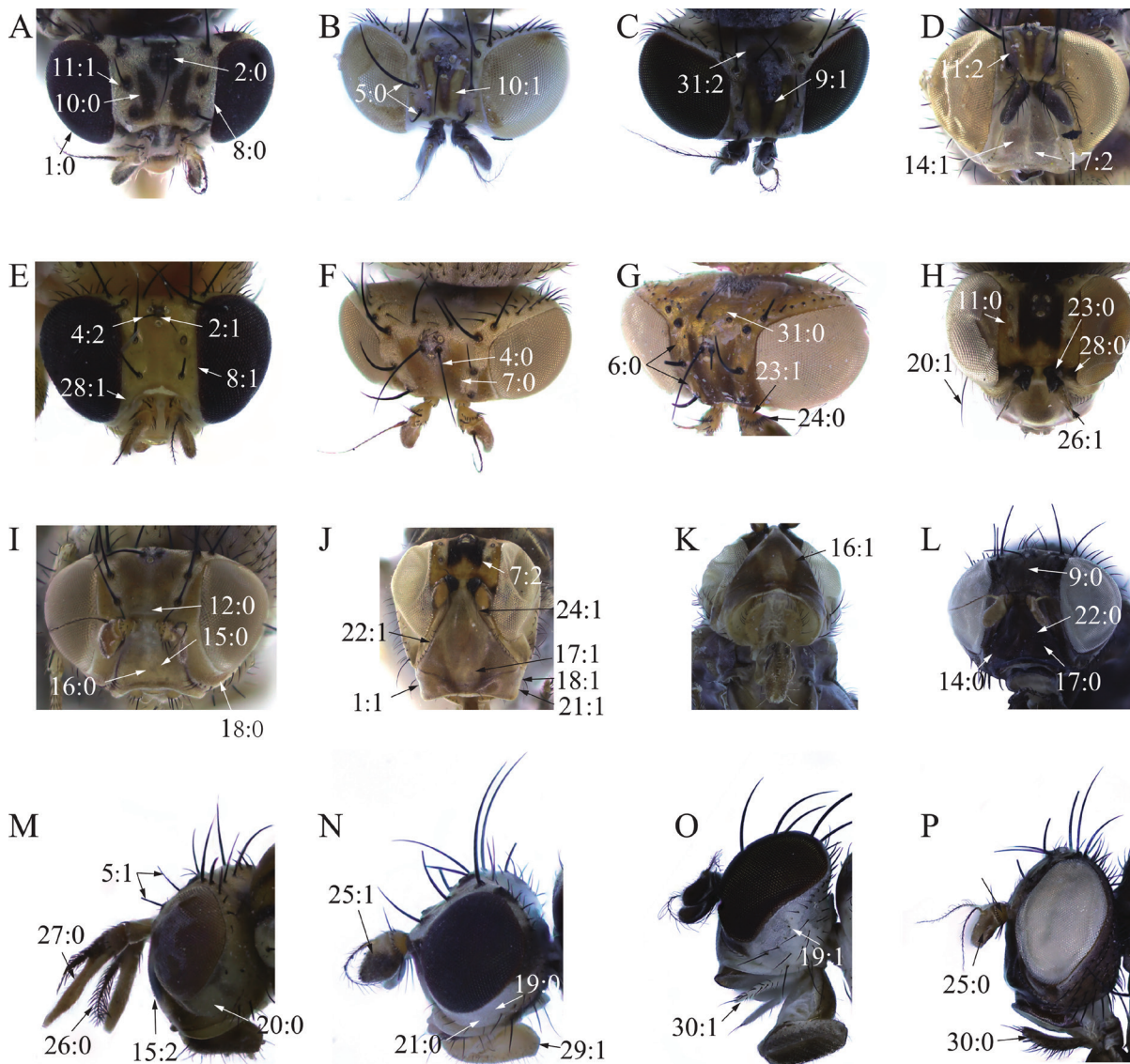
Figure 1. Head characters. *Homoneura* (*Homoneura*) *picta* (de Meijere, 1904) (**A, N**); *Homoneura* (*Homoneura*) *flavida* Shi & Yang, 2009 (**B, C, D, O**); *Homoneura* (*Minettioides*) *orientis* (Hendel, 1908) (**E**); *Homoneura* (*Euhomoneura*) *yanqingensis* Shi, Gao & Li, 2017 (**F, I**); *Homoneura* (*Neohomoneura*) *tricuspidata* Shi & Yang, 2008 (**G**); *Prosopophorella yoshiyasui* Sasakawa, 2001 (**H, J, K**); *Minettia* (*Frendelia*) *longipennis* (Fabricius, 1794) (**L, P**); *Pachycerina decemlineata* de Meijere, 1914 (**M**).

25. Color of flagellomere: (0) monochrome (Fig. 1P); (1) bicolor (Fig. 1N).
26. Arista: (0) plumose (arista with longest setulae, not less than the width of the first flagellomere) (Fig. 1M); (1) pubescent (arista with longest setulae shorter than the width of the first flagellomere) (Fig. 1H).
27. Length of the first flagellomere/width of the first flagellomere: (0) ≥ 2 (Fig. 1M); (1) < 2.
28. Spot between base of antennae and inner margin of eye: (0) present (Fig. 1H); (1) absent (Fig. 1E).
29. Color of proboscis: (0) black; (1) brown to yellow (Fig. 1N).
30. Color of palpus: (0) monochrome, black (Fig. 1P); (1) monochrome, brown or yellow (Fig. 1O); (2) bicolor.
31. Occiput: (0) without stripe (Fig. 1G); (1) with distinct narrow stripe (as wide as ocellar triangle); (2) with distinct wide stripe (distinctly longer than ocellar triangle) (Fig. 1C).

Thorax:

32. Mesonotum: (0) with distinct longitudinal stripe (Fig. 2C); (1) without longitudinal stripe (Fig. 2E).
33. Base of dorsocentral seta and prescutellar acrostichal seta: (0) without spot (Fig. 2E); (1) with spot (Fig. 2B).
34. Pre-sutural dorsocentral seta: (0) absent (Fig. 2E); (1) present (Fig. 2D).
35. Post-sutural dorsocentral seta: (0) 3 (Fig. 2A); (1) 2 (Fig. 2D).
36. Rows of acrostichal seta: (0) seven or more rows (Fig. 2E); (1) six or less rows (Fig. 2D).
37. Acrostichal seta: (0) weak, short hair (Fig. 2B); (1) strong seta (Fig. 2D).
38. Mesonotum prescutellar acrostichal seta: (0) longer than acrostichal seta with hair; (1) hair, as long as acrostichal seta with hair.
39. Mesonotum scutellar suture: (0) without spot (Fig. 2D); (1) with spot.
40. Mesonotum pruinose stripe: (0) no pruinose stripe; (1) a broad pruinose stripe from face, antenna, frons, mesonotum to the end of scutellum.
41. Supra-alar seta: (0) one (Fig. 2F); (1) two, the latter is about half as long as the former; (2) two, the latter is about the same length as the former one.
42. Intra-alar seta: (0) one, strong (as long as supra-alar seta); (1) one, weak (half the length of supra-alar seta); (2) 0.
43. Katepisternal seta: (0) two (Fig. 2F); (1) one (Fig. 2C).

Leg:

44. Length of leg/length of body: (0) ≤ 1; (1) > 1.
45. Posterior ventral seta on fore femur: (0) five or more (Fig. 2L); (1) four or less (Fig. 2G).
46. Ctenidium short seta on fore femur: (0) absent; (1) ten or less; (2) eleven or more (Fig. 2G).

47. Anterior seta on mid femur: (0) six or more; (1) five or less (Fig. 2I).
48. Posterior seta on mid tibia: (0) absent (Fig. 2J); (1) present (Fig. 2K).
49. Apical ventral seta on mid tibia: (0) one; (1) two (Fig. 2J); (2) three (Fig. 2K); (3) four.
50. Preapical anterior dorsal seta on hind femur: (0) present (Fig. 2H); (1) absent.
51. Anteroventral seta on hind femur: (0) present; (1) absent.

Wing:

52. Length of wing/width of wing: (0) < 2.7 (Fig. 3A); (1) ≥ 2.7 (Fig. 3D).
53. Wing: (0) most hyaline or pale yellow (five or less spots and wing spots occupy a small area of the wing) (Fig. 3E); (1) most brown or black (six or more spots and wing spots occupy a large area of the wing) (Fig. 3A).
54. Anterior margin of the wing (in front of R2+3): (0) most hyaline or pale yellow (spots on the wings less than half of the anterior margin of the wings) (Fig. 3F); (1) mostly brown or black (spots on the wings not less than half of the wings, while still a little part with no spots) (Fig. 3B); (2) all brown, fading from costa vein to the middle; (3) all brown, no change in color from costa vein to the middle.
55. Short black setae on costal margin of wing: (0) extend to between R_{2+3} and R_{4+5} (Fig. 3G); (1) extend to R_{4+5} (Fig. 3C).
56. Spot on r_1 cell: (0) absent (Fig. 3E); (1) present (Fig. 3C).
57. Spot on R_{2+3}: (0) absent (Fig. 3G); (1) 1, a hyaline space (Fig. 3H); (2) 2 (Fig. 3C); (3) ≥ 3; (4) all brown (Fig. 3A).
58. Tip of R_{4+5}: (0) without spot (Fig. 3E); (1) with one spot (irregular) (Fig. 3H); (2) with two spots (irregular), far away from crossvein r-m (Fig. 3D); (3) with two spots (irregular), next to crossvein r-m (Fig. 3A); (4) with three spots (irregular) (Fig. 3C); (5) many small spots, reticular connection (Fig. 3A); (6) many sexangular spots (a small spot in the middle).
59. Crossvein r-m: (0) without spot (Fig. 3G); (1) only strengthened or with a inconspicuous stripe around (Fig. 3E); (2) distinct spots (Fig. 3H); (3) circular spots (Fig. 3B).
60. Crossvein dm-cu: (0) without spot (Fig. 3G); (1) only overstrike crossvein or an inconspicuous stripe around (Fig. 3E); (2) distinct spots (Fig. 3F); (3) circular spots (Fig. 3D).
61. Tip of M_1: (0) without spot (Fig. 3G); (1) one spot (Fig. 3F); (2) two spots (Fig. 3H); (3) many small spots, reticular connection (Fig. 3A).
62. Stripe on penultimate section of CuA1: (0) absent (Fig. 3F); (1) present (Fig. 3D).
63. Spot on base of radial vein and medial vein: (0) absent (Fig. 3E); (1) present (Fig. 3B).
64. Anal vein: (0) normal (Fig. 3H); (1) lack (Fig. 3B).
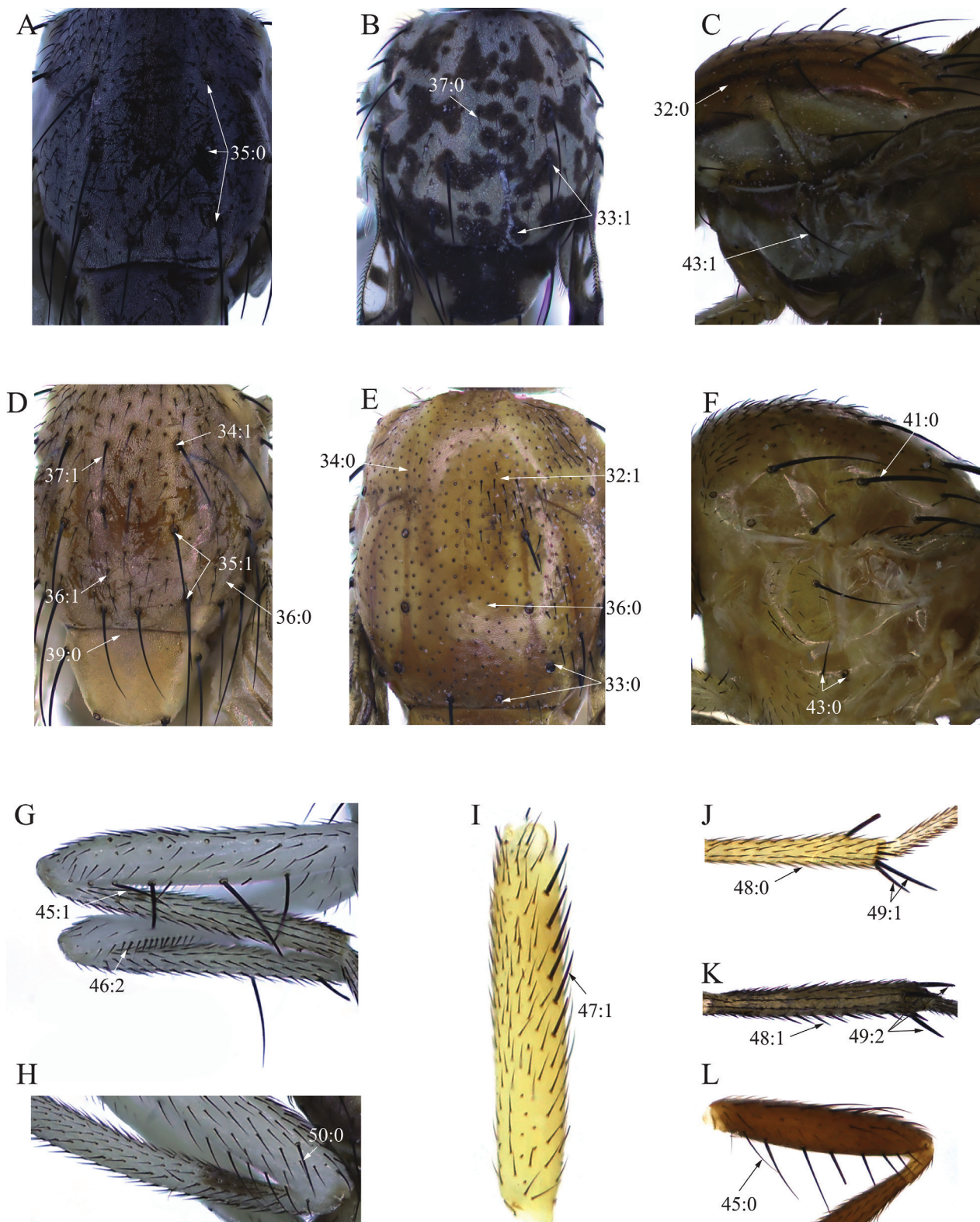
Figure 2. Thoracic and leg characters. *Homoneura* (*Homoneura*) *flavida* Shi & Yang, 2009 (**A, G, H**); *Homoneura* (*Homoneura*) *picta* (de Meijere, 1904) (**B**); *Pachycerina decemlineata* de Meijere, 1914 (**C**); *Homoneura* (*Euhomoneura*) *yanqingensis* Shi, Gao & Li, 2017 (**D, I, J**); *Homoneura* (*Neohomoneura*) *tricuspidata* Shi & Yang, 2008 (**E, K**); *Homoneura* (*Minettioides*) *orientis* (Hendel, 1908) (**F**); *Minettia* (*Frendelia*) *longipennis* (Fabricius, 1794) (**L**).

65. Anterior cubital cell: (0) without spot (Fig. 3C); (1) with spot (Fig. 3A).

66. 2nd (between R_1 and R_{2+3}) section/3rd (between R_{2+3} and R_{4+5}) section: (0) ≥ 3; (1) < 3.

67. 3rd (between R_{2+3} and R_{4+5}) section/4th (between R_{4+5} and M_1) section: (0) ≥ 1.5; (1) < 1.5.

68. The end of R_{2+3}: (0) not bend to costal margin (Fig. 3F); (1) bend to costal margin (Fig. 3C).
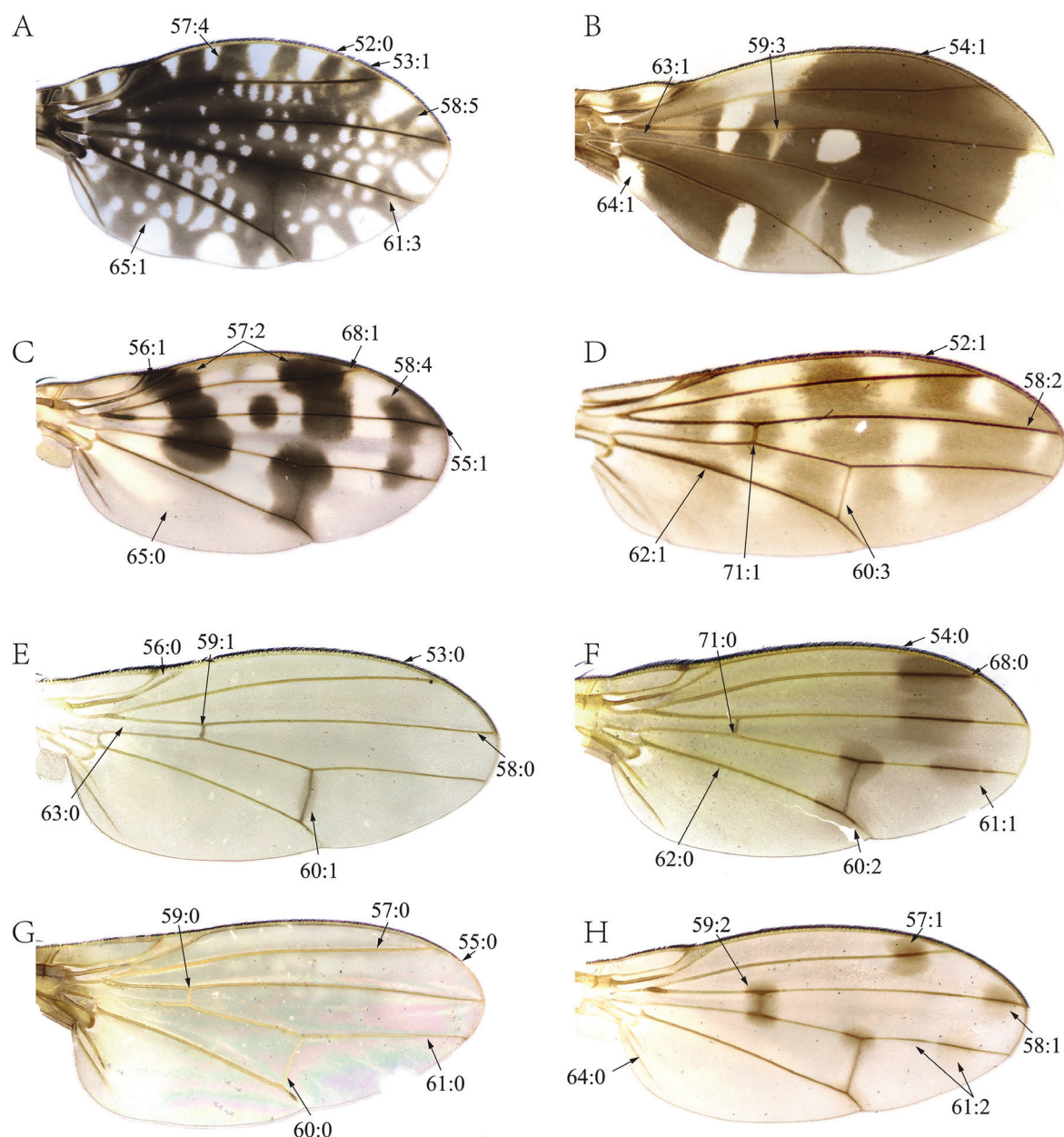
Figure 3. Wing characters. **A.** *Homoneura* (*Homoneura*) *picta* (de Meijere, 1904); **B.** *Noonamyia umbrellata* Shi & Yang, 2009; **C.** *Homoneura* (*Homoneura*) *posterotricuspis* Gao, Shi & Han, 2016; **D.** *Prosopophorella yoshiyasui* Sasakawa, 2001; **E.** *Homoneura* (*Homoneura*) *flavida* Shi & Yang, 2009; **F.** *Homoneura* (*Neohomoneura*) *zengae* Shi & Yang, 2008; **G.** *Minettia* (*Frendelia*) *longipennis* (Fabricius, 1794); **H.** *Homoneura* (*Euhomoneura*) *yanqingensis* Shi, Gao & Li, 2017.

69. Length of the ultimate section of M1/ length of the penultimate section of M1: (0)> 1; (1) ≤ 1.
70. Length of the ultimate section of CuA1/length of the penultimate section of CuA1: (0) < 1/5; (1) ≥ 1/5.
71. Crossvein r-m: (0) before or in the middle of the discal cell (Fig. 3F); (1) behind the middle of the discal cell (Fig. 3D).
72. Color of knob part of haltere: (0) black; (1) brown or yellow.

Abdomen:

73. Spot on middle of tergite 2: (0) absent (Fig. 4B); (1) present (Fig. 4A).

74. Spot on side of tergite 2: (0) absent (Fig. 4F); (1) present (Fig. 4D).
75. Spot on middle of tergite 3: (0) absent (Fig. 4C); (1) present (Fig. 4A).
76. Spot on side of tergite 3: (0) absent (Fig. 4E); (1) present (Fig. 4D).
77. Spot on middle of tergite 4: (0) absent (Fig. 4C); (1) present (Fig. 4A).
78. Spot on side of tergite 4: (0) absent (Fig. 4F); (1) present (Fig. 4D).
79. Spot on middle of tergite 5: (0) absent (Fig. 4C); (1) present (Fig. 4B).
80. Spot on side of tergite 5: (0) absent (Fig. 4F); (1) with striped spot (Fig. 4D); (2) with circular spot (Fig. 4E).
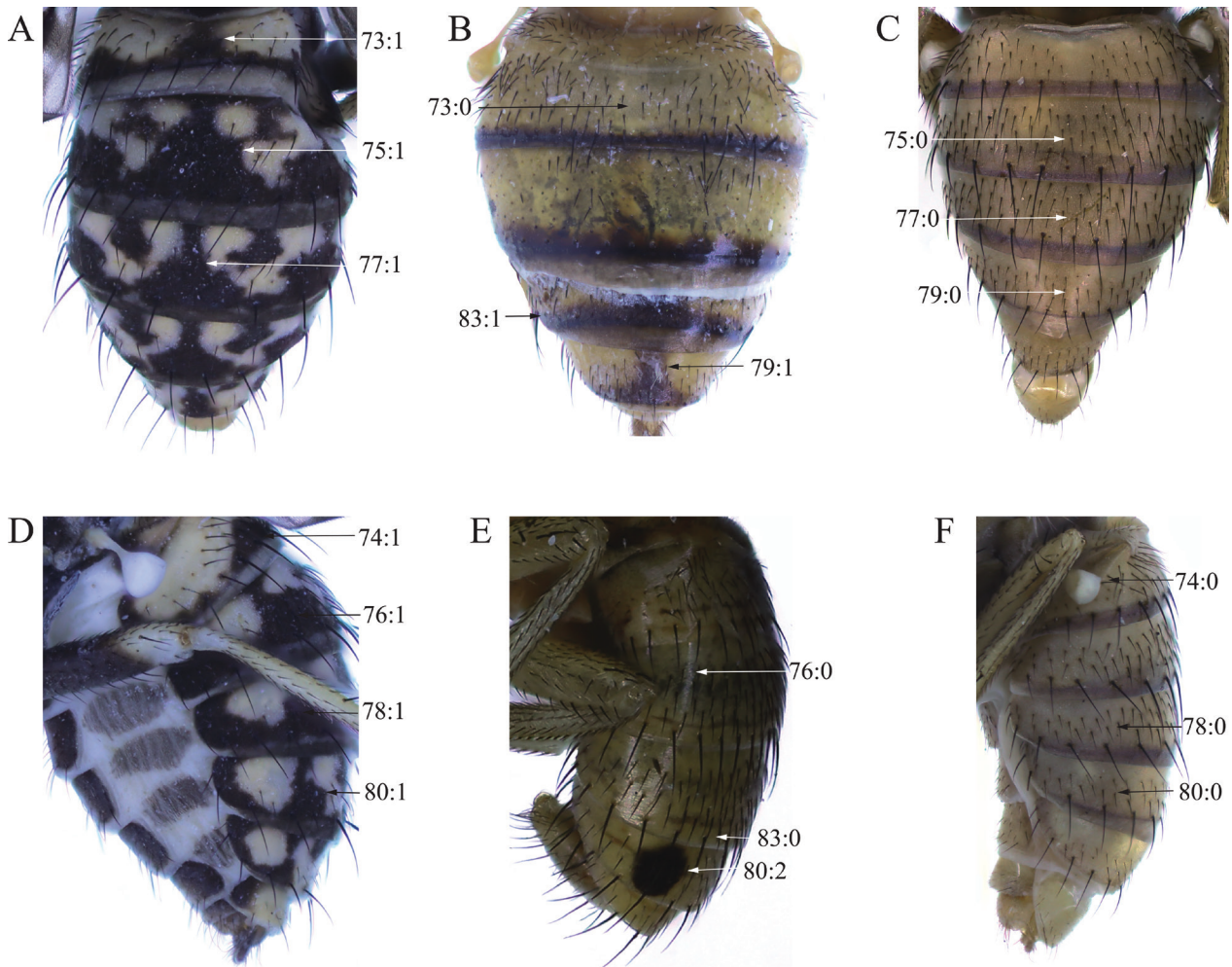
Figure 4. Abdomen characters. *Homoneura* (*Homoneura*) *picta* (de Meijere, 1904) (**A, D**); *Homoneura* (*Neohomoneura*) *tricuspidata* Shi & Yang, 2008 (**B**); *Homoneura* (*Euhomoneura*) *yanqingensis* Shi, Gao & Li, 2017 (**C, F**); *Homoneura* (*Minettioides*) *orientis* (Hendel, 1908) (**E**).

81. Spot on middle of tergite 6: (0) absent; (1) present.
82. Spot on side of tergite 6: (0) absent; (1) present.
83. Posterior margin of tergite: (0) not change color (Fig. 4E); (1) distinct dark brown stripe (2) distinct light brown stripe (Fig. 4B).
84. Sternite 5: (0) not differentiated; (1) differentiated into a digitiform process.
85. Short spine at posterior margin of sternite 5: (0) absent; (1) present.

Male genitalia:

86. Syntergosternite and epandrium: (0) not fused; (1) fused.
87. Shape of syntergosternite: (0) semicircular (Fig. 5C); (1) circular, without ventral processes (Fig. 5A); (2) circular, with ventral processes (Fig. 5B).
88. Length of dorsal margin of syntergosternite/length of posterior margin of syntergosternite: (0) < 2/3; (1) ≥ 2/3.
89. Dorsal margin of syntergosternite: (0) without short hair (Fig. 5C); (1) with short hair (Fig. 5B).

90. Syntergosternite around the spiracle: (0) without short hair (Fig. 5C); (1) with short hair (Fig. 5A).
91. Costal margin of epandrium: (0) with sharp process or concave; (1) without sharp process or without concave.
92. Length of dorsal margin of epandrium/length of ventral margin of epandrium: (0) > 1/2; (1) ≤ 1/2.
93. Surstylus: (0) separated from epandrium (Fig. 6A); (1) not separated from epandrium (Fig. 6D).
94. Length of the longest surstylus/height of epandrium: (0) ≥ 1/2 (Fig. 6D); (1) < 1/2 (Fig. 6B).
95. Shape of the apex of surstylus: (0) sharp (Fig. 6A); (1) blunt (Fig. 6C).
96. Shape of surstylus: (0) bent (Fig. 6A); (1) straight (Fig. 6C).
97. Width of the middle of surstylus/length of surstylus: (0) < 1/2 (Fig. 6B); (1) ≥ 1/2 (Fig. 6A).
98. Fine teeth or terminal processes on surstylus: (0) absent (Fig. 6D); (1) present (Fig. 6C).
99. Hypandrium: (0) present; (1) absent.
100. Middle of hypandrium: (0) connected; (1) unconnected.
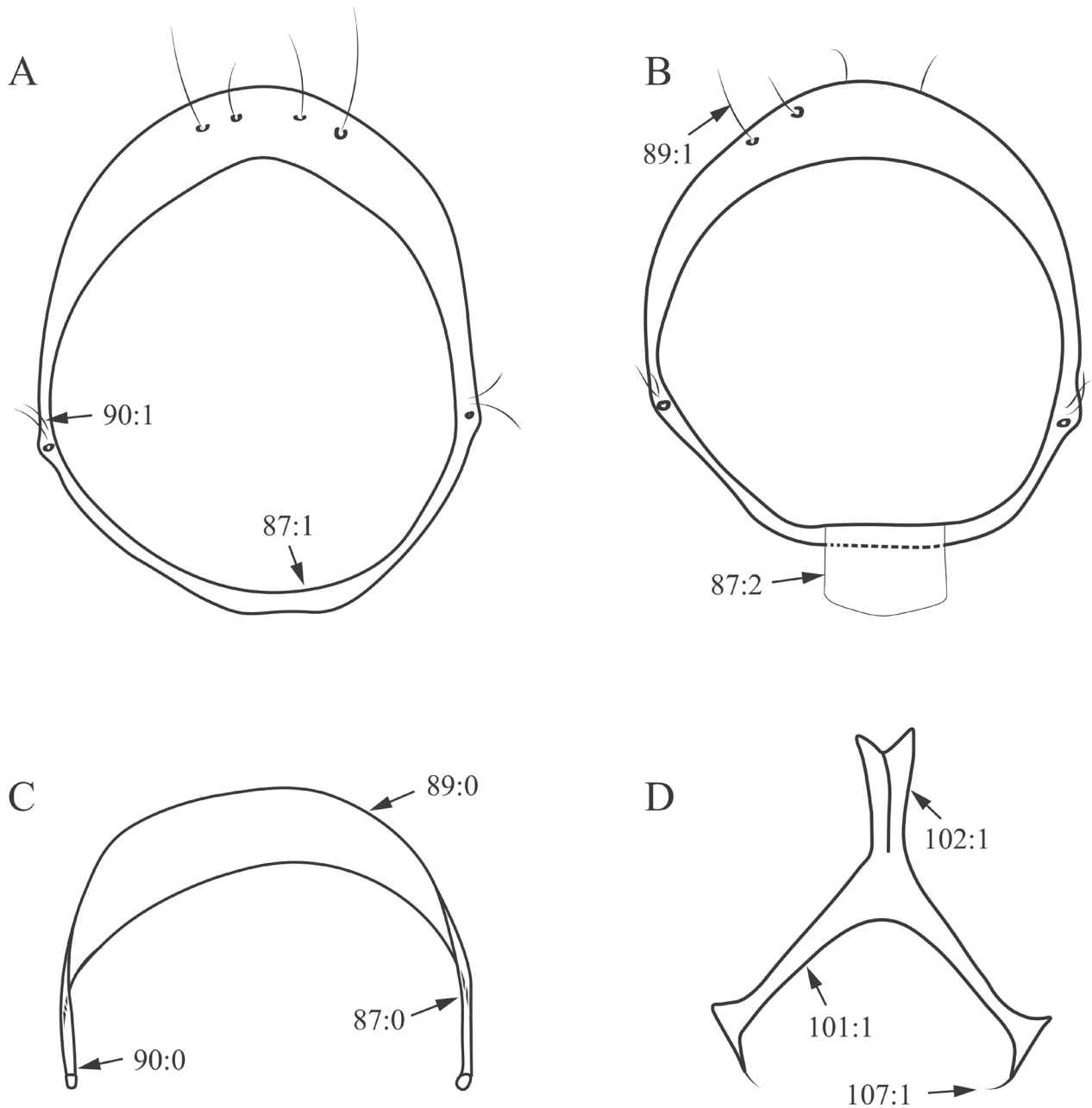
Figure 5. Syntergosternite and hypandrium characters. **A.** *Homoneura* (*Homoneura*) *dorsacerba* Gao, Shi & Han, 2016; **B.** *Homoneura* (*Homoneura*) *posterotricuspis* Gao, Shi & Han, 2016; **C.** *Homoneura* (*Homoneura*) *procerula* Gao & Yang, 2005; **D.** *Cestrotus liui* Shi, Yang & Gaimari, 2009.

101. Shape of hypandrium: (0) U-shaped (Fig. 7A); (1) Y-shaped (Fig. 5D); (2) H-shaped (Fig. 7D); (3) W-shaped (Fig. 7B).

102. Middle of anterior margin of hypandrium: (0) without inner processes (Fig. 7D); (1) with inner processes (Fig. 5D).

103. Both sides at anterior margin of hypandrium: (0) without inner processes; (1) with inner processes.

104. Middle of posterior margin of hypandrium: (0) without ventral process (Fig. 7A); (1) with ventral process (Fig. 7B).

105. Both sides at posterior margin of hypandrium: (0) without ventral process; (1) with ventral process.

106. Gonite: (0) present (Fig. 7D); (1) absent (Fig. 7C).

107. Seta on gonite: (0) present (Fig. 7D); (1) absent (Fig. 7A).

108. Length of gonite/length of phallus: (0) ≥ 1/2 (Fig. 7D); (1) < 1/2 (Fig. 7A).

109. Tip of gonite: (0) sharp (Fig. 7D); (1) blunt (Fig. 7A).

110. Phallus: (0) without thorn or sharp process (Fig. 7C); (1) with thorn or sharp process (Fig. 7B).

111. Lateral view of the tip of phallus: (0) bent (Fig. 7C); (1) straight (Fig. 7A).

112. Tip of phallus: (0) not inflated; (1) blunt round apically.

113. Apex of phallus: (0) sharp (Fig. 7C); (1) not sharp (Fig. 7B).
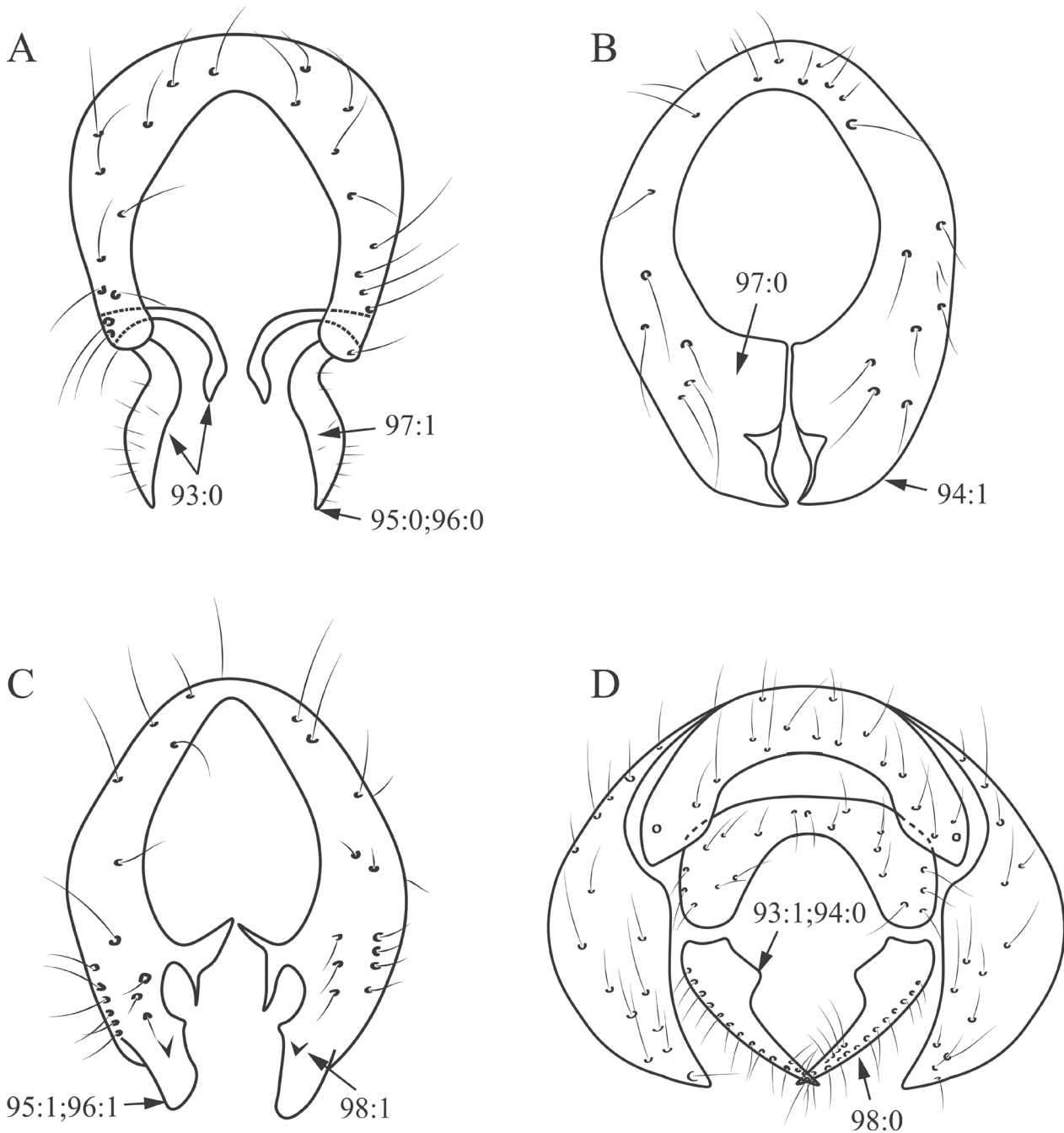
Figure 6. *Epandrium characters.* **A.** *Homoneura* (*Homoneura*) *trispina*; **B.** *Homoneura* (*Homoneura*) *dorsacerba*; **C.** *Homoneura* (*Homoneura*) *posterotricuspis*; **D.** *Pachycerina decemlineata*.

114. Phallus: (0) with distinct apical concavity; (1) without distinct apical concavity (Fig. 7B).
115. Aedeagal apodeme: (0) present; (1) absent.
116. Length of aedeagal apodeme/length of phallus: (0) < 1 (Fig. 7D); (1) ≥ 1 (Fig. 7A).
117. Base of aedeagal apodeme: (0) separate and extend (Fig. 7D); (2) not separate (Fig. 7C).

Phylogenetic analysis

In this research, two species of Lauxaniinae: *Minettia* (*Frendelia*) *longipennis* (Fabricius, 1794) and *Pachycerina decemlineata* Meijere, 1914 and representative species of all genera of Homoneurinae found in China except *Homoneura*, *Cestrotus liui* Li et al., 2009, *Dioides incurvatus* Shi et al., 2009, *Noonamyia umbrellata* Shi et al., 2009, *Phobeticomyia motuoensis* Li et al., 2020. and *Prosopophorella yoshiyasui* Sasakawa, 2001 were used as an outgroup. *Minettia* (*Frendelia*) *longipennis* is the first outgroup.

The phylogenetic construction was conducted using maximum-parsimony analysis. The unambiguous characters were mapped on the tree using WinClada version v1.00.08 (Nixon 2002). The maximum-parsimony tree is shown in Suppl. material 3, Bootstrap values (BS)
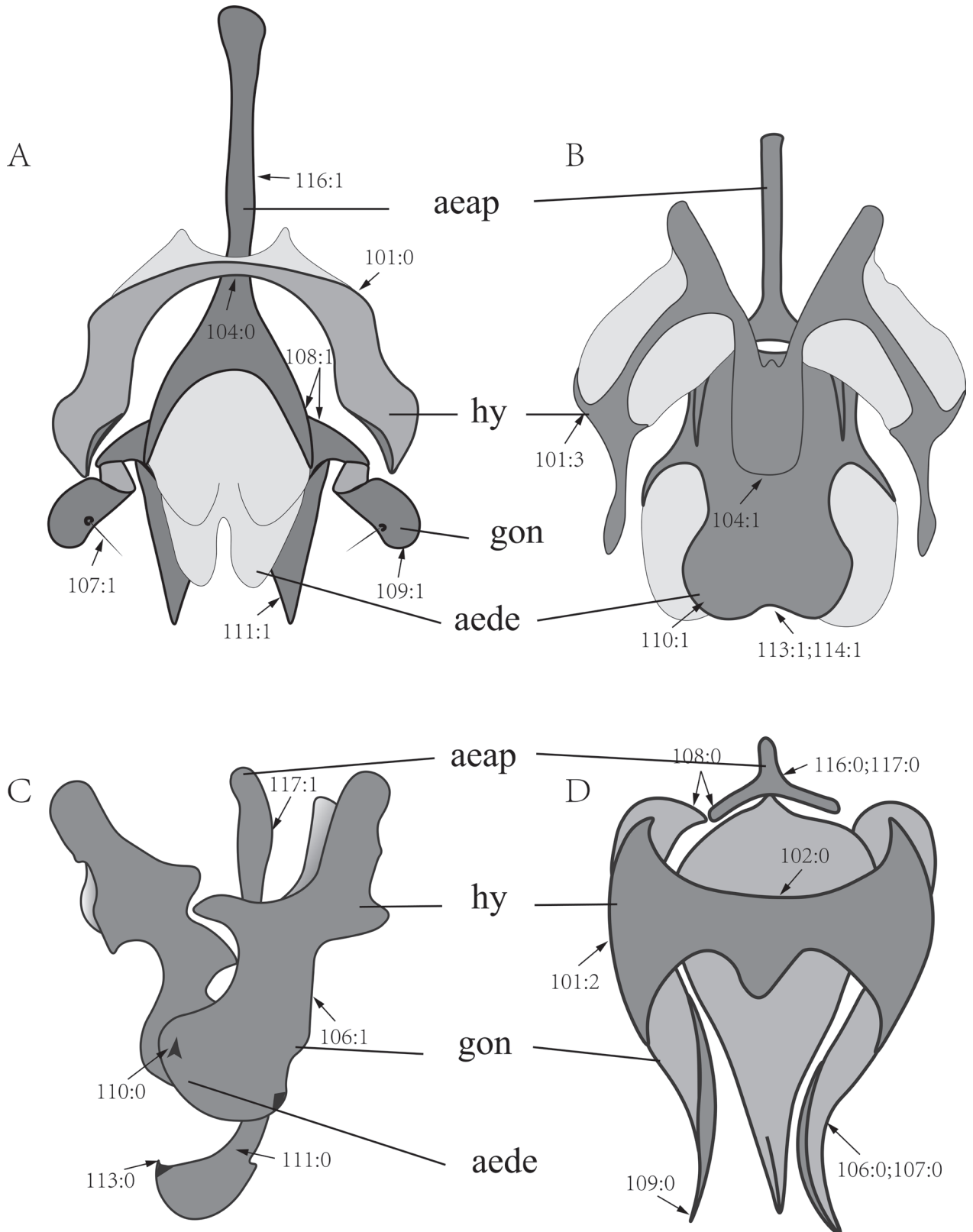
Figure 7. *Aedeagal complex characters.* **A.** *Noonamyia umbrellata*; **B.** *Homoneura* (*Homoneura*) *beckeri*; **C.** *Pachycerina decemlineata*; **D.** *Homoneura* (*Homoneura*) *procerula*.

and Bremer support (B) values are presented next to the nodes. The analysis was performed in TNT (version 1.1; Goloboff et al. 2008) using implied weighting. For the implied weighting analyses, K values of 2–5, 10, 15, 20, 25 and 30 were used, maintaining the maximum number of trees (10000 trees). All analyses were performed using traditional searches, 900 replicates holding up to 45 trees per replication. Branch support values were ver-

Dtsch. Entomol. Z. 71 (2) 2024, 241–254

251

ified through bootstrap analyses on NONA 2.0 (Goloboff 1999). The Bremer support value or decay index was calculated using TNT.

Results

Phylogenetic analysis of *Homoneura*

On the basis of our research, 117 morphological characters were obtained from different body parts of the adults; from the head (31 characters, Fig. 1), thorax (12 charac-

ters, Fig. 2A–F), legs (8 characters, Fig. 2G–L), wings (21 characters, Fig. 3), abdomen (13 characters, Fig. 4), and genitalia (32 characters, Fig. 5–7). Branch length is the shortest and the topology structure no longer changes when K is not less than 20. Forty-five maximum-parsimonious trees were produced when K = 30. Different maximum-parsimonious trees mainly affect the monophyletic and interspecific relationships of *Homoneura* (*Homoneura*) *henanensis* group, and the topology structure of each branch end. The resultant strict consensus tree was calculated using TNT (Fig. 8) [branch length = 1413, consistency index (CI) = 0.11, retention index (RI) = 0.73].

Figure 8. Phylogenetic relationships of *Homoneura*. **I.** *H.* (*H.*) *ornatifrons* group; **II.** *H.* (*H.*) *patella* group; **III.** *H.* (*H.*) *notostigma* group; **IV.** *H.* (*H.*) *nigra* group; **V.** *H.* (*H.*) *nigrifacies* group; **VI.** *H.* (*H.*) *trispina* group; **VII.** *H.* (*H.*) *beckeri* group; **VIII.** *H.* (*H.*) *formosae* group; **IX.** *H.* (*H.*) *laticosta* group; **X.** *H.* (*H.*) *pallida* group; **XI.** *H.* (*H.*) *henanensis* group; **XII.** *H.* (*H.*) *quinquenotata* group. Left, bootstrap values ≥ 50%; right, Bremer support values.

Relationships among the *Homoneura* subgenera occurring in China

The monophyly of the subgenus *Homoneura*, *Neohomoneura*, *Euhomoneura* and *Chaetohomoneura* is not supported. The monophyly of the subgenus *Minettioides* could not be verified due to the limited taxa. One species of the subgenus *Chaetohomoneura* appears at an end node within the subgenus *Neohomoneura*, while the subgenus *Euhomoneura*, *Neohomoneura*, *Minettioides* and *Chaeto-homoneura* also appear mosaically distributed within the subgenus *Homoneura*.

Key to the species groups of the *Homoneura* subgenus based on the maximum-parsimony tree

1   Wing without spots or only with pale spots on crossveins (Fig. 3E, G) 2
–   Wing with many distinct brown spots (Fig. 3A) 10
2   Body yellow or brown (Fig. 2C, D, E, F).. 3
–   Body black (Fig. 2A, B).. 6
3   Two stripes along orbital bristles (Fig. 1A), a triangular brown stripe in the middle of frons (Fig. 1C); hypandrium W-shaped .... *H. (H.) beckeri* group
–   Frons without stripe (Fig. 1B, L); hypandrium not W-shaped 4
4   Post pedicel bicolor (Fig. 1N); mesonotum scutoscutellar suture with black spots (Fig. 1H)..... *H. (H.) notostigma* group
–   Flagellomere yellow (Fig. 1P); mesonotum scutellar suture without spot (Fig. 2D)....................................... 5
5   Length of ocellar seta is shorter than the length of anterior fronto-orbital seta (Fig. 1E)................*H. (H.) patella* group
–   Length of ocellar seta is longer than the length of anterior fronto-orbital seta (Fig. 1F) .... *H. (H.) laticosta* group
6   Prescutellar acrostichal seta weak, same as acrostichal seta.. *H. (H.) ornatifrons* group
–   Prescutellar acrostichal seta strong, longer than acrostichal seta.. 7
7   With a broad white pruinose stripe from face to the end of scutellum (Fig. 4B) .... *H. (H.) nigra* group
–   Without pruinose stripe from face to scutellum (Fig. 4E) 8
8   Tergite 5 with a pair of black spots (Fig. 4B)... *H. (H.) formosae* group
–   Tergite 5 without spots (Fig. 4C) 9
9   Base of fronto-orbital seta with a stripe (Fig. 1D); stripe on the middle of frons extending to ocellar triangle (Fig. 1C).. ....*H. (H.) nigrifacies* group
–   Base of fronto-orbital setae without a stripe; only costal margin of frons yellow (Fig. 1E) ....*H. (H.) trispina* group
10   Wing without spots on crossvein r-m (Fig. 3G)... 11
–   Wing with spots on crossvein r-m (Fig. 3E)..*H. (H.) quinquenotata* group
11   R_{4+5} without spots between r-m and apical spot (Fig. 3E)..*H. (H.) pallida* group
– R_{4+5} with spots between r-m and apical spot (Fig. 3D) .... *H. (H.) henanensis* group

Discussion

Our study proposes a phylogenetic relationship hypothesis for the genus and subgenus *Homoneura* using morphological data. In this study, five genera of Homoneurinae except for *Homoneura* were included for the purpose of serving as an outgroup. Previously, Kong et al. (2022) published the phylogeny of the Chinese subgenera of *Homoneura* based on morphological characters, and obtained the conclusion that the monophyly of the genus and subgenus *Homoneura* is not supported, and this conclusion is further verified in this study. Some relationships among genera are in close agreement with the literature, suggesting that traditional taxonomic characters are more reliable at the generic level. Although the non-monophyly of *Homoneura* was strongly supported, the position of the species groups across the subgenus *Homoneura* was less consistent.

Based on the increment of available morphological characters and on the result of our analyses, we propose to divide the subgenus *Homoneura*. This is different from the the method of dividing the subgenus

Homoneura solely based on spots on the wing. Based on the resultant strict consensus tree we propose to reduce the 21 species groups into 12 species groups by establishing three new species groups: *H. (H.) nigrifacies*, *H. (H.) pallida*, and *H. (H.) patella*; keeping seven species groups: *H. (H.) beckeri*, *H. (H.) formosae*, *H. (H.) henanensis*, *H. (H.) nigra*, *H. (H.) notostigma*, *H. (H.) ornatifrons*, and *H. (H.) trispina*; and combining the remaining species groups into two new species groups: *H. (H.) laticosta*, and *H. (H.) quinquenotata*. However, we advise for caution since these possible placements are tentative at best and further studies are needed to verify these observations.

Previously, the only existing molecular phylogenetic study of the generic level relationships of Lauxaniidae, Shi et al. (2017) explored the phylogeny of the subgenus *Homoneura* based on two mitochondrial and two nuclear markers. But the results did not support the published taxonomy of the species groups of the subgenus *Homoneura* in China (Shi and Yang 2014). All of these indicates that there are many problems in the division of species group of the subgenus *Homoneura*.

Dtsch. Entomol. Z. 71 (2) 2024, 241–254

253

In our research, we provide solid evidence that the currently recognized genus and subgenus *Homoneura* are not monophyletic. Thus, our results indicate that the current classification of the *Homoneura* does not accurately reflect the evolutionary history of the group. This result is consistent with the results obtained by Shi and Yang (2014). We do not seek to formally propose one of these changes here because the resolution of these clades is poor and because our taxon sampling is limited (only Chinese species are involved). We can only try to separate species groups of the subgenus *Homoneura*. Furthermore, we need to take a closer inspection of the morphology, focusing on an alternative level of analysis. Therefore, in order to enable such taxonomic decisions, we urge for a complete phylogeny of the *Homoneura* with datasets including more morphological and molecular data.

Conclusions

Our research results show that the monophyly of the genus and subgenus *Homoneura* is not supported, and the confusion of the subgeneric division is one of the main problems of this genus, which makes some scholars ignore the subgeneric rank in their works, and there are often taxonomists who misclassify subgenera when describing species. The main reason is that the key characteristics and validity of subgeneric level classification are not clear. Although not the primary focus of this study, our results also provide a preliminary glimpse of potential major relationships within the genus *Homoneura*. Nevertheless, we emphasize that this study was focused on testing the monophyly and the relationships of the species groups within the subgenus *Homoneura*. Thus, our findings regarding the major relationships within the entire genus should be considered, at best, preliminary. And although these conclusions are based on a small sample size compared with the diversity of the genus as a whole, our results indicate that the classification of the genus at the subgenus and species group levels will require a thorough reformulation that reflects the family's evolutionary history. In these cases, we should re-analyze the morphological data, trying to look for misinterpretations of morphological characters.

As a next step for the phylogeny and classification of the genus and the subgenus, we will try to find synapomorphies of early diverging lineages, whose phylogenetic placements are not well supported in our study. Additionally, the phylogeny of each subgenus of *Homoneura* is still unclear, and the monophyly and phylogenetic relationship of species groups is still blank, and none of them have been examined using molecular data. The availability of molecular data for species of *Homoneura* has increased during recent years, and we encourage the phylogenetic analysis among the species groups at the subgeneric level using a combination of morpho-

logical and molecular data. Furthermore, we will review specimens from other zoogeographical regions and revise the species groups of the *Homoneura* subgenera by using geographic distribution information to reconstruct the phylogeny of the genus *Homoneura* making taxonomic revisions.

Acknowledgements

References

Chen XL (2022) Taxonomy of *Homoneura* in China. D. M.S. Henan University of Science and Technology, 247 pp.

Cumming JM, Wood DM (2017) Adult morphology and terminology. In: Kirk-Spriggs AH, Sinclair BJ(Eds) Manual of Afrotropical Diptera. South African National Biodiversity Institute: Pretoria, South Africa Vol. 1, 89–133.

Gaimari SD, Miller, RM (2021) Lauxaniidae (Lauxaniid flies). In Manual of Afrotropical Diptera. Kirk-Spriggs, A.H., Sinclair, B.J., Eds.; South African National Biodiversity Institute: Pretoria, South Africa Volume 3: 1757–1781.

Goloboff PA (1999) NONA (NO NAME) ver. 2.0. Z. Published by the author, Tucumán, Argentina.

Goloboff PA, Farris JS, Nixon KC (2008) TNT, a free program for phylogenetic analysis. Cladistics 24: 774–786. https://doi.org/10.1111/j.1096-0031.2008.00217.x

Kim SP (1994) Australian Lauxaniid Flies. Revision of the Australian Species of *Homoneura* van der Wulp, Trypetisoma Malloch, and Allied Genera (Diptera, Lauxaniidae). Monographs on Invertebrate Taxonomy 1: 1–445. https://doi.org/10.1071/9780643105164

Kong CY, Feng KL, Zhao SJ, Li WL, Li XK (2022) Phylogeny of the Chinese Subgenera of the Genus *Homoneura* (Diptera, Lauxaniidae, Homoneurinae) Based on Morphological Characters. Insects 13: 665. https://doi.org/10.3390/insects13080665

Miller RM (1977a) Taxonomy and biology of the Nearctic species of *Homoneura* (Diptera: Lauxaniidae) I. Subgenera *Mallochomyza* and *Tarsohomoneura*. Iowa State Journal Research 52(1): 147–176.

Miller RM (1977b) Taxonomy and biology of the Nearctic species of *Homoneura* (Diptera: Lauxaniidae) II. Subgenenus *Homoneura*. Iowa State Journal Research 52(2): 177–252.

Nixon, KC (2002) WinClada; ver. 1.00.08; Nixon, K.C.: Ithaca, NY, USA.

Papp L. (1978) Constrisution to the revision of the Palaearctic Lauxaniidae (Diptera). Annales Historico-Naturales Musei Nationalis Hungarici 70: 213–231.

Papp L, Merz B, Foldvari M (2006) Diptera of Thailand. A summary of the families and genera with references to the species representations. Acta Zoologica Academiae Scientiarum Hungaricae 52(2): 97–269.

Sasakawa M (1992) Lauxaniidae (Diptera) of Malaysia (part 2): a revision of *Homoneura* van der Wulp. Insecta Matsumurana 46: 133–210.

Shi L, Yang D (2014) Supplements to species groups of the subgenus *Homoneura* in China (Diptera: Lauxaniidae: *Homoneura*), with descriptions of twenty new species. Zootaxa 3890.1: 1–117. https://doi.org/10.11646/zootaxa.3890.1.1

Shi L, Zhang MJ, Shen RR, Li SD, Bai J, Wang YJ, He GW, Cui Y (2017) Preliminary study on phylogeny of species groups in subgenus *Homoneura*. Environmental Entomology 39: 351–356.

Stuckenberg BR (1971) A review of the Old World genera of Lauxaniidae (Diptera). Annals of the Natal Museum 20: 499–610.

You PY, Chen XL, Li WL (2023) Four new species of the subgenus *Homoneura* from Yintiaoling Nature Reserve, China (Diptera: Lauxaniidae: *Homoneura*). Zootaxa 5257: 143–159. https://doi.org/10.11646/zootaxa.5257.1.11

Supplementary material 1

The species studied

Author: Yao Yao
Data type: pdf
Link: https://doi.org/10.3897/dez.71.120389.suppl1

Supplementary material 2

Morphological dataset used for the analysis of the phylogeny

Author: Yao Yao
Data type: pdf
Link: https://doi.org/10.3897/dez.71.120389.suppl2

Supplementary material 3

Maximum parsimony tree

Authors: Yao Yao, Chaoyang Kong, Pu Miao, Shengjuan Zhao, Wenliang Li
Data type: zip
Link: https://doi.org/10.3897/dez.71.120389.suppl3

A new species of the mantidfly genus *Euclimacia* from Vietnam (Neuroptera, Mantispidae)

Sarah Ehlers[1], Hongyu Li[2], Lukas Kirschey[1], Michael Ohl[1]

1 Leibniz-Institut für Evolutions- und Biodiversitätsforschung, Museum für Naturkunde, Invalidenstr. 43, D-10115 Berlin, Germany

2 Department of Entomology, China Agricultural University, Beijing 100091, China

https://zoobank.org/DF838760-FA62-45C0-9063-ACFE010B0170

Corresponding author: Sarah Ehlers (sarah.ehlers@mfn.berlin)

Abstract

A new species of the family Mantispidae (Neuroptera) from Vietnam is described. *Euclimacia radioquaesentis* **sp. nov.** shows a unique colour pattern, which is distinctive within the genus. The colouration and morphology of both sexes of the new species are described in detail and illustrated. The naming of the new species is linked to a popular citizen-science event in choosing the name for this species (and three other species from different undescribed species by taxonomists of the Museum für Naturkunde Berlin).

Key Words

Introduction

The Mantispidae is a family within the holometabolous order Neuroptera, which has a remarkable morphology and interesting, but so far scarcely studied biology. The larvae of the subfamily Mantispinae are predatory and feeding on spider eggs (Snyman et al. 2020). The larvae of Symphrasinae were observed on various insect pupae and, for Drepanicinae, there is one recorded interaction with a spider (Theridiidae) without further details (Austin 1985). So far, there is only one report on Calomantispinae from a laboratory experiment. Here, larvae were reared on various insect pupae and larvae, as well as on spider eggs and paralysed spiders (MacLeod and Redborg 1982). Mantispidae larvae undergo a hypermetamorphosis with first developmental stage mobile and actively search for food sources (Snyman et al. 2020). An interesting type of behaviour is spider boarding, exhibited by some species of the subfamily Mantispinae. In this case, a larva of the first instar climbs on to a female spider and remains there until she begins to produce her egg sac (Redborg 1998). The larva then intrudes into the egg sac and develops into the second and later third instar. The legs of the third in-

star are significantly smaller, which restricts locomotion (Snyman et al. 2020).

Adult mantispids are characterised by a triangular head, raptorial forelegs and an elongated tubular prothorax, which makes them appear very similar to mantids (Ardila-Camacho et al. 2021). Adult mantispids are effective ambush predators on other insects. In some species, it is known that they also feed on pollen and nectar (Boyden 1983). Many species show wasp mimicry (Snyman et al. 2018).

Formerly, this family was assumed to be monophyletic, with its extant members classified into four subfamilies: Mantispinae, Calomantispinae, Symphrasinae and Drepanicinae (e.g. Lambkin (1986a, b)). However, recent morphological and molecular studies have convincingly demonstrated that Mantispidae is paraphyletic, with the Symphrasinae being a subfamily in the Rhachiberothidae (Winterton et al. 2018; Ardila-Camacho et al. 2021). The relationships amongst the Calomantispinae, Drepanicinae and Mantispinae, which might be considered as the Mantispidae *sensu stricto*, are still controversial (see Ardila-Camacho et al. (2023).

Euclimacia Enderlein, 1910 belongs to the most diverse subfamily Mantispinae, which comprises of 320

species in 35 genera (Ohl 2004b; Oswald and Machado 2018). Adult *Euclimacia* can be easily distinguished from other mantispid genera by the disc-like and symmetrical flagellomeres, the short pronotum (approximately of the same length as the pterothorax), pronounced dorsal humps and lateral maculae and a forked 2A vein in the fore-wing. Species of *Euclimacia* exhibit a high degree of colour variation. Many mimic different species of aculeate wasps from different families. Colour patterns in *Euclimacia* vary from almost completely black body colour with blue shimmering wings similar to some Pompilidae to bright yellow and black-striped species, which resemble species of the social wasp family Vespidae (Ohl 2004a; Soh et al. 2022). Currently, there are 33 valid species in this genus, distributed in Oriental and Australasia (Ohl 2004b; Kaur et al. 2021), summarised in Table 1. In 1910, Enderlein initially described *Euclimacia*, designating *E. partita* as the type species. The most comprehensive revision of this genus was performed by Handschin in 1961. At that time, only 19 species were known in *Euclimacia*, but Handschin only included those that were available to him, i.e. a total of 11 species. Of these 11 species, however, he could

only personally study the types of four species. In addition, Handschin described six new species.

In the present study, we describe a new species from Vietnam (Fig. 1B), showcasing a unique colour pattern, which distinguishes it from all other described species in *Euclimacia*.

Material and methods

The type series is part of the large collection of Southeast Asian Mantispidae deposited in the Royal Belgium Institute of Natural Sciences, Brussels, Belgium. One paratype is housed in the collections of the Museum für Naturkunde, Berlin, Germany.

The genital preparation was made from one paratype. Punctures were made in the area of the fourth abdominal segment with the aid of an insect pin size 0. Polyethylene foam was cut into required pieces, which were attached to the pinned specimen with needles to stabilise it for the preparation. The abdomen was very carefully perforated all around until the posterior part could be detached by

Table 1. Overview of the currently valid *Euclimacia* species and their known distribution.

Species	Distribution
Euclimacia badia Okamoto, 1910	Taiwan, Japan
Euclimacia basiflava Handschin, 1961	Malaysia
Euclimacia burmanella (Westwood, 1867)	Myanmar
Euclimacia celebica Handschin, 1961	Indonesia (Sulawesi)
Euclimacia cottami Navás, 1914	India (Sikkim)
Euclimacia flavicauda Esben-Petersen, 1917	Indonesia (Sumatra)
Euclimacia flavocincta Stitz, 1913	Solomon Islands
Euclimacia fusca Stitz, 1913	Taiwan, Japan
Euclimacia gerstaeckeri Banks, 1920	Singapore, Malaysia
Euclimacia grandis (Guérin-Méneville, 1831)	Indonesia (Ambon)
Euclimacia horstaspoecki Ohl, 2004	Thailand
Euclimacia jacobsoni Handschin, 1961	Indonesia (Sumatra)
Euclimacia metallica Esben-Petersen, 1917	Indonesia (Sulawesi, Sumatra)
Euclimacia morosa (Gerstaecker, 1893)	Borneo, Philippines (Palawan)
Euclimacia nelsoni Navás, 1914	Sri Lanka
Euclimacia nicobarica Kaur, 2021	India (Andaman Islands, Nicobar Islands)
Euclimacia nigra Handschin, 1961	Indonesia (Java)
Euclimacia nodosa (Westwood, 1847)	India (Assam)
Euclimacia nuchalis (Gerstaecker, 1985)	Australia (New South Wales, Northern Territory, Queensland).
Euclimacia partita Enderlein, 1910	Indonesia (Sulawesi)
Euclimacia radioquaesentis Ehlers, sp. nov.	Vietnam
Euclimacia regina Esben-Petersen, 1917	Indonesia (Java, Sunda Islands), Singapore
Euclimacia rhombica Navás, 1914	Myanmar
Euclimacia rufa Esben-Peterson, 1928	Indonesia (Sumatra)
Euclimacia ruficauda Enderlein, 1910	Indonesia (Sulawesi)
Euclimacia rufocincta Handschin, 1961	Borneo
Euclimacia similis Kaur, 2021	India (Madhya Pradesh)
Euclimacia superba Lambkin, 1987	Australia (Queensland)
Euclimacia tagalensis Banks, 1914	Philippines (Luzon)
Euclimacia torquata Navás, 1914	Australia (New South Wales, Queensland), New Guinea
Euclimacia triangularis Handschin, 1961	Philippines
Euclimacia vespiformis Okamoto, 1910	Taiwan, Japan
Euclimacia woodhousei Navás, 1914	India (Sikkim)
Euclimacia zonalis Navás, 1914	Indonesia (Sulawesi)
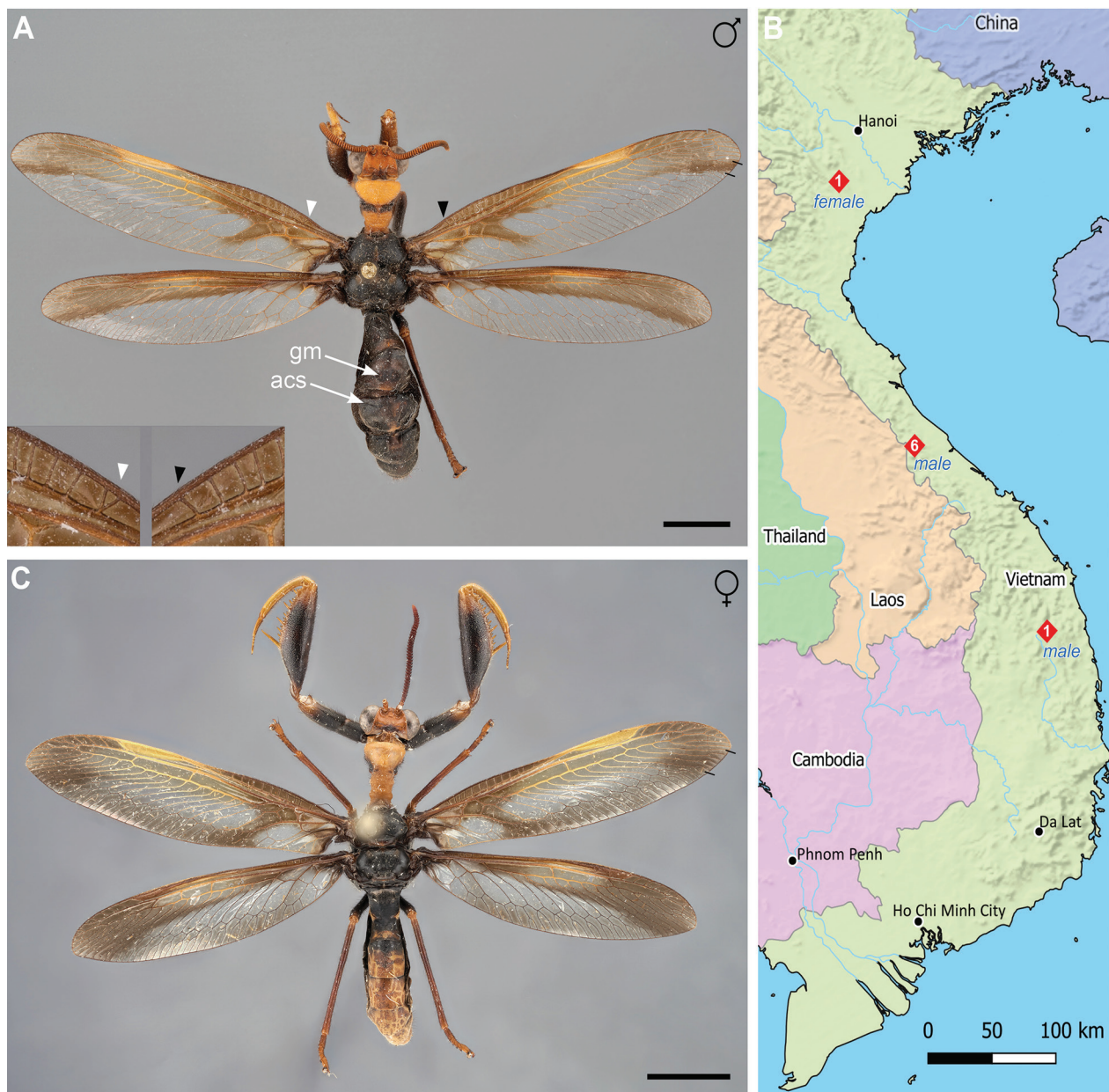
Figure 1. *Euclimacia radioquaesentis* sp. nov. male holotype and female paratype with distribution map. **A.** Habitus dorsal holotype male. Insert shows asymmetrical bifurcation between left and right costal area of fore-wings. Antecostal sutures (*acs*) and glabrous marks (*gm*) visible. The two black lines on the margin of the wing apex of the right fore-wing indicate the width of the oblique apical dark band; **B.** Localities (red rhombus) in Vietnam of the *radioquaesentis* type series. The number in the rhombus symbol indicates the count of specimens in this locality; **C.** Female paratype *radioquaesentis* dorsal view. The two black lines on the margin of the wing apex of the right fore-wing indicate the width of the oblique apical dark band. Scale bars: 5 mm (**A, B**).

a gentle levering action of the needle. The dissected abdominal end was left in 15% potassium hydroxide solution for approx. 21 h, then rinsed with distilled water and transferred to glycerol.

Images were taken with a Sony a7rIII and a Sony Makro G OSS 90mm f 2.8 lens for the habitus and a Canon MP-E 65mm f 2.8 lens for the details. Multi-focus imaging was facilitated by a Novoflex Castel-Mikro stepping motor-controlled focusing rack. To take the images, the software Capture One was used. For stacking, the software Helicon Focus was used. Genital images were made with a Leica Z16 APO A motorised macroscope with a Leica DFC camera. Measurements were done with Fiji (ImageJ) Version 2.1.0/1.53c.

Photos were post-processed with Adobe Photoshop version CC 2019 an arranged and labelled with Adobe InDesign version 19.2.

Illustrations were made with Adobe Illustrator version 25.0.

Distribution map was generated with QGIS version 3.16 Hannover, Natural Earth Data and Adobe Photoshop version CC 2019.

The terminology is based on Snodgrass (1935), Lambkin (1986a), U. Aspöck and H. Aspöck (2008) and Ardila-Camacho (2021).

Results

Class Insecta Linnaeus, 1758
Order Neuroptera Linnaeus, 1758
Family Mantispidae Leach, 1815
Subfamily Mantispinae Leach, 1815

Genus *Euclimacia* Enderlein, 1910

Type species. *Euclimacia partita* Enderlein, 1910: 366, by original designation.

Euclimacia radioquaesentis sp. nov.
https://zoobank.org/2EB67902-20D0-495C-837B-CF63114BD194

Etymology. The species epithet is made up of two words 'radio' and 'quaesentis'. The latter derives from Latin and means 'searched for'. The name was chosen as part of a radio show. Citizens were invited to submit name suggestions. The most suitable was *radioquaesentis* – searched for on the radio.

Material examined. *Holotype.* Vietnam • ♂; Quang Tri, Huong Hoa Nature Reserve; 16°56'15"N, 106°34'52"E; 400 m; 7–10 Nov. 2007; G. Csorba leg., T. S. Nguyen leg., D. T. Pham leg., T. T. Nguyen leg., X. N. Nguyen leg.; light trap; CSOVI – Vietnam No. 92; coll. mfn-berlin.de_u_8bfa03; ISNB.

Paratypes. Vietnam • 4 ♂; Quang Tri, Huong Hoa Nature Reserve; 16°56'15"N, 106°34'52"E; 400 m; 7–10 Nov. 2007; G. Csorba leg., T. S. Nguyen leg., D. T. Pham leg., T. T. Nguyen leg., X. N. Nguyen leg.; light trap; CSO-VI – Vietnam No. 92; coll.mfn-berlin.de_u_7e303d, coll. mfn-berlin.de_u_29a944, coll.mfn-berlin.de_u_199711, coll.mfn-berlin.de_u_93bd60; ISNB • 1 ♂; same collection data as for preceding; coll.mfn-berlin.de_u_5ea2b5; ZBM • 1 ♂; Gia Lai, Kon Chu Rang Nature Reserve; 14°28'28"N, 108°32'27"E; 1200 m; 13–20 Jul. 2018; J. Constant leg., J. Bresseel leg., X. Vermeersch leg.; GTI Project, I.G.: 33.769; coll.mfn-berlin.de_u_6c2cbd; ISNB • 1 ♀; Ninh Bình, Cuc Phuong National Park; 11–18 Jul. 2010; J. Constant leg., P. Limbourg leg.; ISNB.

Diagnosis. The combination of colour characters in the new species is unique within *Euclimacia*. The contrast between the head and prothorax and the rest of the thorax and abdomen is striking. The prothorax and head have a distinct yellow colour, the remaining thorax is almost uniformly black. The abdomen of the male is also almost completely black with only a few brown markings. The female has a brownish abdomen with a black base. The wing colour is also unique in combination with the body colouration. The wings of *E radioquaesentis* have the prominent feature of differently-coloured pterostigmata in fore and hind wing. Whereas the fore-wing pterostigma is yellow, the hind-wing pterostigma is brown. There are currently six species in *Euclimacia* with this diagnostic character, but these species differ distinctly in body colouration. Whereas in *E. radioquaesentis* sp. nov., the head and the prothorax are markedly yellow, in the other six species both parts are either ferruginous (*E. rhombica* Navás, 1914), reddish-brown (*E. morosa* (Gerstäcker, 1893); *E. zonalis* Navás, 1914; *E. regina* Esben-Petersen, 1917; *E. rufocincta* Handschin, 1961) or completely black (*E. gerstaeckeri* Banks, 1920).

Description. *Measurements and ratios* [in mm]. The given size range of each defined measurement area comprises minimum and maximum measured values of all seven specimens: Minimum frontal eye distance [WBE]: male 1.32–1.56; female 1.05. Maximum frontal head width including eyes [WAE]: male 3.96–4.44; female 3.25. Pronatal length, measured lateral from the anterior margin of the prozona to the dorsal basis of the prothorax [PL]: male 3.6–4.53; female 3.6. Pronatal width at maculae [WAM]: male 1.92–2.41; female 1.5. Pronatal ratio (length: width) [PL: WAM]: male 1.81–2.03; female 2.4. Maximum fore femoral length [LFF]: male 6.42–7.39; female 5.44. Maximum fore femoral width [WFF]: male 21–2.52; female 1.6. Fore femoral ratio (length: width) [LFF: WFF]: male 2.55–3.52; female 3.4. Maximum hind femoral length [LHF]: male 4.61–5.46; female 3.85. Hind femoral ratio (Hind femoral length: head width including eyes) [LHF: WAE]: male 1.08–1.38; female 1.18. Fore-wing length (measured at the middle of the humeral plate to the outer apex of the wing) [LFW]: male 22.21–25.1; female 17. Fore-wing width (measured down from the base of the pterostigma at a right angle) [WFW]: male 4.8–5.1; female 4.08. Fore-wing ratio (length: width) [LFW: WFW]: male 4.48–4.95; female 4.15. Maximum length of fore-wing anterior radial cell II [Lrarp2]: male 4.19–5.2; female 3.02. Maximum width of fore-wing anterior radial cell II [Wrarp2]: male 0.46–0.57; female 0.45. Fore-wing 2R1 ratio (length: width) [$L2R_1$: $W2R_1$]: male 8.6–10.57; female 6.71. Maximum hind-wing length (measured at the middle of the humeral plate to the outer apex of the wing): male 19.57–21.9; female 15.55. Maximum hind-wing width (measured down from the base of the pterostigma at a right angle): male 4.26–5.1; female 3.62. Hind-wing ratio (length: width): male 4.29–4.69; female 4.3.

Head. Holotype: Left antenna with 47 flagellomeres, right with 46 flagellomeres. Antennae of male paratypes ranging from 42 to 47 flagellomeres, left and right antennae with different number of flagellomeres in all specimens. Female: 41 flagellomeres right, left antennae missing.

Frons approximately square-shaped basically with outwardly curved lateral subantennal sutures (Fig. 2A). Frons glabrous, pilosity indistinct, frontal surface wrinkled (Fig. 2A). Clypeus trapezoidal, with long parallel side adjacent to frons and short parallel side adjacent to labrum, smoother surface than frons. Labrum ovoid, surface smooth with sparse pilosity. Frontal sutures form a curved line (Fig. 2B). Coronal suture runs straight from junction of frontal sutures to occiput.

Figure 2. *Euclimacia radioquaesentis* male. **A.** Head frontal view. The subantennal suture (*sas*) is curved outwards; **B.** Head and thorax in dorsal view. The epicranial sutures are comprised by the frontal sutures (*fs*) and the coronal suture (*cs*). A black transversal band runs along the pronatal groove over the maculae (*mc*) and the pronatal humps (*ph*). The horizontal dashed lines indicate the three areas of the prothorax, the prozona (*p1*), the metazona (*p2*) and the pronatal base (*p3*); **C.** Lateral view on head, thorax and forelegs. Scale bars: 1 mm (**A**); 2 mm (**B, C**).

Prothorax. Pronatal humps distinctly protruding (Fig. 3A). Female pronatal humps flat, weakly developed (Fig. 3B).

Wings. Number of subcostal veinlets and their bifurcations are asymmetric. Holotype: Left fore-wing costal space proximal to pterostigma with 17 subcostal veinlets, first (most proximal) subcostal veinlet counted as one, but with bifurcation in anterior direction (Fig. 1A). Right fore-wing with same number of subcostal veinlets, but without any bifurcation. Costal space of left hind-wing with 15 subcostal veinlets, right one with 14. Paratypes: Costal space with 11 to 16 subcostal veinlets, different in each wing of each specimen. Five of seven specimens with at least one bifurcated subcostal veinlet within costal space of fore-wing. Bifurcations never on both costal spaces in fore-wings, absent in costal spaces of hind-wings and subcostal spaces. One specimen with three bifurcations in one fore-wing. Female: Left fore-wing costal space with 12 subcostal veinlets, right fore-wing with 13 subcostal veinlets. Costal space of left hind-wing with 12 subcostal veinlets, right one with 16. Anterior ra-

dial cell II (*rarp2*) of the left hind-wing with cross-vein approximately centrally.

Abdomen. Abdominal segments with indistinct pilosity, dull appearance, without enlarged membranes or pores (Fig. 4E). Antecostal sutures (attachment for the longitudinal muscles) clearly visible in tergite III–VI in holotype and two further specimens (Fig. 1A). One transverse suture on each side of anterior margin of tergite, 1.5–1.8 mm long, smooth and without setae. Sutures not merging dorsally. Additional small (0.15 mm – 0.35 mm) circular and glabrous areas on tergum III–VIII, two on each side in the posterior third, below each other, one more dorsally and one at lower part of tergum, similar to surface of tergal sutures (Fig. 1A). Similar arrangement of those marks visible on sternum III–VII.

Male genitalia. Tergite IX laterally about three times as wide as dorsally (Fig. 4A, C). Sternite IX sternite posterior with apex pointing downwards (Fig. 4C). Ectoprocts with median lobes with short thick black setae (Fig. 4A). Mediuncus (gonocoxites X) elongated and arched from ventral to dorsal, approximately 1.1 mm long, anteri-
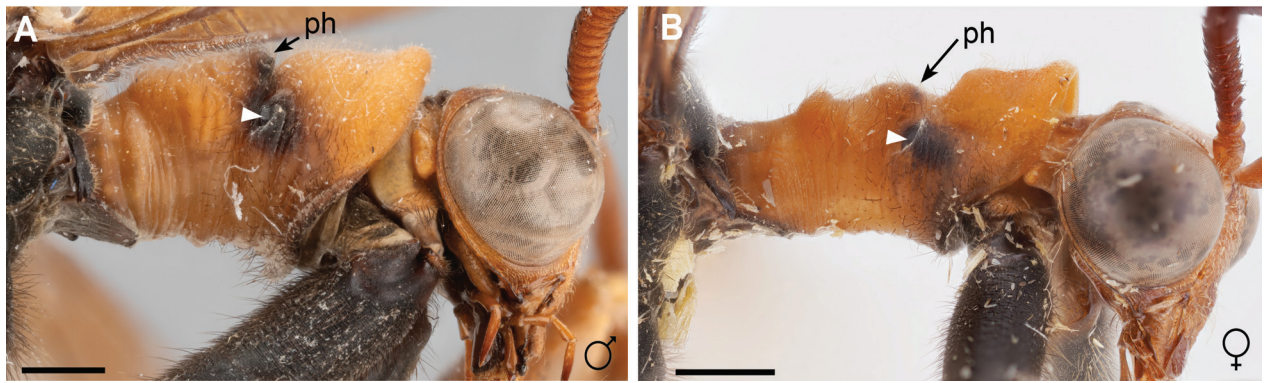
Figure 3. *Euclimacia radioquaesentis* prothorax of both sexes in lateral view. **A.** Male. Pronatal hump (white arrowhead) distinctly protruding. The black marking on the pronatal hump and the black marking on the macula are connected; **B.** Female. Pronatal hump (white arrowhead) barely protrudes. Dark marking on pronatal hump faintly present and not interfering with the black mark of the macula. Scale bars: 5 mm (**A, B**).
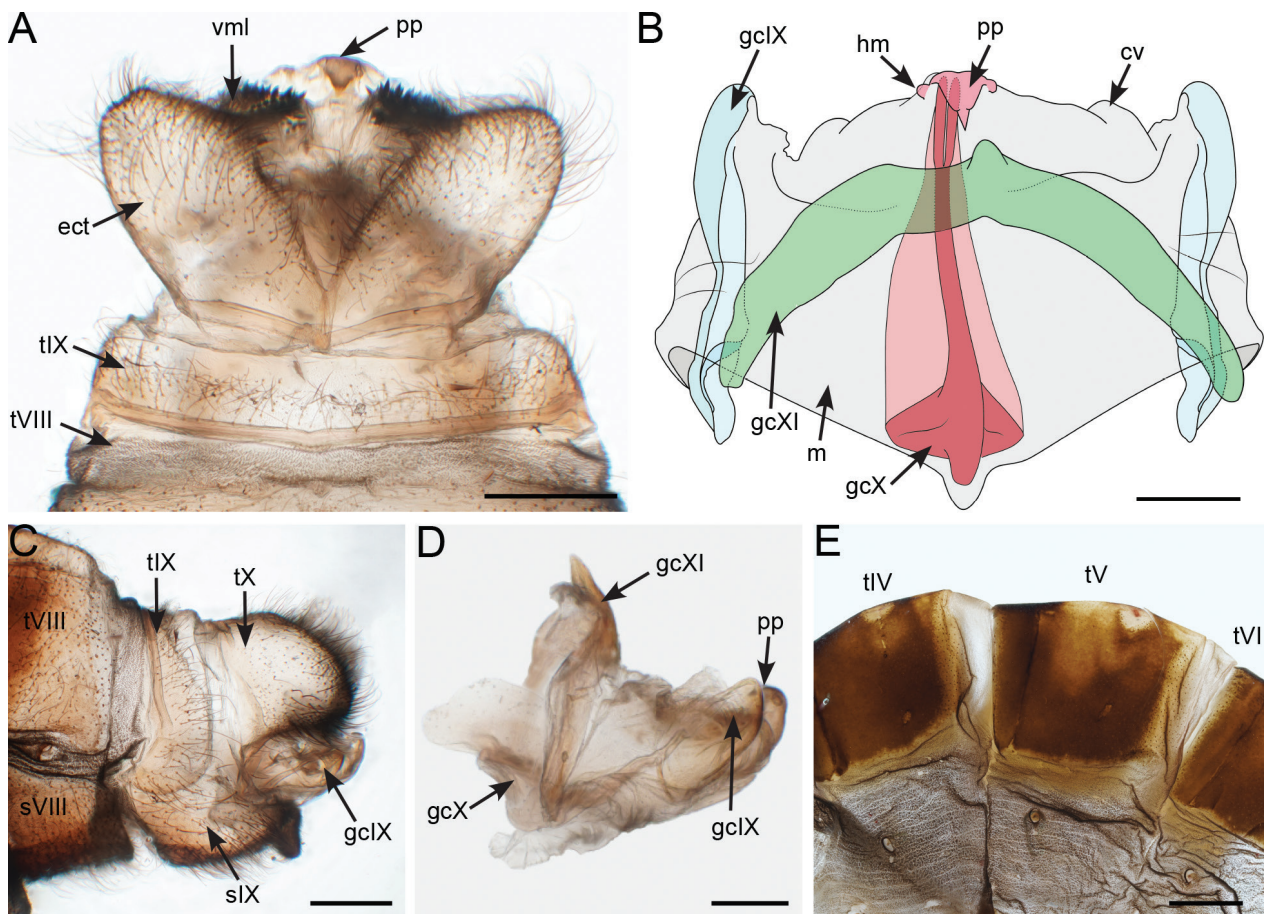
Figure 4. *Euclimacia radioquaesentis* male terminalia and inner genitals. **A.** Dorsal view of abdominal segment VII–IX; **B.** Illustration of the inner genitals from dorsal view with same orientation as in A; **C.** Male terminalia lateral view; **D.** Inner genitals from lateral view with same orientation as in C; **E.** Tergites IV–VI in lateral view. Abbreviations: cv, convex area; ect, ectoproct; gc, gonocoxite; hm, hypomere; m, membrane; pp, pseudopenis; s, sternite; t, tergite; vml, ventromedial lobus. Scale bars: 0.25 mm (**A, B**); 0.5 mm (**C**); 0.2 mm (**D**); 1 mm (**E**).

or two-thirds slender, posterior part broadened with two flanks, apex bifid (Fig. 4B, D). Pseudopenis (gonostyli X) originates posterior to apex of mediuncus, with broadened sclerotised trapezoidal lower region, short and acute process, strongly curved backwards (cranial direction). Two

globular protrusions (hypomeres) lateral at base of pseudopenis. Parameres (gonocoxites IX) slightly s-shaped in lateral plane, one part strongly sclerotised, pigmented, narrow in lower half and widens threefold in upper half, lobe-like shape. Inwardly projecting and less pigmented area

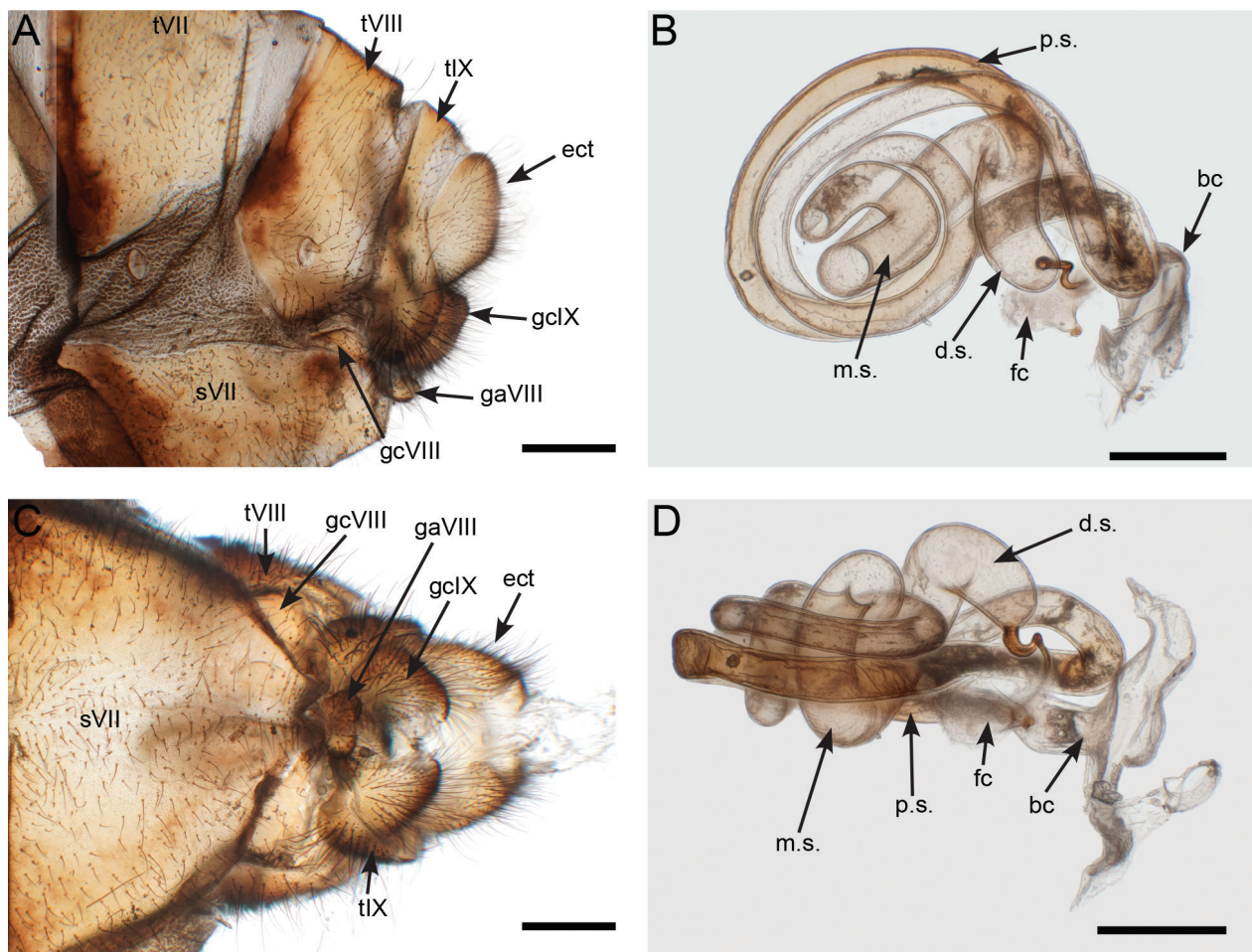**Figure 5.** *Euclimacia radioquaesentis* female terminalia and inner genitals. **A.** Female terminalia lateral view; **B.** Spermatheca with bursa copulatrix lateral view; **C.** Terminalia ventral view; **D.** Spermatheca with bursa copulatrix ventral view. Abbreviations: *b.c.*, bursa copulatrix; *d.s.*, distal section of spermatheca; ect, ectoproct; *fc*, fertilisation canal; *fcd*, fertilisation canal duct; *ga*, gonapophysis; *gc*, gonocoxite; *m.s.*, medial section of spermatheca; *p.s.*, proximal section of spermatheca; *d.s.*, distal section of spermatheca; *s*, sternite; *t*, tergite. Scale bars: 0.25 mm (**A, B**); 0.5 mm (**C**); 0.2 mm (**D**); 1 mm (**E**).

that surrounds sclerotised part, merges into the connecting membrane. Membranous areas and most parts of pseudopenis covered with microspinulae. Gonarcus (gonocoxites XI) arch-shaped from dorsal view, with medial and slightly upwards pointing lobe, located on top of mediuncus-paramere-complex (Fig. 4B), connected to mediuncus and parameres via connecting membrane, remaining part freely movable. Connecting membrane barely sclerotised and flexible, but with definite shape (Fig. 4B, D). Anterior margin between mediuncus/pseudopenis and parameres from dorsal view shoulder-shaped, with strongly convex (*cv*) area in distal 2/3.

Female genetalia. Gonocoxite VIII located between enlarged sternite VII and tergite VIII (Fig. 5A, C). Gonapophysis located as small lobe ventrally between gonocoxites IX. Spermatheca approximate of equal thickness (Fig. 5B, D), spirally coiled, with two inner coils of medial area and two coils of distal area. Short fertilisation duct and fertilisation channel.

Colour. Head. Yellowish with a slightly reddish tinge that contrasts with yellow colour of prozona (Figs 1A,

C, 2B). Vertex with dark brown uneven transversal band on posterior margin, band spreads from crest of vertex symmetrically to both sides without reaching eyes. Mouthparts same colour as head, except of black tips of mandibles (Fig. 2A, C). Antennae yellowish with a slightly reddish tinge. **Prothorax.** Basic colour yellow. Prozona lighter than metazona (Fig. 1A, C). Dorsolateral, a black transversal band appears over maculae, pronatal groove and pronatal humps. Band comprised by laterally connected black spots over maculae and pronatal humps (Figs 1A, 2B, 3A). Spots on pronatal humps do not converge centrally (Fig. 2B). Female: Only hinted black marks on pronatal humps. Black spot over maculae as in male (Fig. 3B). Black spots over maculae and pronatal humps not connected laterally (Fig. 3B). **Meso- and metathorax.** Uniformly black. **Foreleg.** Coxa and separation ring black with small yellow area distally (Fig. 2C). Trochanter yellowish-brown with a red tinge. Ventral lower margin of femur light brown to yellowish. Tibia and tarsus light brown to yellowish. **Mid- and hindleg.** Coxae and trochanters black. Femora black, very

distal part brownish. Tibiae and tarsi reddish-brown with a small black spot dorsally in the proximal third. **Abdomen.** Basic colour black. Anterior area of second pleurite yellowish, tergites with pale marking medially on posterior margin (Fig. 1A), sternite VIII with orange-brown longitudinal stripe medially. Tergite X (ectroproct) reddish-brown. Female abdomen orange-brown (Fig. 1C). Tergite I black, tergite II black with posterior margin orange-brown, tergite III orange-brown with anterior margin black (Fig. 1C). Sternite I–III black, sternite IV–VI black with posterior margin orange-brown. **Fore-wing.** Brown anterior wing band, oblique brown band runs over 3M, not reaching posterior margin of wing (Fig. 1A). Oblique apical dark band at posterior wing margin, comprises branches from first and second proximal radial veins originating from *rarp3* (Fig. 1A). Central area of wing and 1CuA hyaline. Posterior margin of wing pale light brown. Pterostigma light yellow. Wing veining predominantly brown, veins of pterostigma and anterior radial cell II (*rarp2*), veins adjacent of *rarp2* and distal part of veins of *rarp1* yellow (Fig. 1A). Female with 3M reaching posterior wing margin (Fig. 1C). Oblique apical dark band at posterior wing margin, comprises branches from last three distal radial veins originating from *rarp2* and first and second proximal radial veins originating from *rarp3* (Fig. 1C). Posterior wing margin distinctly darker pigmented than in male. **Hind-wing.** Brown anterior wing band, hyaline median stripe and lower pale brownish margin. Pterostigma brown with proximal part of underlying subcosta yellow. Veins of *rarp2* slightly yellowish, remaining veins brown (Fig. 1A). Female with posterior wing margin distinctly darker pigmented than in male (Fig. 1C).

Discussion

Euclimacia is a small, but morphologically markedly diverse genus. Despite the considerable size of individual specimens, which can reach sometimes up to 3 cm body length and their striking colouration in many cases, the number of specimens in scientific collections is very limited. So far, there is still no accurate information about their behaviour and their habitats during the day and at night. *Euclimacia* often represent a by-catch that is caught by scientists specialised in other taxa during light trapping. However, there is no evidence that they are nocturnal. Specific light trapping for *Euclimacia* has, so far, resulted in low numbers of specimens. It can be assumed that, similar to the genus *Climaciella*, during the day, they eat pollen and nectar on flowering plants and prey on other insects (Boyden 1983). Presumably they also occur temporarily in higher tree levels.

Of the 33 species described so far, 30 were described on the basis of a single specimen. The remaining two species were described, based on two (*Euclimacia superba* Lambkin, 1987) and three (*Euclimacia nicobarica* Kaur, 2021) specimens. The series of eight specimens of the here newly-described species *Euclimacia radioquaesentis* sp. nov. is thus comparatively large.

Seven males and one female of *E. radioquaesentis* were examined. The availability of both sexes provides rare data on potential sexual dimorphism in this genus. Only the descriptions of *E. superba* and *E. nicobarica* are based on both sexes. In *E. nicobarica*, the colour pattern of the female is described as similar to the male, although the female is slightly smaller than the male. In *E. superba*, there are a few differences in the colour pattern and size. The colour differences occur in slightly different colour shades and a few markings. The head of the female is slightly paler and it possesses a transverse band across the antennae basis, which is absent in the male. The female possesses a large dark transverse band on tergite III, the male in the same location possesses a small black median mark. In the female, the ectoproct is black-brown with a brownish-yellow spot. The ectoproct of the male is dark orange-brown without any spot. Wings and other body parts have the same colour. The female is slightly larger than the male. The size depends to a certain extent on the larvae's food supply (size of the spider egg sac) and is, therefore, considered natural and not as a sexual trait (Lietzenmayer et al. 2022). In addition, Handschin's re-description of *Euclimacia morosa* was based on three non-type specimens of both sexes. Handschin described the female and the male as identical in colour (Handschin 1961).

In *E. radioquaesentis*, there are differences in colouration between females and males. One difference is the transversal band on the prothorax, which is present in both sexes, but reduced in the female. In the males, the pronatal hump is fully covered by a dark mark and this dark mark merges with the dark mark that covers the macula. The pronatal hump of the female has a very faint dark mark at the apex, which does not merge with the dark mark of the macula. In general, the prothorax of the female appears narrower and less wrinkled than of the male (Fig. 3). The pronatal humps are barely developed (Fig. 3B). Whether this is a sexual dimorphism or whether these differences are based on the smaller body size of the female cannot be finally clarified here.

Furthermore, the abdomen of the male is predominantly black with a few brownish markings. The abdomen of the female has a significantly higher amount of brown, so that, apart from the anterior two black segments, the abdomen appears predominantly brown. The predisposition for this brown colouration of the abdomen is also present in the males, as the brown markings on the tergites indicate. The wings also differ, although only slightly, in colouration. The wings of the female appear more contrasting. The area along the posterior wing margin is darker than in the male and the oblique band above 3M in the fore-wing reaches the posterior wing margin. As a result, the hyaline median stripe is enhanced, especially in the fore-wing (Fig. 1C). The most striking feature of the differently-coloured pterostigmata and the adjacent veining is identical.

Intraspecific variation in *Euclimacia* has also been recorded only occasionally. There are observations of intraspecific variations in *Euclimacia badia* Okamoto, 1910. Ohl (2004b) examined about 20 specimens from Taiwan, from where the type specimen was collected. The basic colour ranges from reddish-brown to almost black. Within the 20 specimens, there is a morphotype type with a predominantly reddish colour, another morphotype with a predominantly black colour and numerous intermediate stages. Variations within *E. radioquaesentis* are hardly recognisable. The differences are limited to slight variations in the yellowish shades, which may also be due to the drying process. Colouration can deviate from that of the living specimen due to the drying and ageing process. From observations of other specimens of *Euclimacia* of which the appearance in the dried and living state is known, it can be said that black colour patterns fade to dark brownish and yellow colouring appears less intense in the dried state, but rather goes into ochre or sand colour.

Furthermore, the individuals differ slightly in size. Variation also occurs in the wing venation. There are variations between specimens, but also asymmetry within the same specimen. The asymmetry of subcostal veinlets within the wings of one specimen seems to be the norm.

Intraspecific variability within this genus is still difficult to assess and, in an ongoing revision, as much material as possible from this genus will be investigated. The trend indicates that there are species with hardly any intraspecific variability, as in the example of *radioquaesentis* and species with clear intraspecific variability, as in *badia*. Adaptation to morphologically different mimicry models (i.e. aculeate wasps) in different regions may result in intraspecific variability.

The description of *E. radioquaesentis* was linked to a popular science event of the Museum für Naturkunde Berlin and 'Inforadio vom rbb', one of Berlin's local radio stations, in choosing the name for this species. Three more species from different taxa were also involved, the descriptions of two of which have already been published (a species of shrimp by Klotz et al. (2023); a staphylinid species by Frisch and Mainda (2022)). A species profile was broadcast by 'Inforadio' and listeners were asked to propose a scientific name (the species epithet). Amongst the suggestions submitted, the species name *E. radioquaesentis* was picked as being most suitable for species named by radio listeners. The goal of this radio event was to raise awareness of the high number of still undescribed species and to let interested citizens participate in taxonomic projects.

Acknowledgements

References

Ardila-Camacho A, Califre Martins C, Aspöck U, Contreras-Ramos A (2021) Comparative morphology of extant raptorial Mantispoidea (Neuroptera: Mantispidae, Rhachiberothidae) suggests a non-monophyletic Mantispidae and a single origin of the raptorial condition within the superfamily. Zootaxa 4992(1): 1–89. https://doi.org/10.11646/zootaxa.4992.1.1

Ardila-Camacho A, Winterton SL, Contreras-Ramos A (2023) The genus *Climaciella* Enderlein, 1910 (Neuroptera, Mantispidae) in French Guiana. ZooKeys 1153: 37–64. https://doi.org/10.3897/zookeys.1153.95960

Aspöck U, Aspöck H (2008) Phylogenetic relevance of the genital sclerites of Neuropterida (Insecta: Holometabola). Systematic Entomology 33(1): 97–127. https://doi.org/10.1111/j.1365-3113.2007.00396.x

Austin AD (1985) The function of spider egg sacs in relation to parasitoids and predators, with special reference to the australian fauna. Journal of Natural History 19(2): 359–376. https://doi.org/10.1080/00222938500770261

Banks N (1920) New neuropteroid insects. Bulletin of the Museum of Comparative Zoology 64(3): 297–362. https://doi.org/10.5962/bhl.title.28705

Boyden TC (1983) Mimicry, predation and potential pollination by the mantispid, *Climaciella brunnea* var. instabilis (Say) (Mantispidae: Neuroptera). Journal of the New York Entomological Society 91(4): 508–511.

Enderlein G (1910) Klassifikation der Mantispiden nach dem Material des Stettiner Zoologischen Museums. Stettiner Entomologische Zeitung 71(1): 341–379.

Esben-Petersen P (1917) Neue und wenig bekannte Mantispiden. Arkiv För Zoologi 11(10): 1–15. https://doi.org/10.5962/bhl.part.1498

Frisch J, Mainda T (2022) The *Scopaeus kokodanus* species group (Coleoptera: Staphylinidae: Paederinae) from New Guinea and the Solomon Islands, with description of three new species. Soil Organisms 94(3): 139–147. https://doi.org/10.25674/so94iss3id303

Gerstäcker A (1893) Ueber neue und weniger gekannte Neuropteren aus der Familie Megaloptera Burm. Mittheilungen aus dem naturwissenschaftlichen Vereine von Neu-Vorpommern und Rügen 25: 93–173.

Handschin E (1961) Beitrage zur Kenntnis der Gattungen Euclimacia, *Climaciella* und *Entanoneura* Enderlein 1910 im indo-australischen Faunengebiet. Nova Guinea, Zoology 15: 253–301.

Kaur S, Pandher MS, Chandra K, Dubey AK (2021) Subfamily Mantispinae Enderlein, 1910 (Insecta: Neuroptera) in India. Zootaxa 5068(3): 355–377. https://doi.org/10.11646/zootaxa.5068.3.2

Klotz W, von Rintelen T, Annawaty A, Wowor D, von Rintelen K (2023) *Caridina clandestina*, new species, an unusual new fresh-

water shrimp (Crustacea: Decapoda: Atyidae) from the remote high elevation Napu Valley of Sulawesi, Indonesia. Raffles Bulletin of Zoology 71: 12–25. https://doi.org/10.26107/RBZ-2023-0002

Lambkin K (1986a) A revision of the Australian Mantispidae (Insecta: Neuroptera) with a contribution to the classification of the family. I. General and Drepanicinae. Australian Journal of Zoology Supplementary Series 116: 1–142. https://doi.org/10.1071/AJZS116

Lambkin K (1986b) A revision of the Australian Mantispidae (Insecta: Neuroptera) with a contribution to the classification of the family. II.* Calomantispinae and Mantispinae. Australian Journal of Zoology (Supplementary Series) 117: 1–113. https://doi.org/10.1071/AJZS117

Lambkin KJ (1987) The Australian Mantispidae (Neuroptera): supplementary notes. General and Applied Entomology 19: 11–14.

Lietzenmayer LB, Goldstein LM, Pasche JM, Taylor LA (2022) Extreme natural size variation in both sexes of a sexually cannibalistic mantidfly. Royal Society Open Science 9(8): 220544. https://doi.org/10.1098/rsos.220544

MacLeod EG, Redborg KE (1982) Larval Platymantispine Mantispids (Neuroptera: Planipennia): Possibly a subfamiliy of generalist predators. Neuroptera International 2(1): 37–41.

Navás L (1914) Mantíspidos nuevos (Segunda [II] serie). Memorias de la Real Academia de Ciencias y Artes de Barcelona 11(3): 83–103.

Ohl M (2004a) A new wasp-mimicking species of the genus *Euclimacia* from Thailand. Denisia 13: 193–196.

Ohl M (2004b) Annotated catalog of the Mantispidae of the World (Neuroptera). Contributions on Entomology, International 5(3): 131–262.

Oswald JD, Machado RJP (2018) Biodiversity of the Neuropterida (Insecta: Neuroptera, Megaloptera, and Raphidioptera). In: Foottit RG (Ed.) Insect Biodiversity. John Wiley & Sons, Ltd, Chichester, UK, 627–672. https://doi.org/10.1002/9781118945582.ch21

Redborg KE (1998) Biology of the Mantispidae. Annual Review of Entomology 43: 175–194. https://doi.org/10.1146/annurev.ento.43.1.175

Snodgrass RE (1935) Principles of Insect Morphology. McGraw-Hill Book Company, New York, 768 pp. https://doi.org/10.2307/3223017

Snyman LP, Sole CL, Ohl M (2018) A revision of and keys to the genera of the Mantispinae of the Oriental and Palearctic regions (Neuroptera: Mantispidae). Zootaxa 4450(5): 501–549. https://doi.org/10.11646/zootaxa.4450.5.1

Snyman LP, Ohl M, Pirk CWW, Sole CL (2020) A review of the biology and biogeography of Mantispidae (Neuroptera). Insect Systematics & Evolution 52(2): 1–42. https://doi.org/10.1163/1876312X-bja10002

Soh Z, Ng Margus, F. C, Gan, Cheong W, Ohl M (2022) Biodiversity Record: Rediscovery of the mantisfly, *Euclimacia gerstaeckeri*, in Singapore and first record for Malaysia, with notes on putative models. Nature in Singapore 15: e2022032. https://doi.org/10.26107/NIS-2022-0032

Winterton SL, Lemmon AR, Gillung JP, Garzon IJ, Badano D, Bakkes DK, Breitkreuz LCV, Engel MS, Lemmon EM, Liu X, Machado RJP, Skevington JH, Oswald JD (2018) Evolution of lacewings and allied orders using anchored phylogenomics (Neuroptera, Megaloptera, Raphidioptera). Systematic Entomology 43(2): 330–354. https://doi.org/10.1111/syen.12278

PENSOFT.

MUSEUM FÜR
NATURKUNDE
BERLIN

Integrative taxonomic revision of the grasshopper genera *Parapetasia* Bolívar, 1884, and *Loveridgacris* Rehn, 1954 (Orthoptera, Pyrgomorphidae), with description of a new species of *Loveridgacris*

Jeanne Agrippine Yetchom Fondjo[1,2], Martin Husemann[2], Armand Richard Nzoko Fiemapong[3], Alain Didier Missoup[1], Martin Kenne[1], Maurice Tindo[1], Oliver Hawlitschek[4], Tarekegn Fite Duressa[2,5], Sheng-Quan Xu[6], Wenhui Zhu[6], Claudia Hemp[7]

1   *Zoology Unit, Laboratory of Biology and Physiology of Animal Organisms, Graduate School in Fundamental and Applied Sciences, University of Douala, Douala, Cameroon*

2   *Staatliches Museum für Naturkunde Karlsruhe, Karlsruhe, Germany*

3   *University of Neuchâtel, Neuchâtel, Switzerland*

4   *Department of Evolutionary Biology and Environmental Studies, Universität Zürich, Zürich, Switzerland*

5   *School of Plant Sciences, College of Agriculture and Environmental Sciences, Haramaya University, Dire Dawa, Ethiopia*

6   *College of Life Sciences, Shaanxi Normal University, Xi´an, China*

7   *Senckenberg Biodiversity and Climate Research Center, Frankfurt, Germany*

https://zoobank.org/8108C5B0-40C9-40CA-A38B-8805F173900D

Corresponding author: Jeanne Agrippine Yetchom Fondjo (jayetchomfondjo@gmail.com)

Abstract

The taxonomic status of the Pyrgomorphid genera *Parapetasia* Bolívar, 1884, and *Loveridgacris* Rehn, 1954 is complex and challenging. Here, we use a combination of morphological, distributional, and genetic data to revise the two genera and provide new information on their diversity. We describe a new species, *Loveridgacris tectiferus* **sp. nov.**, from Tanzania and formally resurrect the status of *Parapetasia rammei* as a valid species within *Parapetasia*, resulting in two species in *Parapetasia* (*P. femorata* and *P. rammei*) and two in *Loveridgacris* (*L. impotens* and *L. tectiferus* **sp. nov.**). We also sequenced the COI and 16S genes of 10 Pyrgomorphidae species and provided the first phylogeny of the group. Our data show that all species are clearly distinct and represent molecular operational taxonomic units (mOTUs), with the exceptions of *L. impotens* and *L. tectiferus* **sp. nov.**, which are morphologically clearly distinct but for which the concatenated sequence alignments of the two individual gene datasets (COI and 16S) do not provide sufficient information. In addition, high interspecific distances were found between *Parapetasia* and *Loveridgacris*. Moreover, the complete mitogenomes of *L. impotens* and *L. tectiferus* **sp. nov.** were sequenced using next-generation sequencing technology. The total lengths of the assembled mitogenomes were 15,592 bp and 15,737 bp, representing 13 protein-coding genes, 22 transfer RNA genes, two ribosomal RNA genes and one D-loop region, respectively. To aid in identification, we present a key for the two genera, including a key to species. This study provides insights into the morphology, distribution, and phylogeny of Pyrgomorphidae in Africa.

Key Words

Introduction

The family Pyrgomorphidae, which has the type genus *Pyrgomorpha* Seville, 1838, is easily identifiable due to its unique phallic complex, which is relatively uniform within the family, as described by Dirsh in 1961. Members of this family are commonly referred to as gaudy grasshoppers and are renowned for their strikingly vivid coloration, which serves as a warning to predators. Pyrgomorphidae can sequester and accumulate plant secondary compounds, such as cardiac glycosides, from the toxic plants on which they feed. This accumulation leads to many species displaying aposematism, signaling their toxicity through conspicuous coloration. The Pyrgomorphidae family is the only member of the superfamily Pyrgomorphoidea and is closely related to the superfamily Acridoidea (Song et al. 2015). The presence of a groove in the fastigium and distinctive male phallic structures, including the cingulum that extends around the ventral side, medially directed endophallic apodemes, an ejaculatory sac that opens to the genital chamber, and undivided valves of the penis, differentiate the Pyrgomorphidae from other families, as noted by Kevan and Akbar (1964) and Dirsh (1961). Eades (2000) also described an ejaculatory sac opening to the genital chamber as a distinguishing characteristic.

The Pyrgomorphidae include 31 tribes, 149 genera, and 487 species (Mariño-Pérez and Song 2018) and are globally distributed. Most species of Pyrgomorphidae occur in tropical and subtropical countries of Africa, Asia, and Australia (Kevan and Akbar 1964; Mariño-Pérez and Song 2018). The tribe Dictyophorini, which includes only five genera with a small number of species each, namely, *Dictyophorus* Thunberg, 1815; *Maura* Stål, 1873; *Camoensia* Bolívar, 1882; *Parapetasia* Bolívar, 1884; and *Loveridgacris* Rehn, 1954, is distributed in Africa south of the Sahara (Kevan et al. 1974). The classification of the genera *Parapetasia* and *Loveridgacris*, as well as the species included in them, is complex. *Parapetasia* was first established by Bolívar in 1884 with *Parapetasia femorata* Bolívar, 1884, as the type by monotypy. *Loveridgacris* was first described by Karsch in 1888, with *Petasia impotens* Karsch, 1888, as the type that was later transferred to *Parapetasia* (Bolívar, 1904). Many researchers followed this classification and referred to *Petasia impotens* as *Parapetasia*. *Parapetasia rammei* Sjöstedt, 1923, the second species of *Parapetasia*, was described approximately 40 years later. Rehn (1953) conducted a partial revision of the genus *Parapetasia* in 1953 and separated the genus into two subgeneric entities based on the morphology of the pronotum and the size of the tegmina: *Parapetasia* (s.str) and *Loveridgea* (designated as a new subgenus). Rehn also distinguished two species within the subgenus *Parapetasia* (*Parapetasia*) based on female morphological features: the type species *Parapetasia femorata* and the newly described *Parapetasia calabarica* Rehn, 1953. In the subgenus *Loveridgea*, Rehn included two species, *P.* (*L.*) *impotens* and *P.* (*L.*) *ulugurensis*. Additionally, Rehn (1953) placed *P. rammei* Sjöstedt, 1923, in the subgenus *Parapetasia* (*Loveridgea*). Shortly

thereafter, Rehn (1954) elevated the subgenus *Parapetasia* (*Loveridgea*) Rehn to *Loveridgacris* Rehn. Dirsh (1956), Johnston (1956), and Kevan (1962) maintained *P. rammei* in the subgenus *Loveridgacris* until Akbar and Kevan (1964) later raised the subgenus *Parapetasia* (*Loveridgacris*) to the generic status of *Loveridgacris* on the basis of phallic structures, with *L. impotens* and *L. ulugurensis* as the two species of this genus. Dirsh (1965), in his work on the genus *Parapetasia*, included five species distributed in Central, East, and West African forests, based on Rehn's descriptions: *Parapetasia femorata*, which was recorded in the lowlands of West African forest areas of the less elevated parts of Cameroon (Rehn 1953); *Parapetasia calabarica*, known only from southern Nigeria (Rehn 1953); *Parapetasia impotens* from Tanzania and southeastern Kenya; *Parapetasia ulugurensis* Rehn, 1953 from the Uluguru Mountains of Tanzania; and *P. rammei*, which was restricted to the more elevated areas of Cameroon. Shortly thereafter, Kevan et al. (1974) identified *L. ulugurensis* as a synonym of *L. impotens* and regarded *P. calabarica* and *P. rammei* as "almost undoubtedly mere forms of *P. femorata*." Later, Kevan (1977) effectively designated *P. calabarica* and *P. rammei* as true synonyms of *P. femorata*, with *P. calabarica* being the micropterous form and *P. rammei* being the brachypterous form. Mestre and Chiffaud (2009), based on Kevan's (1977) analysis, concluded that the genus *Parapetasia* is a monotypic Afrotropical genus.

The taxonomic status of species belonging to the genera *Parapetasia* and *Loveridgacris* remains challenging despite Kevan's (1977) attempt to synonymize some of the species. Some researchers, including Hochkirch (1998) and Seino and Njoya (2018), still consider certain species, such as *L. impotens*, *L. ulugurensis*, *P. femorata*, and *P. rammei*, to be distinct. Additionally, *P. rammei* shares many similarities with *L. impotens* in terms of morphology, coloration, and ecological preference, making it difficult to clearly differentiate between the two genera. To resolve this taxonomic confusion, molecular data may be useful. While some studies have generated DNA sequence data for *P. femorata*, none have focused on all species of these genera. Thus, we have conducted a comprehensive revision of the genera *Parapetasia* and *Loveridgacris* using an integrative approach that combines morphological studies, particularly of the phallic complex, with molecular analysis. Our study includes the description of a new *Loveridgacris* species and proposes a key to distinguishing valid species in both genera.

Materials and methods

Materials

Field collections and observations were made between 2020 and 2022 at five localities in three regions of Cameroon: Bekob and Iboti (Ebo forest in the littoral region), Manengouba Mountain (littoral region), Fotouni in the western highlands of Cameroon, and Somalomo in the Dja

Biosphere Reserve (eastern region). Furthermore, additional field trips were made at several locations in Tanzania. Individuals were collected by sight and hand using a sweep net. The collected specimens were deposited in the collections of the Karlsruhe Natural History Museum (SMNK) and the private collection of Claudia Hemp (CCH). In addition, some historical specimens belonging to the following collections have also been examined: the Hamburg Zoological Museum, Germany (ZMH), and the Museum für Naturkunde Berlin, Germany (MfN). Paratypes of *P. rammei* deposited at MfN Berlin and erroneously labeled as type (male) and allotype (female) were also examined.

Depositories

MfN: Museum für Naturkunde, Leibniz-Institut für Evolutions- und Biodiversitätsforschung, Berlin, Germany; **SMNK:** Staatliches Museum für Naturkunde Karlsruhe, Karlsruhe, Germany; **ZMH:** Zoologisches Museum Hamburg, Leibniz-Institut für Analyse des Biodiversitätwandels, Hamburg, Germany; **CCH:** Collection of Claudia Hemp.

Morphological analysis

Observations of external and internal morphological features were made with a Leica M165 C binocular microscope. Photographs of whole specimens were made with a high-resolution DUN Inc. stacking system (DUN Inc., California, USA).

Measurements were obtained using a digital caliper (at a scale of 0.01 mm). All measurements are given in millimeters (mm). For all measurements, males and females were measured separately. For each species, the following characters were examined: **HeadL:** length of head; **HeadW:** width of head; **AntenL:** length of antenna; **I.O.D.:** interocular distance; **FastigL:** length of fastigium of vertex; **PronotL:** pronotum length; **PronotW:** pronotum width; **TegL:** length of tegmina; **TL:** hind tibia length; **FL:** hind femur length; **fW:** hind femur width; and **BodyL:** body length, measured from the tip of the frons to the hindmost tip of the abdomen. The measurements of the specimens correspond to the average value of the different body parts plus the standard deviation (SD) of all newly collected samples, as well as all historical samples held by the ZMH and MfN (Germany).

Dissections and preparations of male and female genitalia followed the standard methods of Kevan et al. (1969) and Martinelli et al. (2017). The extracted internal genitalia were placed in a 1.5 mL microcentrifuge tube containing a solution of 5 µL proteinase K (20 mg/mL) and 25 µL buffer (pH 8.0, 10 mM Tris-Cl, 25 mM EDTA, 100 mM NaCl, 0.5% SDS) and were kept overnight in an incubator at 55 °C. The genitalia were gently separated from the digestion solution and then kept at 95 °C for 10 minutes to inactivate the enzyme. Preparations were then washed with double-distilled water (ddH$_2$O). Photographs of male and female genitalia were obtained with a Keyence VHX-7000 digital microscope (Clustermarket London, United Kingdom). The terminology for male genitalia and female spermatheca followed Dirsh (1956, 1957, 1970), Kevan et al. (1974), and Rowell (2013).

Distribution of species

Distributional data were obtained from geographical coordinates recorded during field observations, from locality records taken from specimen labels in different collections of museums, and from records available in the literature. A distribution map of the species was made using QGIS 3.28.3 "Firenze" (2023).

DNA extraction, PCR amplification, sequencing, and data depository

DNA was extracted from the femoral muscle tissue of 24 specimens stored in 96% ethanol. The species considered in this study are large; hence, only fragments of femoral muscles were used for DNA extraction at the Museum der Natur Hamburg. A high-salt extraction method was used (Paxton et al. 1996). The primer pair LCO and HCO (Folmer et al. 1994) was used for amplification of the COI gene, while the primer pair 16S-F and 16S-R (Palumbi et al. 1991) was used to amplify the 16S markers. The thermocycling conditions consisted of an initial denaturation at 94 °C (3 min), 35 cycles at 94 °C (denaturation, 30 s), 50 °C (annealing, 45 s), 72 °C (extension, 1 min), and a final extension at 72 °C (10 min). Samples were run on a 1% agarose gel stained with GelRed (Biotium, Remont, CA, USA) to test for amplification. Successfully amplified samples were purified with an ExoSap Enyzme cocktail (VWR, Pennsylvania, USA). The purified PCR products were then sequenced in both directions by Macrogen Europe (Amsterdam, Netherlands).

Phylogenetic analyses

Sequences were aligned and checked in GENEIOUS PRO (Kearse et al. 2012) using the MUSCLE algorithm (Edgar 2004). The aligned sequences included each one sequence of *Parapetasia femorata* (MT011522) and *Zonocerus elegans* (MT011544), which were downloaded from GenBank. We checked for pseudogenes (Numts) by translating sequences into amino acids using the invertebrate mitochondrial code and checking for frame shifts. Furthermore, the National Center for Biotechnology Information (NCBI) Blast and BOLD databases were used to check for species identity (a few related taxa are available in the databases). We used MRBAYES 3.2 (Ronquist et al. 2012) to reconstruct the phylogeny. For this, we used the reversible jump model. *Zonocerus elegans* was defined

as the outgroup. Analyses were run for 1 million generations, sampling every 100 generations for a total of 10 000 trees. The first 25% of the samples were discarded as burn-in. The average split frequencies were less than 0.01, indicating convergence of the analyses. The final tree was visualized with FIGTREE v.1.4.2 (Rambaut 2010). The net evolutionary divergence between groups of sequences was estimated using MEGA11 (Tamura et al. 2021).

Complete mitochondrial genome assembly, annotation, and analysis

For *L. impotens* and *L. tectiferus*, for which the phylogeny was not resolved when using only COI, the complete mitochondrial genome was sequenced by Novogene, China. Thereafter, the sequences were checked and assembled using MitoZ (Meng et al. 2019). All mitochondrial genes were further adjusted and corrected using GENEIOUS 10.1.3 (Kearse et al. 2012) with the reference mitogenome of *Oxya sinensis* (Thunberg, 1815). The base composition, codon distribution, and length of the protein-coding genes were calculated in Geneious Prime 2023.1.2 (Kearse et al. 2012). Nucleotide compositional differences (composition skew) were measured using the formula $(A - T)/(A + T)$ for AT skew and $(G - C)/(G + C)$ for GC skew (Perna & Kocher, 1995). The genetic distances for different PCGs among the two *Loveridgacris* species were estimated using MEGA 11 (Tamura et al. 2021).

Results

Taxonomy

Key to *Parapetasia* Bolívar and *Loveridgacris* Rehn

The genus *Parapetasia* can be easily distinguished from the genus *Loveridgacris* by several characters:

1 (2) Fastigium of vertex triangular; eyes small, hemispherical, prominent; pronotal disc sellate; posterior part of metazona raised, swollen, with median margin slightly or strongly emarginate (Fig. 2A, B, G, H); hind femora upper-median margin distinctly raised; elytra shortened, or, if brachypterous, slightly reticulated; male subgenital plate with slightly incised and parallel margins (Fig. 2E); epiphallic bridge narrow; appendices subparallel; ectophallus short; ventral process of cingulum broadly triangular (Fig. 6A, B, D, E, G, H, J, K) ....*Parapetasia* Bolívar, 1884 (West and Central Africa)

2 (1) Fastigium of vertex rounded; eyes of moderate size, oval, not prominent; pronotal disc not sellate; posterior part of metazona not notably raised nor swollen, its median margin not emarginate (Fig. 2C, F, I); hind femora upper-median margin flat, not raised; elytra brachypterous, strongly reticulated; male subgenital plate with fused margins (Fig. 5A, B); epiphallic bridge wide or broad; appendices divergent; ectophallus elongate; ventral process of cingulum subtriangular (Fig. 6C, F, I, L)... *Loveridgacris* Rehn, 1954 (East Africa)

Genus *Parapetasia* Bolívar, 1884

Parapetasia Bolívar, 1884 (type species: *Parapetasia femorata* Bolívar, 1884b, by monotypy).
Parapetasia (*Parapetasia*) Rehn, 1953
Parapetasia (*Loveridgea*) Rehn, 1953
Parapetasia (*Loveridgacris*) Rehn, 1954

Diagnosis of the genus *Parapetasia* Bolívar. Fastigium of vertex triangular; tegmina vestigial, or if brachypterous, strongly reticulated; the eyes small, hemispherical, and prominent; posterior part of metazona raised, swollen, with median margin slightly or strongly emarginate; hind femora upper-median margin distinctly raised; male subgenital plate with slightly incised and parallel margins; epiphallic bridge narrow; appendices subparallel; ectophallus short; ventral process of cingulum broadly triangular.

Differential diagnoses for species of *Parapetasia*. *Parapetasia femorata* can be easily distinguished from *Parapetasia rammei* by the following characters: tegmina dark brown, strongly reduced, vestigial, (yellow–brown with brown veins, shortened or brachypterous, semilobed

in *P. rammei*); first and/or second abdominal segments with a lateral black band behind the insertion points of the femora (absent in *P. rammei*); anterior projections of epiphallus large (small in *P. rammei*); lateral plates subparallel (oblique or divergent in *P. rammei*); lophi large, strongly curved (very small, slightly curved in *P. rammei*); suprazygomal plate widely rounded (U-shaped in *P. rammei*); apodemal lobes only slightly produced ventrally (strongly produced ventrally in *P. rammei*); basal emargination of cingulum shallow (very deep in *P. rammei*); endophallic apodemes short (strongly elongate or slender in *P. rammei*).

Parapetasia femorata Bolívar, 1884
Figs 1A, B, 2A, D, G, 6A, D, G, J, 7A, D, G

Holotype. GABON • ♀; 6687; Natural History Museum Vienna, Austria.

Synonyms. *Parapetasia* (*Parapetasia*) *calabarica* Rehn, 1953: 121, 122–124, pl. 2: f. 17, pl. 3: f. 26. Kevan et al. (1974): 229; Kevan (1977): 318 (new synonym).

Figure 1. Habitus images of *Parapetasia* and *Loveridgacris* species. **A.** *P. femorata* nymph; **B.** *P. rammei* nymph; **C.** *P. femorata* adult; **D.** *P. rammei* adult; **E.** *L. impotens* nymph; **F.** *L. impotens* adult (the black arrow points at the yellowish foamy secretion on the abdominal segment).

Parapetasia rammei Sjöstedt, 1923, p. 10–11, pl. 1: f. 1, 2. Kevan et al. (1974): 229; Kevan (1977): 318 (new synonym).

Material examined. CAMEROON • 1 male, 1 female; Iboti in the Ebo Forest; 4.450°N, 10.450°E; 736 m; 07 Jan. 2022; J.A. Yetchom Fondjo leg. and A.R. Nzoko leg.; SMNK; CMJ244. • 1 female; Iboti in the Ebo Forest; 4.450°N, 10.450°E; 736 m; 07 Jan. 2022; J.A. Yetchom Fondjo leg.; SMNK; CMJ245. • 1 female; Somalomo in the Dja Biosphere Reserve; 3.371°N, 12.733°E; 06 Jun. 2022; A.R. Nzoko leg.; SMNK; CMJ1439. • 1 male; Bekob in the Ebo Forest; 4.350°N, 10.420°E; 936 m; 20 Mar. 2021; J.A. Yetchom Fondjo leg.; SMNK; CMJ598. • 6 females; Mukondje Farm, Mundame-Mungo Fluss; 25 Nov. 1904; R. Rohde leg.; ZMH. • 1 male, 4 females and 1 nymph; Esosung, Bakossi-Gebirge; 10 Sep. 1909; C. Räthke leg.; ZMH. • 3 males, 4 females, 4 nymphs; Esosung, Bakossi-Gebirge; 01 Nov. 1912; R. Rohde leg.; ZMH. • 1 male; Esosung, Bakossi-Gebirge; 1913; ZMH. • 2 females; Esosung, Bakossi-Gebirge; 1930; O. Kröber leg.; ZMH. • 3 males; Buea, south-West; 1891; S. Preuss leg.; MfN. • 1 male, 3 females; South; 1891; S. Preuss leg.; MfN. • 1 male, 1 female; Station Jaunde [Yaoundé], Centre; Mar. 1997; V. Carnap S.G. leg.; MfN. • 1 male, 1 female; Dibongo of Sanaga, Littoral; Ld. Kam leg.; MfN. • 1 male, 1 female; Lolodorf, South; L. Conradt S. leg.; MfN. • 1 female; Victoria [Limbe], south-West; S. Preuss leg.; MfN. • 1 female; Barombi station, south-West; Preuss S. leg.; MfN. • 1 male; Duala [Douala], Littoral; Dr Schäfer leg.; MfN. • 1 female; Nlobe-Ndunge; 500–700 m from Edea-Douala, Littoral; Dr Schäfer leg.; MfN. • 1 female; Longi; Jun. 1904; MfN. • 1 nymph; Japoma, Littoral; Dr Schäfer leg.; MfN. • 1 nymph; Victoria [Limbé], south-West; Jan. 1898–1899; MfN. • 2 females; north
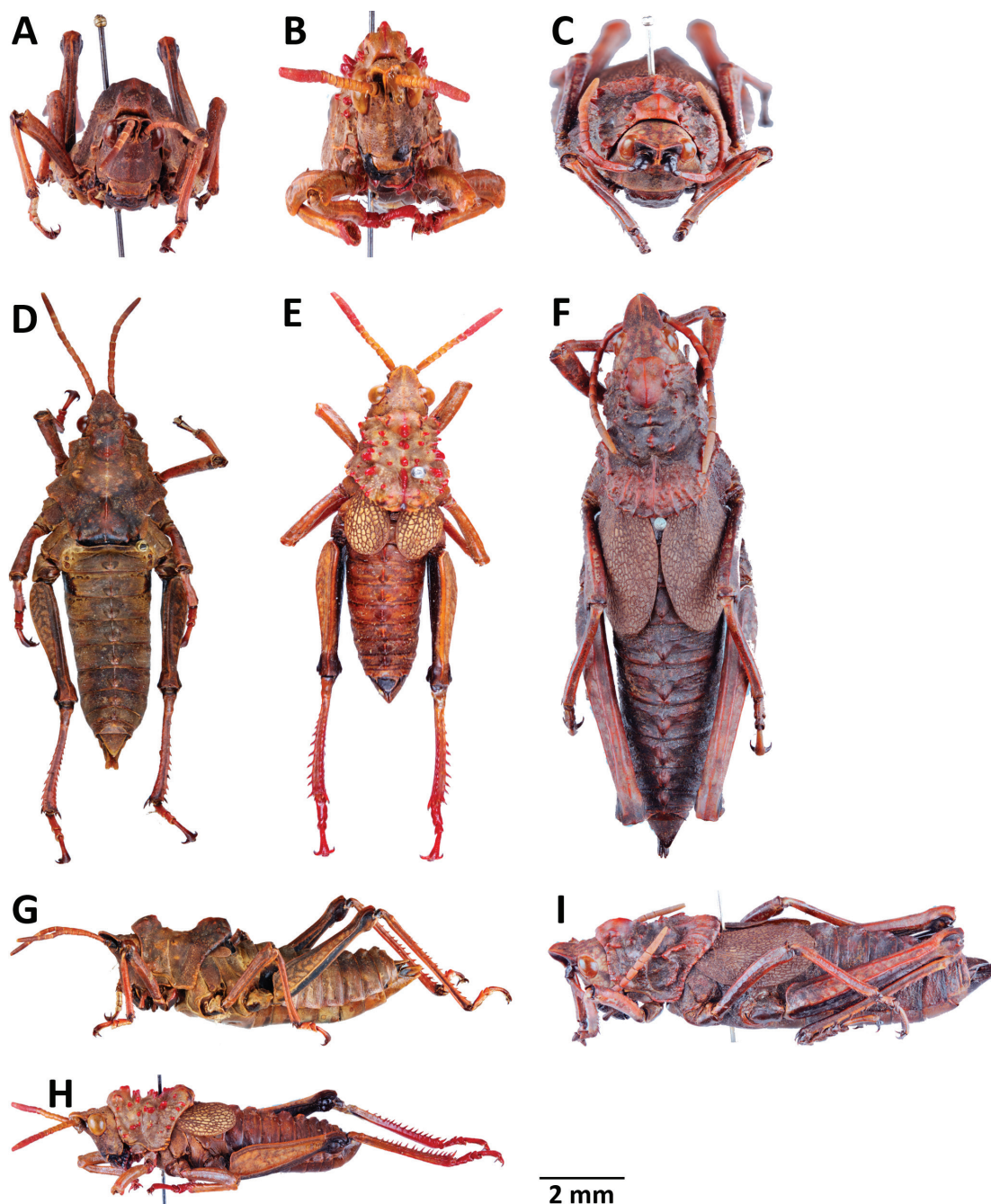
Figure 2. Frontal, dorsal and lateral views. **A–C.** Frontal view; **A.** *P. femorata*; **B.** *P. rammei*; **C.** *L. impotens*; **D–F.** Dorsal view; **D.** *P. femorata*; **E.** *P. rammei*; **F.** *L. impotens*; **G–I.** Lateral view; **G.** *P. femorata*; **H.** *P. rammei*; **I.** *L. impotens*.

Mundame, Elephantensee; 21 Jan.–15 Feb. 1996; S. Conradt leg.; MfN. • 1 female; Buea, south-West; MfN. • 1 female; Mundame; 1896; MfN. • 2 males; Bissika, Span. Guinea; Dr Escherich leg.; MfN.

Redescription. Male. *Body*: robust, depressed, with very finely or moderately rugose and tuberculated integument. ***Head*** (Figs 1A, 2A, D, G): acutely conical; fastigium of vertex slightly curved upwards, flat, slightly concave in basal part, distinctly triangular, narrowing toward apex (Fig. 2D); frontal carina hardly visible; antennae thick, shorter, or only slightly longer than head and pronotum together, with short transverse or subtransverse segments, the last apical segment being distinctly longer than others. ***Thorax*** (Fig. 2D, G): pronotum with large inflation in front of first sulcus, strongly tuberculated in anterior part of prozona and posterior part of metazona, with the posterior part of the prozona and anterior part of the metazona being very finely tuberculated; median carinae inconspicuous and interrupted, lateral carinae absent; inferior margins of lateral lobes of pronotum straight; prozona shorter than metazona; posterior margin of metazona strongly emarginate; prosternal process very short, subacute or obtuse-angular; mesosternal interspace wider than long. ***Legs*** (Fig. 2D, G): hind femur slender, its external area not expanded, its upper-median margin distinctly
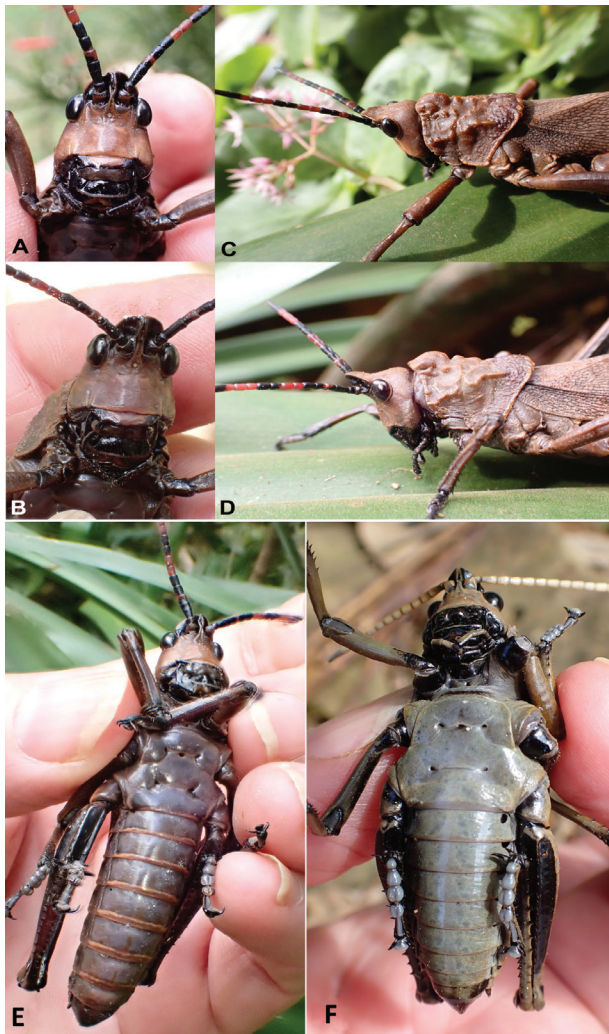
Dtsch. Entomol. Z. 71 (2) 2024, 265–287

271

Figure 3. A–E. *L. tectiferus* sp. nov. **A.** Male in frontal view; **B.** Female in frontal view; **C.** Male head and pronotum; **D.** Female head and pronotum; **E.** Male in ventral view; **F.** Male of *L. impotens* in ventral view.

raised; obliquely expanded area at the base of hind femur strongly pronounced; external apical spine of hind tibiae present; hind tarsal segments not elongate. *Elytra* (Fig. 2G): strongly reduced, micropterous, not reaching point of insertion of metathoracic legs, with rounded posterior margins. *Abdomen* (Fig. 2D): often annulated; abdominal tergites each with a trigonal medio-dorsal tubercle; male supra-anal plate subtriangular; male subgenital plate compressed toward apex above, margins slightly incised, parallel; male cerci conical (Fig. 7A). *Epiphallus* (Fig. 6A): bridge narrow, its anterior margin emarginate; anterior projections large, fairly prominent, not broadly rounded; appendices broad, subparallel, with apical lobes having smaller and broader processes, attached marginally to the basal part of the lateral plates; lateral plates subparallel, almost straight, directed posteriorly, with external margins not expanded; lophi large, strongly curved upward, anteriorly directed with acute apex. *Ectophallus* (Fig. 6D, G, J): central membrane fairly narrow, rather triangular or subtriangular, marked

at its lateral margins by furrows; zygoma broadly transverse, not extending halfway along the cingulum; suprazygomal plate widely rounded, moderately wide, highly shorter than the zygoma; apodemal lobes only slightly produced ventrally, the apices fairly wide apart; valves of cingulum small, narrow, and divergent in dorsal view; rami of cingulum rather broad in dorsal view, extending into sheath; dorsal cleft of cingulum rather narrow, ventral cleft small; suprarami well developed; basal emargination of cingulum shallow; sheats rather well developed; ventral process of cingulum short, not reaching the apex of endophallic apodemes nor the basal thickening of cingulum in ventral view. *Endophallus* (Fig. 6D, G, J): endophallic apodemes broad or stout, rather short, not reaching the basal emargination of cingulum in ventral; aedeagal valves narrow, slender with button-like apices; aedeagal sclerites stout and shorter, ventrally directed; spermatophore sac small, ovoid, not extending beyond the lateral limits of endophallic apodemes; gonopore at the middle.

Female. As in male, but larger. *Abdomen* (Fig. 7D): subgenital plate in female without carina or keel, its posterior margin rounded and smooth; egg guide prominent, conical, and slightly elongated; ovipositor valves large, not sinuate. *Genitalia* (Fig. 7G): spermatheca thick, lacking an apical pocket, with a laminated appearance in the apical part; median longitudinal groove of genital chamber reduced; spermatheca duct short, with an elongate, terminally thickened region; secondary diverticulum of spermathecal appendage of varying shape.

Color. Predominantly brownish, sometimes with orange or red markings; eyes entirely black in adults; antennal scape black; head brownish, margin of vertex, antennae light brown or dark brown in some parts in adults; sternum light brown and black in some parts; dorsal part of mesothorax with a broad black band bordered laterally by the elytra; elytra dark brown; first and/or second abdominal segments with a lateral black band behind the insertion points of the femora; lower external, lower internal, and medial internal hind femoral areas blackish; fore and middle femora, outer-medial, upper-external and upper-internal areas of hind femora dark-brown; hind tibiae light brown; tarsi light brown; cerci black.

Nymph (Fig. 1A). Eyes dark-red; antennae predominantly black with yellow apex; hind knee predominantly yellow with black median mark.

Measurements. Male. Body length 37.80–40.45 mm; Female. Body length 45.98–62.69 mm. Adult *P. femorata* individuals exhibit very large size variations in both sexes. Additional information on the measurements is given in Table 1.

Geographical distribution (Fig. 8). *Parapetasia femorata* has been recorded from Gabon, Cameroon, Nigeria, and Equatorial Guinea. In Cameroon, *P. femorata* was discovered in two localities within the proposed Ebo Forest, namely, Bekob and Iboti, as well as in Somalomo, a location within the Dja Biosphere Reserve, and Ngoutadjap and Zamakoe.

Table 1. Measurements in millimeters (mm) of the examined *Parapetasia* and *Loveridgacris* species; n: number of individuals; FastigL: length of fastigium of vertex; PronotL: pronotum length; PronotW: pronotum width; TegL: length of wings; TL: hind tibia length; FL: hind femur length; Fw: hind femur width; and BodyL: body length, measured from the tip of the frons to the hindmost tip of the abdomen.

Species	*Parapetasia femorata* Bolívar, 1884				*Parapetasia rammei* Sjöstedt, 1923			
Parameters	Male		Female		Male		Female	
	(Mean ± SD)	(Range)	(Mean ± SD)	(Range)	(Mean ± SD)	(Range)	(Mean ± SD)	(Range)
HeadL	6.06 ± 0.43 (n = 5)	5.69–6.54	7.30 ± 0.98 (n = 15)	5.50–9.11	5.18 ± 0.32 (n = 2)	4.95–5.40	6.23 ± 0.57 (n = 7)	5.32–6.81
HeadW	5.03 ± 0.42 (n = 5)	4.53–5.58	6.22 ± 0.31 (n = 15)	5.53–6.61	4.51 ± 0.05 (n = 2)	4.47–4.54	5.33 ± 0.31 (n = 7)	5.09–5.96
AntenL	14.99 ± 1.33 (n = 5)	13.13–16.49	16.68 ± 1.56 (n = 15)	12.84–18.61	11.65 ± 0.53 (n = 2)	11.27–12.02	13.85 ± 0.61 (n = 7)	13.00–14.52
I.O.D.	2.69 ± 0.14 (n = 5)	2.51–2.82	3.34 ± 0.17 (n = 15)	3.06–3.63	2.77 ± 0.02 (n = 2)	7.75–2.78	3.30 ± 0.17 (n = 7)	3.15–3.66
FastigL	2.24 ± 0.27 (n = 5)	1.83–2.54	3.02 ± 0.39 (n = 15)	2.46–3.80	1.88 ± 0.01 (n = 2)	1.87–1.89	2.78 ± 0.30 (n = 7)	2.41–3.04
PronotL	10.94 ± 0.73 (n = 5)	10.08–11.64	13.84 ± 0.92 (n = 15)	12.41–15.37	10.37 ± 0.11 (n = 2)	10.29–10.44	13.50 ± 0.77 (n = 7)	12.63–14.64
PronotW	9.59 ± 0.58 (n = 5)	8.73–10.25	12.81 ± 0.79 (n = 15)	11.41–14.22	0.81 ± 0.59 (n = 2)	8.39–9.23	11.28 ± 0.61 (n = 7)	10.26–12.11
TegL	2.71 ± 0.82 (n = 5)	1.96–3.86	4.14 ± 0.89 (n = 15)	2.53–5.48	10.29 ± 0.76 (n = 2)	9.75–10.83	15.03 ± 1.11 (n = 7)	13.15–16.60
TL	16.01 ± 0.87 (n = 5)	15.15–17.27	19.69 ± 1.26 (n = 15)	17.10–21.26	13.07 ± 0.83 (n = 2)	12.48–13.65	17.23 ± 0.81 (n = 7)	15.86–18.04
FL	17.62 ± 1.04 (n = 5)	16.47–19.12	21.89 ± 1.31 (n = 15)	19.15–23.47	15.10 ± 0.21 (n = 2)	14.95–15.25	19.64 ± 0.58 (n = 7)	18.83–20.31
FW	3.65 ± 0.07 (n = 5)	3.55–3.71	4.47 ± 0.37 (n = 15)	3.77–5.08	3.55 ± 0.27 (n = 2)	3.36–3.74	4.17 ± 0.21 (n = 7)	3.87–4.49
BodyL	38.60 ± 1.06 (n = 5)	37.80–40.45	54.00 ± 5.06 (n = 15)	45.98–62.69	31.10 ± 1.80 (n = 2)	32.83–35.37	45.75 ± 2.40 (n = 7)	43.22–49.73
Species	*Loveridgacris impotens* (Karsch, 1888)				*Loveridgacris tectiferus* Hemp sp. nov.			
Parameters	Male		Female		Male		Female	
	(Mean ± SD)	(Range)	(Mean ± SD)	(Range)	(Mean ± SD)	(Range)	(Mean ± SD)	(Range)
HeadL	8.32 ± 0.42 (n = 2)	8.02–8.62	8.63 ± 0.48 (n = 4)	8.19–9.12	7.41 (n = 1)	NA	6.87 ± 0.60 (n = 2)	6.44–7.29
HeadW	7.11 ± 1.09 (n = 2)	6.34–7.88	7.10 ± 0.47 (n = 4)	6.40–7.41	8.95 (n = 1)	NA	9.18 ± 0.53 (n = 2)	9.55–8.81
AntenL	19.41 ± 3.13 (n = 2)	17.19–21.62	20.42 ± 1.21 (n = 4)	19.21–22.10	21.30 (n = 1)	NA	19 ± 00 (n = 2)	19.00–19.00
I.O.D.	3.55 ± 0.17 (n = 2)	3.43–3.67	4.17 ± 0.22 (n = 4)	3.99–4.49	4.10 (n = 1)	NA	4.20 ± 0.14 (n = 2)	4.10–4.30
FastigL	3.67 ± 0.34 (n = 2)	3.43–3.91	3.89 ± 0.30 (n = 4)	3.46–4.15	3.50 (n = 1)	NA	3.05 ± 0.07 (n = 2)	3.00–3.10
PronotL	16.05 ± 1.44 (n = 2)	15.03–17.06	16.41 ± 1.75 (n = 4)	14.54–18.70	13.6 (n = 1)	NA	21.60 ± 0.14 (n = 2)	21.50–21.70
PronotW	13.39 ± 1.22 (n = 2)	12.52–14.25	13.53 ± 1.34 (n = 4)	11.89–15.11	9.30 (n = 1)	NA	9.50 ± 00 (n = 2)	9.50–9.50
TegL	14.96 ± 2.02 (n = 2)	13.53–16.38	17.88 ± 1.54 (n = 4)	16.59–19.80	29.00 (n = 1)	NA	27.70 ± 0.71 (n = 2)	27.20–28.20
TL	21.62 ± 1.11 (n = 2)	20.83–22.40	24.20 ± 1.12 (n = 4)	22.99–25.69	20.67 (n = 1)	NA	23.19 ± 00 (n = 2)	23.19–23.19
FL	24.12 ± 0.69 (n = 2)	23.63–24.60	27.29 ± 0.75 (n = 4)	26.19–27.85	25.00 (n = 1)	NA	24.25 ± 0.49 (n = 2)	23.90–24.60
FW	4.25 ± 0.22 (n = 2)	4.09–4.40	4.82 ± 0.34 (n = 4)	4.40–5.11	3.44 (n = 1)	NA	4.65 ± 0.21 (n = 2)	4.80–4.50
BodyL	55.54 ± 6.58 (n = 2)	50.88–60.19	58.66 ± 6.77 (n = 4)	48.72–63.69	51.20 (n = 1)	NA	50.65 ± 4.17 (n = 2)	47.70–53.60

The measurements represent the average value of the different body parts plus the standard deviation (SD). The range reffers to the minimum and maximum values.

Ecology. *Parapetasia femorata* is distributed throughout the lowlands of West and Central Africa and is exclusively found in forest habitats with a closed canopy and close proximity to marshy areas, where litter is abundant. Within forest habitats, the species is geophilous. *Parapetasia femorata* is present throughout the year in Cameroon, with the highest abundance observed during the dry season from November to January. This species is known to produce foamy secretions on tergites 3 and 4.

Parapetasia rammei Sjöstedt, 1923
Figs 1C, D, 2B, E, H, 6B, E, H, K, 7B, E, H

Holotype. Cameroon • ♀; Bare-Dschang, [Stockholm]

Paratypes. Cameroon • 1 ♂, Bamenda; Adametz S.G. leg.; MfN URL: http://cool.mfn-berlin.de/u/bb659e [MfN]. • 1 ♀; Bangwe; 1000 m; Mitte V-Mitte VI. 99 [mid-May.–mid-Jun. 1999]; G. Conrau S. leg.; MfN URL: http://cool.mfn-berlin.de/u/d4c8af [MfN].
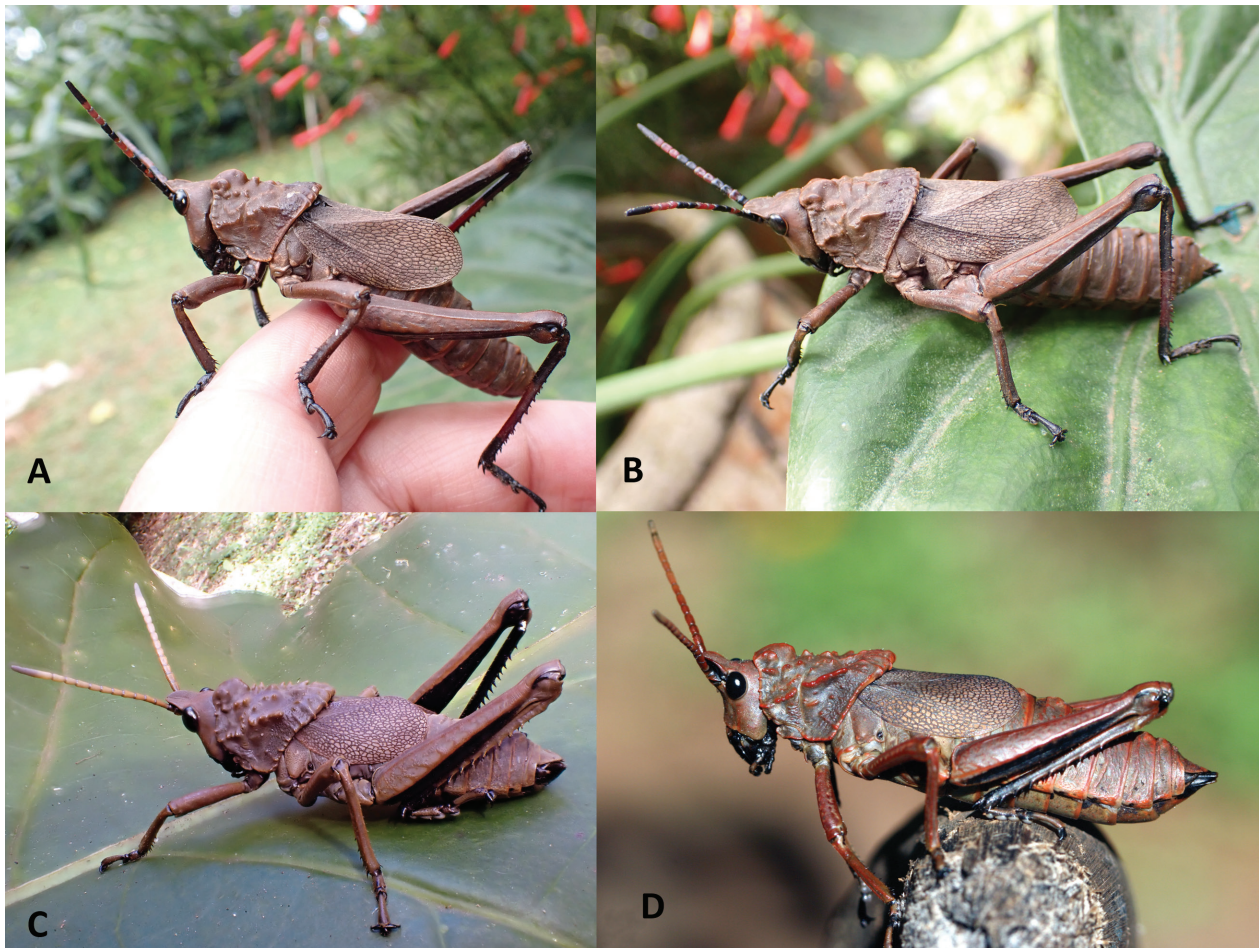
Figure 4. A, B. *L. tectiferus* sp. nov. **A.** Male; **B.** Female; **C, D.** *L. impotens*; **C.** Male; **D.** Female.

Material examined. CAMEROON. • 1 male; Bamenda; Adametz S.G. leg.; URL: http://cool.mfn-berlin.de/u/bb659e (MfN). • 1 female; Bangwe; 1000 m; Mitte V–Mitte VI. 99 [mid-May.–mid-Jun. 1999]; G. Conrau S. leg.; URL: http://cool.mfn-berlin.de/u/d4c8af (MfN). • 1 female; Fotouni, West; 5.362°N, 10.246°E; 15 Jun. 2020; J.A. Yetchom Fondjo; SMNK; CMJ678. • 1 female; Fotouni, West; 5.362°N, 10.246°E; 13 Aug. 2020; J.A. Yetchom Fondjo leg.; SMNK; CMJ61. • 2 males, 2 females; Fotouni, West; 5.362°N, 10.246°E; 16 Jan. 2021; J.A. Yetchom Fondjo; SMNK; CMJ679. • 1 female; Fotouni, West; 5.362°N, 10.246°E; 14 Mar. 2022; J.A. Yetchom Fondjo; SMNK; CMJ63. • 2 females; Fotouni, West; 5.362°N, 10.246°E; 15 Mar. 2022; J.A. Yetchom Fondjo; SMNK; CMJ64.

Redescription. Male. *Body*: robust, depressed, with strongly rugose and tuberculated integument. *Head* (Fig. 2B, E, H): acutely conical; fastigium of vertex slightly curved upwards, flat, slightly concave in basal part, distinctly triangular and narrowing toward apex; antennae thick, shorter than head and pronotum together, with short transverse or subtransverse segments, the last apical segment being distinctly longer than others. *Thorax* (Fig. 2E, H): pronotum with large inflation in front of first sulcus, strongly and intensely rugose with more pointed tubercles; median carinae interrupted, lateral carinae absent;

inferior margins of lateral lobes of pronotum straight; prozona shorter than metazona; posterior margin of metazona slightly emarginate in the middle; prosternal process very short, subacute; mesosternal interspace wider than long. *Legs* (Figs 1D, 2E, H): hind femur slender, its external area not expanded; upper-median margin of hind femora distinctly raised; obliquely expanded area at the base of hind femur strongly pronounced; external apical spine of hind tibiae present; hind tarsal segments not elongate. *Elytra* (Fig. 1D, 2E, H): less reticulated, shortened or brachypterous, oval, semilobed, reaching dorsally the third abdominal tergite, anterior margins rather curved, with very broadly rounded posterior margins. *Abdomen* (Figs 1D, 2E, H): often annulated; abdominal tergites each with a trigonal medio-dorsal tubercle; male subgenital plate compressed toward apex above, margins slightly incised, parallel; male supra-anal plate conical; male cerci (Fig. 7B) conical, straight. *Epiphallus* (Fig. 6B): bridge narrow, its anterior margin curved emarginate, posterior margin almost straight; anterior projections small; lateral plates oblique or divergent, its external margins fairly expanded; appendices of epiphallus narrow, subparallel, with apical lobes having only broader terminal processes, smaller processes absent, attached marginally to the basal part of external expansion of lateral plates, lying marginally to the external expansion of lateral plates; lophi very small or short, slightly curved,
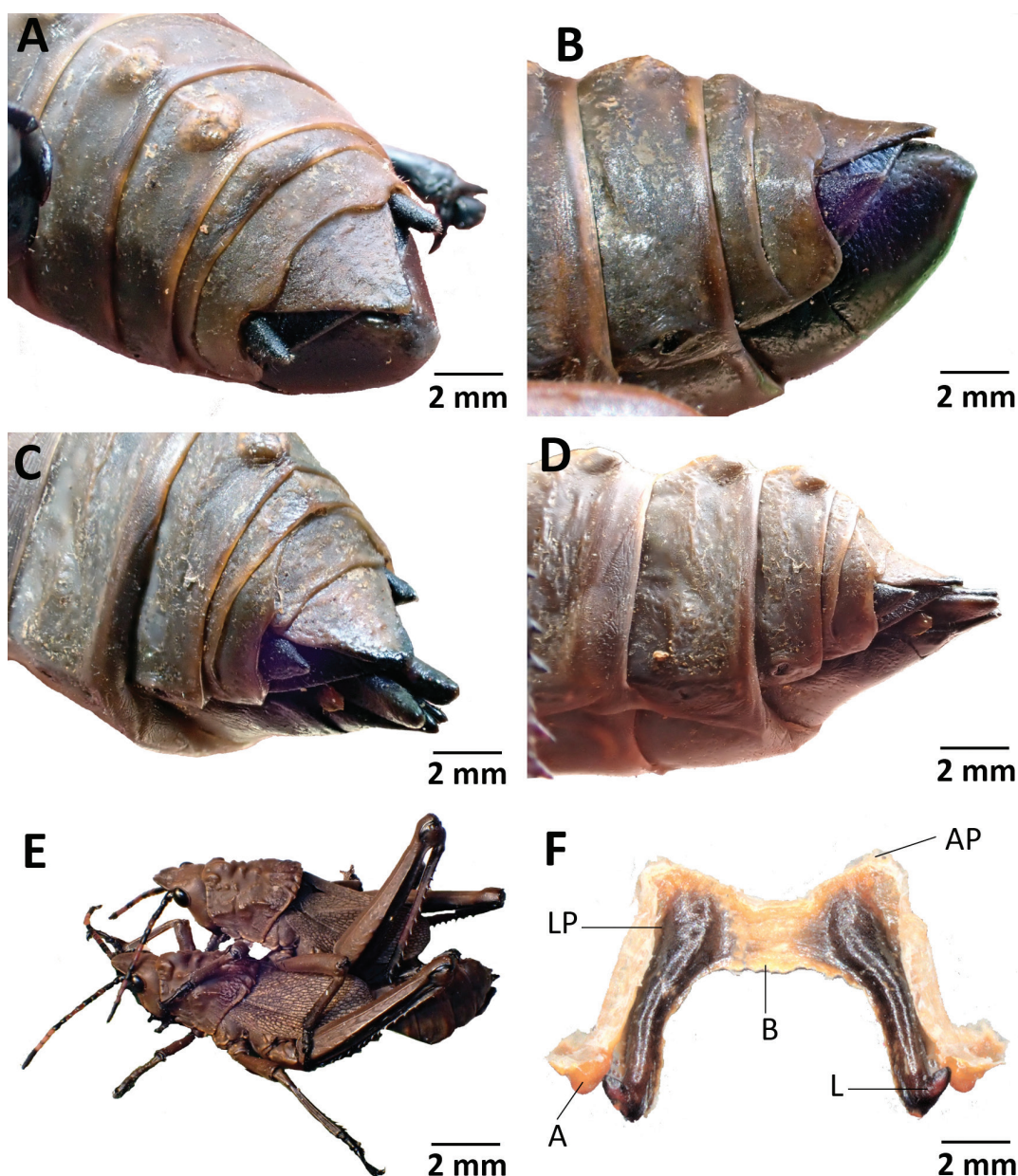
Figure 5. *L. tectiferus* sp. nov. **A.** Male semidorsal; **B.** Male in lateral view; **C.** Female semidorsal; **D.** Female in lateral view; **E.** *L. tectiferus* sp. nov. mating pair; **F.** Epiphallus.

and anteriorly directed with acute apex. *Ectophallus* (Fig. 6E, H, K): central membrane fairly narrow, subtriangular, marked at its lateral margins by furrows; zygoma broadly transverse, not extending halfway along the cingulum; suprazygomal plate rather U-shaped, slightly shorter than the zygoma; apodemal plates strongly produced ventrally, the apices fairly close to each other; valves of cingulum of smaller size, narrow, divergent in dorsal view; rami of cingulum narrow in dorsal view; dorsal cleft of cingulum large, ventral cleft narrow; suprarami well developed, large; sheats of moderate size, the inner margins separated from each other; ventral process of cingulum broadly triangular, slender, almost exceeding beyond endophallic apodemes in ventral view; basal emargination of cingulum very deep; *Endophallus* (Fig. 6E, H, K): endophallic apodemes of medium size, strongly produced

forwards ventrally, exceeding beyond the basal emargination of cingulum; aedeagal valves small, short with button-like apices, with ventrolaterally directed process in its distal part; aedeagal sclerites narrow and of moderate size; pseudoarch small; spermatophore sac small, ovoid, not extending beyond the lateral limits of endophallic apodemes; gonopore at the middle.

Female. Similar to male but larger. *Abdomen* (Fig. 7E): ovipositor valves large, not sinuate; subgenital plate without carina, narrowed posteriorly, slightly emarginate at apex; egg guide prominent, conical, and slightly elongated; median longitudinal groove of genital chamber slender. *Genitalia* (Fig. 7H): spermatheca thick, lacking an apical pocket, with a laminated appearance in the apical part; spermatheca duct short, secondary diverticulum of spermathecal appendage of varying shape.
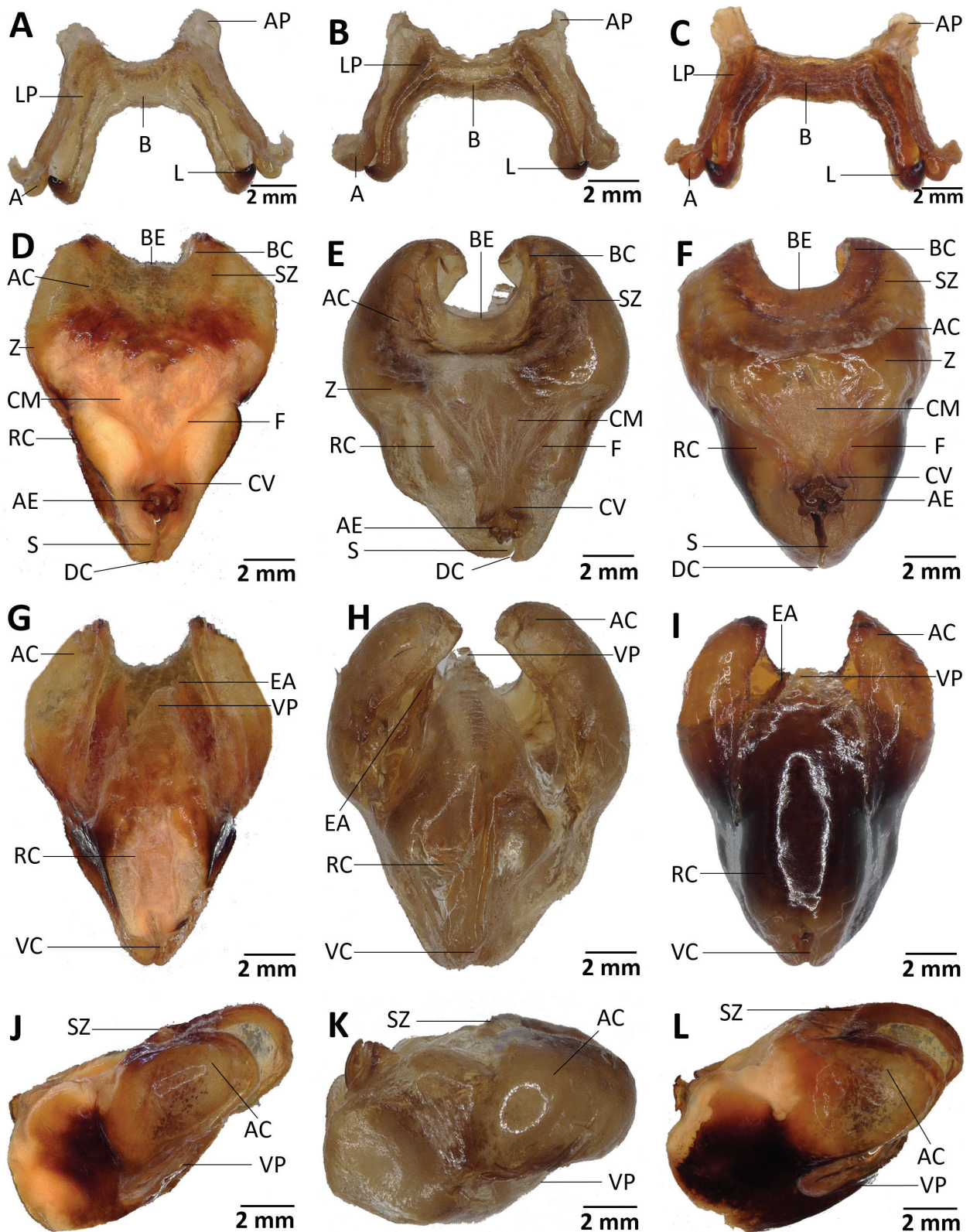
Figure 6. Phallic structures. **A–C.** Epiphallus dorsal view; **A.** *P. femorata*; **B.** *P. rammei*; **C.** *L. impotens*; **D–F.** Ectophallus + Endophallus dorsal view; **D.** *P. femorata*; **E.** *P. rammei*; **F.** *L. impotens*; **G–I.** Ectophallus + Endophallus ventral view; **G.** *P. femorata*; **H.** *P. rammei*; **I.** *L. impotens*; **J–L.** Ectophallus + Endophallus lateral view; **J.** *P. femorata*; **K.** *P. rammei*; **L.** *L. impotens.* A: appendices; AC: apodemal plate of cingulum; AE: aedeagus (aedeagal valves); AP: anterior projection of epiphallus; B: bridge of epiphallus; BC: basal thickening of cingulum; BE: basal emargination of cingulum; CM: central membrane of epiphallus; CV: valve of cingulum; DC: dorsal cleft of cingulum; EA: endophallic apodeme; F, marginal furrow separating suprarami and rami of cingulum; L: lophus of epiphallus; LP: lateral plate of epiphallus; RC: ramus of cingulum; S: sheath of ectophallus; SR: supraramus of cingulum; SZ: suprazygomal plate of cingulum; VC: ventral cleft of cingulum; VP: ventral process of cingulum; Z: zygoma of cingulum.
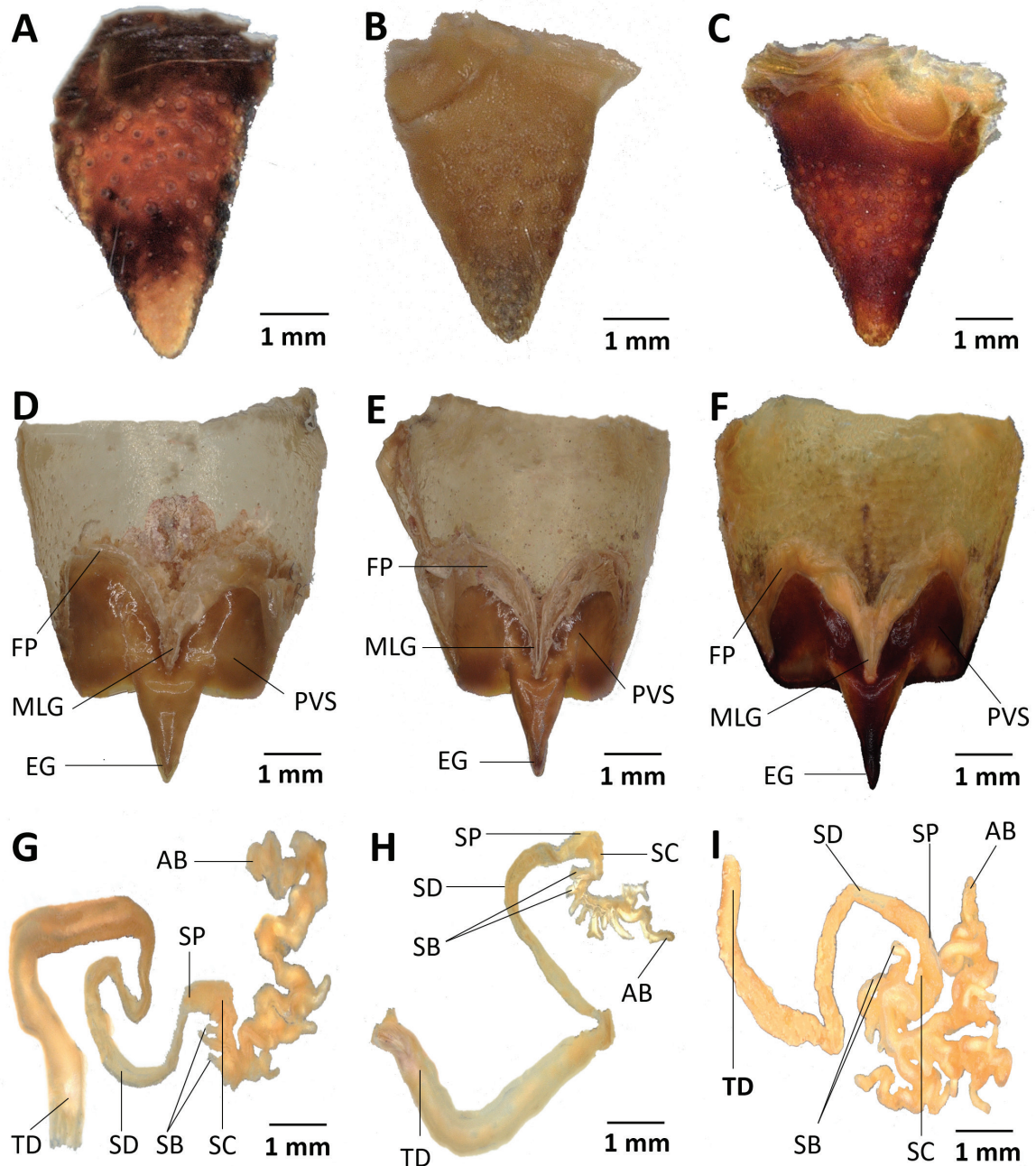
Figure 7. A–C. Male cerci; **A.** *P. femorata*; **B.** *P. rammei*; **C.** *L. impotens*; **D–F.** Female subgenital plates; **D.** *P. femorata*; **E.** *P. rammei.* **F.** *L. impotens.* **G–I.** Female spermatheca; **G.** *P. femorata*; **H.** *P. rammei*; **I.** *L. impotens*. AB: apical bulb of the spermathecal appendage; EG: egg-guide; FP: floor pouch of the female genital chamber; MLG: median longitudinal groove of the female genital chamber; PVS: postvaginal sclerite of the female genital chamber; SB: secondary diverticulum of the cecum of the spermatheca; SC: cecum of the spermatheca; SD: spermathecal duct; SP: spermathecal vesicle; TD: terminal dilatation of the spermathecal duct.

Color. Predominantly grayish; eyes red dark or entirely black in adults; labium, labrum, and mandibles red; hind knee entirely black in adults; elytra yellow-brown with brown veins; cerci yellowish or blackish; abdominal segments all separated by red lines; lower external, lower internal, mid internal, and upper internal hind femoral areas bright black.

Female. Pronotum testaceous brown with blood-like colored tubercles, more or less blackish below; antennae and legs reddish brown, more or less outlined with red; the outer-medial and upper-external area slightly variegated with yellowish brown, the margins more or less red, the tips of the femora black; hind tibiae all reddish brown, sometimes outlined with a blood-like color.

Male. Apex of antennae, apical 2/3 of hind tibiae, and ankles with blood-like colored tubercles; margin of vertex, lower part of antennae, fore and median femora, upper-external and medio-external areas of hind femora, anterior and median tibiae, and basal part of hind tibiae marked with yellow, especially on ribs.

Nymph with entirely black antennae, hind knees completely yellow.

Measurements. Male. Body length 32.83–35.37 mm; Female. Body length 43.22–49.73 mm. Adult individuals of *P. rammei* exhibit very large size variations in both sexes (Table 1).

Geographical distribution. *Parapetasia rammei* (as shown in Fig. 8) is limited to Cameroon. The species has been primarily observed in highland zones and grass fields, specifically in Bare-Dschang (the type locality), Bamenda, Bangwe, Fotouni, and Mt. Manengouba.

Ecology. *Parapetasia rammei* is typically associated with highland ecosystems. The species is commonly found on bare ground, low vegetation, and sometimes on shrubs in open vegetation, such as cultivated farms and fallows, as well as in steppe habitats. In its natural habitat, it can be observed throughout the year, with adults being particularly abundant during the rainy season. Nymphs are more commonly found during this period as well. Foamy secretions on tergites 7 and 8 are notable characteristics of the species and are also common in other pyrgomorphid species.

Key to the species of *Parapetasia*

1(2) Tegmina dark brown, strongly reduced, vestigial; first and/or second abdominal segments with a lateral black band behind the insertion points of the femora; anterior projections of epiphallus large; lateral plates subparallel; lophi large, strongly curved; suprazygomal plate widely rounded; apodemal lobes only slightly produced ventrally; basal emargination of cingulum shallow; endophallic apodemes short ....
.... *Parapetasia femorata* Bolívar, 1884 (Gabon, Cameroon, Equatorial Guinea, Nigeria)

2(1) Tegmina yellow-brown with brown veins, shortened or brachypterous, semilobed; first and/or second abdominal segments without a lateral black band behind the insertion points of the femora; anterior projections of epiphallus small; lateral plates oblique or divergent; lophi very small, slightly curved; suprazygomal plate U-shaped; apodemal lobes strongly produced ventrally; basal emargination of cingulum very deep; endophallic apodemes strongly elongate or slender .... *Parapetasia rammei* Sjöstedt, 1923 (Cameroon)

Genus *Loveridgacris* Rehn, 1954

Parapetasia (*Loveridgea*) Rehn (1953)
Parapetasia (*Loveridgcris*) Rehn (1954)
Parapetasia (*Loveridgeacris*) Kevan (1962) (subsequent misspelling)
Parapetasia (*Loveridgcris*): Akbar & Kevan, (1964)

Diagnosis of the genus *Loveridgacris*. Fastigium of vertex rounded apically; tegmina brachypterous and slightly reticulated; eyes ovate and not prominent; posterior part of metazona not notably raised nor swollen, its median margin not emarginate; hind femora upper-median margin flat, not raised; male subgenital plate with fused margins; epiphallic bridge wide or broad; appendices divergent; ectophallus elongate; ventral process of cingulum subtriangular.

Loveridgacris impotens (Karsch, 1888)

Figs 1E, F; 2C, F, I; 3F, 4C, D, 6C, F, I, L, 7C, F, I

Petasia impotens Karsch, 1888
Parapetasia impotens Karsch

Holotype. Deutsch-Ostafrika [German East Africa]. • 1 male; Uzigna [Usegna]; MfN.

Synonyms. *Loveridgacris ulugurensis* Rehn (1953): 124, 126, pl. 2: f. 18 and 19, pl. 3: f. 23 and 24. Kevan et al. (1972): 223, 229.

Material examined. Deutsch-Ostafrika [German East Africa]. • 1 male; Uzigna [Usegna]; MfN. • 1 male; Amani; 26 Nov. 1906; S.G. Vosseler leg.; MfN. • 1 male; Amani; 1 Nov. 1906; S.G. Vosseler leg.; MfN. • 1 male, 1 female; Amani; Nov. 1906; Vosseler S.G. leg.; MfN. • 2 males; Amani; Nov. 1907; S.G. Vosseler leg.; MfN. • 1 female; Amani; 16 Jan. 1906; S.G. Vosseler leg.; MfN. • 1 male; Amani; 30 Nov.– 5 Dec.1906; S.G. Vosseler leg.; MfN. • 1 male; Amani; S.G. Vosseler leg.; MfN. • 1 male; Amani; 20 Nov.– 5 Dec. 1906; S.G. Vosseler leg.; MfN. • 1 male, 6 females, 1 nymph; Amani; S.G. Vosseler leg.; MfN. Tanzania. • 1 male; Uluguru-Berge; 11 Dec. 1998; S. Götze leg.; MfN. Deutsch-Ostafrika [German East Africa]. • 1 female; Sigital; Jul. 1903; S. Götze; MfN. • 1 female; Muoa, Bez.langa; S. Fischer; MfN. • 1 female; V. Karger leg.; MfN. • 2 males, 3 females; 1903, vend.1 Apr. 1911; Dr F. Eichelbaum; ZMH. Tanzania. • 1 female; Usambara Nguelo; S. Heinsen; MfN. • 1 female; Usambara Nguelo; 14 Jun. 1905; H. Rolle leg.; ZMH. Deutsch-Ostafrika [German East Africa]. • 4 males; 1908; S.G. Vosseler; MfN.

Redescription. Male. *Body*: robust, depressed, with strongly rugose and tuberculated integument. *Head* (Fig. 1F, 2C, F, I): acutely conical; fastigium of vertex slightly curved upward, flat, slightly concave in basal part, with rounded apex in dorsal view; antennae thick, shorter than head and pronotum together, with short transverse or subtransverse segments, the last apical segment being distinctly longer than others; eyes oval, of moderate size. *Thorax* (Figs 2F, I, 3F, 4C, D): pronotum less testaceous, not deeply and concavely saddle-shaped, with large inflation in front of first sulcus, moderately rugose with slightly pointed tubercles; posterior part of metazonal disc not swollen or raised dorsally; median carinae interrupted, lateral carinae absent; lower margins of lateral lobes of

pronotum rather angular; prozona shorter than metazona; median posterior margin of metazona not emarginate; prosternal process very short, triangular, expanded at its base with angular apex; mesosternal interspace wider than long. *Legs* (Figs 2F, I, 3F, 4C, D): hind femur slender; upper-median margin of hind femora flat, not raised, almost of equal height to upper-external margin; obliquely expanded area at the base of hind femur less pronounced; external apical spine of hind tibiae present; hind tarsal segments not elongate. *Elytra* (Figs 1F, 2F, I, 4C, D): shortened or brachypterous, slightly elongated and strongly reticulated, reaching dorsally the third abdominal tergite, with evenly rounded posterior margins. *Abdomen* (Figs 2F, I, 3F, 4C, D): often annulated; abdominal tergites each with a trigonal medio-dorsal tubercle; male subgenital plate compressed toward apex above, margins fused but not separated; male supra-anal plate conical; male cerci conical (Fig. 7C). *Epiphallus* (Fig. 6C): bridge wide or broad, its anterior margin emarginate, and posterior margin almost straight; anterior projections large, fairly prominent; lateral plates almost divergent, its external margins slightly expanded; lophi of larger size, upcurved and anteriorly directed with acute apex; appendices divergent, with broad apical lobes bearing long terminal processes, attached submarginally to the anterior projections and lying close to the lateral plates. *Ectophallus* (Fig. 7F, I, L): elongate, stout; central membrane broad, marked at its lateral margins by furrows; zygoma narrow; suprazygomal plate narrow, slightly shorter than the zygoma, with rather widely rounded apex; apodemal plate broad and rounded in lateral view, lobes slightly produced ventrally, the apices fairly wide apart, without anterior blunt points; valves of cingulum of smaller size, divergent in dorsal view; rami of cingulum extending into sheath; sheath wide, inner margins fairly close to each other; dorsal cleft of cingulum large; ventral cleft of cingulum of moderate size; suprarami well developed, large; sheats well developed; ventral process of cingulum rather subtriangular, broadly covering the endophallic apodemes, slender, but not reaching or extending beyond endophallic apodemes in ventral view; basal emargination of cingulum shallow. *Endophallus* (Fig. 7F, I, L): endophallic apodemes moderately produced forward ventrally, rather broad, and reaching the basal emargination of cingulum; aedeagal valves of smaller size, broad, with button-like apices, and with ventrolaterally directed process in its distal part; aedeagal sclerites stout, slender, and curved; pseudoarch small, distinct, broad; spermatophore sac small, ovoid, extending beyond the lateral limits of endophallic apodemes; gonopore distally placed.

Female. As for male, but larger. *Abdomen* (Figs 4D, 7F): ovipositor valves large, not sinuate; subgenital plate without a carina, its posterior margin rounded and smooth; egg-guide prominent, conical, and highly elongated; median longitudinal groove of genital chamber slender. *Genitalia* (Fig. 7I): spermatheca thick, lacking an apical pocket, with a laminated appearance in the apical part; spermatheca duct slender, secondary diverticulum of spermathecal appendage of varying shape.

Color. General coloration brownish or reddish; eyes entirely black; head dark-red or brownish; labium, labrum, and mandible blackish; elytra light brown with dark-brown veins; lower-external, lower-internal, and medial-internal areas of hind femora blackish; hind tibiae sometimes brown in basal half and black in apical half.

Female. Antennae reddish brown; pronotum brown with dark-red tubercles; fore and middle femora, outer-medial, upper-external, and upper-internal areas of hind femora dark-red; fore and middle tibiae dark red; hind tibiae all brown in basal 2/3 and black in apical parts; tarsi blackish or dark-red; abdomen brownish; the posterior margins of the segments marked by red lines.

Male. Antenna light-brown; pronotum brownish with light-red tubercles in male; fore and middle femora, outer-medial, upper-external, and upper-internal areas of hind femora light-red; fore and middle tibiae light-red; hind tibiae all light-red in outer area and black in inner area; tarsi blackish or brownish.

Measurements. Male. Body length 50.88–60.19 mm; Female. Body length 48.72–63.69 mm. Adults of *L. impotens* exhibit significant size variation in both males and females. Table 1 provides detailed measurements of various body parts for this species.

Geographical distribution (Fig. 8). *Loveridgacris impotens* is a species that is found in East Africa. The species is known only from some of the Eastern Arc Mountains of Tanzania, on Zanzibar, and the Shimba Hills of Kenya.

Ecology. *Loveridgacris impotens* is a geophilous species found in lowland wet forests. The species produces the toxic foams (see the black arrow on Fig. 1F) by combining haemolymph with air through the spiracles.

Loveridgacris tectiferus Hemp, sp. nov.

https://zoobank.org/4A3C74E4-1002-458F-AC93-7F882AD0F4B5
Figs 3A–H, 4A, B, 5C, D

Holotype. Tanzania. • male; Udzungwa Mountains, Mang´ula; in disturbed lowland wet forest at border to National Park; Sep. 2022; Claudia Hemp leg.; Depository: CCH.

Paratypes. Tanzania. • 2 females; same data as for holotype. Depository: CCH.

Measurements. (mm) Males (n = 1): Body length: 51.20; Median length of pronotum: 13.60; length of hind femur: 25.00. Females (n = 2): Body length: 47.70–53.60; Median length of pronotum: 21.50–21.70; length of hind femur: 23.90–24.60.

Diagnosis. *Loveridgacris tectiferus* sp. nov. can be distinguished from *L. impotens* by the coloration of the antennae and hind tibiae. In *L. impotens*, the antennae are light or reddish brown, while in *L. tectiferus* sp. nov., segments alternate between black and orange (Fig. 4C, D). Similarly, the hind tibiae are uniformly brown and become darker at their apical parts in *L. impotens*, but are black with a median dull orange part in *L. tectiferus* sp. nov. The most noticeable difference between the two species is the shape of the tegmina, which are lobe-like and
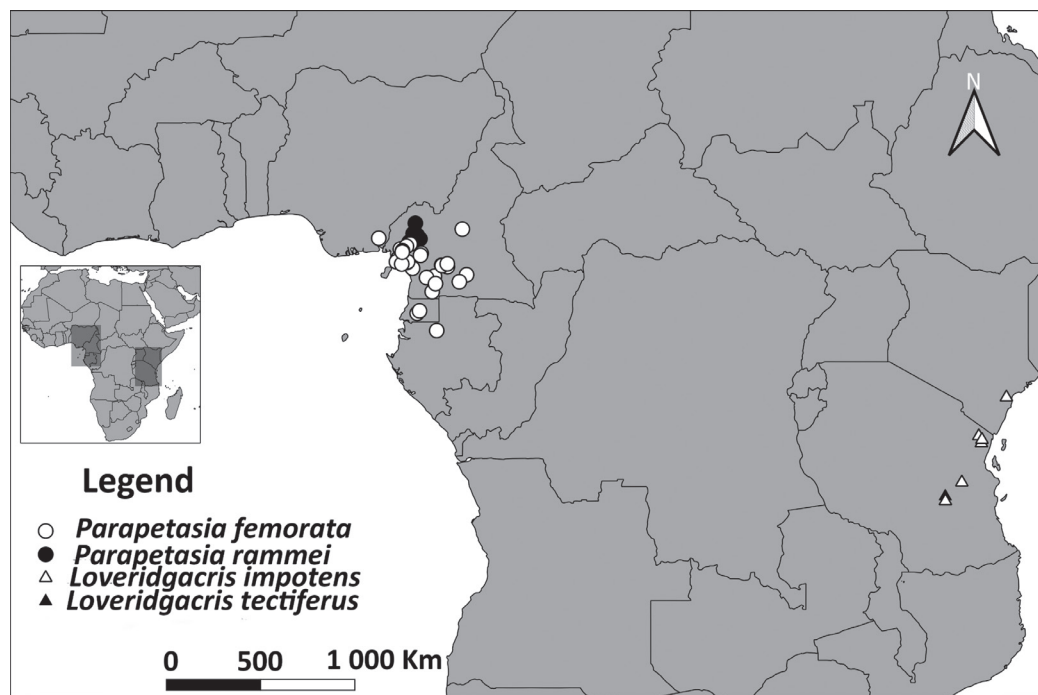
Figure 8. Geographical distribution of species in the genera *Parapetasia* and *Loveridgacris* (*P. femorata*, unfilled circle; *P. rammei*, filled circle; *L. impotens*, unfilled triangle; *L. tectiferus* sp. nov., filled triangle).

attached to the abdomen in *L. impotens*, while tectiform in *L. tectiferus* sp. nov. Both species are very similar in the overall shape of the head, pronotum, legs, and body, as well as in the tegminal pattern of darker veins on a light brown ground and their size. The epiphallus of both species is also very similar, consisting of hooked lophi and elongate appendices with bulbous end parts. However, in *L. tectiferus* sp. nov., the lophi are slender, and the hooks are slightly longer than those in *L. impotens*. Additionally, the appendices of the epiphallus are stouter in *L. impotens*, and the bridge of the epiphallus is slightly longer than that in *L. tectiferus* sp. nov. (see Fig. 5F and 6C for comparison).

Description. Male. *General coloration.* Overall, color brown with antennae with conspicuously black and orange colored segments. Eyes and labrum black. Hind femora ventrally black, hind tibiae black with dull orange middle part (Fig. 4A). ***Head and antennae.*** Antennae thick, rod-like with basal segments black, and then alternating one or two segments orange and black (Fig. 3A, C). Antennae slightly shorter than head and pronotum together. Fastigium of vertex upcurved, slightly concave in the middle, with acute-angular apex. Frons incurved. Frontal ridge narrow, constricted between antennae (Fig. 3A). ***Pronotum and wings.*** Pronotum in front of first sulcus with large hump, remaining pronotum strongly rugose with elevated ridges and tubercles. Median carina irregular, obtuse, lateral carinae absent. Posterior margin of pronotum with ridge-like tubercles along the edge. Prosternal process low, subpyramidal. Mesosternal interspace wider than long, with deep grooves (Fig. 3E). Tegmina tectiform, shortened, slightly exceeding abdominal segment 3. Hind wings absent. ***Abdomen.*** All abdominal segments with dorsal tubercles. Male supra-anal plate tri-

angular (Fig. 5A), cerci laterally compressed, black, with blunt apex. Subgenital plate obtusely conical (Fig. 5B). Internal morphology. Epiphallus typical for Dictyophorini. Lophi of epiphallus strongly sclerotized with well-developed dorsolaterally directed apical hooks. Appendix of the epiphallus with angular externolateral sclerotized processes running parallel to the lophi; apices knob-like with ventral directed dent. Bridge little sclerotized and comparatively narrow.

Female. Larger and stouter than the male, with the same coloration as male; predominantly brown with antennae with black and orange segments, black eyes, and labrum. Underside of hind femora black, hind tibia black with median dull orange part (Fig. 4B). Antennae, head, and pronotum as male. Supra-anal plate triangular with blunt apex (Fig. 5C). Cerci laterally compressed, black (Fig. 5C, D). Ovipositor valves black, straight, rounded, with blunt apices (Fig. 5C, D).

Etymology. From Latin: -*tectum* = roof, because of the tectiform-shaped tegmina.

Habitat. A geophilous species of lowland wet forest.

Ecology. In captivity, individuals have the same preference for monocotyledonous plants as observed for *Dictyophorus griseus* (Rowell et al. 2015). Even when offered various other plants, they preferred to feed on Liliaceae leaves and flowers. Mating took approximately half an hour, and the male sat on top of the female, bending its abdomen under that of the female for copulation (Fig. 5E). Even when roughly handled, no reflex bleeding was observed, as is common in other Dictyophorini species and also observed in *L. impotens* (Fig. 1F).

Nymphs. Unknown but are probably similar to nymphs of *L. impotens* (Fig. 1E).

Distribution. Tanzania, Udzungwa Mountains.

Key to the species of *Loveridgacris*

1(2)   Antennae light or reddish brown; hind tibiae uniformly brown, their apical parts darker; tegmina lobe-like and attached to the abdomen (Fig. 4C, D) ....*Loveridgacris impotens* (Karsch, 1888) (Tanzania, Kenya)

2(1)   Antennal segments alternate between black and orange; hind tibiae black with a median dull orange part; tegmina tectiform (Fig. 4A, B) .... *Loveridgacris tectiferus* Hemp, sp. nov. (Tanzania)

Phylogenetic analysis

In total, 47 DNA barcode sequences belonging to 10 Pyrgomorphidae species were analyzed. The locations of collection of the samples used are presented in Table 4. For the genera *Parapetasia* and *Loveridgacris*, two species representing all known species were analyzed. Six additional species defined as outgroups included *Zonocerus elegans* (Thunberg, 1815), *Phyteumas purpurascens* (Karsch, 1896), *Phymateus viridipes* (Stål, 1873), *Tapronota calliparea calliparea* (Schaum, 1853), *Dictyophorus spumans* (Thunberg, 1787), and *Dictyophorus griseus* (Reiche & Fairmaire, 1849). One phylogenetic tree based on the concatenated sequence alignments of the two individual gene datasets (COI = 565 bp, 16S = 376 bp) was constructed with the BI method (Fig. 9). The concatenated sequence alignment included 941 bp. The most basal clusters of the phylogenetic tree comprised the subtribes Zonocerina (*Zonocerus*), Phymateina (*Phymateus*, *Phyteumas*), and Taphronotina (*Taphronota*). The tribes Taphronotini and Phymateini were well resolved, and all members of these tribes clustered together; similarly,

members of the subtribes Zonocerina and Phymateina were well resolved. The tribe Dictyophorini represented a separate clade relative to Taphronotini and Phymateini. The tribe Dictyophorini was divided into three groups, representing three different genera. We found strong support for the monophyly of the genera *Loveridgacris*, *Parapetasia*, and *Dictyophorus*. The species tree inferred using the BI approach (Fig. 9) clustered. *Loveridgacris* near *Parapetasia* with high posterior probability support (score > 0.95). The cluster, including only the members of *Parapetasia*, was divided into two groups, and *Parapetasia rammei* was the sister to *Parapetasia femorata*. Both had relatively large interspecific distances (3.75%). The two *Loveridgacris* species (*L. impotens* and *L. tectiferus* sp. nov.) showed substantial sequence divergence from the other genera. The distances between *L. impotens* and *P. femorata* (6.70%) and between *L. impotens* and P. *rammei* (7.58%) were relatively large. At the species level, *L. impotens* and *L. tectiferus* sp. nov. are not completely resolved, but *L. tectiferus* sp. nov. is monophyletic with high support; the species show low genetic distance (0.33%).
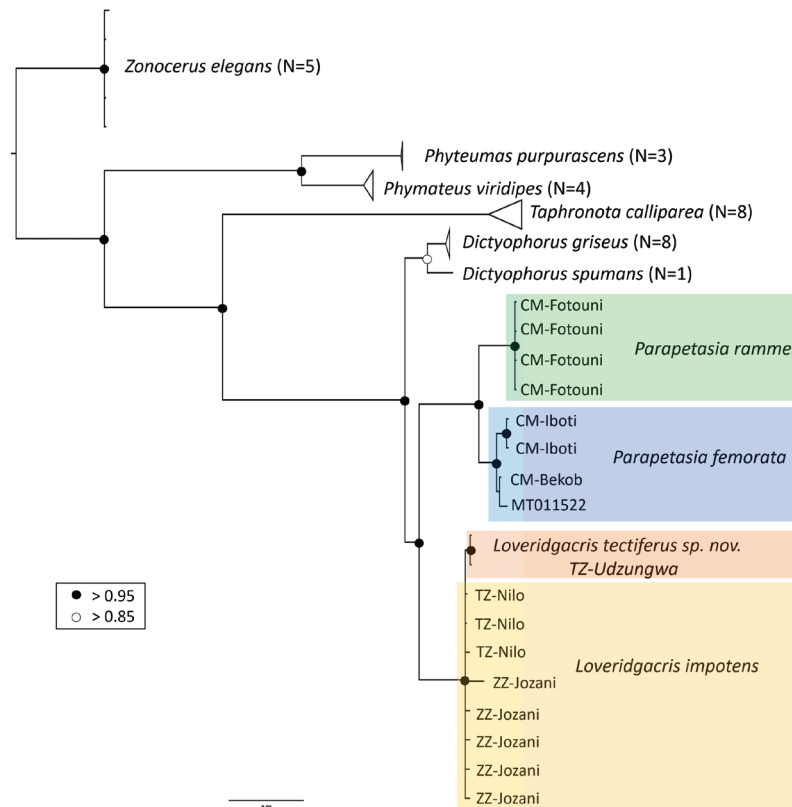

Figure 9. Bayesian inference (BI) tree built from the concatenated sequence alignment of mtDNA COI/16S gene fragments. The Bayesian posterior probabilities (PPs) are shown close to the nodes.

Dtsch. Entomol. Z. 71 (2) 2024, 265–287

281

Mitochondrial genome organization, structure, and base composition in *Loveridgacris*

The mitogenomes of *Loveridgacris impotens* and *Loveridgacris tectiferus* sp. nov. are 15,592 bp and 15,737 bp long, respectively (see Suppl. 1). Both are organized in the typical metazoan mitochondrial gene set consisting of 37 genes, namely, 13 protein-coding genes, 22 transfer RNA genes, two ribosomal RNA genes (rrnL and rrnS), and one A+T-rich control region (Table 2). A comparison of the whole mitogenomes, rrnL genes, rrnS genes, and A+T-rich regions of *L. impotens* and *L. tectiferus* sp. nov. are shown in Table 4. The nucleotide composition of the entire mitochondrial genome of both species is A+T-biased, with contents ranging from 70.0% in *L. impotens* to 74.1% in *L. tectiferus* sp. nov. (Table 3). The skew metrics of the protein-coding genes within *L. impotens* and *L. tectiferus* sp. nov. showed a positive AT-skew and a negative GC-skew, indicating that base C was more abundant than base G in the mitogenomes of both species (Table 3).

The pairwise genetic distances (see Suppl. 2) inferred from all 13 protein-coding genes showed that the interspecies genetic distance ranged from 0% (ATP8) to 0.8% (ND4), indicating relatively low genetic distances between *L. impotens* and *L. tectiferus* sp. nov., regardless of the gene considered. Among the 13 PCGs, ND2, COI, COII, ATP8, ATP6, COIII, ND3, and ND6 CYTB were encoded on the majority strand (J-strand), while ND1, ND4, ND4L, and ND5 were encoded on the minority strand (N-strand) (Table 2). Transfer RNA genes are located on the J strand, except for tRNA-Gln, tRNA-Cys, tRNA-Tyr, tRNA-Phe, tRNA-His, tRNA-Pro, tRNA-Leu1, and tRNA-Val, which are located on the N strand (Table 2). Most of the PCGs (ND2, COII, ATP6, COIII, ND4L, ND6, and CYTB) have ATG as the start codon; ATP8 has ATC as the start codon; COI has ACT as the start codon; ND3 and ND5 have ATT as the start codon, and ND1 has ATA as the start codon. All PCGs use complete TAA as the stop codon, except COIII, ND5, and ND4, which use ACT, ATT, and TAG, respectively, as the stop codon (Table 2).

Discussion

Taxonomy

This study was conducted to investigate the genera *Parapetasia* and *Loveridgacris* using a combination of morphological, distributional, and molecular data. *Parapetasia rammei* has been used by Seino and Njoya (2018); hence, this name is currently considered valid in the OSF (Cigliano et al. 2023). In this study, *Parapetasia rammei* was formally resurrected.

We present herein the description of a new species, *Loveridgacris tectiferus* sp. nov., discovered in Tanzania. Despite exhibiting distinguishable morphological traits, our genetic analysis reveals minimal differences

Table 2. Distribution of protein-coding genes (PCGs), transfer RNA genes, ribosomal RNA genes, and A+T-rich regions in the mitogenome of *Loveridgacris* impotens.

Species	*Loveridgacris impotens*					
Genes	Length (bp)	Position	Start codon	Stop codon	Strand	Anticodon
ND2	1,023	197–1219	ATG	TAA	J	
COX1	1545	1415–2959	ACT	TAA	J	
COX2	684	3029–3712	ATG	TAA	J	
ATP8	159	3858–4016	ATC	TAA	J	
ATP6	678	4010–4687	ATG	TAA	J	
COX3	820	4694–5513	ATG	ACT	J	
ND3	354	5548–5901	ATT	TAA	J	
ND5	1717	6311–8027	ATT	ATT	N	
ND4	1335	8112–9446	GTG	TAG	N	
ND4L	294	9440–9733	ATG	TAA	N	
ND6	522	9871–10392	ATG	TAA	J	
CYTB	1143	10396–11538	ATG	TAG	J	
ND1	945	11625–12569	ATA	TAG	N	
tRNA-Ile	64	1–64	AAT	TAA	J	GAT
tRNA-Gln	69	62–130			N	TTG
tRNA-Met	67	130–196			J	CAT
tRNA-Trp	71	1224–1294			J	TCA
tRNA-Cys	63	1287–1349			N	GCA
tRNA-Tyr	69	1354–1422			N	GTA
tRNA-Leu2	65	2955–3019			J	TAA
tRNA-Asp	64	3711–3774			J	GTC
tRNA-Lys	71	3775–3845			J	CTT
tRNA-Gly	64	5484–5547			J	TCC
tRNA-Ala	66	5902–5967			J	TGC
tRNA-Arg	65	5967–6031			J	TCG
tRNA-Asn	68	6043–6110			J	
tRNA-Ser	70	11537–11606			J	TGA
tRNA-Glu	64	6184–6247			J	TTC
tRNA-Phe	64	6246–6309			N	GAA
tRNA-His	70	8043–8112			N	GTG
tRNA-Thr	68	9736–9803			J	TGT
tRNA-Pro	65	9804–9868			N	TGG
tRNA-Ser2	68	6111–6178			J	GCT
tRNA-Leu1	65	1273–12637			N	TAG
tRNA-Val	68	13939–14006			N	TAC
L-rRNA	1252	13897–12646			J	
S-rRNA	785	14017–14801			N	
A+T-rich region	791	14802–15592			J	N/A

Table 3. Nucleotide composition of the complete mitogenome for each *Loveridgacris* species examined.

Species		*Loveridgacris impotens*	*Loveridgacris tectiferus* sp. nov.
Accession number		OR730795	OR730794
Length (bp)		15592	15737
Whole mitogenome	A	6869 (40.0%)	6947 (44.1%)
	T	4679 (30.0%)	4709 (29.9%)
	G	1539 (9.9%)	1543 (9.8%)
	C	2507 (16.1%)	2538 (16.1%)
	A+T	11546 (70.0%)	11656 (74.1%)
	G+C	4046 (26.0%)	4081 (25.9%)
	AT-skew	0.14	0.19
	GC-skew	-0.24	-0.24

between *Loveridgacris tectiferus* sp. nov. and *L. impotens*. This suggests that *Loveridgacris tectiferus* sp. nov. is likely a recently evolved species, indicative of its youth within the taxonomic hierarchy. Indeed, *L. impotens* and

Table 4. Taxon sampling and GenBank accession numbers.

Species	Country	Locality	Specimen codes	GenBank Accession number COI	16S	GenSeq Nomenclature	References
Dictyophorus griseus (Reiche & Fairmaire, 1849)	Cameroon	Fotouni	CMJ65 (non-type specimen voucher)	OR583878	PP552786	genseq-4 COI, 16S	This study
Dictyophorus griseus (Reiche & Fairmaire, 1849)	Cameroon	Fotouni	CMJ66 (non-type specimen voucher)	OR583879	PP552787	genseq-4 COI, 16S	This study
Dictyophorus griseus (Reiche & Fairmaire, 1849)	Cameroon	Fotouni	CMJ67 (non-type specimen voucher)	OR583880	PP552788	genseq-4 COI, 16S	This study
Dictyophorus griseus (Reiche & Fairmaire, 1849)	Cameroon	Fotouni	CMJ70 (non-type specimen voucher)	OR583881	PP552789	genseq-4 COI, 16S	This study
Dictyophorus griseus (Reiche & Fairmaire, 1849)	Cameroon	Fotouni	CMJ72 (non-type specimen voucher)	OR583882	PP552790	genseq-4 COI, 16S	This study
Dictyophorus griseus (Reiche & Fairmaire, 1849)	Cameroon	Fotouni	CMJ814 (non-type specimen voucher)	OR583885	PP552791	genseq-4 COI, 16S	This study
Dictyophorus griseus (Reiche & Fairmaire, 1849)	Cameroon	Fotouni	CMJ816 (non-type specimen voucher)	OR583886	PP552792	genseq-4 COI, 16S	This study
Dictyophorus griseus (Reiche & Fairmaire, 1849)	Cameroon	Fotouni	CMJ817 (non-type specimen voucher)	OR583887	PP552793	genseq-4 COI, 16S	This study
Dictyophorus spumans (Thunberg, 1787)	South Africa	Western Cape	ORTH48 (non-type specimen voucher)	NA	PP552794	genseq-4 16S	This study
Loveridgacris impotens (Karsch, 1888)	Tanzania	Nilo	TZC1351 (non-type specimen voucher)	NA	PP552822	genseq-4 16S	This study
Loveridgacris impotens (Karsch, 1888)	Tanzania	Nilo	TZC1379 (non-type specimen voucher)	OR578932	PP552823	genseq-4 COI, 16S	This study
Loveridgacris impotens (Karsch, 1888)	Tanzania	Nilo	TZC1380 (non-type specimen voucher)	NA	PP552824	genseq-4 16S	This study
Loveridgacris impotens (Karsch, 1888)	Tanzania	Nilo	TZC1381 (non-type specimen voucher)	OR578933	NA	genseq-4 COI	This study
Loveridgacris impotens (Karsch, 1888)	Zanzibar	Jozani	ZZC1434 (non-type specimen voucher)	NA	PP552980	genseq-4 16S	This study
Loveridgacris impotens (Karsch, 1888)	Zanzibar	Jozani	ZZC1435 (non-type specimen voucher)	NA	PP552825	genseq-4 16S	This study
Loveridgacris impotens (Karsch, 1888)	Zanzibar	Jozani	ZZC1436 (non-type specimen voucher)	NA	PP552826	genseq-4 16S	This study
Loveridgacris impotens (Karsch, 1888)	Zanzibar	Jozani	ZZC1437 (non-type specimen voucher)	NA	PP552827	genseq-4 16S	This study
Loveridgacris impotens (Karsch, 1888)	Zanzibar	Jozani	ZZC1438 (non-type specimen voucher)	NA	PP552828	genseq-4 16S	This study
Loveridgacris tectiferus sp. nov.	Tanzania	Udzungwa	TZC1336 (holotype)	OR730794	PP552820	genseq-1 COI, 16S	This study
Loveridgacris tectiferus sp. nov.	Tanzania	Udzungwa	TZC1352 (paratype)	OR583893	PP552821	genseq-2 COI, 16S	This study
Parapetasia femorata Bolívar, 1884	NA	NA	NA	MT011522	NA	genseq-4 COI	Song et al. (2020)
Parapetasia femorata Bolívar, 1884	Cameroon	Iboti	CMJ244 (non-type specimen vouvher)	OR583883	PP552818	genseq-4 COI, 16S	This study
Parapetasia femorata Bolívar, 1884	Cameroon	Iboti	CMJ245 (non-type specimen vouvher)	OR578931	PP552979	genseq-4 COI, 16S	This study
Parapetasia femorata Bolívar, 1884	Cameroon	Bekob	CMJ598 (non-type specimen vouvher)	OR583884	PP552819	genseq-4 COI, 16S	This study
Parapetasia rammei Sjöstedt, 1923	Cameroon	Fotouni	CMJ61 (non-type specimen vouvher)	OR583875	PP552814	genseq-4 COI, 16S	This study
Parapetasia rammei Sjöstedt, 1923	Cameroon	Fotouni	CMJ62 (non-type specimen voucher)	OR583876	PP552815	genseq-4 COI, 16S	This study
Parapetasia rammei Sjöstedt, 1923	Cameroon	Fotouni	CMJ63 (non-type specimen voucher)	OR578930	PP552816	genseq-4 COI, 16S	This study
Parapetasia rammei Sjöstedt, 1923	Cameroon	Fotouni	CMJ64 (non-type specimen voucher)	OR583877	PP552817	genseq-4 COI, 16S	This study
Phymateus viridipes (Stål, 1873)	Tanzania	Nguru	TZC1339 (non-type specimen voucher)	NA	PP552803	genseq-4 16S	This study
Phymateus viridipes (Stål, 1873)	Tanzania	Nguru	TZC1340 (non-type specimen voucher)	OR583890	PP552804	genseq-4 COI, 16S	This study
Phymateus viridipes (Stål, 1873)	Tanzania	Nguru	TZC1354 (non-type specimen voucher)	NA	PP552805	genseq-4 16S	This study
Phymateus viridipes (Stål, 1873)	Tanzania	Nguru	TZC1355 (non-type specimen voucher)	OR583894	PP552806	genseq-4 COI, 16S	This study
Phyteumas purpurascens (Karsch, 1896)	Tanzania	Nguru	TZC1343 (non-type specimen voucher)	OR583892	PP552807	genseq-4 COI, 16S	This study
Phyteumas purpurascens (Karsch, 1896)	Tanzania	Wikwescho	TZC1388 (non-type specimen voucher)	OR578937	PP552808	genseq-4 COI, 16S	This study
Phyteumas purpurascens (Karsch, 1896)	Tanzania	Wikwescho	TZC1389 (non-type specimen voucher)	OR578938	PP552809	genseq-4 COI, 16S	This study

Species	Country	Locality	Specimen codes	GenBank Accession number		GenSeq Nomenclature	References
				COI	16S		
Taphronota calliparea (Schaum, 1853)	Tanzania	Kimboza	TZC1335 (non-type specimen voucher)	OR583888	PP552795	genseq-4 COI, 16S	This study
Taphronota calliparea (Schaum, 1853)	Tanzania	Nguru	TZC1341 (non-type specimen voucher)	NA	PP552796	genseq-4 16S	This study
Taphronota calliparea (Schaum, 1853)	Tanzania	Nguru	TZC1342 (non-type specimen voucher)	OR583891	PP552797	genseq-4 COI, 16S	This study
Taphronota calliparea (Schaum, 1853)	Tanzania	Nilo	TZC1383 (non-type specimen voucher)	OR583895	PP552798	genseq-4 COI, 16S	This study
Taphronota calliparea (Schaum, 1853)	Tanzania	Nilo	TZC1384 (non-type specimen voucher)	OR583896	PP552799	genseq-4 COI, 16S	This study
Taphronota calliparea (Schaum, 1853)	Tanzania	Nilo	TZC1385 (non-type specimen voucher)	OR578934	PP552800	genseq-4 COI, 16S	This study
Taphronota calliparea (Schaum, 1853)	Tanzania	Nguru	TZC1386 (non-type specimen voucher)	OR578935	PP552801	genseq-4 COI, 16S	This study
Taphronota calliparea (Schaum, 1853)	Tanzania	Nguru	TZC1387 (non-type specimen voucher)	OR578936	PP552802	genseq-4 COI, 16S	This study
Zonocerus elegans (Thunberg, 1815)	Tanzania	Nguru	TZC1337 (non-type specimen voucher)	NA	PP552810	genseq-4 16S	This study
Zonocerus elegans (Thunberg, 1815)	Tanzania	Nguru	TZC1338 (non-type specimen voucher)	OR583889	PP552811	genseq-4 COI, 16S	This study
Zonocerus elegans (Thunberg, 1815)	Tanzania	Nilo	TZC1390 (non-type specimen voucher)	NA	PP552812	genseq-4 16S	This study
Zonocerus elegans (Thunberg, 1815)	Tanzania	Nilo	TZC1391 (non-type specimen voucher)	OR578939	PP552813	genseq-4 COI, 16S	This study
Zonocerus elegans (Thunberg, 1815)	–	–	MT011544	NA	genseq-4 COI, 16S	Song et al. (2020)

L. tectiferus sp. nov. inhabit different mountain habitats in Tanzania, with *L. impotens* being widely distributed, while *L. tectiferus* is restricted to Udzungwa mountain so far. This suggests a possibility of sympatric speciation due to habitat isolation, which may cause disruption of gene flow. Our findings align with prior investigations of Orthopteran taxa, particularly those inhabiting the Eastern Arc Mountains. These studies indicate that while genera within this region have ancient origins, speciation at the species level appears to be relatively young. This pattern is attributed to historical climatic fluctuations, which have intermittently fragmented and interconnected habitats, facilitating both isolation and subsequent diversification. Similar mechanisms have been documented in various Orthopteran groups, including Lentulidae (Hemp et al. 2020), the coptacrine genus *Parepistaurus* (Hemp et al. 2015), the hexacentrine genus *Aerotegmina* (Grzywacz et al. 2021), and the meconematine genus *Amytta* (Hemp et al. 2018). These studies collectively underscore the dynamic interplay between historical environmental factors and evolutionary processes, shaping the diversity of Orthopteran fauna in the Eastern Arc Mountains and beyond. Two species are now included in both *Parapetasia* (*P. femorata* and *P. rammei*) and *Loveridgacris* (*L. impotens* and *Loveridgacris tectiferus* sp. nov.).

Akbar and Kevan (1964) used external morphology and phallic structures to distinguish between the genera *Parapetasia* and *Loveridgacris*. Although they did not examine the phallic structures of *P. rammei*, they concluded that *Parapetasia* has an epiphallus with subparallel lateral plates and appendices, a triangular fastigium of the vertex, and other anatomical features similar to those of *P. femorata*. However, the phallic structures of *P. rammei*, as illustrated in this study, reveal that the epiphallus has a narrow bridge but divergent lateral plates, resembling those of *Loveridgacris* rather than *Parapetasia*.

Akbar and Kevan (1964) noted that *Parapetasia* species, specifically *P. femorata*, have epiphallus appendices with smaller and broader terminal processes. However, *P. rammei* has appendices with broader terminal processes and lacks smaller terminal processes. The bridge of the epiphallus is also longer in *P. rammei* than in *P. femorata*. Additionally, our findings indicate that the lophi in *P. rammei* are smaller than those in *Loveridgacris*, contradicting Akbar and Kevan's claim that *Loveridgacris* has small lophi.

According to Kevan et al. (1974), *P. calabarica* and *P. rammei* are likely variations of *P. femorata* with smaller wings. Later, Kevan (1977) combined all three species into *P. femorata* based on their shared geographic range and morphological similarities. However, DNA evidence and differences in external morphology and phallic structures show that *P. femorata* and *P. rammei* are distinct species. Therefore, *P. rammei* should be recognized as a separate species within the genus *Parapetasia*.

The present study highlights the importance of combining multiple sources of information and DNA markers for the identification of Afrotropical grasshopper species of the genera *Parapetasia* and *Loveridgacris*.

Distribution

The type specimen of *P. rammei* was found in Bare-Dschang, a high-altitude location in western Cameroon. Two specimens at MfN labeled holotype (male) and allotype (female) were actually paratypes and collected from Bamenda and Bangwe in the northwestern region

of Cameroon. The true holotype, a female specimen, is housed in the Stockholm Museum. Seino and Njoya (2018) also collected *P. rammei* from the northwestern region of Cameroon, which is known for its high altitude. We found *P. rammei* in Fotouni in the western highlands and in the steppe habitats of the Manengouba Mountains. Our observations are supported by Rehn (1953), who suggested that *P. rammei* is limited to the highest areas of Cameroon. Our research, together with museum data, indicates that *P. femorata* inhabits forested areas in Western and Central African countries such as Cameroon, Equatorial Guinea, Gabon, and Nigeria. Although the species is widespread in Cameroon, its distribution in neighboring countries may be underestimated due to a lack of sampling. Hence, our results show that *P. femorata* and *P. rammei* occupy different ecological niches.

Loveridgacris impotens and *L. tectiferus* sp. nov. are found only in Tanzania and Kenya. Therefore, the genus *Parapetasia* is restricted to western and central Africa, while *Loveridgacris* is exclusive to East Africa. The new species *L. tectiferus* has to be considered a narrow range endemic, whereas *L. impotens* is widespread in eastern Africa.

Phylogeny

Although *Parapetasia* and *Loveridgacris* have been the subject of taxonomic discussions since I. Bolívar (1884), their taxonomy and systematic status have remained complex and challenging; thus, we provide the first attempt at a molecular phylogeny for the tribe Dictyophorini.

Our results divided the studied Pyrgomorphidae into three main tribes (Dictyophorini, Phymateini, and Taphronotini). Taphronotini, which includes a single species, *Taphronota calliparea*, is closely related to Dictyophorini, which includes three genera (*Dictyophorus*, *Loveridgacris*, and *Parapetasia*). In addition, the genera *Zonocerus*, *Phyteumas*, and *Phymateus* are closely related, indicating their inclusion in the tribe Phymateini. The close relationships among Pyrgomorphid tribes and genera have previously been documented by several authors. For instance, Kevan et al. (1974) suggested a close relationship between Taphronotini and Dictyophorini according to copulatory structures. Similarly, Mariño-Perez and Song (2018) reported a close relationship between Taphronotini and Dictyophorini, as well as among *Zonocerus*, including *Zonocerus variegatus*, and *Phymateus*, including *Phymateus saxosus*.

When comparing our tree with the molecular phylogeny of Zahid et al. (2021), we found concordance regarding the monophyly of Dictyophorini. Similarly, we found concordance regarding the monophyly of Phymateini when comparing our phylogenetic tree with the morphological phylogenetic tree by Mariño-Pérez and Song (2018). In addition, the monophyly of Phymateini recovered in our tree was not supported by the molecular phylogeny of Zahid et al. (2021), as this tribe was found to be paraphyletic. In addition, Mariño-Pérez and Song (2019) reported that *Monistria* Stål, *Dictyophorus*,

Phymateus, and *Poekilocerus* Serville were scattered throughout the phylogeny, forming paraphyletic groups. Such discordances in the topologies are not surprising, as previous studies, e.g., Baker et al. (1998), Friedrich et al. (2014), Kjer et al. (2016), and Peters et al. (2014), have demonstrated. However, as our study was limited in terms of taxon sampling to clarify the taxonomic position of *Parapetasia* and *Loveridgacris* species, we did not include many species from other tribes. Hence, we are not able to address these problems with our dataset.

We obtained robust evidence supporting the distinct status of the genus *Parapetasia*. Specifically, *Parapetasia rammei* has been confirmed as the sister taxon to *Parapetasia femorata*, and this distinction is further reinforced by morphological and phallic structure diagnostic traits. Furthermore, our phylogenetic tree revealed substantial genetic differentiation between the genera *Loveridgacris* and *Parapetasia*. Consequently, Kevan's (1977) proposal to synonymize *P. rammei* and *L. impotens* with *P. femorata*, primarily based on their shared geographic distribution and some morphological resemblances, is now questioned. This study marks the first integrative examination of the phylogeny of Dictyophorini, which revealed a consistently structured topology. Nonetheless, to fully resolve the phylogenetic relationships within Dictyophorini, it is imperative to include additional genera and their respective species in future investigations, as well as additional genetic markers.

The findings from the maximum likelihood (ML) and Bayesian inference (BI) analyses and the examination of the complete mitogenome indicate that it is challenging to establish a phylogenetic relationship between *L. impotens* and the newly described species *L. tectiferus* sp. nov. using the COI gene alone. Even the complete mitogenome revealed only minor divergence in this regard. Generally, it is likely that *L. tectiferus* sp. nov. represents a relatively young species in the early stages of speciation. To gain more conclusive insights into its taxonomic status and evolutionary trajectory, broader sampling of specimens is needed.

Conclusion

This study offers a reassessment of the Pyrgomorphid grasshopper genera *Parapetasia* and *Loveridgacris*, along with the first-ever analysis of the mitochondrial genome in the genus *Loveridgacris*. Our research unequivocally demonstrated that the genus *Parapetasia* comprises two distinct species, *P. femorata* and *P. rammei*, characterized by both pronounced morphological and genetic disparities. Additionally, we underscore the substantial differences, both morphologically and genetically, between the genera *Parapetasia* and *Loveridgacris*. Consequently, the previous doubts regarding their taxonomic position are dispelled. Therefore, we confirm that *Parapetasia* and *Loveridgacris* are unequivocally recognized as two distinct genera. Finally, we describe a new *Loveridgacris* species adding to the diversity of the group.

Dtsch. Entomol. Z. 71 (2) 2024, 265–287

285

Acknowledgments

References

Akbar SS, Kevan McEDK (1964) Two subgenera of Pyrgomorphidae (Orth., Acridoidea) raised to generic status on the basis of their phallic structures. Entomologist's Monthly Magazine 99: 90–95.

Baker RH, Yu X, DeSalle R (1998) Assessing the relative contribution of molecular and morphological characters in simultaneous analysis trees. Molecular Phylogenetics and Evolution 9(3): 427–436. https://doi.org/10.1006/mpev.1998.0519

Bolivar I (1904) Notas sobre los Pirgomorfidos (Pyrgomorphidae). Boletín de la Real Sociedad española de Historia natural 4: 89–111.

Bolivar I (1884) Monografia de los Pirgomorfinos. Anales de la Sociedad española de Historia natural 13: 419–500. [pls. 1–4]

Cigliano MM, Braun H, Eades DC, Otte D (2023) Orthoptera Species File. Version 5.0/5.0. http://Orthoptera.SpeciesFile.org [02.09.2023]

Dirsh VM (1956) The phallic complex in Acridoidea (Orthoptera) in relation to taxonomy. Transactions of the Royal Entomological Society of London 108(7): 223–356. https://doi.org/10.1111/j.1365-2311.1956.tb02270.x

Dirsh VM (1957) The spermatheca as a taxonomic character in Acridoidea (Orthoptera). Proceedings of the Royal Entomological Society of London. Series A, General Entomology 32(7–9): 107–114. https://doi.org/10.1111/j.1365-3032.1957.tb00380.x

Dirsh VM (1961) A preliminary revision of the families and subfamilies of Acridoidea (Orthoptera, Insecta). Bulletin of the British Museum (Natural History) Entomology 10: 351–419. https://doi.org/10.5962/bhl.part.16264

Dirsh VM (1965) The African genera of Acridoidea. Cambridge University Press for the Anti-Locust Research Centre, London, xiii + 579 pp.

Dirsh VM (1970) Acridoidea of the Congo (Orthoptera). Annales du Musée Royal de l'Afrique Centrale (série Sciences zoologiques), Tervuren 182: [6] + 605 pp.

Eades DC (2000) Evolutionary relationships of phallic structures of Acridomorpha (Orthoptera). Journal of Orthoptera Research 9(9): 181–210. https://doi.org/10.2307/3503648

Edgar RC (2004) MUSCLE: A multiple sequence alignment method with reduced time and space complexity. BMC Bioinformatics 5(1): 113. https://doi.org/10.1186/1471-2105-5-113

Folmer O, Black M, Hoeh W, Lutz R, Vrijenhoek R (1994) DNA primers for amplification of mitochondrial cytochrome *c* oxidase subunit I from diverse metazoan invertebrates. Molecular Marine Biology and Biotechnology 3: 294–299.

Friedrich F, Matsumura Y, Pohl H, Bai M, Hörnschemeyer T, Beutel RG (2014) Insect morphology in the age of phylogenomics: Innovative techniques and its future role in systematics. Entomological Science 17(1): 1–24. https://doi.org/10.1111/ens.12053

Grzywacz B, Warchałowska-Śliwa E, Kociński M, Heller K-G, Hemp C (2021) Diversification of the Balloon bushcrickets (Orthoptera, Hexacentrinae, *Aerotegmina*) in the East African mountains. Scientific Reports 11(1): 9878. https://doi.org/10.1038/s41598-021-89364-4

Hemp C, Kehl S, Schultz O, Wägele W, Hemp A (2015) Climatic fluctuations and topography as motor for speciation: case study on *Parepistaurus* Karsch, 1896 (Orthoptera: Acrididae, Coptacridinae). Systematic Entomology 40(1): 17–34. https://doi.org/10.1111/syen.12092

Hemp C, Heller K-G, Hemp A, Warchalowska-Sliwa E, Grzywacz B (2018) A molecular phylogeny of East African *Amytta* (Orthoptera: Tettigoniidae, Meconematinae) with data on their karyotypes. Systematic Entomology 43(2): 239–249. https://doi.org/10.1111/syen.12269

Hemp C, Scherer C, Brandl R, Pinkert S (2020) The origin of the endemic African grasshopper family Lentulidae (Orthoptera: Acridoidea) and its climate-induced diversification. Journal of Biogeography 47(8): 1805–1815. https://doi.org/10.1111/jbi.13880

Hochkirch A (1998) A comparison of the grasshopper fauna (Orthoptera: Acridoidea & Eumastacoidea) of the Uluguru mountains and the East Usambara mountains, Tanzania. Journal of East African Natural History 87(1): 221–232. https://doi.org/10.2982/0012-8317(1998)87[221:ACOTGF]2.0.CO;2

Johnston HB (1956) Annotated catalogue of African grasshoppers. Cambridge University Press for the Anti-Locust Research Centre, London, xxii + 883 pp.

Karsch F (1888) Beitrage zu Ignacio Bolivar's Monografia de los Pirgomorfinos (Madrid, 1884). Entomologisches Nachrichtenblatt (Vienna, Austria) 14(21): 328–335.

Kearse M, Moir R, Wilson A, Stones-Havas S, Cheung M, Sturrock S, Buxton S, Cooper A, Markowitz S, Duran C, Thierer T, Ashton B, Meintjes P, Drummond A (2012) Geneious Basic: An integrated and extendable desktop software platform for the organization and analysis of sequence data. Bioinformatics (Oxford, England) 28(12): 1647–1649. https://doi.org/10.1093/bioinformatics/bts199

Kevan DKM (1962) Pyrgomorphidae (Orthoptera: Acridoidea) collected in Africa by E.S. Ross and R.E. Leech, 1957–1958, with descriptions of new species. Proceedings of the California Academy of Sciences, fourth series 31(9): 227–248.

Kevan DKM (1977) Ordo Orthoptera s. str. (= Saltatoria-Caelifera) Subordo Acridodea Infraordo Acridomorpha Superfam. Acridoidea Fam. Pyrgomorphidae. In: Beier M (Ed.) Orthopterorum Catalogus, W. Junk, La Hague 16, iv + 656 pp. [+ 7 pp].

Kevan DKM, Akbar SS (1964) The Pyrgomorphidae (Orthoptera: Acridoidea): Their systematics, tribal divisions and distribution. Canadian Entomologist 96(12): 1505–1536. https://doi.org/10.4039/Ent961505-12

Kevan DKM, Akbar SS, Chang YC (1969) The concealed copulatory structures of Pyrgomorphidae (Orthoptera: Acridoidea). Part I. General introduction. Eos, Revista española de Entomología 44: 165–266.

Kevan DKM, Akbar SS, Chang YC (1972) The concealed copulatory structures of the Pyrgomorphidae (Orthoptera: Acridoidea). Part IV. Tribes Desmopterini, Monistriini, Chlorizeinini, Poekilocerini and Phymateini. Eos, Revista española de Entomología 47: 137–234.

Kevan DKM, Akbar SS, Chang YC (1974) The concealed copulatory structures of the Pyrgomorphidae (Orthoptera: Acridoidea). Part V. Tribes Schulthessiini, Taphronotini, Dictyophorini, Tagastini, Pseudomorphacridini, Atractomorphini, Sphenariini and Omurini. Eos, Revista española de Entomología 48: 203–294.

Kjer K, Borowiec ML, Frandsen PB, Ware J, Wiegmann BM (2016) Advances using molecular data in insect systematics. Current Opinion in Insect Science 18: 40–47. https://doi.org/10.1016/j.cois.2016.09.006

Mariño-Pérez R, Song H (2018) Phylogeny of the grasshopper family Pyrgomorphidae (Caelifera, Orthoptera) based on morphology. Systematic Entomology 43(1): 90–108. https://doi.org/10.1111/syen.12251

Mariño-Pérez R, Song H (2019) On the origin of the New World Pyrgomorphidae (Insecta: Orthoptera). Molecular Phylogenetics and Evolution 139: 106537. https://doi.org/10.1016/j.ympev.2019.106537

Martinelli AB, Waichert C, Barbosa DN, Fagundes V, Azevedo C (2017) The use of Proteinase K to access genitalia morphology, vouchering and DNA extraction in minute wasps. Anais da Academia Brasileira de Ciências 89(3): 1629–1633. https://doi.org/10.1590/0001-3765201720160825

Meng GL, Li YY, Yang CT, Liu S (2019) MitoZ: Atoolkit for animal mitochondrial genome assembly, annotation and visualization. Nucleic Acids Research 47(11): e63. https://doi.org/10.1093/nar/gkz173

Mestre J, Chiffaud J (2009) Acridiens du Cameroun et de République centrafricaine (Orthoptera Caelifera). Supplément au catalogue et atlas des acridiens d'Afrique de l'Ouest. http://acrida.info/PDF2009/Catalogue-Acridiens-2009.pd

Palumbi SR, Martin A, Romano S, McMillan WO, Stice L, Garbowski G (1991) The simple fools guide to PCR. A collection of PCR protocols, version 2. University of Hawaii, Honolulu.

Paxton RJ, Thorén PA, Tengö J, Estoup A, Pamilo P (1996) Mating structure and nestmate relatedness in a communal bee, *Andrena jacobi* (Hymenoptera, Andrenidae), using microsatellites. Molecular Ecology 5(4): 511–519. https://doi.org/10.1111/j.1365-294X.1996.tb00343.x

Perna NT, Kocher TD (1995) Patterns of nucleotide composition at fourfold degenerate sites of animal mitochondrial genomes. Journal of Molecular Evolution 41(3): 353–358. https://doi.org/10.1007/BF01215182

Peters RS, Meusemann K, Petersen M, Mayer C, Wilbrandt J, Ziesmann T, Donath A, Kjer KM, Aspöck U, Aspöck H, Aberer A, Stamatakis A, Friedrich F, Hünefeld F, Niehuis O, Beutel RG, Misof B (2014) The evolutionary history of holometabolous insects inferred from transcriptome-based phylogeny and comprehensive morphological data. BMC Evolutionary Biology 14(1): 52. https://doi.org/10.1186/1471-2148-14-52

Rambaut A (2010) FigTree v1.3.1. Institute of Evolutionary Biology, University of Edinburgh, Edinburgh. http://tree.bio.ed.ac.uk/software/figtree/

Rehn JAG (1953) Records and descriptions of Pyrgomorphinae (Orthoptera: Acrididae), with critical notes on certain genera. Transactions of the American Entomological Society 99: 99–149.

Rehn JAG (1954) Loveridgacris. Entomological News 65(5): 128.

Ronquist F, Teslenko M, Van Der Mark P, Ayres DL, Darling A, Hohn S, Larget B, Liu L, Suchard MA, Huelsenbeck JP (2012) MrBayes 3.2: Efficient Bayesian Phylogenetic Inference and Model Choice Across a Large Model Space. Systematic Biology 61(3): 539–542. https://doi.org/10.1093/sysbio/sys029

Rowell CHF (2013) The grasshoppers (Caelifera) of Costa Rica and Panama. The Orthopterists' Society, 611 pp.

Rowell CHF, Hemp C, Harvey AW (2015) Jago's Grasshoppers of East and North East Africa, Vol. 1: Pneumoridae, Pyrgomorphidae, Lentulidae, Pamphagidae, and Dericorythidae. San Francisco, Blurb Publishers, 237 pp.

Seino RA, Njoya MTM (2018) Species diversity of pyrgomorphidae (Orthoptera: Caelifera) grasshoppers in the North West region of Cameroon. International Journal of Zoology and Applied Biosciences 3(1): 104–109.

Song H, Amédégnato C, Cigliano MM, Desutter-Grandcolas L, Heads SW, Huang Y, Otte D, Whiting MF (2015) 300 million years of diversification: Elucidating the patterns of orthopteran evolution based on comprehensive taxon and gene sampling. Cladistics 31(6): 621–626. https://doi.org/10.1111/cla.12116

Tamura K, Stecher G, Kumar S (2021) MEGA11: Molecular Evolutionary Genetics Analysis Version 11. Molecular Biology and Evolution 38(7): 3022–3027. https://doi.org/10.1093/molbev/msab120

Zahid S, Mariño-Pérez R, Song H (2021) Molecular phylogeny of the grasshopper family Pyrgomorphidae (Caelifera, Orthoptera) reveals rampant paraphyly and convergence of traditionally used taxonomic characters. Zootaxa 4969(1): 101–118. https://doi.org/10.11646/zootaxa.4969.1.5

Dtsch. Entomol. Z. 71 (2) 2024, 265–287

287

Supplementary material 1

Complete mitochondrial genomes of *Loveridgacris impotens* and *Loveridgacris tectiferus* sp. nov.

Authors: Jeanne Agrippine Yetchom Fondjo, Martin Husemann, Armand Richard Nzoko Fiemapong, Alain Didier Missoup, Martin Kenne, Maurice Tindo, Oliver Hawlitschek, Tarekegn Fite Duressa, Sheng-Quan Xu, Wenhui Zhu, Claudia Hemp

Data type: tif

Explanation note: In this supplementary material, the mitogenomes of *Loveridgacris impotens* and *Loveridgacris tectiferus* sp. nov. are presented. The lenght of the genomes, their organization and nucleotide composition are also shown on the file.

Link: https://doi.org/10.3897/dez.71.125877.suppl1

Supplementary material 2

Genetic distance of the 13 protein-coding genes between *Loveridgacris impotens* and *Loveridgacris tectiferus* sp. nov.

Authors: Jeanne Agrippine Yetchom Fondjo, Martin Husemann, Armand Richard Nzoko Fiemapong, Alain Didier Missoup, Martin Kenne, Maurice Tindo, Oliver Hawlitschek, Tarekegn Fite Duressa, Sheng-Quan Xu, Wenhui Zhu, Claudia Hemp

Data type: tif

Explanation note: This supplemtary material shows the pairwise genetic distances inferred from all 13 protein-coding genes between *Loveridgacris impotens* and *Loveridgacris tectiferus* sp. nov.

Link: https://doi.org/10.3897/dez.71.125877.suppl2

Supplementary material 3

Localities and coordinates of *Parapetasia* and *Loveridgacris*

Authors: Jeanne Agrippine Yetchom Fondjo, Martin Husemann, Armand Richard Nzoko Fiemapong, Alain Didier Missoup, Martin Kenne, Maurice Tindo, Oliver Hawlitschek, Tarekegn Fite Duressa, Sheng-Quan Xu, Wenhui Zhu, Claudia Hemp

Data type: docx

Link: https://doi.org/10.3897/dez.71.125877.suppl3

PENSOFT.

MUSEUM FÜR
NATURKUNDE
BERLIN

The genus *Colydium* Fabricius in Europe (Coleoptera, Zopheridae, Colydiinae) with description of a new species, *Colydium noblecourti* sp. nov.

Guilhem Parmain[1,2], Andreas Eckelt[3], Rudolf Schuh[4]

1   INRAE, Laboratoire d'entomologie Forestière, Nogent sur Vernisson, Loiret, France

2   ONF, Laboratoire National d'Entomologie Forestière, Quillan, Aude, France

3   Tiroler Landesmuseen-Betriebsgesellschaft, Innsbruck, Austria

4   Kapellauweg 16, Katzelsdorf, Austria

https://zoobank.org/E585053C-4ECC-4F72-A226-F25C351B8B39

Corresponding author: Rudolf Schuh (rudolf.schuh@a1.net)

Abstract

A new species of the genus *Colydium* Fabricius, 1792 (Coleoptera, Zopheridae, Colydiinae), *Colydium noblecourti* **sp. nov.** is described. An illustrated and updated key for the identification of the Western Palearctic species of *Colydium* is presented. Distribution maps for the three species are provided.

Key Words

Introduction

The family *Zopheridae* Solier, 1834 is widely distributed throughout the world. In the Palearctic region, this family is represented by 287 species grouped into 46 genera (Schuh 2020). The genus *Colydium* was revised by Węgrczynowicz (1999) and currently contains 32 species. Until now, only two species in the genus *Colydium* were known to inhabit the Palearctic area: *Colydium elongatum* (Fabricius, 1787) and *Colydium filiforme* Fabricius, 1792 (Schuh 2020). They live under the bark of dead or dying trees inside the galleries of other wood-dwelling insects. Both species are members of the saproxylic guild (Alexander 2008), although the details of their ecology are largely unstudied. They may prey on other beetles or their larvae living under the bark, or they may only clean the galleries (commensalism) (Dajoz 1977; Węgrczynowicz 1999; Bouget et al. 2019).

The authors found two different morphological forms of *Colydium* Fabricius (tentatively assigned to *C. elongatum* (Fabricius, 1787)) during past ecological and faunistic research projects. Additionally, these forms were found to occur in several countries across Europe. This initiated the present study with the aim to resolve their identities. As a result, a new species of *Colydium* is described here and a key for the three Western Palearctic species of this genus is presented to provide means of reliable identification. Recent fieldwork has yielded additional geographic country records which, together with new data on their habitat, will contribute to a better understanding of their distribution and should facilitate further studies on their ecology.

Material and methods

We studied several private and institutional collections of *Colydium* specimens sampled throughout the West Palearctic region.

Acronyms for collections and depositories

AE	Andreas Eckelt collection, Austria
AJ	Anthony Jeanneau collection, France
BM	Bruno Mériguet collection, France
CASP	Czech Academy of Sciences, Prague, Czech Republic
CBF	Heinz Bussler collection, Feuchtwangen, Germany
CEW	Manfred Egger collection, Wattens, Austria
CHV	Carolus Holzschuh collection, Villach, Austria
CSW	Rudolf Schuh collection, Wiener Neustadt, Austria
CVM	Cyrille Van Meer collection, France
FA	Frédéric Arnaboldi collection, France
GP	Guillem Parmain collection, France
HB	Hervé Brustel collection, France
INRAE	National Institute for Agricultural and Environmental Research (INRAE) Nogent-sur-Vernisson, France
IR	Inaki Recalde Iruzun collection, Spain
KM	Kiel Natural History Museum, Germany
LF	Laurent Ferchaud collection, France
LuF	Ludovic Fuchs collection, France
LL	Laurent Lathuillière collection, France
LM	Lilian Micas collection, France
LNEF	Office National des Forets-Laboratoire National d'Entomologie Forestière Quillan, France
LV	Laurent Velle collection, France
MNHNP	Muséum National d'Histoire Naturelle, Paris, France
NME	Naturkundemuseum Erfurt, Germany
NMW	Naturhistorisches Museum Wien, Austria
OC	Olivier Courtin collection, France
OR	Olivier Rose collection, France
PM	Philippe Millarakis collection, France
PZ	Pierre Zagatti collection, France
RM	Raphael Megrat collection, France
SE	Sébastien Etienne collection, France
SNBS	Bavarian State Collection for Zoology, Munich, Germany
ST	Simon Thorn collection, Germany
TLF	Tiroler Landesmuseum Ferdinandeum, Innsbruck, Austria
ZFMK	Zoologisches Forschungsmuseum Alexander König, Bonn, Germany
ZMUO	Zoological Museum, University of Oulu, Oulu, Finland

Morphological measurements

Morphological terminology follows Lawrence and Ślipiński (2013). In most available identification keys, the pronotal length to width ratio (PL/PW) is used to separate *C. elongatum* from *C. filiforme*. However, Węgrczynowicz (1999) suggested that this measurement may be inefficient to separate the two species. Possibly, the third West Palearctic species described herein was complicating identification. We measured the total length to maximum elytral width ratio (TL/EW) and the pronotal length to maximum pronotal width ratio (PL/PW) of 313 specimens representing all three species to test the pertinence of this ratio. Morphometric analyses and maps were made using R and Vegan package (R Core Team, 2024). The distribution maps were made using the following packages: plotKML, rnaturalearth and ggplot2 (R Core Team 2024).

The following abbreviations will be used hereafter in the article:

EL	elytral length, along the suture from the base of the scutellum to the elytral apex
EW	elytral width between humeri
HW	maximum head width between the eyes
PL	pronotal length, along the midline
PW	maximum pronotal width
TL	total length from frontal margin of the epistoma to elytral apex

DNA sequencing and analysis

All mitochondrial cytochrome oxidase subunit 1 (COI) barcode sequences from 29 *Colydium* specimens as well as the outgroup sequence (*Lasconotus jelskii* (Wankow)) are accessed from the Barcode of Life Data System (BOLD; Ratnasingham and Hebert 2007). Samples from 14 *Colydium* individuals were collected by the authors (all samples from Austria and Italy) and made publicly available via BOLD. The COI barcode samples from all the *Colydium* specimens were processed at the Canadian Centre for DNA Barcoding (CCDB, Biodiversity Institute of Ontario, University of Guelph) according to the standard high-throughput protocol described in De Waard et al. (2008). We used the Kimura's 2-parameter model of nucleotide substitution and analytical tools in the BOLD systems v. 3.0. (http://www.boldsystems. org) to calculate the degree of intra- and interspecific variation of the COI barcode fragment. The maximum likelihood (ML) tree was constructed via the Phylosuite v.1.2.2 platform (Zhang et al. 2020). The following plugins were used: The alignment was performed with MAFFT v7.313 (Katoh and Standley 2013). The best fitting model was calculated with Modelfinder (IQ-TREE v.1.6.8) (Kalyaanamoorthy et al. 2017) and the maximum likelihood phylogenies were inferred using IQ-TREE v (Nguyen et al. 2015) under Edge-linked partition model for 1000 ultrafast (Minh et al. 2013) bootstraps. The tree was visualized with FigTree v1.4.4 (Rambaut 2015) and edited in Adobe Photoshop version 25 (Adobe Inc. (2024)).

The sequences are publicly available in the Dataset DS-COL0815 (*Colydium* species in Europe) on the BOLD homepage (https://www.boldsystems.org/index.php), and the respective BOLD-IDs are listed in Table 1.

Table 1. List of Sequence ID`s with country of origin and depository information.

BOLD-ID	Sample ID	COI-5P bp-Length	Country	Depository
TDAAT1092-20	ABOL-BioBlitz 2019 19-1071	614[0n]	Austria	NMW
FBCOB785-10	BC ZSM COL 01640	658[0n]	Germany	SNBS
PSFOR791-13	BC-PNEF-PSFOR0668	658[0n]	France	LNEF
FBCOJ850-13	BCZSM_COLA_01705	658[0n]	Austria	SNBS
FBCOJ851-13	BCZSM_COLA_01706	658[0n]	Austria	SNBS
FBCOJ852-13	BCZSM_COLA_01707	658[0n]	Austria	SNBS
FBCOJ854-13	BCZSM_COLA_01709	658[0n]	Austria	SNBS
FBCOH482-12	BFB_Col_FK_6466	605[0n]	Germany	SNBS
GBCOC535-12	GBOL_Col_FK_1770	658[0n]	Germany	SNBS
GBCOF156-13	GBOL_Col_FK_5571	658[0n]	Germany	SNBS
GBCOD830-13	GBOL_Col_FK_5770	658[0n]	Germany	SNBS
GBCOD950-13	GBOL_Col_FK_5985	627[0n]	Germany	SNBS
AALCO178-17	TLMF Col 00463	658[0n]	Italy	TLF
AALCO181-17	TLMF Col 00466	658[0n]	Austria	TLF
AALCO182-17	TLMF Col 00467	658[0n]	Austria	TLF
AALCO183-17	TLMF Col 00468	658[0n]	Austria	TLF
AALCO185-17	TLMF Col 00470	618[0n]	Austria	TLF
ABBAT203-16	TLMF Col. 00203	658[0n]	Austria	TLF
ABBAT204-16	TLMF Col. 00204	658[0n]	Austria	TLF
ABBAT205-16	TLMF Col. 00205	658[0n]	Austria	TLF
AALCO094-16	TLMF Col. 00379	658[0n]	Italy	TLF
GCOL7655-16	ZFMK-TIS-2511588	658[0n]	Germany	ZFMK
GCOL7678-16	ZFMK-TIS-2511657	658[0n]	Germany	ZFMK
GCOL7679-16	ZFMK-TIS-2511658	658[0n]	Germany	ZFMK
GCOL7680-16	ZFMK-TIS-2511659	658[0n]	Germany	ZFMK
GCOL11496-16	ZFMK-TIS-2530109	658[0n]	Germany	ZFMK
GCOL11624-16	ZFMK-TIS-2530820	658[0n]	Germany	ZFMK
GCOL12018-16	ZFMK-TIS-2532271	658[0n]	Germany	ZFMK
GCOL12030-16	ZFMK-TIS-2532288	658[0n]	Germany	ZFMK
LEFIJ2542-15	ZMUO.023616	658[0n]	Finland	ZMUO

Results

We studied 830 specimens of *Colydium* from various collections. Type specimens for the European species were studied through high quality pictures provided by Dr. Michael Kuhlmann from the Zoological Museum of Kiel University.
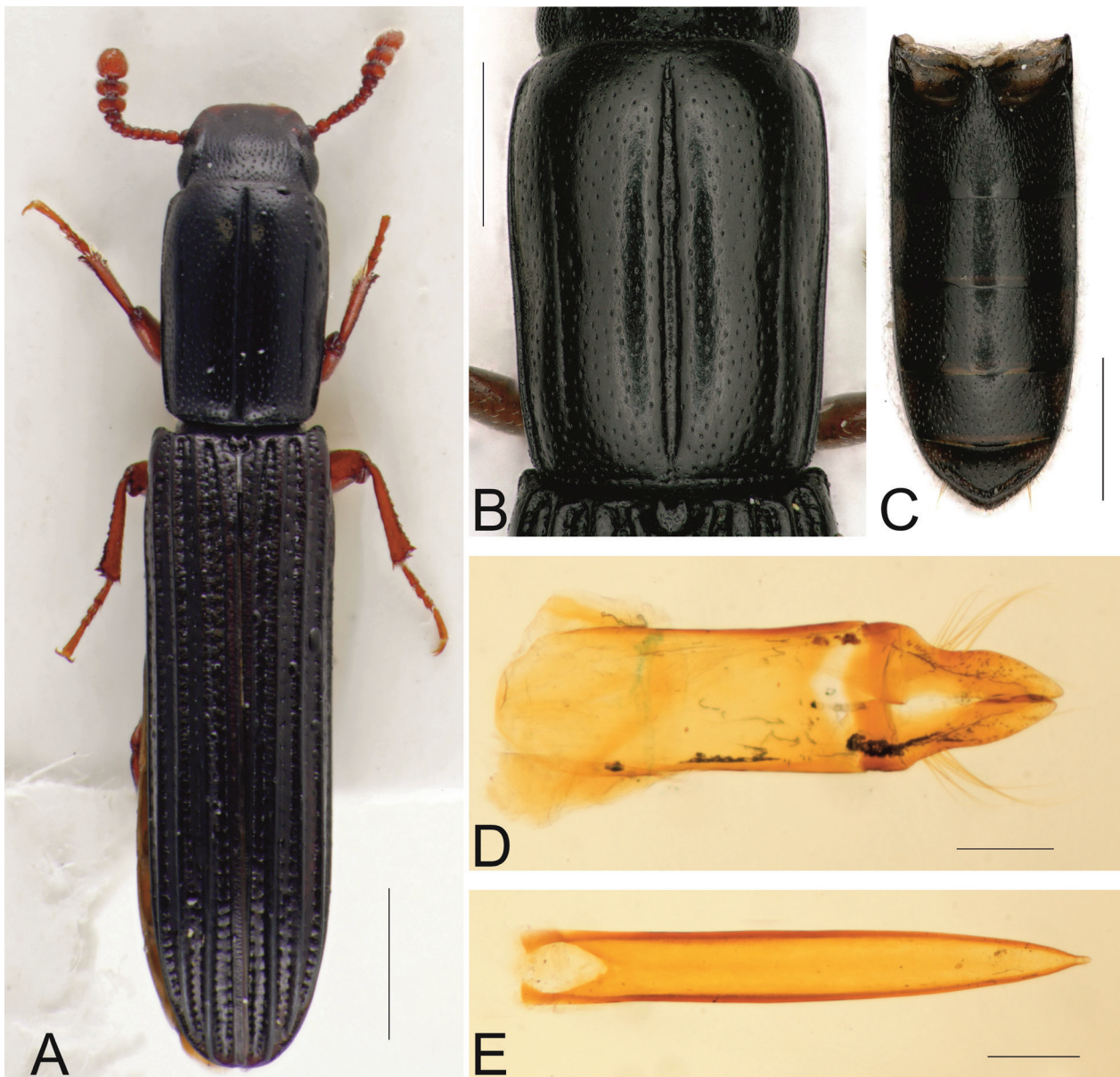
Colydium noblecourti sp. nov.

https://zoobank.org/F7254A03-E80C-458A-8B8A-73DD9CF22527

Figs 1A–E, 5, 6

Type locality. Austria, Wien, 13. Bezirk, Lainzer Tiergarten, Johannserkogel, 320 m a.s.l., 48°11'36"N, 16°13'10"E.

Type material. *Holotype* • ♂ (Fig. 1A–E); Original label: "AUT. W. Lainzer Tiergarten, Johannserkogel N, 16.21968/48.19335 320 m, 28.IV.2016 leg. Eckelt A." "DNA Barcode, TLMF Col 00203" "HOLOTYPE ♂, Colydium noblecourti sp.nov., des. Parmain, Eckelt and Schuh 2024 [red printed label]" (TLF). *Paratypes*. (250 exx.); **Andorra** • 1 ♀; La Massana; 16. Jan. 1998, H. Brustel leg. (HB) • 3 ♂; La Massana, 25. Feb. 2008, H. Brustel leg. (HB). **Austria** – **Wien** • 1 ♀; Lainzer Tiergarten; 24. Jul. 1965; Vogl leg. (CSW) • 1 ♂; Lainzer Tiergarten; 8. May 1996; E. Holzer leg. (CSW) • 1 ♂; Lainzer Tiergarten, 2. Jul. 1966; C. Holzschuh leg. (CSW) • 1 ♂; Lainzer Tiergarten, Johannser Kogel, Nordseite,

300 m a.s.l.; 19. Apr. 1995; M. Kahlen leg. (TLF) • 1 ex.; Lainzer Tiergarten, Aug. 1954; F. Schubert leg. (NMW) • 1 ex.; Lainzer Tiergarten, 29. Jul. 1951; C. Holzschuh leg. (CHV) • 1 ex.; Lainzer Tiergarten, 6. Sep. 1969; C. Holzschuh leg. (CHV) • 1 ex.; Lainzer Tiergarten, 14. May 2007; W. Hansely leg. (CSW) – **Niederösterreich** • 2 exx.; Wienerwald; Kubinyi leg. (CHV) • 1 ex.; Wien Umgebung, Mariabrunn; 22. May 1966; C. Holzschuh leg. (CHV) • 2 exx.; Lunz; Kaufmann leg. (NMW) • 1 ex.; Wien Umgebung; Haberditz leg. (NMW) • 1 ex.; Wien Umgebung; Hoffmann leg. (NMW) • 1 ex.; Klosterneuburg, Donau-Auen; 7. Apr. 1947; Lechner leg. (NMW) • 1 ex.; Klosterneuburg, Wienerwald; 8. Apr. 1947; Lechner leg. (NMW) • 2 exx.; Pressbaum; 21. Mar. 1948; Lechner leg. (NMW) • 1 ♂, 1 ♀; Bez. Wiener Neustadt, Bad Fischau, Kürassier, 400 m a.s.l.; 15. Apr. 1990; R. Schuh leg. (CSW) • 1 ♂, 1 ♀; Wiener Neustadt, 1 km SSE Feuerwerksanstalt; 7. Jan. 2007; R. Schuh leg. (CSW) • 1 ♀; Bez. Neunkirchen, Raxgebiet, Hinternasswald, 800 m a.s.l.; 23. May 2005; W. Hansely leg. (CSW) • 1 ♀; Wiener Neustadt, Föhrenwald; 10. Apr. 1993; R. Schuh leg. (CSW) • 1 ♂; Bez. Baden, Helenental, Hoher Lindkogel, Nordseite, Umg. Cholerakapelle, 300 m a.s.l.; 11. May 2024; R. Schuh leg. (CSW) • 1 ♂; Neulengbach; 2. Apr. 1980; A. Dostal leg. (CSW) – **Burgenland** • 6 ♂, 6 ♀; Bez. Mattersburg: Gruskogel Westseite 4 km SSW Marz; 450 m a.s.l.; 8. Apr. 2007; R. Schuh leg. (CSW) – **Steiermark** • 2 exx.; Bez. Hartberg-Fürstenfeld, Vorau;

28. Apr. 1958; C. Holzschuh leg. (CHV) • 3 ♂; Gams bei Frohnleiten; Gamsgraben; 47°18'23,5"N, 15°14'49,3"E; 25. Jul. 2011; A. Eckelt leg. (AE) • 2 exx.; Gams o F; Apr. 1966; (NMW) – **Kärnten** 8 exx.; Bez. Klagenfurt Land, Forchsee; 9. Mar. 1999; C. Holzschuh leg. (CHV, CSW) • 1 ex.; Bez. Villach Land: Gerlitzen, Deutschberg; 1300 m a.s.l.; 10. Jul. 2010; C. Holzschuh leg. (CHV) • 3 exx.; Bez. Spittal an der Drau, Siflitzberg; Konschegg leg. (NMW) • 2 exx.; Villach; Holdhaus leg. (NMW) • 1 ♀; Hermagor; 12. May 1964; C. Holzschuh leg. (CHV) • 1 ♀; Bez. Spittal an der Drau, Edling; 14. Feb. 1961; C. Holzschuh leg. (CHV) • 1 ♂; Bez. Klagenfurt Land, Kreuzbergl; 6. Mar. 1990; R. Preiss leg. (CSW) • 1 ex.; Eisenkappel; 20. Jun. 1968; (NMW) – **Osttirol** • 1 ex.; Lienz, Weg nach Bannberg; 2. Apr. 1967; A. Kofler leg. (TLF) • 1 ♂; Lienz, Tristacher See; 26. Jul. 1961; C. Holzschuh leg. (CHV) – **Tirol** 1 ex.; Karwendel, Absam N, Egg SW, Heuberg-Latschen; 985 m a.s.l.; 10. Apr.– 8. May 2016; M. Kahlen leg; window trap (TLF) • 1 ex.; Karwendel, Absam N, Egg SW, Heuberg-Flecke; 1000–1050 m a.s.l.; 20. Dec. 2015; M. Kahlen leg. (TLF) • 1 ex.; Karwendel, Absam N, Egg SW, Heuberg-Latschen; 1036 m a.s.l.; 8. May – 7. Jun. 2016; M. Kahlen leg.; window trap (TLF) – **Oberösterreich** • 1 ♀; NP Kalkalpen, Brandfläche Hagler; 47°46'24"N, 14°17'48"E; 1500 m a.s.l.; 7. Jul. 2011; A. Eckelt leg. (AE) • 1 ♀; NP Kalkalpen, Bodinggraben, östl. Gamskitzgraben; 47°47'03,1"N, 14°22'16,5"E; 700 m a.s.l.; 7. Jul. 2011; A. Eckelt leg. (AE). **Bosnia** • 3 exx.; District Mostar, Blagaj; 12. Apr. 1920 (NMW). **Croatia** • 1 ♀; ex coll. Oberthür; (CSW). **Czech Republic** 5 ♂, 1 ♀; floodplain of Lower Morava, Dyje; 24. Apr.–16. May 2012; S. Vodka, D. Hauck & L. Cizek leg. (CASP) • 2 ♀; Beskiden [Beskydy mountains]; Borth leg. (CSW, CHV) • 1 ♂; Moravia, Brno; 22. Feb. 1997; P. Čechovsky leg. (CSW) • 1 ♂; central Bohemia, Loučeň; 21. May 2004; L. Daněk leg. (CSW). **France** • 1 ex.; Aube, Maraye-en-Othe; 14. Apr. 2007; F. Soldati leg. (LNEF) • 2 exx.; Loiret, Nogent-sur-Vernisson, Domaine des Barres; 20. Jun. 2022; G. Parmain & C. Moliard leg. (GP) • 1 ♂,1 ♀; Loiret, Nogent-sur-Vernisson, Domaine des Barres; 3. May 2023; G. Parmain & C. Moliard leg. (GP) • 1 ♀; FD Bercé; 13. May 2014; A. Jeanneau leg. (AJ) • 1 ♀; Bois du Château d'Angervilliers; 27. May 2020; B. Mériguet leg. (BM) • 1 ♂, 2 ♀; FD Chantilly; 27. Apr. 2022; C. Moliard leg. (GP) • 2 ♂, 6 ♀; FD Chantilly; 25. May 2022; C. Moliard leg. (GP, INRAE) • 1 ♂, 1 ♀; FD Rambouillet; 3. Feb. 2004; F. Arnaboldi leg. (FA) • 1 ♀; Rambouillet; 19. Mar. 2003; B. Mériguet leg. (PZ) • 1 ♂; FD Rambouillet; 30. May – 30. Jun. 2006; C. Bouget leg. (INRAE) • 1 ♂; FD Rambouillet; 25. Sep. 2006; C. Bouget leg. (INRAE) • 1 ♀; FD Hautil; 21. Jul. 2003; F. Arnaboldi leg. (FA) • 1 ♀; Forêt de St Colombe; 23. Feb. 1999; H. Brustel leg. (HB) • 1 ♂; Armainvilliers; 10. May 2001; C. Bouget leg. (INRAE) •2 ♂, 1 ♀; Armainvilliers; 11. May 2001; C. Bouget leg. (INRAE) • 1 ♀; Armainvilliers; 8. Jun. 2001; C. Bouget leg. (INRAE) • 3 ♂, 2 ♀; Belesta; 13. Jun. 2017; C. Bouget leg. (INRAE)" • 3 ♀; Belvis; 13. Jun.

2017; C. Bouget leg. (INRAE) • 1 ♂; Belvis; 13. Jun. 2017; C. Bouget leg. (PZ) • 1 ♂; Belvis; 1. Jul. 1997; LNEF staff leg. (LNEF) • 1 ♀; Espezel; 13. Jun. 2017; C. Bouget leg. (INRAE) • 1 ♀; FD Karstenwald; 3. Jun. 2009;C. Bouget leg. (INRAE) • 1 ♀; FD Orléans; 6. Jun. 2019; INRAE staff leg. (INRAE) • 1 ♂, 1 ♀; Ferrières-en-brie; 10. May 2001; C. Bouget leg. (INRAE) • 1 ♀; Ferrières-en-brie; 11. May 2001; C. Bouget leg. (INRAE) • 1 ♂; Ferrières-en-brie; 8. Jun. 2001; C. Bouget leg. (PZ) • 1 ♀; Ferrières; 10. May – 5. Jun. 2001; C. Bouget leg. (INRAE) • 1 ♂, 1 ♀; Fougax-et-Barrineuf; 13. Jun. 2017; C. Bouget leg. (INRAE) • 8 ♂, 4 ♀; Gambaseuil; 24. Apr. 2007; C. Bouget leg. (INRAE) • 1 ♀; Gambaseuil; 24. Apr. 2007; C. Bouget leg. (PZ) • 2 ♂, 1 ♀; Gex; 20. Jul. 2013; C. Bouget leg. (INRAE) • 1 ♀; Saint-Laurent; 30. May 2016; C. Bouget leg. (INRAE) • 1 ♀; Saint-Laurent-du-Pont; 23. Jun. 2014; P. Janssen leg. (INRAE) • 6 ♂, 2 ♀; Vouzeron; 30. May 2016; C. Bouget leg. (INRAE) • 1 ♀; Bussac; 21. May – 4. Jun. 2019; LNEF staff leg. (LNEF) • 1 ♀; FD Verrières; 14. – 22. Apr. 2003; LNEF staff leg. (LNEF) • 1 ♀; Nebias; 8. Mar. 1994; LNEF staff leg. (LNEF) • 1 ♀; RNN Cerisy; 29. Apr. 2018; S. Etienne leg. (LNEF) •1 ♀; RNN Cerisy; 16. May 2018; S. Etienne leg. (LNEF) • 1 ♀; Ft. pays des étangs; 2. May 2018; L. Fuchs leg. (LuF) • 1 ♀; Marckolsheim, RB Rhinvald; 9. May 2018; L. Fuchs leg. (LuF) • 1 ♂; FD Campagne; 4. Jun. 2019; L. Velle leg. (LV) • 1 ♂; FD Campagne; 12. May 2021; L. Velle leg. (LV) • 1 ♀; FD Campagne; 9. Jun. 2021; L. Velle leg. (LV) • 1 ♀; Saint-Maurice; 15. Jun. 2010; O. Rose leg. (OR) • 1 ♀; Bareilles; 14. Jun. 2017; C. Bouget leg. (PZ) • 1 ♂; Le Val St Germain; 25. May 2021; B. Mériguet leg. (BM) • 1 ♂; Larrau (Iraty); 22. Feb. 2017; C. Van Meer leg. (CVM) • 1 ex.; Pyrénées Atlantiques, Iraty, Forêt d'Iraty; 5. Jun. 1998; H. Brustel leg. (CSW) • 1 ♂; Ardengost; 14. Jun. 2017; C. Bouget leg. (INRAE) •1 ♂; Comus; 13. Jun. 2017; C. Bouget leg. (INRAE) • 1 ♂; Hèches; 14. Jun. 2017; C. Bouget leg. (INRAE) • 1 ♂; Niort-de-Sault; 13. Jun. 2017; C. Bouget leg. (INRAE) • 1 ♂; FD Vierzon-Vouzeron; 7. May 2019; Canopee team leg. (INRAE) • 2 ♂; FD Fontainebleau; 13–15. May 2008; LNEF staff leg. (LNEF) • 1 ♂; FD St. Antoine; 22. May 2021; LNEF staff leg. (LNEF) • 1 ♂; Combe Lavaux; 18. May 2021; LNEF staff leg. (LNEF) • 1 ♂; ZNIEFF Puits d'Enfer; 4. May 2021; LNEF staff leg. (LNEF) • 1 ♂; La Broque; 25. Apr. 2011; L. Fuchs leg. (LuF) • 1 ♂; La Wantzenau, RB confluence III-Rhin; 7. May 2018; L. Fuchs leg. (LuF) • 1 ♂; La Wantzenau, RB confluence III-Rhin; 22. May 2018; L. Fuchs leg. (LuF) • 1 ♂; La Wantzenau, RB confluence III-Rhin; 16. Jul. 2018; L. Fuchs leg. (LuF) • 1 ♂; FD Vallée Doller, Oberbruck; 31. May 2017; L. Fuchs leg. (LuF) • 1 ♂; FD Vallée Doller, Oberbruck; 26. Jul. 2017; L. Fuchs leg. (LuF) • 1 ♂; FD Vallée Doller, Oberbruck; 1. Jun. 2018; L. Fuchs leg. (LuF) • 1 ♂; FD Vierzon-Vouzeron; 16. May 2014; L. Velle leg. (LV) • 1 ♂; Saint-Barthélemy-de-Séchilienne, ile Falcon; 13. Aug. 2019; Y. Braud leg. (OC) • 1 ♂; Saint-Barthélemy-de-Séchilienne, ile Falcon; 17. Aug. 2019; Y. Braud leg. (OC) •1 ♂; Moussey;

Figures 1. A–E. Holotype of *Colydium noblecourti* sp. nov. **A.** Dorsal view; **B.** Dorsal view of pronotum; **C.** Ventral view of abdomen; **D.** Tegmen; **E.** Median lobe. Scale bars: 0.5 mm (**A–C**); 0.1 mm (**D, E**).

24. May 2011; O. Rose leg. (OR) • 1 ♂; Sturzelbronn; 30. Apr. 2015; P. Millarakis leg. (PM) • 1 ♂; FD de Brotonne; 23. May 2017; S. Etienne leg. (SE) • 1 ♂; FD de Brotonne; 6. Jun. 2017; S. Etienne leg. (SE) • 1 ♂; FD de Brotonne; 29. May 2018; S. Etienne leg. (SE). **Germany – Bayern** • 1 ex.; Scheidegg, NSG Rohrbachtobel; Jun. 2017; H. Bussler leg. (CBF) • 1 ex.; Ebrach, Brunnst.; 15. May 2017; S. Thorn leg. (ST) • 3 ♂, 3 ♀; Rauhenebrach; 16. Aug. 2016; S. Thorn leg. (ST) • 2 exx.; Rauhenebrach; 18. Aug. 2016; S. Thorn leg. (ST) • 3 exx.; Rauhenebrach; 25. Aug. 2016; S. Thorn leg. (ST). **Iran** • 1 ex.; Prov. Mazandaran, Now Shahr, Kheiroud Kanar Forest; 40–200 m a.s.l.; 36°36'35"N, 51°34'10"E; 3–4. May 2010; D. Frenzel leg. (NME). **Italy** • 1 ex.; Süd-Tirol [= prov. Alto Adige], Burgraviato, Bad Grill W, Gampental; 1300 m a.s.l.; 22.Jul. 2013; M. Kahlen leg. (TLF). **Slovakia** • 1 ♀; Hronská Dúbrava; 26. Apr. 2000; P. Hlaváč leg.

(CSW) • 1 ♂; Bratislava, Badín; 21. Oct. 1987; I. Martinů leg. (CSW) • 1 ♀; "Hungaria: Neutraer Comitat" [= Slovakia: District Nitra]; (CSW). **Slovenia** • 18 exx.; Buje – Kozanje; 30. May 2010; M. Egger leg. (CEW, CSW) • 3 exx.; "Carniolia: Gottschee" [=Kočevje]; 1911; Naser leg. (NMW) • 3 exx.; "Untersteiermark: Windisch Landsberg" [= region Štajerska: Podčetrtek]; 1882; Ganglbauer leg. (NMW). **Spain** • 1 ex.; Prov. León, Ponferrada; Paganetti leg. (NMW). **Turkey** • 1 ex.; N Anatolia, Yenice – Karabük; May 1962; F. Schubert leg. (NMW).

Additional material. 1 ♂ (KM): "No locality on labels, no date. Paralectotypus *Bostricilus elongatus* Fabricius des. P. Wegrzynowicz". This specimen was included as a paralectotype of *Colydium elongatum* (Fabricius) by Węgrczynowicz (1999). Genitalia of this specimen were recently dissected and our studies revealed that it does not belong to *C. elongatum* but rather to *C. noblecourti*

sp. nov.. We identified this specimen by only using high resolution photographs of it and its genitalia provided by Dr. Michael Kuhlmann (KM) and were not able to study the specimen itself. Therefore, we refrain from listing it as a paratype of *C. noblecourti* sp. nov..

Etymology. The new species *Colydium noblecourti* sp. nov. is named after Thierry Noblecourt, one of the mentors of the first author. Noblecourt worked in the French National Forest Office (ONF) for many years. He developed a network of French entomologists, made huge contributions to the general knowledge of saproxylic beetles in France and raised public interest in these insects. Noblecourt is also a specialist in Symphyta (Hymenoptera) and has described several new species. The name *noblecourti* is a noun in the genitive case derived in honour of Thierry Noblecourt.

Description. *Habitus.* (TL 5.1–7.4 mm) relatively robust; head, pronotum, elytra and ventral side uniformly black (except in teneral specimens); legs and antennae reddish brown. Fig. 1A.

Head. (HW/PW: 0.78–0.88) Lateral margins of frons and epistoma converging towards apex, anterior margin of epistoma straight, with yellow setation; periocular carinae as long as eye. Punctures on central part of frons elongate, distance between them about 1 to 2 diameters; punctures denser and more circular on the fronto-epistomal depression. Antennomere 1 not completely visible in dorsal aspect, 1.2 times as long as wide; antennomere 2 narrower, 1.25 times as long as wide; antennomere 3 of same width as 2 and 1.2 times as long as wide; antennomeres 4 to 7 of same width (length to width ratios: 4: 1.0; 5: 1.0; 6: 0.8; 7: 0.6); antennomere 8 slightly wider than the preceding ones and 1.75 times as wide as long; antennomeres 9 to 11 form a three-segmented club (2.5 times as wide as the funicule), antennomere 9 wider than preceding ones, twice as wide as long; antennomere 10 is 1.1 times wider than 9, twice as wide as long; antennomere 11 narrower than 10 and 1.1 times as wide as long. Setation of antennomeres 4 to 8 similar in both sexes, a few longer setae occur on the inner side of antennae; antennomeres 9, 10 and 11 densely setose.

Pronotum. (PL/PW: 1.27–1.56) (Fig. 1B) In dorsal view lateral margins slightly diverging from base to apical quarter in straight line, then slightly narrowing apicad; anterior angles narrowly rounded; lateral margin bordered from base to apex; apical margin not bordered near anterior angles. Median line sulciform from anterior margin to basal transverse groove. Admedian lines slightly impressed (never sulciform), more or less obsolete on anterior third. Punctures on disc slightly elongate and 2 to 4 diameters apart. Microsculpture punctiform, microreticulated near anterior angles. Pronotal hypomera with round, small punctures, four diameters apart. Prosternum smooth, transversely wrinkled.

Elytra. (EL/EW: 3.00–3.31) Parallel-sided in dorsal view; humeral angles protruding forward; elytral apices conjointly broadly rounded. Striae slightly impressed; strial punctures separated from each other by a distance of 1 to 2 diameters. Sutural interval (= interval 1) raised, but not carinate except laterally along scutellary striole, flat–topped and finely wrinkled along most of its length. Uneven intervals bluntly carinate; carina on interval 3 reaching elytral apex; carina on interval 5 not reaching elytral apical rim; carina on interval 7 still shorter. Even intervals flat, smooth, indistinctly transversely wrinkled.

Ventral side of pterothorax. Mesanepisterna roughly and densely punctured. Metaventrite with complete median sulcus; very finely punctured, except for an area posterior to mesocoxae with larger punctures, partly connected by irregular lines. Metanepisterna smooth. Abdominal ventrites (Fig. 1C) shiny, weakly microreticulate, finely punctured; punctures separated by a distance of 3 to 4 diameters, each bearing very short seta; sculpture on ventrite 1 consisting of irregular wavy or zigzag lines, forming a scaly pattern; sculpture on ventrite 2 consisting of a few irregular lines or wrinkles, particularly laterad; ventrite 5 with a deep preapical groove, apical margin obtusely angled in the middle in both sexes, setose and with two groups of long setae laterally. Relative lengths of ventrites: 1: 1.9–2.2; 2: 1.3–1.5; 3: 1.2–1.4; 4: 1.0–1.2; 5: 1.0. *Male genitalia.* Tegmen (Fig. 1D) 4 times as long as its maximum width; basal part 2.5 times longer than parameres; parameres in dorsal aspect lamelliform, narrowed apicad, in lateral aspect s-shaped, continuously narrowed to tip; not lying in same plane, but inclined toward each other at a blunt angle; median lobe (Fig. 1E) 8 to 9 times as long as wide, 1.5 times longer than tegmen; in dorsal aspect almost parallel-sided, narrowing continuously from mid–length to apex; in lateral aspect slightly bent; apex prolonged into a narrow tip.

Variability some characters are subject to a certain degree of variation. Body proportions vary, as shown in the morphological measurements sections below. The admedian lines on the pronotum vary considerably: from absent in some specimens, only detectable by an elongate, narrow depression (minimal development) to an impressed, but irregularly interrupted line (maximal development). Elytral carina 5 is never completely connected to the apical elytral margin, but in a few cases it may reach it. The sculpture on the lateral parts of abdominal ventrite 2 is generally shallow. The extent of the sculptured area is variable.

Differential diagnosis. *Colydium noblecourti* sp. nov. can be distinguished from the two other European species of *Colydium* as follows:

From *Colydium elongatum* (Fabricius) (Fig. 2A–E) *Colydium noblecourti* sp. nov. differs in the uniformly black colour of its elytra (humeral region brown or elytral base obscurely reddish in *C. elongatum*); pronotum more globose apically; admedian lines weak, irregular and interrupted or absent; anterior pronotal angles not bordered by a prolongation of the lateral marginal line; carina on elytral interval 5 not reaching elytral apical rim; sculpture on the lateral parts of abdominal ventrites 2, 3 and 4 is less developed than on ventrite 1, or even absent, and never similar to ventrite 1; apical margin of abdominal ventrite 5 is obtusely angled in the middle (semicircular in *C. elongatum*); aedeagus with parameres that are
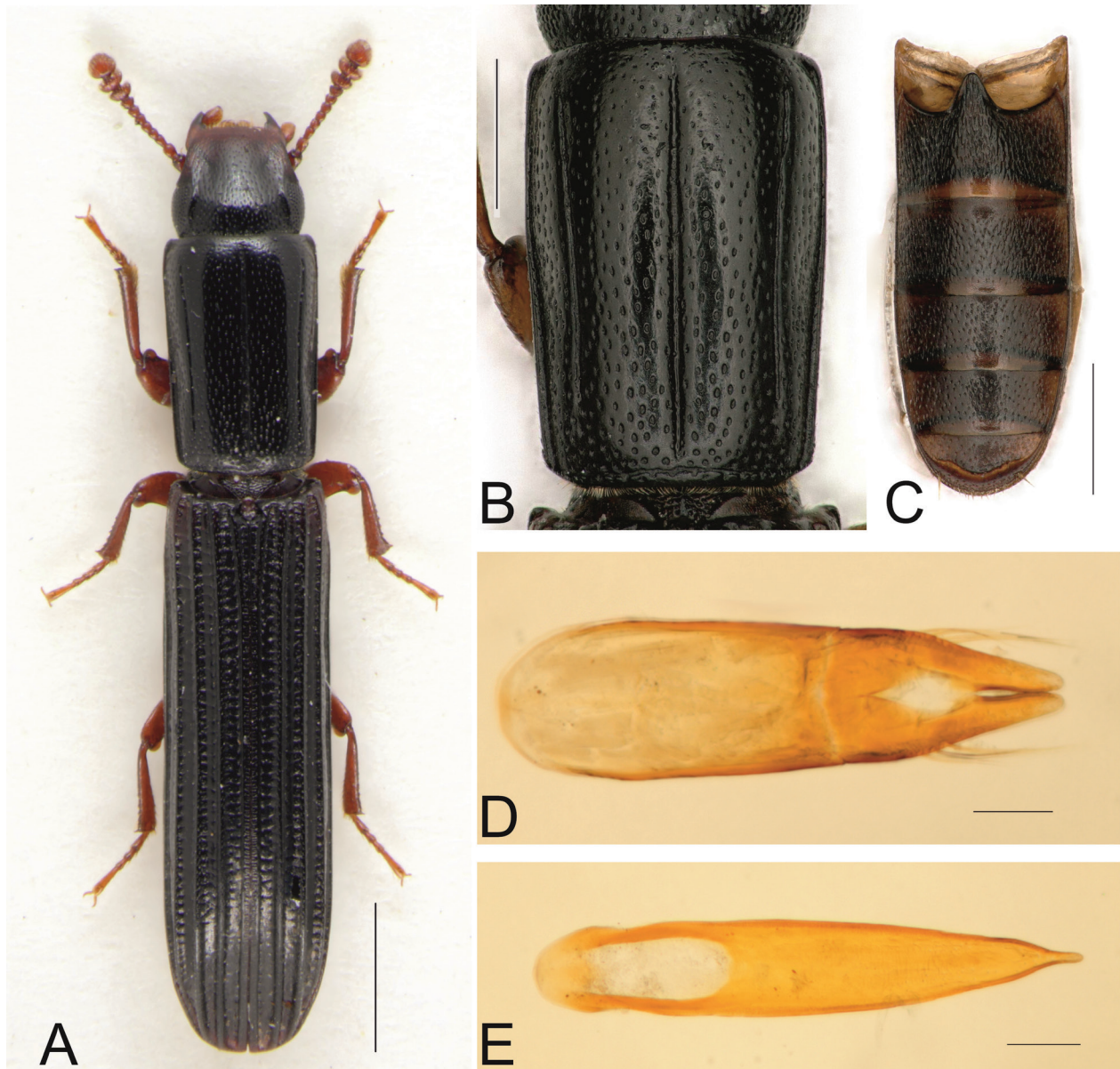
Figures 2. A–E. *Colydium elongatum* (Fabricius). **A.** Dorsal view; **B.** Dorsal view of pronotum; **C.** Ventral view of abdomen; **D.** Tegmen; **E.** Median lobe. Scale bars: 0.5 mm (**A–C**); 0.1 mm (**D, E**).

broader lamelliform, s-shaped in lateral aspect, inclined toward each other, not lying in the same plane (straight or slightly bent and narrow in *C. elongatum*).

From *Colydium filiforme* Fabricius (Fig. 3A–E) *Colydium noblecourti* sp. nov. differs in uniformly black colour of its elytra (elytral base distinctively reddish in *C. filiforme*); pronotum in general less elongate, PL/PW up to 1.56 (PL/PW up to 1.65 in *C. filiforme*) and more globose apically; admedian lines weak, irregular and interrupted or absent; anterior pronotal angles not bordered by a prolongation of the lateral marginal line; sculpture on the lateral parts of abdominal ventrites 2, 3 and 4 less developed than on ventrite 1, or even absent, never similar to ventrite 1; apical margin of abdominal ventrite 5 obtusely angled in the middle (semicircular in *C. filiforme*); aedeagus with longer median lobe, its apex is acutely angled but never prolonged into a narrow tip.

Distribution. We assume a similar distribution range as for *Colydium elongatum*. To date, *Colydium noblecourti* sp. nov. has been recorded in the following countries: Austria, Andorra, Bosnia, Croatia, Czech Republic, France, Germany, Iran, Italy, Slovakia, Slovenia, Spain and Turkey (Fig. 6).

Distribution maps of the studied material are presented for *Colydium noblecourti* sp. nov. (Fig. 6), *C. elongatum* (Fig. 7) and *C. filiforme* (Fig. 8). Since C. *filiforme* is well separated from the other European species of *Colydium*, we include locality records from Węgrczynowicz (1999).

Bionomics. The specimens were found on dead or decaying wood of the following tree genera: *Picea* A. Dietrich spp., *Abies* Miller spp., *Pinus* Linné spp. (all Pinaceae), *Fagus* Linné spp., *Quercus* Linné spp. (both Fagaceae), and *Carpinus* Linné spp. (Betulaceae).
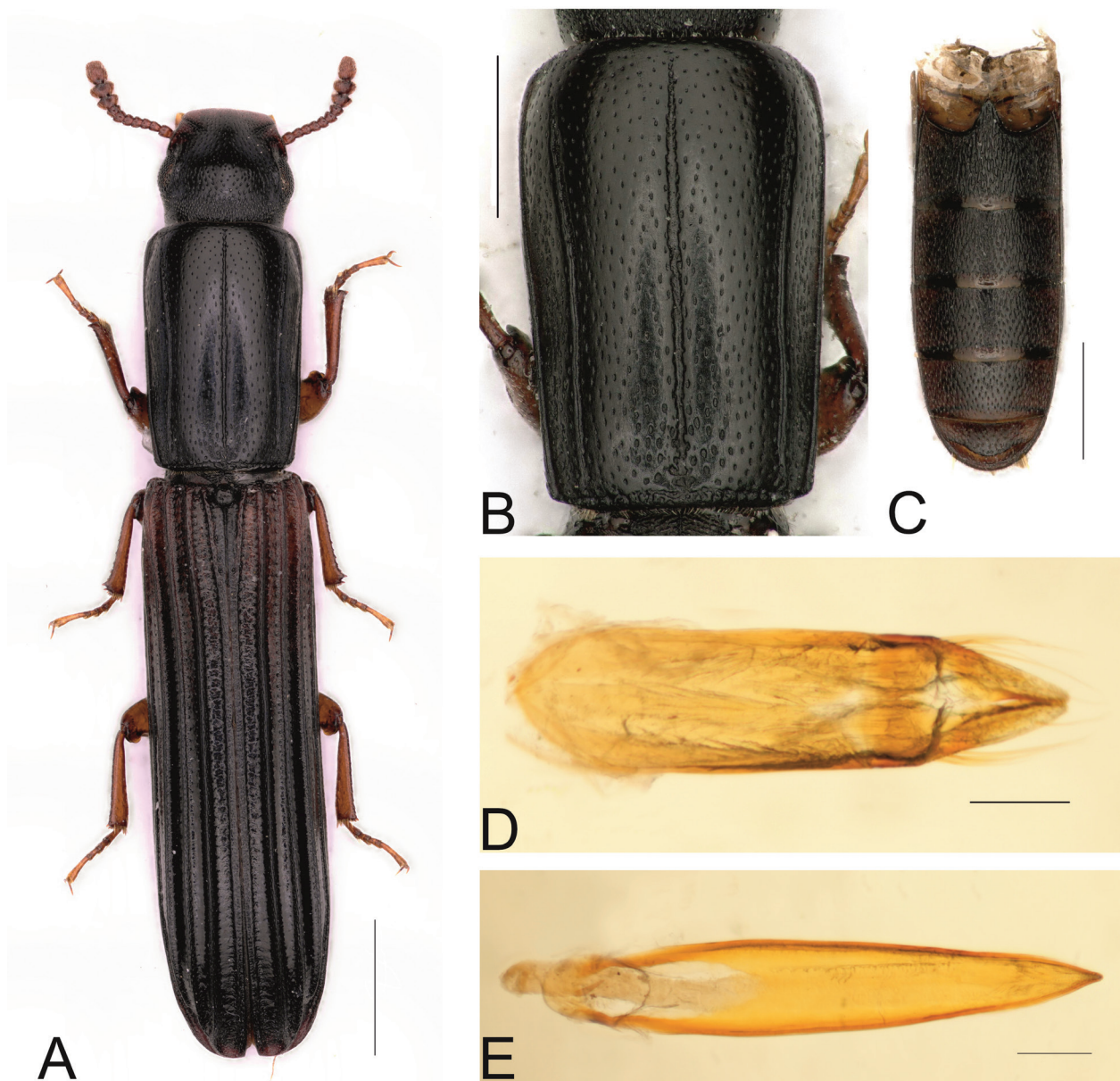
Figures 3. A–E. *Colydium filiforme* Fabricius. **A.** Dorsal view; **B.** Dorsal view of pronotum; **C.** Ventral view of abdomen; **D.** Tegmen; **E.** Median lobe. Scale bars: 0.5 mm (**A–C**); 0.1 mm (**D, E**).

Genetic analysis

A maximum likelihood tree analysis was derived from COI barcode sequences of the three European species of the genus *Colydium*. Forming distinct clades, the support values (bootstrap with 1,000 replicates) show a robust backing for the new *Colydium* species (Fig. 4). Considering a mean interspecific distance of 4.83% (minimum 4.1%, maximum 5.6%) within the genus, *C. noblecourti* sp. nov. shows a distance of 4.3% to its closest neighbour, *Colydium filiforme* Fabricius, 1792, while the distance is more than 4.5% to *Colydium elongatum* (Fabricius, 1787).

The sequences are publicly available in the Dataset DS-COL0815 (*Colydium* species in Europe, https://dx.doi.org/10.5883/DS-COL0815) on the BOLD homepage (https://www.boldsystems.org/index.php), and the respective BOLD-IDs are listed in Table 1.

Morphological measurements

The total length to elytral width ratio (TL/EW) (Fig. 5A) does not show distinct clusters for the three species. There is mutual overlap, which does not allow a clear separation of the species by body shape alone. *Colydium filiforme* has a small range, from 4.62 to 5.28 (mean = 4.91; SD = 0.15); *Colydium elongatum* has a wide range, from 3.81 to 5.19 (mean = 4.71; SD = 0.18); and *Colydium noblecourti* sp. nov. a small range from 4.20 to 4.82 (mean = 4.60; SD = 0.13).

A similar situation can be seen for the proportions of the pronotum. The results of our measurements show no significant specific differences in the PL/PW-ratios (Fig. 5B). *Colydium filiforme* has a range, from 1.42 to 1.65 (mean = 1.53; SD = 0.05), *Colydium elongatum* from 1.35 to 1.58 (mean = 1.47; SD = 0.04) and *Colydium noblecourti* sp. nov. from 1.37 to 1.56 (mean = 1.46; SD = 0.04).
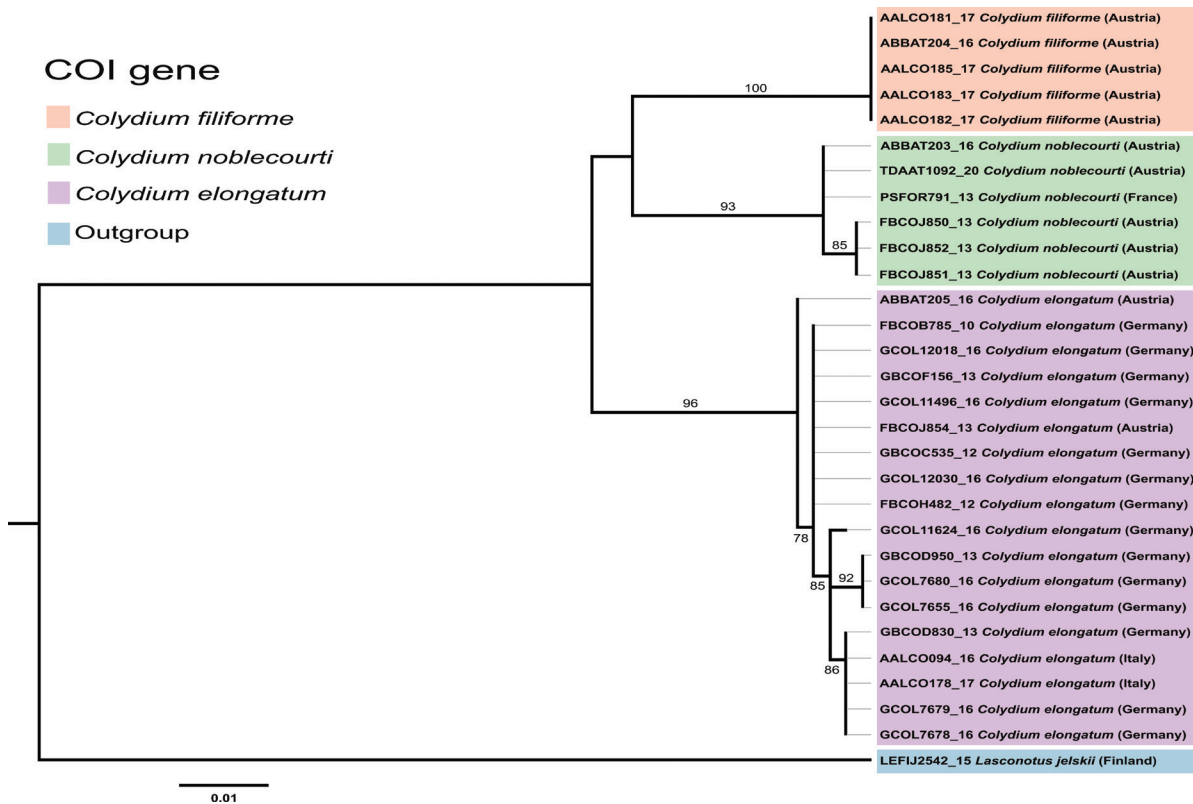
Figure 4. ML tree, based on COI barcode data for *Colydium* specimens from Austria, France, Germany and Italy. The fine, light grey branches that connect labels are not to scale. Support values (bootstrap with 1,000 replicates) are indicated on the respective branches.

The differences in the PL/PW-ratios and the TL/EW-ratios show, at most, slight specific tendencies in proportions of pronotum and body, but without diagnostic value. The PCA analysis (Fig. 5C) reflects this situation, as there is no obvious clustering of the specific data.

Ecology of Western Palearctic species of Colydium

All previous publications on the ecology and biology of Palearctic *Colydium* show similar behaviour for all the species (Dajoz 1977; Węgrczynowicz 1999; Bouget et al. 2019). They live in the galleries of other saproxylic beetles. There is no clear evidence as to whether they are predators or cleaners, or possibly both depending on the stage of development (larva or adult). They are associated with different tree species.

Colydium elongatum (Fabricius) inhabits deciduous trees like *Quercus* Linné spp., *Fagus sylvatica* Linné and *Juglans regia* Linné (Juglandaceae), at least in Central Europe, but it has also been reported from coniferous trees (*Abies* Miller spp.) in France and Greece.

Colydium filiforme Fabricius has hitherto been found exclusively on *Quercus* Linné spp.

Colydium noblecourti sp. nov. seems to show a slight preference for coniferous trees (*Pinus* Linné spp., *Abies alba* Miller, *Picea abies* (Linné) H.Karsten), although it has also been found on deciduous trees like *Fagus sylvatica* Linné and *Carpinus betulus* Linné. One of the authors (R. Schuh, personal observation) has collected

C. noblecourti sp. nov. several times in the eastern part of Austria (alluvial floodplains 200–300 m a.s.l.). All these specimens were collected by hand on dead but still standing *Pinus nigra* Arnold, under mouldy or rotten bark. The *Colydium noblecourti* sp. nov. specimens were hiding in abandoned galleries of Scolytinae (Curculionidae) or Cerambycidae. Collecting was largely carried out from December to April, although some was performed during other parts of the year, but with less success. Some specimens from other collections bear notes about collecting circumstances on their labels, which might give more information on the species bionomics. A short list of these data follows: "in galleries of *Xyloterus lineatus* (Ol.) (Curculionidae: Scolytinae) on *Picea abies* (L.) Karst." (Austria: Carinthia: Hermagor, leg. C. Holzschuh); "in galleries of *Orthotomicus laricis* (F.) (Curculionidae: Scolytinae) on *Picea abies* (L.) Karst." (Austria: Tyrol: Lienz, leg. A. Kofler); "under bark of burnt *Picea*" (Austria: Tyrol, Karwendel, leg. M. Kahlen); "under bark of *Pinus* or *Picea*" (Austria: Carinthia, several localities, leg. C. Holzschuh); "in window trap on dead *Abies alba* Mill." (Germany: Bayern, leg. H. Bussler); "on *Fagus*" (France: Forêt d'Iraty, leg. H. Brustel); "in the night on trunks of *Fagus*" (Austria: Vienna, leg. M. Kahlen); "in galleries of *Xyloterus domesticus* (L.) (Curculionidae: Scolytinae) on *Carpinus betulus* L." (Austria: Vienna, leg. C. Holzschuh).

These labels represent only single data points, however, and a full ecological analysis is therefore not yet possible. Further investigations are required to reveal the true bionomics of *C. noblecourti* sp. nov.
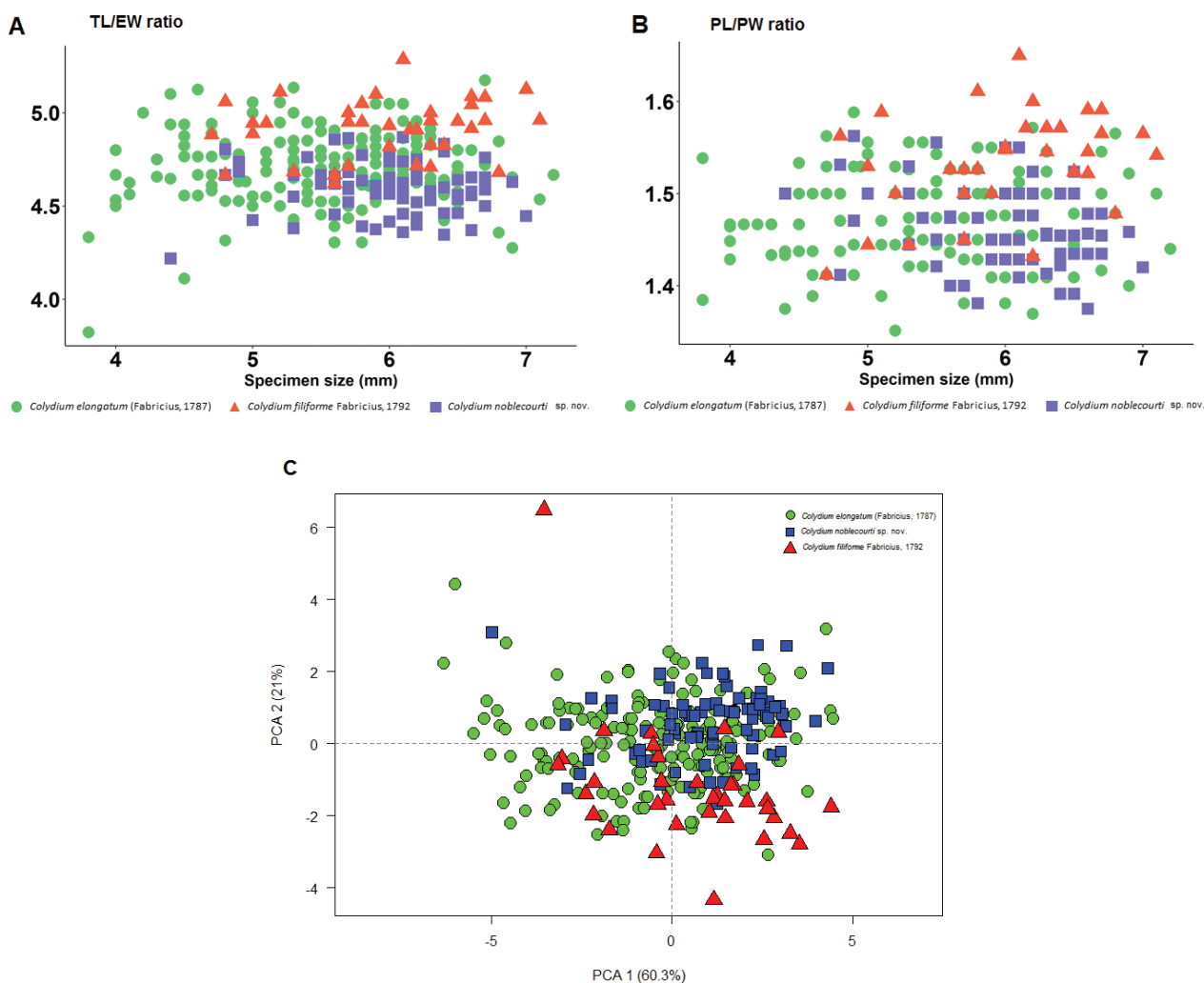
Figures 5. A–C. Morphometric diagrams. **A.**Total length / elytral width ratios; **B.** Pronotal length / pronotal width ratios; **C.** PCA analysis.

Identification key

Note: the three species are not easy to separate. In the authors' opinion the most efficient criterion for separating species are the male genitalia. The morphometric values proposed by Porta (1929), Dajoz (1977) and Vogt (1967) as diagnostic are not efficient, as Węgrczynowicz (1999) has already suggested. The description of *Colydium noblecourti* sp. nov. is the perfect opportunity to propose a new identification key with more useful characteristics.

1   Admedian lines of pronotum absent or only slightly impressed (Fig. 1B). Apex of apical ventrite angled in both sexes (Fig. 1C). Punctures on pronotal base on average smaller (separated by one to two of their diameters), of same size as on pronotal disc. Elytra generally completely black. Aedeagus as in Fig. 1D, E. Parameres not in the same plane, inclined toward each other; the apex of median lobe prolonged into a narrow tip (Fig. 1E) ....*Colydium noblecourti* sp. nov.

–   Admedian lines of pronotum strongly impressed (Figs 2B and 3B). Apex of apical ventrite rounded (Figs 2C and 3C). Punctures on pronotal base on average larger (separated by half to 1.5 of their diameters), larger and denser than on pronotal disc. Humeral angles of the elytra at least with a brown spot or the basal third of the elytra completely reddish. Aedeagus differently shaped... 2

2   Periocular carina well defined and sharply cariniform (well visible from above). Humeral angles of elytra brown. Elytral interval 3 elevated at the apex but rounded in cross-section; carina on elytral interval 5 connected to interval 9 at apex. Aedeagus as in Fig. 2D, E. Parameres in the same plane, apex of the median lobe prolonged into a narrow tip (Fig. 2E) ....*Colydium elongatum* (Fabricius, 1787)

–   Periocular carina weak, blunt, without a distinct angle (well visible from above). Humeral angles and at least first fifth of elytra reddish brown to brown. Elytral interval 3 distinctly and sharply cariniform at apex; carina on elytral interval 5 not connected to interval 9 at apex. Aedeagus as in Fig. 3D, E. Parameres not in the same plane and inclined toward each other; apex of median lobe sharply angled, but not prolonged into a narrow tip (Fig. 3E)........... *Colydium filiforme* Fabricius, 1792

Discussion

The consistent confusion between the Western Palearctic species of *Colydium* in former times was due to inappropriate identification keys, their very similar biology and the existence of the hitherto unknown *C. noblecourti* sp. nov.. As our study shows, all three species can be separated by external characters and specific differences in male genitalia. The genetic analysis of COI barcode sequences further confirms that the morphological differences identified between the species are sufficient to distinguish them clearly.

The aim of the morphometric analysis was to test the value of length/width-ratios to describe the body shape of these species. Particularly, the PL/PW-ratio has been used widely to separate *C. elongatum* (Fabricius) and *C. filiforme* Fabricius (Vogt 1967; Dajoz 1977; Węgrzynowicz 1999). For example, the PL/PW-ratio of *C. elongatum* according to Vogt (1967) and Dajoz (1977) is 1.5 and for *C. filiforme* the PL/PW-ratio is stated as "above 1.5" (Vogt 1967) and as 1.75 (Dajoz 1977). More thorough results are published by Węgrzynowicz (1999) with PL/PW-ratio of *C. elongatum* as 1.29–1.52 and 1.41–1.66 of *C. filiforme* respectively. This shows, that the values for those ratios in previous literature are not useful for separation of the Western Palearctic *Colydium* species. In this study, with the new situation of a third species it was important to elaborate how descriptive those ratios are, including the data of *C. noblecourti* sp. nov. too. The results show that morphometric characters do not represent a reliable identification tool, particularly for separation of *C. elongatum* and *C. noblecourti* sp. nov..

All three species can be found under the same type of bark (observation by the second author). This makes the available ecological and distributional data in the literature difficult to interpret. We have provided distribution maps for each species (Figs 6–8).

C. noblecourti sp. nov. is only known from the records provided in the present study. We studied specimens from Austria, Andorra, Bosnia, Croatia, Czech Republic, France, Germany, Iran, Italy, Slovakia, Slovenia, Spain and Turkey (Fig. 6). Compared to the two other species, *C. noblecourti* sp. nov. seems more or less rare, depending on the country of origin. According to the available data, this species is more common in France than *C. filiforme*, whereas in Germany and the Czech Republic, *C. filiforme* is more common than *C. noblecourti* sp. nov. More data are needed to assess the real conservation status of this new species.

Colydium elongatum is widespread in Europe (33 countries: AB; AL; AR; AU; BE; BH; BU; BY; CR; CT; CZ; DE; FI; FR; GB; GE; GR; HU; IT; LT; MC; NL; PL; RO; SK; SL; SP; ST; SW; SZ; TR; UK; YU. Abbreviations according to Iwan and Löbl (2020)). This was the most common species among the studied material. The data we gathered suggest that it might be distributed throughout French territory, including Corsica (Fig. 7). It is considered "of least concern" in Italy (http://www.iucn.it/scheda.php?id=-1019656031) and "endangered" in Norway (https://artfakta.artdatabanken.se/taxon/100701). It is absent from the European list of "primeval forest relict beetles" (Eckelt et al. 2017). In France, the recent catalogue of saproxylic beetles (Bouget et al. 2019) gives it a value of 1, which indicates a common species.
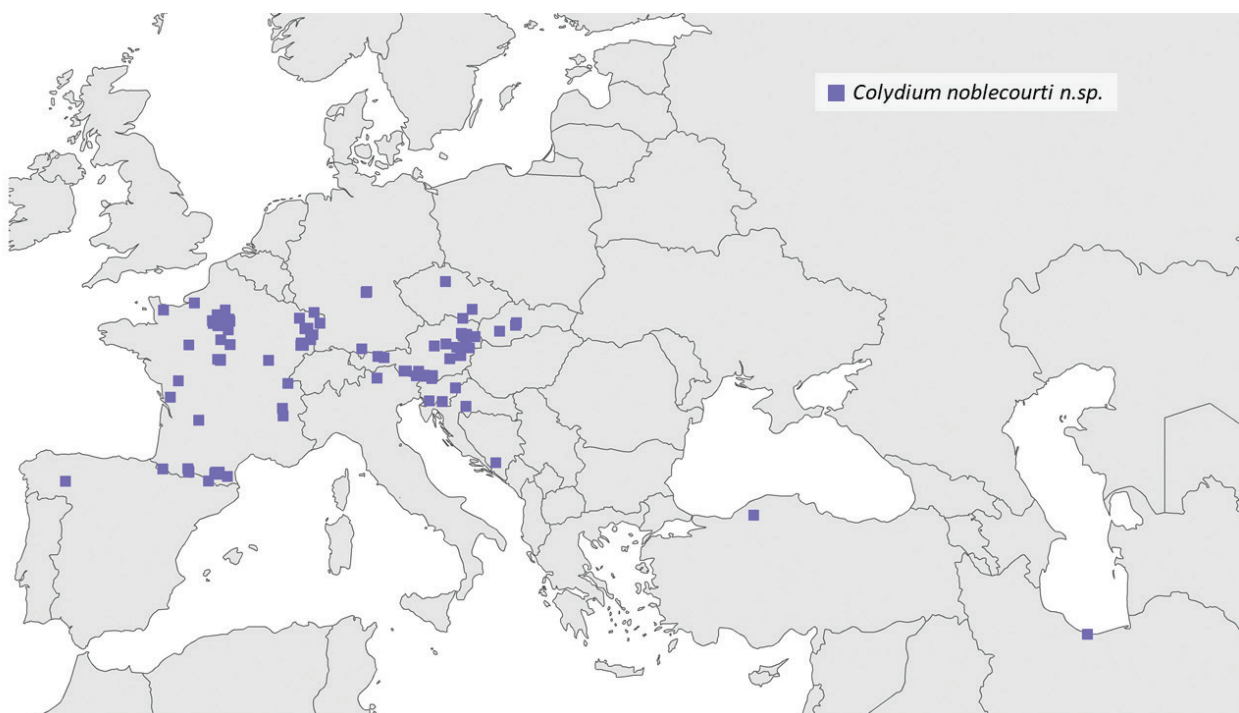

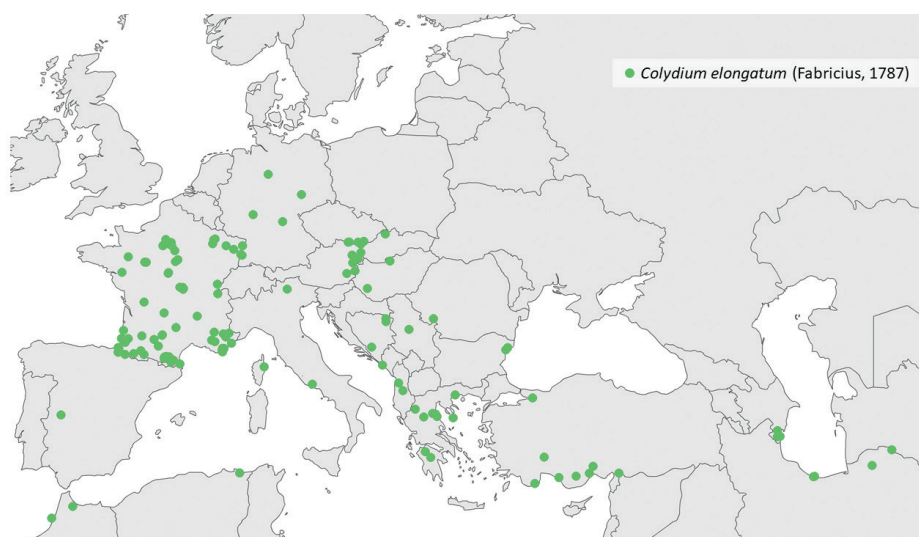**Figure 6.** Geographical distribution of *Colydium noblecourti* sp. nov.

Figure 7. Geographical distribution of *Colydium elongatum* (Fabricius).

Figure 8. Geographical distribution of *Colydium filiforme* Fabricius.

Colydium filiforme is known in 23 countries in Europe (AB; AU; BE; BH; BU; BY; CR; CZ; FR; GE; GG; GR; HU; IT; LA; LS; NR; PL; SK; SP; ST; SV; SZ. Abbreviations according to Iwan and Löbl (2020)). It is a rare species in Western Europe, while it seems more common in Eastern Europe. According to Brustel (2014), this species is indicated as rare but widespread in France. However, despite studying more than 290 *Colydium* specimens from France, we identified only two French specimens of *C. filiforme*, one from Saint Auban (Dépt. Alpes-Maritimes) trapped in a *Pinus* stand and one from La Wantzeau (Dépt. Bas-Rhin) trapped in a riverine *Fraxinus* and *Quercus* forest. No specimens are known from Corsica, but the species might be found there (Fig. 8). It is included in the list of European "primeval forest relict beetles" (Müller et al. 2005; and the updated edition, Eckelt et al. 2017). This assessment confirms its high conservation importance. It is considered "near threatened" in Italy (http://www.iucn.it/scheda.php?id=-1991355085) and "endangered" in Norway (https://artfakta.artdatabanken.

se/taxon/100702). In Spain, only a few localities are known to host the species (Dieguez-Fernandez et al. 2012). We were able to study the specimen mentioned in Recalde Irurzun (2015). In France, the recent catalogue of saproxylic beetles (Bouget et al. 2019) gives it a value of 3, which indicates a rare species of important conservation interest.

Conclusion

Widely distributed species can sometimes hide a complex of several cryptic species. Closely studying morphology and male genitalia in association with genetic analysis is an efficient way to detect new species. We believe that many species remain undiscovered in Europe, and are simply hidden among more common ones. In the material we gathered, we detected *Colydium noblecourti* sp. nov. in thirteen countries. We assume that *Colydium noblecourti* sp. nov. will be found in other European countries as well.

Acknowledgements

References

Adobe Inc. (2024) Adobe Photoshop version 25. https://www.adobe.com/products/photoshop.html

Alexander KNA (2008) Tree biology and saproxylic coleoptera: issues of definitions and conservation language. Revue d'Écologie (Terre Vie) 63: 1–7. https://doi.org/10.3406/revec.2008.1455

Bouget C, Brustel H, Noblecourt T, Zagatti P (2019) Les Coleoptères saproxyliques de France. Catalogue écologique illustré. Muséum national d'histoire naturelle, Publications scientifiques, Patrimoines naturels 79. Paris, 744 pp.

Brustel H (2014) Famille Zopheridae Solier, 1834. In: Tronquet M (Ed.) Catalogue des coléoptères de France. Association Roussillonnaise d'Entomologie, Supplément au tome XXII. Perpignan, 525–527.

Dajoz R (1977) Coléoptères Colydiidae et Anommatidae paléarctiques. Masson, Paris, 275 pp.

De Waard JR, Ivanova NV, Hajibabaei M, Hebert PDN (2008) Assembling DNA Barcodes: Analytical Protocols. In: Cristofre M (Ed.) Methods in Molecular Biology: Environmental Genetics. Humana Press Inc., Totowa, USA, 275–293. https://doi.org/10.1007/978-1-59745-548-0_15

Dieguez-Fernandez JM, Recalde-Irurzun JI, Schuh R (2012) Contributions to the chorology of Iberian Zopheridae (Coleoptera). Aportaciones a la corologia de los Zopheridae ibericos (Coleoptera). Heteropterus Revista de Entomologia 12(1): 107–114.

Eckelt A, Müller J, Bense U, Brustel H, Bußler H, Chittaro Y, Cizek L, Frei A, Holzer E, Kadej M, Kahlen M, Köhler F, Möller G, Mühle H, Sanchez A, Schaffrath U, Schmidl J, Smolis A, Szallies A, Németh T, Wurst C, Thorn S, Christensen RHB, Seibold S (2017) "Primeval forest relict beetles" of Central Europe: a set of 168 umbrella species for the protection of primeval forest remnants. Journal of Insect Conservation 22: 15–28. https://doi.org/10.1007/s10841-017-0028-6

Iwan D, Löbl I (2020) Distributional information. In: Iwan D, Löbl I (Eds) Catalogue of Palearctic Coleoptera. Vol. 5, Revised and Updated Second Edition, Tenebrionoidea. Brill Books, Leiden, Boston, XII–XVII. https://doi.org/10.1163/9789004434998

Kalyaanamoorthy S, Minh BQ, Wong TKF, von Haeseler A, Jermiin LS (2017) ModelFinder: fast model selection for accurate phylogenetic estimates. Nature Methods 14: 587–589. https://doi.org/10.1038/nmeth.4285

Katoh K, Standley DM (2013) MAFFT Multiple Sequence Alignment Software Version 7: Improvements in Performance and Usability. Molecular Biology and Evolution 30: 772–780. https://doi.org/10.1093/molbev/mst010

Lawrence JF, Ślipiński A (2013) Australian Beetles, Vol 1. Morphology, Classification and Keys. CSIRO Publishing, Collingwood, 561 pp. https://doi.org/10.1071/9780643097292

Minh BQ, Nguyen MA, von Haeseler A (2013) Ultrafast approximation for phylogenetic bootstrap. Molecular Biology and Evolution 30: 1188–1195. https://doi.org/10.1093/molbev/mst024

Müller J, Bussler H, Bense U, Brustel H, Flechtner G, Fowles A, Kahlen M, Möller G, Mühle H, Schmidl J, Zabransky P (2005) Urwald relict species – Saproxylic beetles indicating structural qualities and habitat tradition. Waldökologie Online 2: 106–113.

Nguyen LT, Schmidt HA, von Haeseler A, Minh BQ (2015) IQ-TREE: a fast and effective stochastic algorithm for estimating maximum-likelihood phylogenies. Molecular Biology and Evolution 32: 268–274. https://doi.org/10.1093/molbev/msu300

Porta A (1929) Fauna Coleopterum Italica, Vol III, Diversicornia. Stabilimente Tipographico Piacentino, Piacenza, 466 pp.

R Core Team (2024) R: A language and environment for statistical computing. Version 4.4.1. R Foundation for Statistical Computing, Vienna, Austria. https://www.R-project.org/

Rambaut A (2015) FigTree. Edinburgh, Scotland. http://tree.bio.ed.ac.uk/software/figtree/

Ratnasingham S, Hebert PDN (2007) BOLD: The Barcode of Life Data System (http://www.barcodinglife. org). Molecular Ecology Notes 7: 355–364. https://doi.org/10.1111/j.1471-8286.2007.01678.x

Recalde Iruzun JI (2015) Aproximacion a la fauna de escarabajos saproxilicos (Coleoptera) del Parque Natural del Senorio de Bertiz (Navarra). Heteropterus Revista de Entomologia 15(1): 43–57.

Schuh R (2020): Zopheridae. In: Iwan D, Löbl I (Eds) Catalogue of Palearctic Coleoptera, Vol.5, Revised and Updated 2nd edn, Tenebrionoidea. Brill Books, Leiden, Boston, 66–79.

Vogt H (1967) 60. Fam. Colydiidae. In: Freude H, Harde KW, Lohse GA (Eds) Die Käfer Mitteleuropas, Band 7. Goecke & Evers, Krefeld, 197–216.

Węgrzynowicz P (1999) A revision of the genus *Colydium* Fabricius, 1792 (Coleoptera: Zopheridae; Colydiinae). Annales Zoologici 49(3): 265–328.

Zhang D, Gao F, Jakovlić I, Zou H, Zhang J, Li WX, Wang GT (2020) PhyloSuite: An integrated and scalable desktop platform for streamlined molecular sequence data management and evolutionary phylogenetics studies. Molecular Ecology Resources. 20(1): 348–355. https://doi.org/10.1111/1755-0998.13096

PENSOFT.

MUSEUM FÜR
NATURKUNDE
BERLIN

Description of the immature stages and bionomics of *Anthonomus* (*Anthonomus*) *brunnipennis* Curtis, 1840 (Coleoptera, Curculionidae, Anthonomini)

Rafał Gosik[1], Peter Sprick[2]

1   *Department of Zoology and Nature Protection, Maria Curie–Skłodowska University, Akademicka 19, 20–033 Lublin, Poland*

2   *Curculio–Institute e.V. (CURCI), Weckenstraße 15, 30451 Hannover, Germany*

https://zoobank.org/A6236EAE-1EAC-497F-A0EF-5B9ADC884640

Corresponding author: Rafał Gosik (r.gosik@poczta.umcs.lublin.pl)

Abstract

The developmental stages (larva, pupa) of *Anthonomus brunnipennis* are fully described for the first time. Despite great similarities of the adults of *A. brunnipennis* and *A. rubi* the differences between immature stages of both species could be demonstrated. Two different habitats of *A. brunnipennis* in Germany are described, and host plant data are critically reviewed. The only well-documented host plant of *A. brunnipennis* is *Potentilla erecta*.

Key Words

Introduction

With more than 500 species, the genus *Anthonomus* Germar, 1817 (Curculioninae, Curculioninae) is the largest genus in the tribe Anthonomini (Clark 2005, 2013; Caldara 2013). Approximately 400 of them occur in the Neotropics, 73 in the Palaearctic, 3 in the Afrotropics, 11 in the Oriental Region, and 2 in the Australian and Pacific Regions (Clark 2005, 2013; Caldara 2013; Sprick and Floren 2018). They are characterized by small to medium-sized bodies (1.7–5.0 mm), elongate rostra, long antennae, somewhat convex eyes, small pro-femorae and teeth on the pro- and mesofemorae (Smreczyński 1972; Burke 1976). *Anthonomus* weevils are known to inhabit 22 different plant families (Dieckmann 1968; Anderson 1993; Jones 2001). The majority of them feed on dicotyledonous plants, the larvae develop in flower buds, and pupation takes place in flower buds or rarely in soil (Koch 1992). Certain larvae, like those of *A. phyllocola* (Herbst, 1795), develop in conifer flowers. A small number of larvae are known to develop as inquilines of galls (e.g., *Anthonomus vis* Clark, 1992 on *Leandra aurea* Cogn. (Melastomataceae) produced by momphid moth larvae (Lepidoptera, Momphidae) (Gates and Burke 1972).

Knowledge about the morphology of immature Anthonomini stages is restricted to around 10% of the species, but compared with other speciose genera or tribes, it is at a quite good but still nowhere near sufficient level, as descriptions from some subgenera are non-existent (Zabaluev 2021). Burke (1968) published descriptions and illustrations of the pupae of 47 species, which were later supplemented by descriptions of the larvae of several dozen Anthonomini species by Ahmad and Burke (1972) and Burke and Gates (1974). The latest comprehensive contribution with first descriptions of some Palaearctic species – *Anthonomus* (*Anthonomidius*) *rubripes* Gyllenhal, 1835, *A.* (s. str.) *incurvus* (Panzer, 1795), *A.* (s. str.) *conspersus* Desbrochers des Loges, 1868, and *A.* (s. str.) *latior* Pic, 1902 – was provided by Zabaluev (2021). Other studies give information on the biology and morphology of immatures of the Nearctic

species *A. monostigma* Champion, 1903 (Chacón-Madrigal et al. 2012), *A. rubricosus* Boheman, 1859 (Loiácono et al. 2004), *A. vis* (Bená and Vanin 2013) and *A. santacruzi* Hustache, 1924 (Gosik et al. 2017).

Although certain species, such as *Anthonomus rubi* (Herbst, 1795), *A. pomorum* (Linnaeus, 1758), *A. vestitus* Boheman, 1859 and *A. grandis* Boheman, 1843, have been identified as significant pests (Scherf 1964; Burke 1976), and conversely, *A. santacruzi*, *A. morticinus* Clark, 1998 and *A. monostigma* are employed as biocontrol agents of weeds (Burke 1976; Olckers 1999; Caxambu 2003; Chacón-Madrigal et al. 2012), knowledge of the biology of many other Anthonomini species is rudimentary. According to Zabaluev (2021), the bionomics of fewer than 12% of Palaearctic *Anthonomus* species have been studied to date.

Anthonomus brunnipennis is a European species with a range limited to several countries in the western and northern part of the continent, namely, Belgium, Denmark, Great Britain, Northern Germany, France, Ireland and Switzerland; in Scandinavia and north-eastern Europe it occurs in Finland, Norway and Sweden, also in Latvia, Lithuania and the northern part of European Russia (Alonso–Zarzaga et al. 2023). According to Hoffmann (1954), Dieckmann (1968), Palm (1992) and Morris (2012), *Comarum palustre* L., *Dryas octopetala* L., *Filipendula ulmaria* (L.) Maxim. and *Potentilla erecta* (L.) Raeusch. (all Rosaceae) are mentioned as host plants of *A. brunnipennis*.

Our aim is to describe the morphology of the immature stages, larva and pupa of *Anthonomus brunnipennis*, with particular emphasis on the differences between this species and its sibling species *A. rubi*, and to update and expand knowledge about the bionomics of *A. brunnipennis*.

In addition, based on the available descriptions of larvae, in particular by Ahmad and Burke (1972), Burke and Gates (1974), Zabaluev (2021), the differences between genera of the tribe Anthonomini have been formulated.

Materials and methods

Insect collection

Larvae: 9 exx. of various instars: collected on 15.06.2022: 3 exx. breeding to 23.06.2022; 1 ex. breeding to 23.06.2022; 4 exx. breeding to 17.06.2022; 1 ex. breeding to 05.07.2022.

Pupae: 4 exx. collected on 15.06.2022, 1 ex. breeding to 05.07.2022.

All specimens collected in Germany, National Park Harz, mountain meadow, in part wet, from *Potentilla erecta* (L.) Raeusch.

In order to confirm species affiliation, some of the larvae obtained in the field were left to metamorphose under laboratory conditions (Fig. 1A, B). The adults were determined based on the morphological features proposed by Palm (1992).

Morphological descriptions

All larval and pupal specimens described were fixed in 95% ethanol and examined under an optical stereomicroscope (Olympus SZ 60 and SZ11) with calibrated oculars. The following measurements of larval instars were made: body length (BL), body width (BW) (at the second abdominal segment) and width of the head capsule (HW). The body length (BL) of pupae was measured without urogomphi.

Slide preparation basically followed May (1994). Larvae selected for study under a microscope were dissected, cleared in potassium hydroxide (KOH, 10%), then rinsed in distilled water. After clearing, the head and mouthparts were separated and mounted on permanent microscope slides in Faure–Berlese fluid (50 g gum arabic and 45 g chloral hydrate dissolved in 80 g of distilled water and 60 cm³ of glycerol) (Hille Ris Lambers 1950).
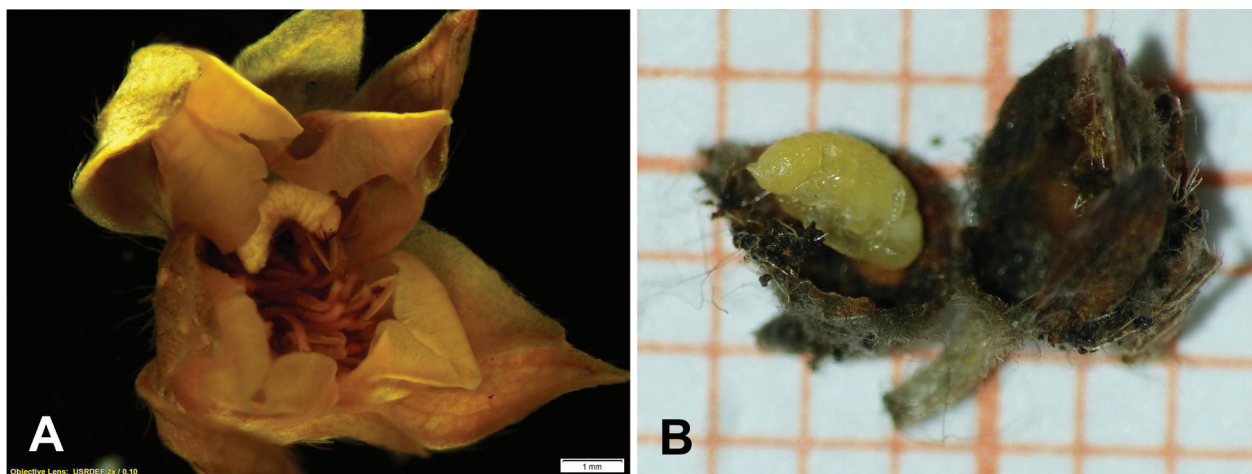

Figure 1. Breeding of *Anthonomus brunnipennis*. **A.** Young larva in a flower bud of *Potentilla erecta*; **B.** Pupa in a flower bud of *Potentilla erecta* after the 11th day of breeding.

Dtsch. Entomol. Z. 71 (2) 2024, 303–318

305

Photographs were taken using an Olympus BX63 microscope and processed with Olympus cellSens Dimension software. The larvae selected for SEM imaging (scanning electron microscope) were first dried in absolute ethanol (99.8%), then rinsed in acetone, treated by CPD (Critical Point Drying) and finally gold–plated. TESCAN Vega 3 SEM was used to examine selected structures. The general terminology and chaetotaxy follow Anderson (1947), May (1994), Marvaldi (1997, 1998, 1999, 2003) and Skuhrovec et al. (2015), while the antennae terminology follows Zacharuk (1985). In the case of the description of the pupa, we followed the terminology proposed by Skuhrovec et al. (2015).

Morphological abbreviations

Abd. I–X–abdominal segments 1–10, **Th. I–III**–thoracic segments 1–3, **at**–antenna, **clss**–clypeal sensorium, **ds**–digitiform sensillum, **st**–stemmata, **Se**–sensorium, **sa**–sensillum ampullaceum, **sb**–sensillum basiconicum, **snp**–sensilla pores, **tra**–terminal receptive area, **lr**–labral rods, **ur**–urogomphus; setae: *als*–anterolateral, *ams*–anteromedial, *as*–apical (pupa), *cls*–clypeal, *d*–dorsal (pupal abdomen), *des*–dorsal (larval head), *dms*–dorsal malar, *ds*–discal (pupal prothorax), *ds*–dorsal (larval abdomen), *eps*–epipleural, *eus*–eusternal, *fs*–frontal, *les*–lateral epicranial, *ligs*–ligular, *lrs*–labral, *ls*–lateral, *lsts*–laterosternal, *mbs*–malar basiventral, *mds*–mandibular, *mes*–median, *mps*–maxillary palp, *pda*–pedal, *pds*–postdorsal, *pls*–posterolateral, *pes*–postepicranial, *pfs*–palpiferal, *pms*–postlabial, *prms*–prelabial, *prns*–pronotal, *prs*–prodorsal, *ps*–pleural, *sls*–superlateral, *sos*–superorbital, *ss*–spiracular, *stps*–stipal, *ves*–ventral, *vms*–ventral malar, *vs*–vertical. **HW**–head width, **BL**–body length, **BW**–body width.

Results

Habitat and host plant

The habitat (Fig. 2A–C) in the National Park Harz near Drei Annen Hohne, Sachsen-Anhalt (Fig. 2A, B, E), is a nutrient and base-poor wet meadow on a slightly inclined slope of the types Junco acutiflori-Molinietum and Crepido-Juncetum acutiflori (see Preising et al. 1997) with plants such as *Crepis paludosa* (L.) Moench, *Deschampsia cespitosa* (L.) P. Beauv., *Filipendula ulmaria*, *Galium uliginosum* L., *Hypericum maculatum* Crantz, *Juncus acutiflorus* Ehrh. ex Hoffm., *Plantago lanceolata* L., *Potentilla erecta* (host plant of *A. brunnipennis*), *Ranunculus acris* L., *Rubus idaeus* (host plant of *A. rubi*), *Senecio ovatus* (Gaertn. et al.) Willd., *Succisa pratensis* Moench, *Valeriana dioica* L., *Valeriana excelsa* Poir. s. str. and many others.

The habitat of *Anthonomus brunnipennis* in the Hechtmoor in Mittelangeln, northern Schleswig-Holstein (Fig. 2C, D, F) is part of a peat bog. At the *A. brunnipennis* site it contains plant species such as *Calluna vulgaris* (L.) Hull, *Comarum palustre* (syn. *Potentilla palustris*), *Erica tetralix* L., *Eriophorum angustifolium* Honck., *Lysimachia vulgaris* L., *Molinia caerulea* (L.) Moench, *Potentilla erecta* (host plant), *Sphagnum* spec., and *Vaccinium oxycoccos* L. Due to a lack of a complete plant recording the plant community is not exactly known, it could belong to Sphagno-Juncetum acutiflori or Carici-Agrostietum caninae, which unites the presence of all, or most, recorded plant species (see Preising et al. 2012).

This plant community, more characterized by peat bog rather than wet meadow conditions, may describe another extreme of the plant communities, in which *P. erecta* and *A. brunnipennis* can be found in Germany.

Morphology

Description of the mature larva of *A. brunnipennis*

BL: 2.46–2.66 mm; BW: 0.70–0.83 mm; HW: 0.53–0.56 mm.

General habitus (Fig. 3A, B). Colour of living larva and pupa yellowish; head capsule always light brown.

Body strongly curved, rounded in cross section. Prothorax prominent, pronotal shield weakly isolated, not more sclerotized than rest of prothorax; meso- and metathorax almost equal in size. Meso- and metathorax each divided dorsally into two folds (prodorsal folds small, postdorsal folds prominent). Pedal lobes of thoracic segments weakly isolated and flattened. Abdominal segments I–V of a similar, medium size, with next segments tapering towards posterior body end. Abdominal segments I–VII, each with three dorsal folds, prodorsal and postdorsal folds well developed, the later divided into two parts (the first narrow, the second slightly wider and much higher than the first). The divisions and subdivisions are most visible on abdominal segments I-V and become gradually faint from abdominal segment VI onwards. Segment VIII with a wide prodorsal fold and a narrow, undivided postdorsal fold. Abdominal segment IX undivided dorsally. Epipleural, laterosternal and eusternal folds of segments I–VIII slightly conical and weakly isolated. Abdominal segment X divided into four folds of almost equal size, completely hidden within segment nine. Anus situated ventrally. All spiracles bicameral: thoracic ones (Fig. 3C) placed medio-laterally on the prothorax, abdominal ones (Fig. 3D) placed medio-laterally on segments I–VIII. Body cuticle densely covered with nodular asperities and only partially smooth (Fig. 4A–D).

Chaetotaxy (the number of setae is given for one side of the body) (Fig. 4A–D). Setae of various lengths, from elongate to minute, always hair-like. Thorax (Fig. 4A): prothorax with 9 elongate and 1 short *prns* (6 on the pronotal sclerite, the next 3 above the spiracle), 2 elongate
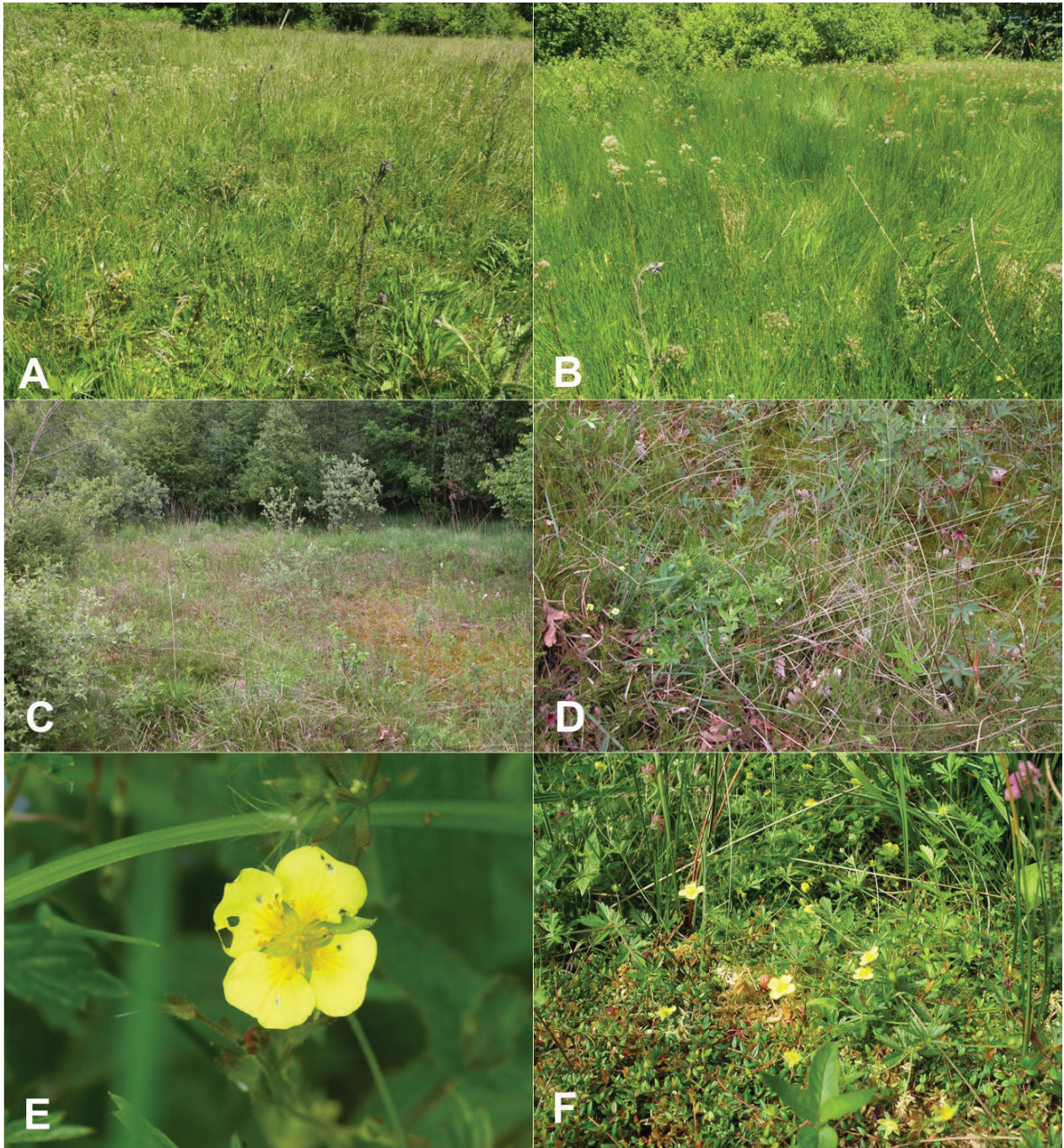
Figure 2. Habitat of *Anthonomus brunnipennis* in the Harz Mountains and in Schleswig-Holstein. **A.** Wet meadow of the type Junco-Molinietum with *Potentilla erecta* in the National Park Harz near Drei Annen Hohne; **B.** Wet meadow with large stands of *Juncus acutiflorus* in the Harz Mountains, in direct contact to the habitat depicted on A; **C.** Habitat of *A. brunnipennis* in the Hechtmoor in Schleswig-Holstein; **D.** Habitat in the Hechtmoor with *Comarum palustre* and *Potentilla erecta*. **E.** *Potentilla erecta* in the habitat of *A. brunnipennis* in the Harz Mts. with feeding holes. **F.** Detail from the habitat in the Hechtmoor with *Potentilla erecta* and *Vaccinium oxycoccos*.

ps, and a single elongate *eus*. Meso- and metathorax each with 1 minute and 1 medium *prs*, 4 *pds* of various lengths (first long, second medium, third and fourth long), spiracular area with 2 *ss* of various lengths (1 long and 1 minute), 1 long *eps*, and 1 long *ps*. Pedal areas of thoracic segments, each with two elongate and one medium *pda*. Abdomen (Fig. 4B, C): segments I–VIII with 1 minute and 1 medium *prs*, 4 *pds* (first and third elongate, second

and fourth medium), 2 *ss* (first minute, second medium), 2 *eps* (1 medium and 1 minute), 1 minute *lsts*, and a single minute (sometimes absent) *eus*. Abdominal segment IX with 3 very long *ds* and 2 *ps* (1 long, 1 minute). Segment X: anal lobes without setae (Fig. 4D).

Head (Figs 5A–C, 6A, B, 7A, B). Head capsule almost rounded; endocarinal line long, two-thirds as long as frons; frontal sutures distinct along entire length up to
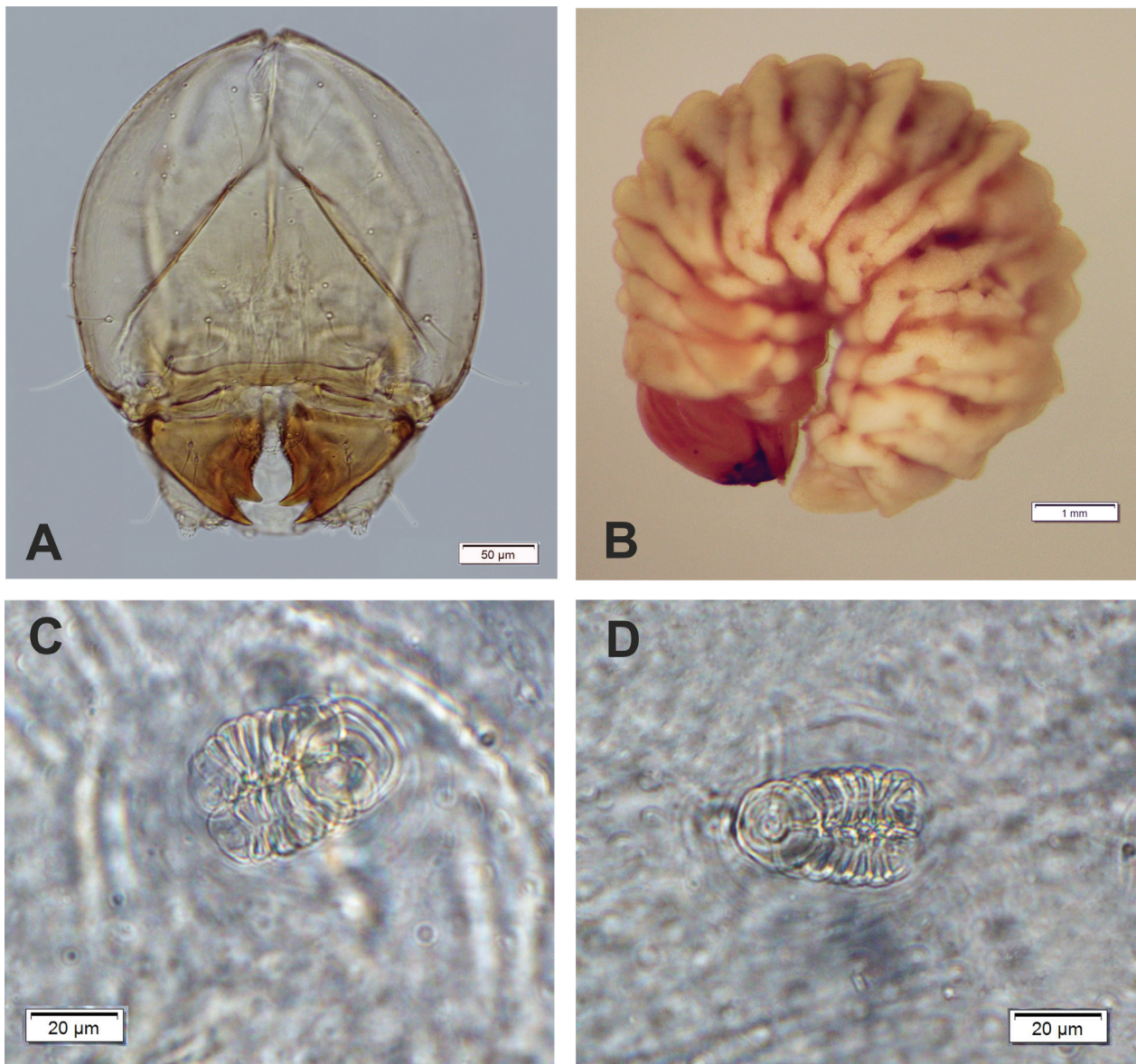
Figure 3. *Anthonomus brunnipennis.* **A.** Head; **B.** Larva, habitus, lateral view; **C.** Spiracle of prothorax; **D.** Spiracle of abdominal segment I.

antennae; one single stemma present on each side (st) in form of prominent dark pigmented spots with convex cornea, placed anterolaterally (Fig. 5A). Each hemisphere of head with 16 setae of various lengths, from medium to minute. Cranial setae: des_1 medium, placed medially, des_2 medium, placed posterolaterally, des_3 medium size, placed on epicranium close to frontal suture, des_4 short, placed anteromedially, des_5 medium, placed anterolaterally, fs_1 minute, placed posteriorly, fs_3 minute, placed anteromedially, fs_4 medium, placed anteromedially and fs_5 medium, placed close to epistome, les_1 short, les_2 as long as des_5, two *ves*: first minute, second medium, postepicranial area with 3 minute *pes*.

Antennae (Fig. 6A, B) with frontal position on each side at anterior margin of head; membranous basal segment convex, semi–spherical, bearing conical, elongate sensorium and 6 sensilla: 5 basiconica (sb) and 1 ampullaceum (sa).

Mouthparts (Figs 7A–E, 8, 9A, B, 10A–D). Clypeus (Fig. 7A, B) approximately 3× wider than long, cls_{1-2} short, placed posterolaterally. Anterior margin of clypeus almost straight. Labrum (Fig. 7A, C, D) trapezium-shaped, approximately 2.3× wider than long; lrs_1 long, placed medially, lrs_2 long, placed antero-laterally and lrs_3 short, placed antero-laterally. Epipharynx (Fig. 7E) with 3 digitate *als*, equal in length, 3 *ams*, various in size and shape: ams_1 elongate, rod-like, ams_2 thin, ams_3 very short and curved; mes_1 short, mes_2 robust, curved. Labral rods (lr) elongate, more sclerotized at apex, distinctly converging posteriorly. Sensilla pores (snp) arranged in a single median cluster of 4 units, close to *ams.*. Surface of epipharynx between labral rods smooth. Mandibles (Fig. 8) with 2 apical teeth of unequal height, the inner one apical and very robust. Cutting edge between apex and middle of mandible smooth. Both setae, mds_1 and mds_2, medium, placed medially in shallow depressions.
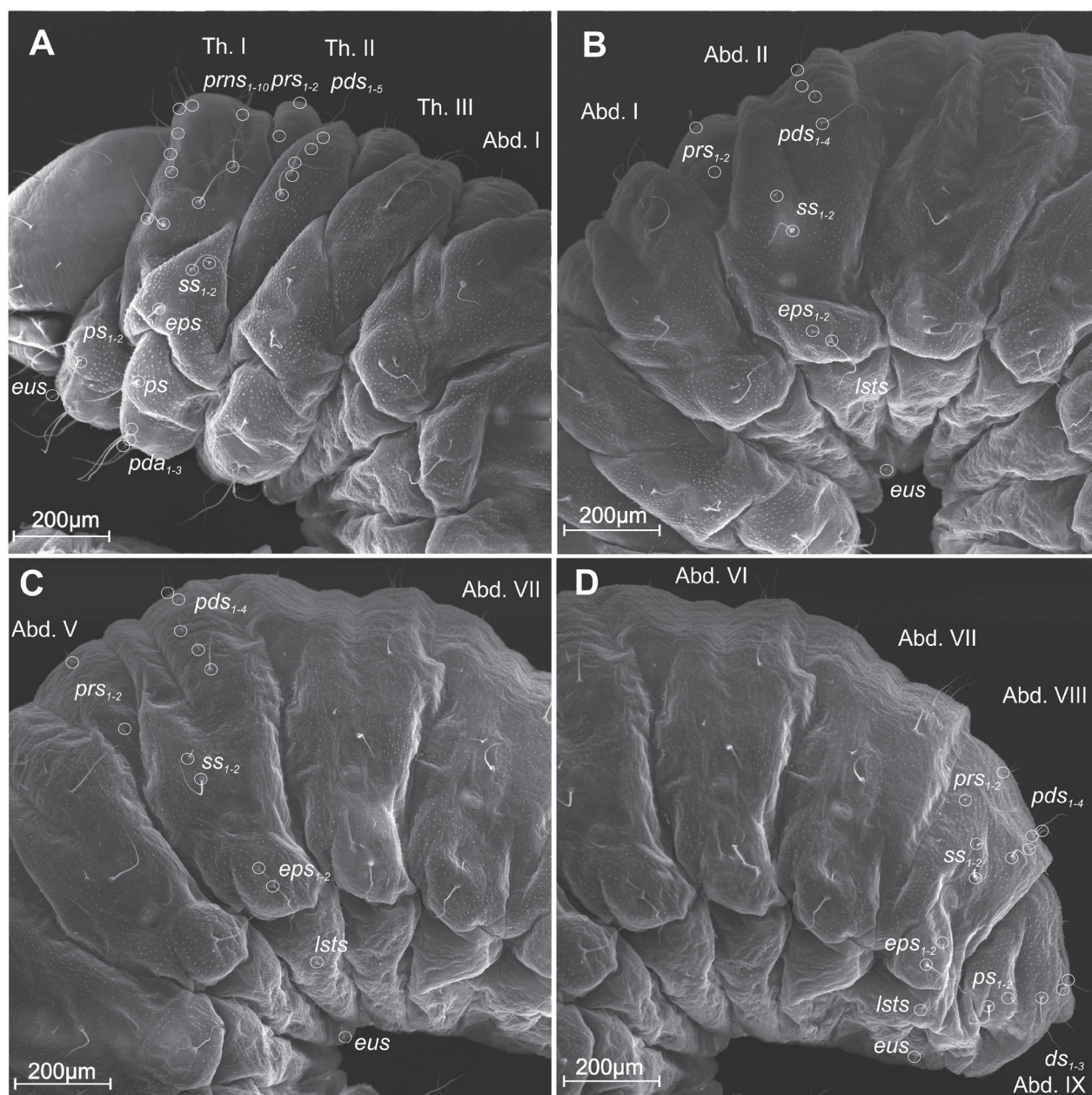
Figure 4. *Anthonomus brunnipennis* mature larva, habitus and chaetotaxy, lateral view (SEM micrographs). **A.** Head and thorax; **B.** Abdominal segments I–III; **C.** Abdominal segments IV–VII; **D.** Abdominal segments VI–IX (setae: *ds*–dorsal, *ps*–pleural, *eps*–epipleural, *eus*–eusternal, *lsts*–laterosternal, *pda*–pedal, *pds*–postdorsal, *prns*–pronotal, *prs*–prodorsal, *ss*–spiracular).

Maxillolabial complex (Figs 7B, 9A–C, 10A–D) on stipes with 1 elongate *stps* and 2 medium size *pfs*. Mala with a row of 6 digitate, almost equally sized *dms* and 4 rod-like *vms* (2 medium and 2 short). Maxillary palps with two palpomeres; basal palpomere distinctly wider than distal one. Length ratio of basal to distal palpomeres almost 1:1. Basal palpomere with medium *mps* and 2 pores, distal palpomere (Fig. 9A–C) with 1 pore, 1 digitiform sensillum (ds) and a group of 10 apical sensilla (8 basiconica and 2 ampullacea) on terminal receptive area (tra) (Fig. 10A–D). Dorsal parts of mala smooth. Labium with prementum cup–shaped, with 1 medium *prms* placed medially. Ligula concave, semicircular at margin, with 3 *ligs* (one short,

two minute). Premental sclerite trident–shaped (median branch weakly sclerotized), posterior extension with elongate, sharp apex; postmentum moderately narrow, membranous, triangular, divided by two furrows into three parts of different size; 3 *pms*, various in size: pms_1 medium, located medially, pms_2 elongate, mediolaterally and pms_3 short, placed anterolaterally. Labial palps two–segmented; basal palpomere wider and much shorter than distal one. Length ratio of basal to distal palpomeres almost 0.5:1. Basal palpomere with two pores, distal with a single pore and a group of 9 apical sensilla (basiconica) on a terminal receptive area. Posterior and posterolateral parts of labium covered with prominent, nodular asperities (Fig. 9A).
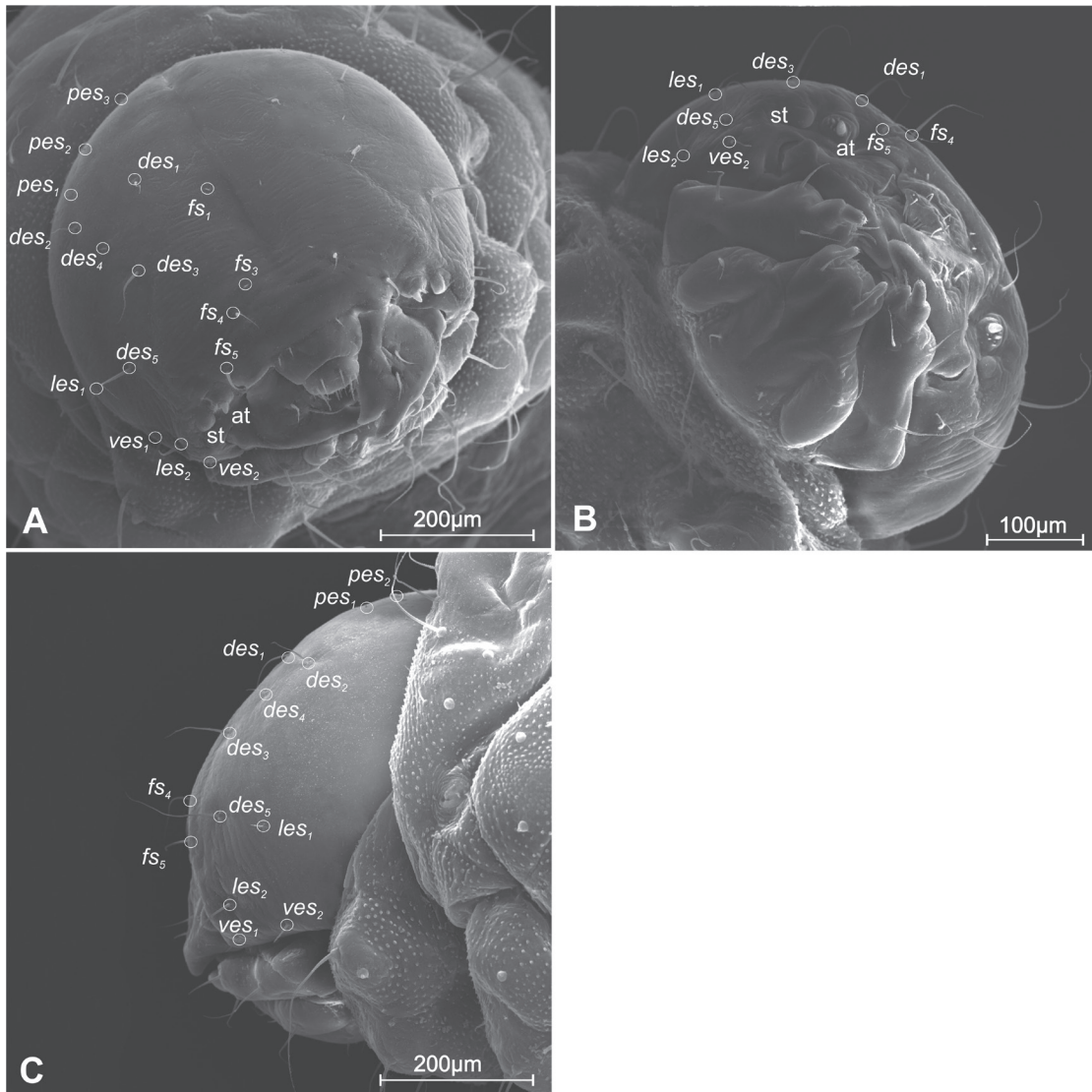
Figure 5. *Anthonomus brunnipennis* larva, head. **A.** Mature instar, frontal view; **B.** Mature instar, ventral view; **C.** Mature instar, lateral view, scheme (at–antenna, st–stemmata, setae: *des*–dorsal epicranial, *fs*–frontal, *ls*–lateral epicranial, *pes*–postepicranial, *ves*–ventroepicranial).
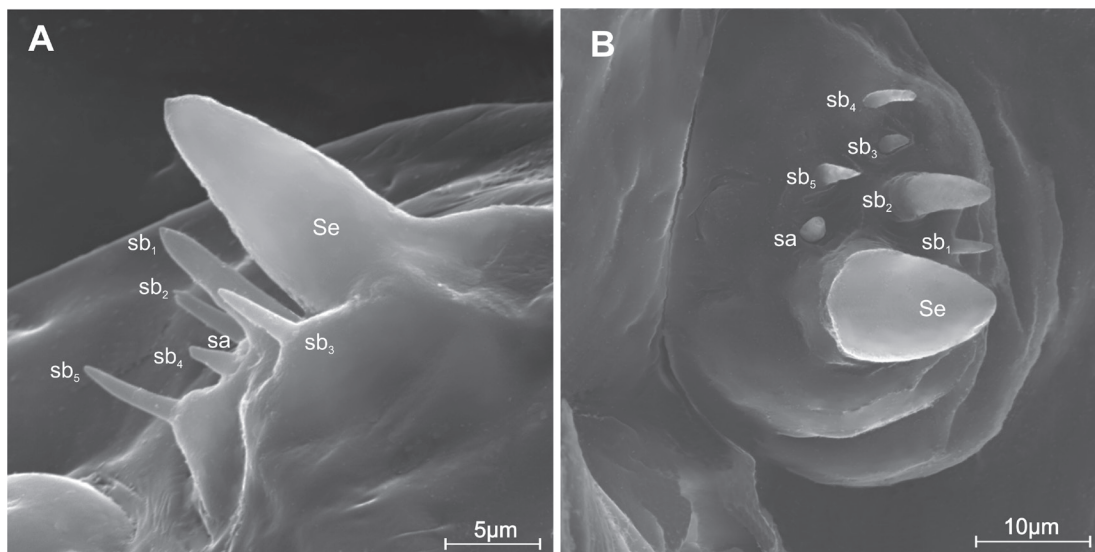

Figure 6. *Anthonomus brunnipennis* mature larva, antenna (SEM micrograph). **A.** Lateral view; **B.** Dorsal view (sa–sensillum ampullaceum, Se–sensorium, sb–sensillum basiconicum).
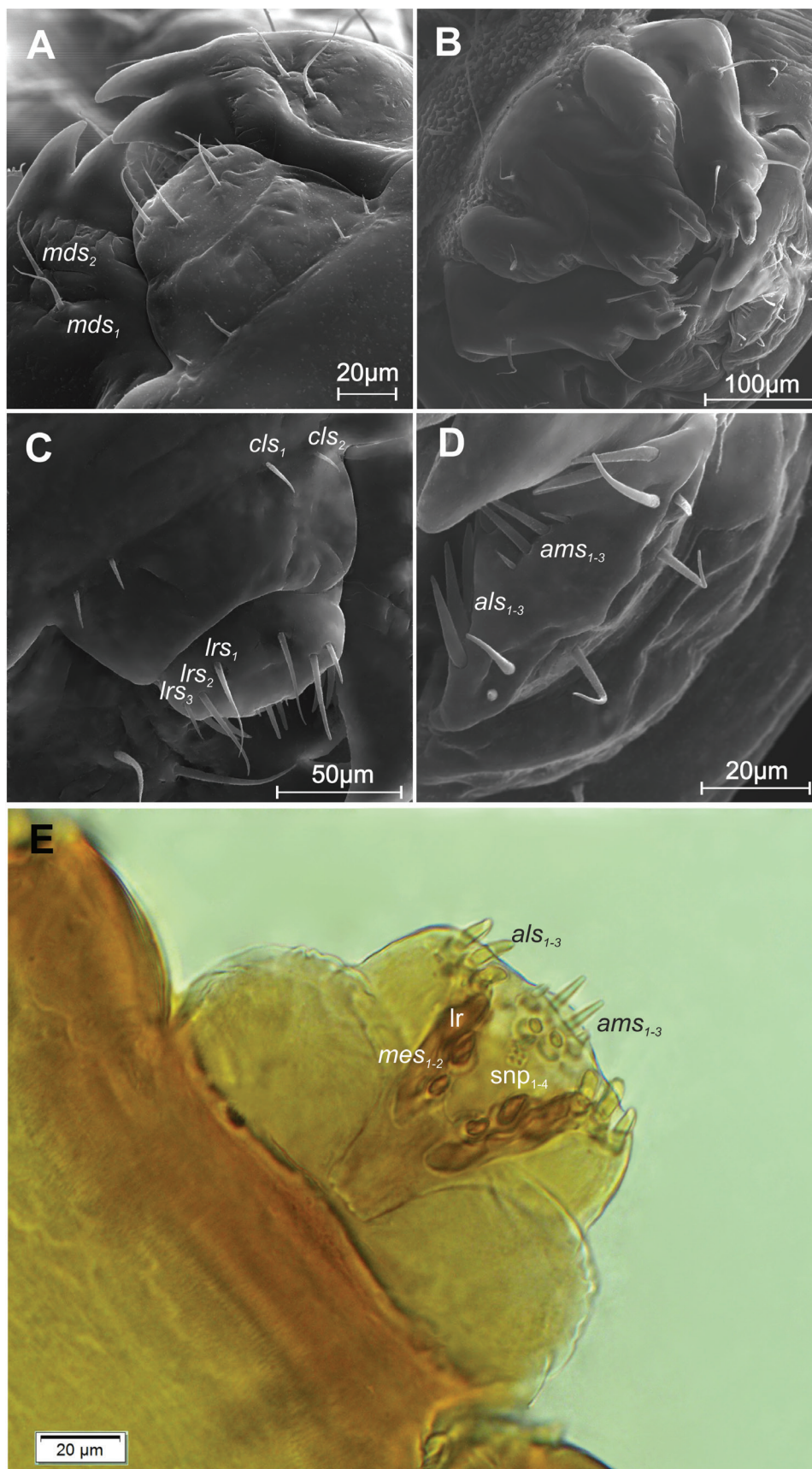
Figure 7. *Anthonomus brunnipennis* mature larva, mouthparts. **A.** Total, dorsal view (SEM micrograph); **B.** Total, ventral view, (SEM micrograph); **C.** Clypeus and labrum, dorsal view, (SEM micrograph); **C.** Clypeus and labrum, dorsal view (SEM micrograph); **D.** Labrum, frontal view, (SEM micrograph); **E.** Epipharynx, (photo) (lr–labral rods, snp–sensilla pores, setae: *als*–antero-lateral, *mds*–mandibular, *ams*–anteromedial, *cls*–clypeal, *lrs*–labral, *mes*–median).

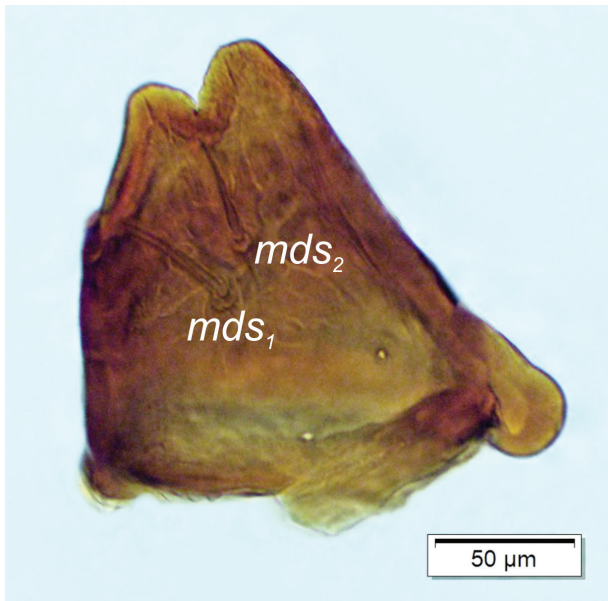**Figure 8.** *Anthonomus brunnipennis* mature larva, right mandible, (photo) (*mds*–mandibular seta).

Description of the pupa of *Anthonomus brunnipennis*

General habitus and chaetotaxy (Figs 11, 12A, B). Body yellowish, 1.90–2.30 mm in length, stout, cuticle partially covered with fine, nodular asperities (Fig. 12D). Rostrum very elongate, 6× as long as wide, almost reaching gonothecae. Pronotum 2.5× wider than long, trapezium-shaped. Prothoracic depression present. Mesonotum narrower than metanotum. Abdominal segments I–V of equal length, segments VI and VII tapering gradually towards end of body, segment VIII narrow, segment IX terminal, with urogomphi (ur) medially situated, straight, rather short, fused. Only the apical parts of urogomphi free, apices curving to the outside. Surface of urogomphi covered with asperities. Male gonothecae undivided, female gonothecae divided, with tubercles on subcontiguous lobes (Fig. 13C, D). Spiracles placed dorso–laterally on abdominal segments I–VI, functional on segments I–V, vestigial on segment VI.

Chaetotaxy (setal numbers given for one side of the body): setae variable in size, hair–like, placed on conical or thorn-like protuberances. Head with short, 1 *vs* and 2 *sos* short, rostrum with 1 *rs* minute. All setae on head and rostrum placed on small, conical protuberances (Fig. 12C, D). Pronotum with 1 *as*, 2 *sls*, 2 *ds* and 3 *pls* almost equal in size. Ds_1 placed on robust, thorn-like protuberance, ds_2 and pls_{1-3} placed on medium-sized, thorn-like protuberances; $ls_{1,2}$ placed on small, conical protuberances. Meso– and metathorax with 3 setae, various in length, placed medially on dorsum. Abdominal segments I–VII with 5 setae, various in length (seg. VII without d_4) even setae are visibly shorter than the odd ones, d_{1-3} located along posterior margin of the segment, d_4 placed antero-laterally and d_5 medio-laterally. Setae: $d_{1,2,4}$ placed on small conical protuberances, $d_{3,5}$ placed on thorn-like protuberances. Segment VIII with 2 elongate setae, placed on robust, thorn-like protuberances (Fig. 13B). Segment IX without setae. Each urogomphus with 3 minute setae placed dorso-laterally. Lateral parts of abdominal segments I–VIII with single, short setae. Ventral parts of abdominal segments I–VIII without setae. Each femur without setae (Fig. 12A, B).

Discussion

Morphology

There are several species in the genus *Anthonomus*, including *A. terreus* Gyllenhal, 1835, Curtis, 1840, *A. costipennis* Fairmaire, 1889 and especially *A. rubi*, whose morphology is very similar to that of *A. brunnipennis*. The systematic status and distribution of some of these taxa are still under debate (Legalov 2000; Alonso-Zarazaga et al. 2023).

Adults of *Anthonomus brunnipennis* are very similar to *A. rubi* and can be distinguished by differences in body size (albeit with an overlap), 1.7–2.1 mm in *A. brunnipennis*, and 2.0–3.5 mm in *A. rubi* according to Dieckmann (1968) and 1.5–2.4 mm in *A. brunnipennis*

Table 1. Morphological differences between larvae and pupae of *Anthonomus brunnipennis* and *A. rubi*.

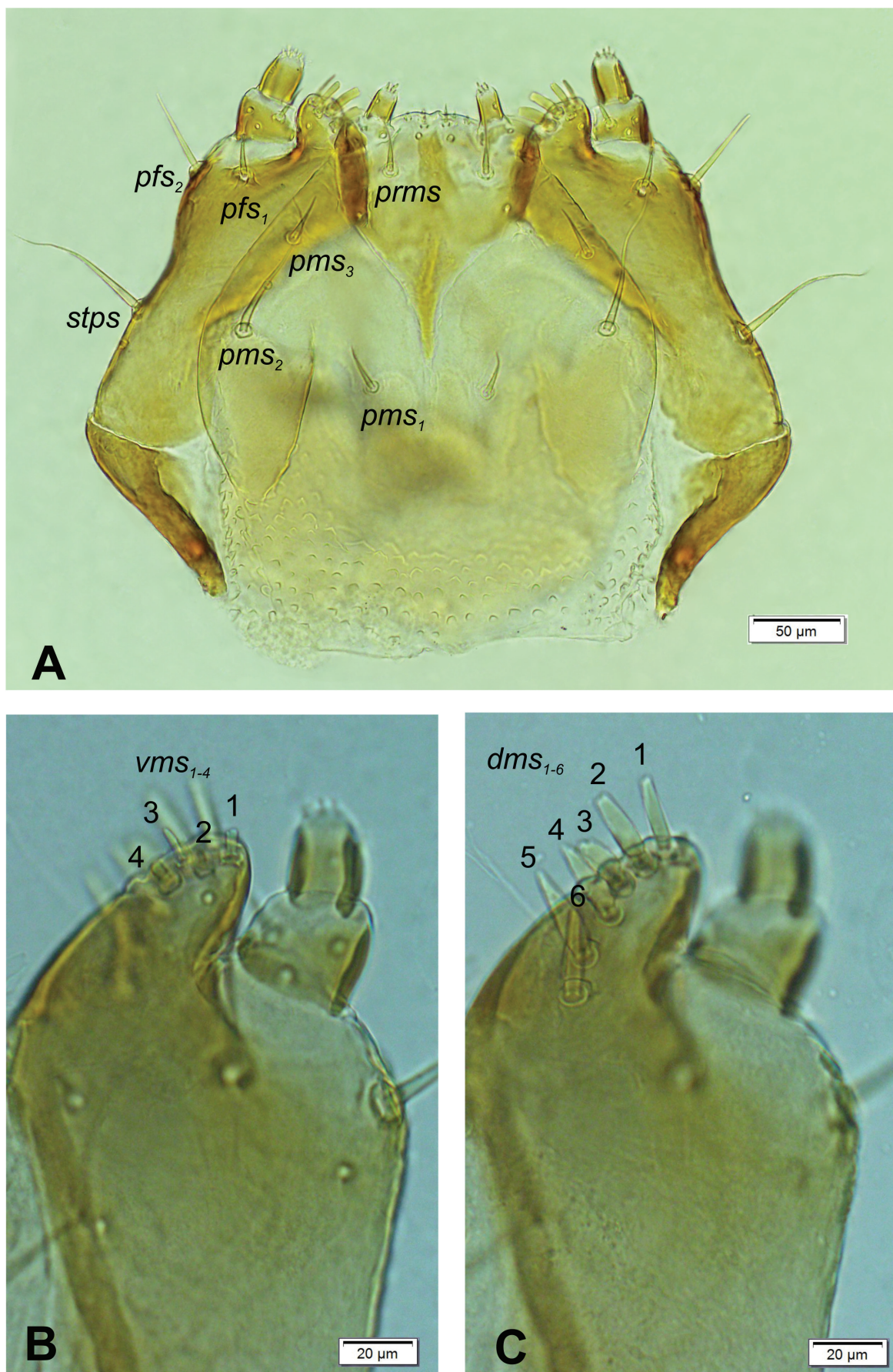|	*Anthonomus brunnipennis*	*Anthonomus rubi*
larva	body yellow, strongly curved, length up to 2.66 mm	body whitish to yellowish, length up to 3.42 mm
	head brown, up to 0.56 mm in length, with 3 *pes* and 2 *ves*	head yellowish, up to 0.67 mm in length, with 4 *pes* and 0 *ves*
	thorax with 10 *prns*, 2 *prs*, 5 *pds*, 2 *ss* and 3 *pda*	thorax with 11 *prns*, 1 *prs*, 4 *pds*, 1 *as*, 3 *ss* and 5 *pda* (+2 sensillae)
	abdominal segments I–VIII with 2 *prs*, 4 *pds*, 0 *ps* and 1 *eus*	abdominal segments I-VIII with 1 *prs*, 5 *pds*, 1 *ps* and 2 *eus*
	abdominal segment IX with 3 *ds* and 0 *sts*	abdominal segment IX with 6 *ds* and 2 *sts*
	clypeus without clss	clypeus with 1 clss
	labrum with 3 *ams*,	labrum with 2 *ams*
	epipharynx with 4 snp in single cluster	epipharynx with 4 snp in two separate clusters
	labial palpi two-segmented, with 6 *dms* and 4 *vms*	labial palpi one-segmented, with 5 *dms* and 5 *vms*
pupa	body length up to 2.30 mm	body length up to 3.42 mm,
	rostrum with 1 *rs*	rostrum without *rs*,
	head with 2 *sos* and 0 *os*	head with 1 *sos*, 1 *os*
	clubs covered with conical asperities	clubs smooth
	abdominal segments I–VII with 5 *d*	abdominal segments I–VII with 3 *d*
	urogomphi fused, with separate apical parts	urogomphi paired, located close together throughout their length

Figure 9. *Anthonomus brunnipennis* mature larva, maxillolabial complex (photos). **A.** Maxillolabial complex, ventral aspect; **B.** Apical part of right maxilla, ventral aspect; **C.** Apical part of right maxilla, dorsal aspect, (*dms*–dorsal malar, *pfs*–palpiferal, *prms*–prelabial, *pms*–postlabial, *stps*–stipal, *vms*–ventral malar, 1–6– malar setae numbers).
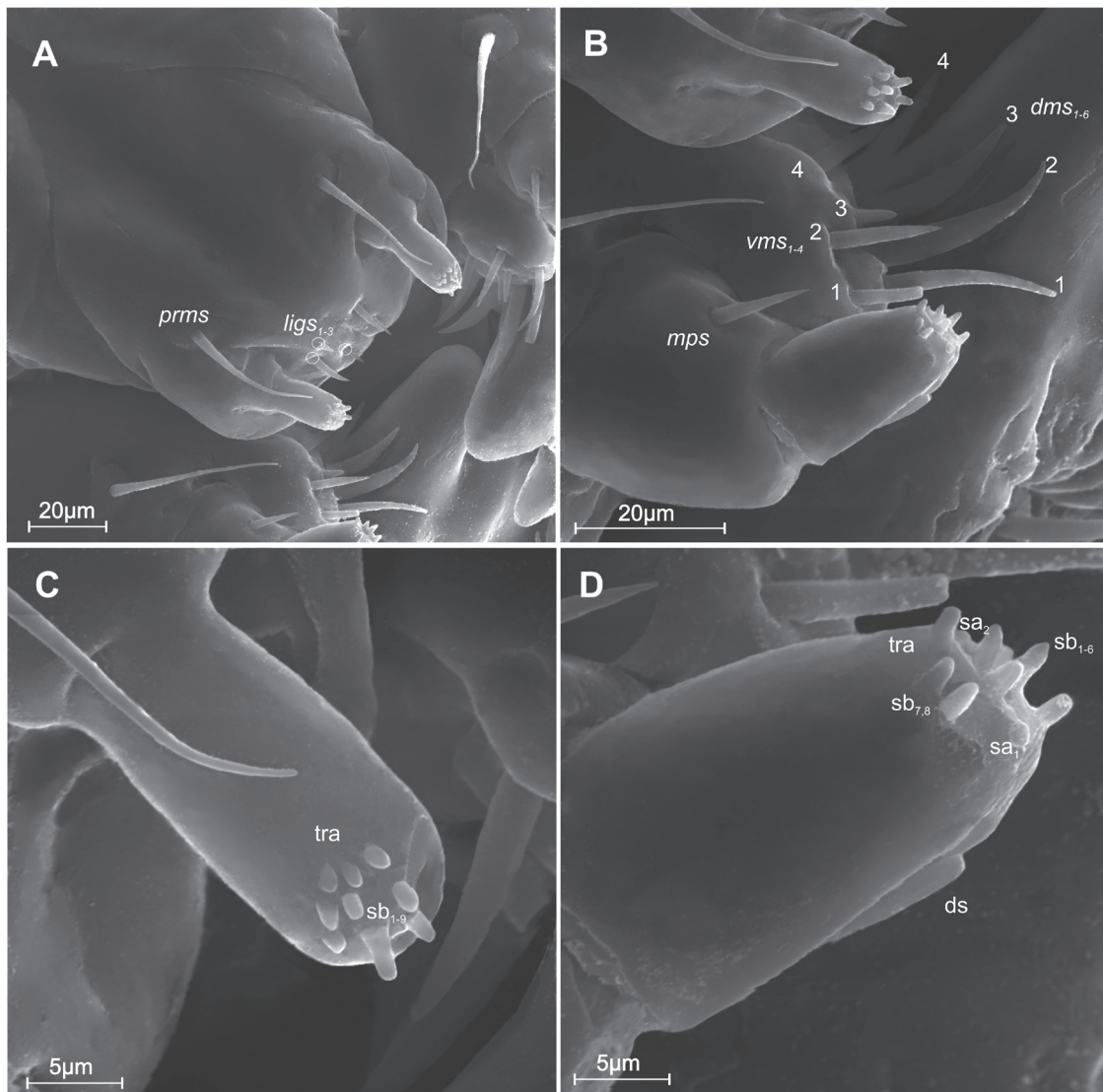
Figure 10. *Anthonomus brunnipennis* mature larva, maxillolabial complex (SEM micrographs). **A.** Prementum, ventral aspect; **B.** Apical part of right maxilla, lateral aspect; **C.** Distal, labial palpomere; **D.** Distal, maxillary palpomere (setae: *dms*–dorsal malar, *mps*–maxillary, *prms*–prelabial, *vms*–ventral malar palp; sensilla: ds–digitiform, sa–ampullaceum, sb–basiconicum; tra–terminal receptive area).

and 2.0–3.2 mm in *A. rubi* according to Palm 1992) by two separate light longitudinal fields on the aedeagus in *A. brunnipennis*, which are confluent in *A. rubi* (view from above; Palm 1992), and by the size of the aedeagus (Kevan 1965): 0.65–0.77 mm in *A. rubi* and 0.50–0.625 mm in *A. brunnipennis*. Kevan (1965) pointed out the length difference in the first antennomere of the funicle and Gurney (without date) in the second: both are more slender in *A. rubi* (Fig. 14). Other differences, e.g. body colour (Fig. 15), are not conclusive and are only of secondary importance, even if *A. brunnipennis* does tend to be dark reddish to dark brown in colour and *A. rubi* black. But immature adults may cloud this picture.

The immature stages of *A. rubi* were previously described by Scherf (1964) and Burke (1976), but the work of Zabaluev (2021) provided the most complete and detailed attempt. Thus, the immature stages of both species differ distinctly in the characters presented in Table 1.

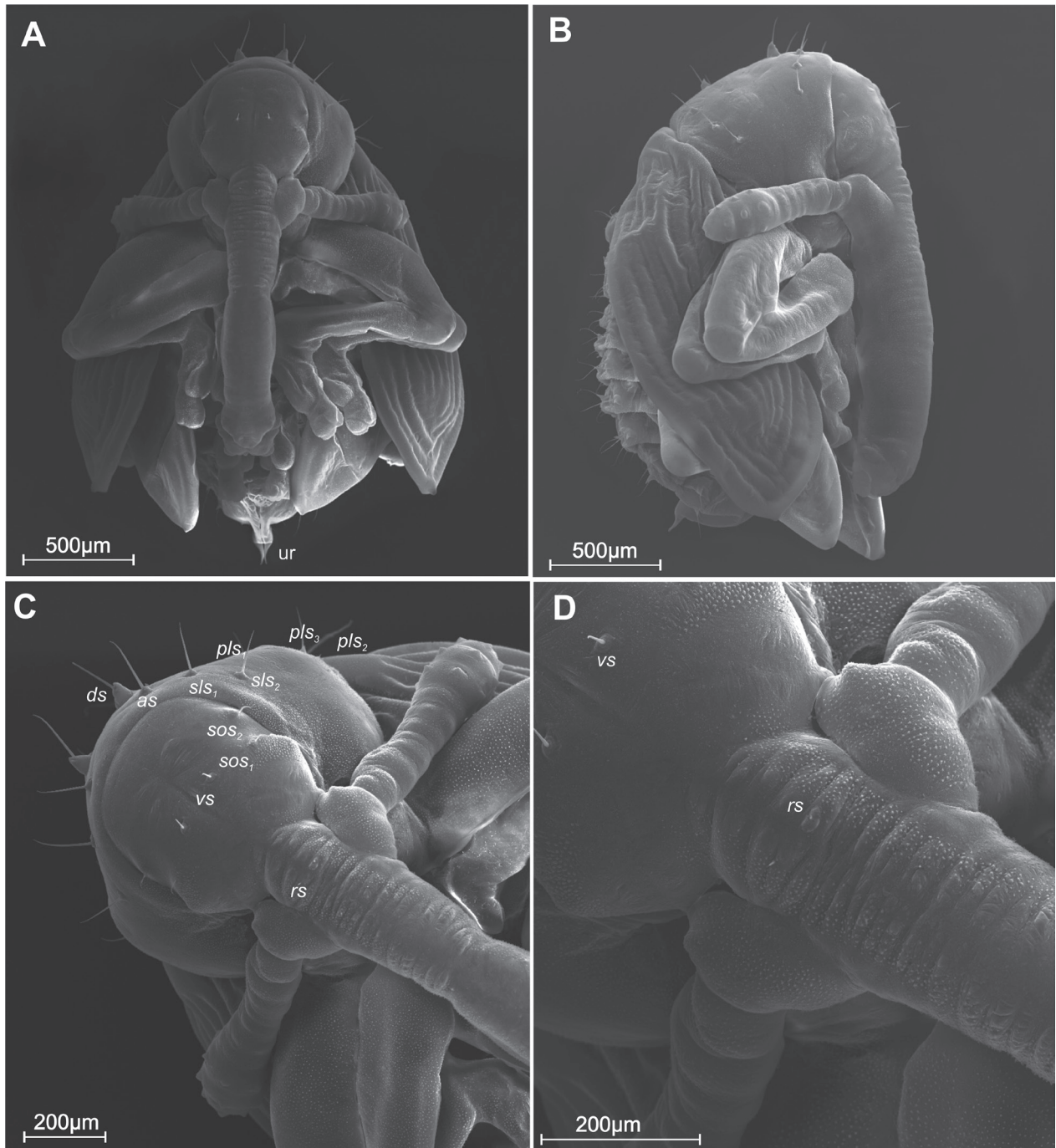**Figure 11.** *Anthonomus brunnipennis* pupa, habitus.

Figure 12. *Anthonomus brunnipennis* pupa (SEM micrographs). **A.** Habitus, ventral view; **B.** Habitus, lateral view; **C.** Head and rostrum base; **D.** Rostrum base magnification (ur–urogomphus, setae: *as*–apical, *ds*–discal, *sls*–lateral, *sos*–superorbital, *pls*–posterolateral, *rs*–rostral).

Based on the morphological structure of preimaginal stages, Zabaluev (2021) proposed a preliminary division of the genus *Anthonomus* into five species groups. In this division, group 3 contains *A. rubi* and *A. rubripes* Gyllenhal, 1836. Interestingly, despite the significant similarity of the adult stages, the larva of *A. brunnipennis* does not have any of the features characteristic of group 3, namely, 11 *prns* and the epipharynx with two separate clusters vs 10 *prns* and a single cluster on *A. brunnipennis*, whilst the pupa has well-defined features, prothoracic depressions and the presence of *sos*. It therefore seems that the

division into species groups within the genus *Anthonomus* requires redefinition.

It should be noted that both the larva and the pupa of *A. brunnipennis* have features found almost exclusively in Nearctic species (e.g. *A. nebulosus* LeConte, *A. grandis* Boheman, *A. stupulosus* Champion, *A. flavus* LeConte, *A. texanus* Dietz and *A. albopilosus* Dietz): snp organized in a single cluster, labial palpi two-segmented; in the pupal stage: a prothoracic depression, and abdominal segments I–VIII bearing five pairs of setae, placed on protuberances; setae alternating in length with noticeably
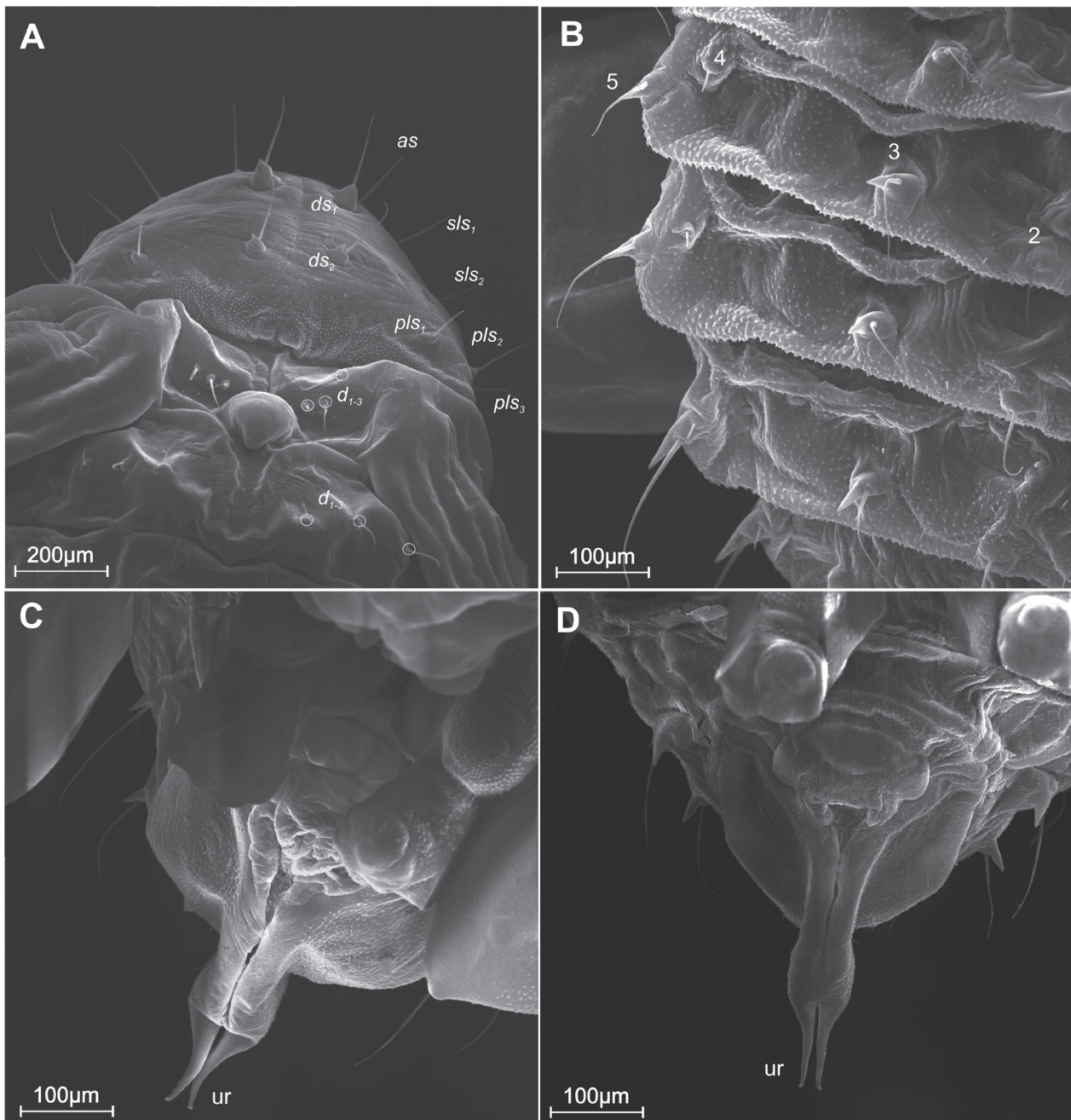
Figure 13. *Anthonomus brunnipennis* pupa, habitus and chaetotaxy. **A.** Pro–, meso– and metathorax dorsal view; **B.** Abdominal segments; **C.** Females abdominal terminal segments; **D.** Males abdominal terminal segments, magnification (ur–urogomphus, setae: *as*–apical, *d*–dorsal, *ds*–discal, *sls*–lateral, *pls*–posterolateral, 1–5– dorsal setae numbers).

shorter setae in the odd intervals. The characteristic features at the generic level of both the larva and the pupa of the genus *Anthonomus* were specified precisely by Zabaluev (2021). Hence, they do not require further elaboration. In turn, based on available descriptions (Burke 1968; Ahmad and Burke 1972; Vanin et al. 2013), the following characters are diagnostic of the genus *Anthonomus* at the larval stage and distinguish it from other genera of the tribe Anthonomini: (1) always 3 *als* (*Furcipus* Desbrochers with 2 *als*), (2) except in *A. rubi* and *A. rubripes*, snp arranged in a single median cluster of 4 units (*Smicraulax* Pierce without snp; *Anthonomopsis*

Dietz, *Loncophorus* Chevrolat and *Tachypterellus* Fall & Cockerell snp arranged in two lateral clusters, (3) labral rods separate (*Pseudanthonomus* Dietz and *Coccotorus* LeConte labral rods posteriorly fused).

The pupa of *Anthonomus brunnipennis* exhibits evident sexual dimorphism in the gonotheca – divided in the female, undivided in the male – with tubercles on subcontiguous lobes. Similar structures have also been observed in the genus *Aspidapion* Schilsky, 1901 (Gosik, in press) and in *Smicronyx smreczynskii* Solari, 1952 (Sprick and Gosik 2023). According to Burke (1968) a bilobed gonotheca is a characteristic feature of female pupae.
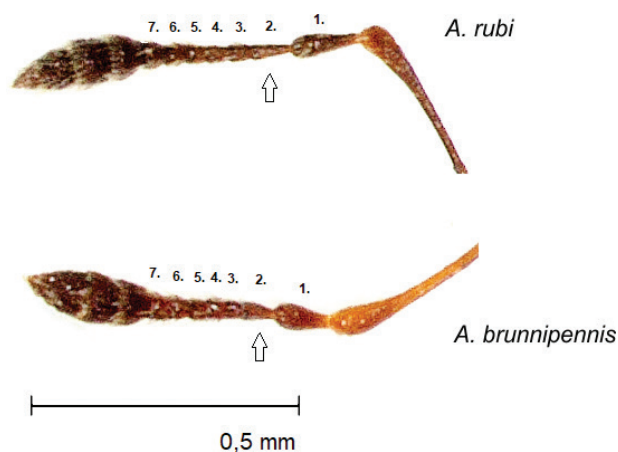
Figure 14. Comparison of antennae of *Anthonomus brunnipennis* and *A.rubi*.

Bionomics

According to literature data, *Anthonomus brunnipennis* is an oligophagous species that feeds on several plants from the family Rosaceae Juss. Dieckmann (1968), Hoffmann (1954), Koch (1992), Palm (1992) and Morris (2012) list *Comarum palustre* L. (syn. *Potentilla palustris* (L.) Scop.), *Dryas octopetala* L., *Filipendula ulmaria* and *Potentilla erecta* (L.) Raeusch. Its presence on the genus *Helianthemum* Mill. (family Cistaceae Juss.) was recorded by Tempère and Péricart (1989), even though it seems highly improbable that this genus and family are host plants of *A. brunnipennis*. Another explanation could be that weevils migrate to a plant with similar small, yellow flowers before *Potentilla erecta* starts to flower. According to Hoffmann (1954), *Filipendula ulmaria* (L.) Maxim. is also mentioned as a host plant of *A. brunnipennis*. However, the relationship between *A. brunnipennis* and this morphologically rather different species seems doubtful and requires confirmation by detailed field observations, e.g. oviposition behaviour or the presence of larvae. In Schleswig-Holstein, to date the region with the only German localities, R. Suikat found this species only on *Potentilla erecta*, even though *Comarum palustre* was growing nearby at the same locality (pers. comm. 2024) (habitat, see Fig. 2). Morris (2012) described this situation in similar words: "On *Potentilla erecta*, possibly other *Potentilla* species, and *Comarum palustre*". Dieckmann (1968) cited Crotch, who found a form of *A. brunnipennis* on *Comarum palustre* in Scotland only in very wet localities. To clarify this situation, data regarding host plants apart from *Potentilla erecta* should be confirmed by records of larvae.

On current British websites, only *Potentilla erecta* is listed as a host plant (https://www.ukbeetles.co.uk/curculioninae). Earlier data from *Comarum palustre* or some other plants, such as the widespread *Filipendula ulmaria*, have for some unknown reason not been repeated. The use of *Potentilla erecta* as a host plant in Denmark was confirmed by Palm (1992).

Figure 15. Comparison. **A.** *Anthonomus brunnipennis* male, habitus; **B.** *A. rubi* male, habitus.

It can be stated that Hoffmann (1954) lists only *Comarum palustre*, *Dryas octopetala*, and *Filipendula ulmaria* as host plants of *Anthonomus brunnipennis*, but he overlooked the main host plant, *Potentilla erecta*, what means that all his host plant data are of low reliability.

At present, only *Potentilla erecta* can be regarded as a host plant of *Anthonomus brunnipennis*, and the status of *Comarum palustre* and *Dryas octopetala* requires confirmation. The presence of *A. brunnipennis* adults in the flowers of Cistaceae, as reported by Tempère and Péricart (1989), remains doubtful. In a current barcoding study Germann et al. (2017) did not find any difference to *A. rubi* in Alpine populations collected from *Helianthemum* (Cistaceae) and from *Dryas octopetala*. At this moment Cistaceae cannot be regarded as host plant either of *A. rubi* or of *A. brunnipennis*, and Germann (2017) recommended to delete *A. brunnipennis* from the checklist of Swiss weevils.

Anthonomus brunnipennis is classified as a stenotopic, hygrophilous species and inhabits cold and usually wet, nutrient-poor sites like certain swamps, bogs, mountain and moor meadows (Koch 1992 and our own observations). Interestingly, the northern distribution of this species coincides with the previously described relationships of characters of immatures with Nearctic (northern) species. The distribution at the southern boundary of its range may be limited by warm climate conditions and may be restricted to bogs and fens, and to mountain areas, a phenomenon which is observed in other weevils, too, e.g. *Otiorhynchus*

rugifrons or *Sitona lineellus* (see Heijerman and Hodge 2005; Rheinheimer and Hassler 2010; Germann 2013).

Unlike *Anthonomus rubi*, which is a ubiquitous species, *Anthonomus brunnipennis* is a strictly stenotopic species and occurs at only a few sites with a high degree of naturalness (National Parks, reserves), especially in the southern parts of its range in middle Europe. Because these ecosystems are threatened by nitrogen entries from the atmosphere and subsequent changes to the vegetation, and also by the effects of climate warming (drought, temperature increases), *A. brunnipennis* has been identified as a highly endangered species in Germany (see Sprick et al. 2021), and may be a candidate for such a status in other countries along the southern boundary of its range.

Author Contributions

Acknowledgements

References

Ahmad M, Burke HR (1972) Larvae of the weevil tribe Anthonomini. Miscellaneous Publications of the Entomological Society of America 8: 31–80. https://doi.org/10.4182/SPOJ1513.8-2.33

Alonso-Zarazaga MA, Barrios H, Borovec R, Bouchard P, Caldara R, Colonnelli E, Gültekin L, Hlaváč P, Korotyaev B, Lyal CHC, Machado A, Meregalli M, Pierotti H, Ren L, Sánchez–Ruiz M, Sforzi A, Silfverberg H, Skuhrovec J, Trýzna M, Velázquez de Castro AJ, Yunakov NN (2023) Cooperative Catalogue of Palaearctic Coleoptera Curculionoidea, 2nd edn. Sociedad Entomológica Aragonesa, *Monografías electrónicas SEA*, 14, 780 pp. www.sea–entomologia.org [accessed on 03 April 2024]

Anderson WH (1947) A terminology for the anatomical characters useful in the taxonomy of weevil larvae. Proceedings of the Entomological Society of Washington 49: 123–132.

Anderson RS (1993) Weevils and plants: Phylogenetic versus ecological mediation of evolution of host plant associations in Curculionidae (Curculioninae). Memoirs of the Entomological Society of Canada 125: 197–232. https://doi.org/10.4039/entm125165197-1

Bená D, Vanin SA (2013) Description of the immature stages of the weevil *Anthonomus vis* Clark (Coleoptera, Curculionidae), inquiline into the gall of *Leandra aurea* (Melastomataceae). Revista Brasileira de Entomologia 57: 367–373. https://doi.org/10.1590/S0085-56262013005000032

Burke HR (1968) Pupae of the weevil tribe Anthonomini (Coleoptera, Curculionidae). Texas Agricultural Experiment Station Technical Monograph 5: 1–92.

Burke HR (1976) Bionomics of the Anthonomine weevils. Annual Review of Entomology 21: 283–303. https://doi.org/10.1146/annurev.en.21.010176.001435

Burke HR, Gates DB (1974) Bionomics of several North American species of Anthonomus (Coleoptera: Curculionidae). Southwestern Naturalist 19: 313–327. https://doi.org/10.2307/3669937

Caldara R (2013) Curculioninae In: Löbl I and Smetana A (Eds.), Catalogue of Palaearctic Coleoptera. Vol. 8. Curculionoidea II. Brill. Leiden, Boston, 700 pp.

Caxambu MG (2003) *Anthonomus partiarius* Boheman, 1843 (Coleoptera, Curculionidae) associado a Tibouchina cerastifolia (Naud.) Cogniaux (Melastomataceae): formas imaturas, aspectos bioecológicos e testes de especificidade. Doctoral thesis, Universidade Federal do Paraná, Brazil, 71 pp.

Chacón-Madrigal EJ, Johnson TM, Hanson P (2012) The life history and immature stages of the weevil *Anthonomus monostigma* Champion (Coleoptera: Curculionidae) on *Miconia calvescens* DC (Melastomataceae). Proceedings of the Entomological Society of Washington 114: 173–185. https://doi.org/10.4289/0013-8797.114.2.173.

Clark WE (2005) Revision of the subgenus *Cnemocyllus* Dietz of the weevil genus *Anthonomus* Germar (Coleoptera: Curculionidae, Anthonomini). Insecta Mundi 19: 1–54.

Clark WE (2013) List of Species of Curculionidae (Coleoptera) assigned to the tribe Anthonomini. Auburn University. http://www.auburn.edu/;clarkwe/anthspp.htm [accessed 24 January 2017]

Dieckmann L (1968) Revision der westpaläarktischen Anthonomini (Coleoptera: Curculionidae). Beiträge zur Entomologie 17(3/4): 377–564.

Gates DB, Burke HR (1972) Review of the gall-inhabiting weevils of the genus *Anthonomus*, with description and biology of a new species (Coleoptera: Curculionidae). Annals of the Entomological Society of America 65: 1215–1224. https://doi.org/10.1093/aesa/65.5.1215

Germann Ch (2013) Erster Nachtrag zur Checkliste der Rüsselkäfer der Schweiz (Coleoptera, Curculionoidea). Mitteilungen der Schweizerischen Entomologischen Gesellschaft 86: 151–164.

Germann Ch (2017) Zweiter Nachtrag zur Rüsselkäfer-Fauna der Schweiz (Coleoptera, Curculionoidea). Alpine Entomology 1: 43–49. https://doi.org/10.3897/alpento.1.17788

Germann Ch, Wyler S, Bernasconi MV (2017) DNA barcoding of selected alpine beetles with focus on Curculionoidea (Coleoptera). Revue suisse de Zoologie 124(1): 15–38.

Gosik R (in press) Evidence from immature stages in support of systematic separateness between the genera *Aspidapion* Schilsky, 1901 and *Pseudaspidapion* Wanat, 1990 (Coleoptera, Brentidae, Apioninae). Zootaxa Gurney M (without date): *Anthonomus* and *Furcipus*. https://quelestcetanimal-lagalerie.com/wp-content/uploads/2018/11/Anthonomus-and-Furcipus.pdf [accessed on 05.06.2024]

Gosik R, Sasa A, Witkowski ETF (2017) Description of the mature larva and pupa of *Anthonomus santacruzi* Hustache (Coleoptera, Curculionidae), a biological control agent of Solanum mauritianum

Scop. (Solanaceae), and remarks about its biology. Zootaxa 4294: 545–558. https://doi.org/10.11646/zootaxa.4294.5.4

Heijerman T, Hodge PJ (2005) Bisexual populations of *Otiorhynchus rugifrons* (Coleoptera: Curculionidae). Entomologische Berichten 65(3): 66–69.

Hille Ris Lambers D (1950) On mounting aphids and other soft–skinned insects. Entomologische Berichten 13: 55–58.

Hoffmann A (1954) Coleopteres Curculionides II. Faune de France 59: 487–1208. https://doi.org/10.3406/bsef.1954.18700

Jones RW (2001) Evolution of the host plant associations of the *Anthonomus grandis* species group (Coleoptera: Curculionidae): Phylogenetic tests of various hypotheses. Annals of the Entomological Society of America 94: 51–58. https://doi.org/10.1603/0013-8746(2001)094[0051:EOTHPA]2.0.CO;2

Kevan DK (1965) *Anthonomus rubi* Herbst var. *brunneipennis* Curtis, a separate species. - Col. Curculioniade. Entomologist's monthly Magazine 101: 203–205.

Koch K (1992) Die Käfer Mitteleuropas. Vol. 3 (Ökologie), Goecke and Evers, Krefeld, 380 pp.

Legalov AA (2000) To identification of *Anthonomus rubi* (Coleoptera, Curculionidae) in Asian part of Russia and adjacent territories. Zoologichesky Zhurnal 79(2): 247–250. [In Russian]

Loiácono MS, Marvaldi AE, Lanteri AA (2004) Description of larva and new host plants for *Anthonomus rubricosus* Boheman (Coleoptera: Curculionidae). Entomological News 114: 69–74.

Marvaldi AE (1997) Higher level phylogeny of Curculionidae (Coleoptera: Curculionoidea) based mainly on larval characters, with special reference to broad–nosed weevils. Cladistics 13: 285–312. https://doi.org/10.1006/clad.1997.0049

Marvaldi AE (1998) Larvae of South American Rhytirrhininae (Coleoptera: Curculionidae). The Coleopterists Bulletin 52: 71–89.

Marvaldi AE (1999) Morfología larval en Curculionidae. Acta zoológica Lilloana 45: 7–24.

Marvaldi AE (2003) Key to larvae of the South American subfamilies of weevils (Coleoptera, Curculionoidea). Revista Chilena de Historia Natural 76: 603–612. https://doi.org/10.4067/S0716-078X2003000400005

May BM (1994) An introduction to the immature stages of Australian Curculionoidea. In Australian weevils. Zimmerman, E.C. Eds.; Brentidae, Eurhynchidae, Apionidae and a chapter on immature stages by Brenda May. Volume II. CSIRO, Melbourne.

Morris MG (2012) True Weevils 3: Coleoptera: Curculionidae (Curculioninae, Baridinae, Orobitidinae). Handbooks for the Identification of British Insects Royal Entomological Society, Vol. 5/17d, 136 pp.

Olckers T (1999) Biological control of *Solanum mauritianum* Scopoli (Solanaceae) in South Africa: a review of candidate agents, progress and future prospects. African Entomology Memoir 1: 65–73.

Palm E (1992) *Anthonomus brunnipennis* Curtis 1840 er utbredt i Norden! (Coleoptera, Curculionidae). Entomologisk Tidskrift 113: 52–54.

Preising E, Vahle H-C, Brandes D, Hofmeister H, Tüxen J, Weber HE 1997 Die Pflanzengesellschaften Niedersachsens. Rasen-, Fels- und Geröllgesellschaften. Naturschutz und Landschaftspflege in Niedersachsen 20(5): 1–146.

Preising E, Vahle H-C, Tüxen J (2012) Die Pflanzengesellschaften Niedersachsens – Heide-, Moor- und Quellgesellschaften. Naturschutz und Landschaftspflege in Niedersachsen 20(1+3): 1–114. [+ CD ROM]

Rheinheimer J, Hassler M (2010) Die Rüsselkäfer Baden-Württembergs. Naturschutz-Spectrum, Themen 99; verlag regionalkultur, 944 pp.

Scherf H (1964) Die Entwicklungsstadien der mitteleuropäischen Curculioniden (Morphologie, Bionomie, Ökologie). Abhandlungen der Senckenbergischen Naturforschenden Gesellschaft 506: 335.

Skuhrovec J, Gosik R, Caldara R, Košťál M (2015) Immatures of Palaearctic species of the weevil genus Sibinia (Coleoptera, Curculionidae): new descriptions and new bionomic data with suggestions on their potential value in a phylogenetic reconstruction of the genus. Zootaxa 3955: 151–187. https://doi.org/10.11646/zootaxa.3955.2.1

Smreczyński S (1972) Ryjkowce – Curculionidae: Podrodzina Curculioninae. Klucze do Oznaczania Owadów Polski 77: 195. [in Polish]

Sprick P, Floren A (2018) Diversity of Curculionoidea in Humid Rain Forest Canopies of Borneo: A Taxonomic Blank Spot. Diversity 10(116): 20. https://doi.org/10.3390/d10040116

Sprick P, Gosik R (2023) Biological data on *Smicronyx* species with a first description of immature stages of *Smicronyx smreczynskii* Solari, 1952 (Coleoptera, Curculionidae). Weevil News 110: 15.

Sprick P, Behne L, Maus C (2021) Rote Liste und Gesamtartenliste der Rüsselkäfer (i.e.S.) Deutschlands (Überfamilie Curculionoidea; exklusive Anthribidae, Scolytidae, Platypodidae). Naturschutz und Biologische Vielfalt 70(5): 335–412.

Tempère G, Péricart J (1989) Coléoptères Curculionidae. 4. Compléments aux trois volumes d'Adolphe Hoffmann: corrections, additions et répertoire. Faune de France 74: 536 pp.

Vanin SA, Cassia Bená D, Albertoni FF (2013) Description of immatures and natural history of the weevil *Loncophorus pustulatus* (Champion, 1903) (Coleoptera: Curculionidae: Curculioninae) associated with flowers of *Ceiba speciosa* (A. St.-Hil.) Ravenna (Bombacoideae: Malvaceae) in southeast Brazil. Zootaxa 3636: 451–462. https://doi.org/10.11646/zootaxa.3636.3.4

Zabaluev IA (2021) Contribution to the knowledge of the immature stages of Palaearctic species of the genus *Anthonomus* Germar (Coleoptera: Curculionidae). Zootaxa 5032(4): 451–488. https://doi.org/10.11646/zootaxa.5032.4.1

Zacharuk RY (1985) Antennae and sensilla. In: Comparative Insects Physiology, Chemistry and Pharmacology. Kerkut GA, Gilbert LI (Eds) Pergamon Press, Oxford, Vol. 6, 69 pp.

MUSEUM FÜR
NATURKUNDE
BERLIN

Phylogenetic analysis of the circum-Antarctic Subfamily Migadopinae (Coleoptera, Carabidae) and assessment of the trans-Tasman *Amarotypus* clade

James K. Liebherr[1], Sergio Roig-Juñent[2], Kipling W. Will[3]

1   *Cornell University Insect Collection, Ithaca, NY 14853-2601 USA*

2   *Laboratorio de Entomología, Instituto Argentina de Investigaciones de las Zonas Áridas (IADIZA, CCT–CONICET, Mendoza), 5500 Mendoza, Argentina*

3   *Essig Museum of Entomology, University of California, Berkeley, CA, 94720-3112 USA*

https://zoobank.org/A1638EDA-A566-4837-A558-AA2707FBD0EB

Corresponding author: James K. Liebherr (jkl5@cornell.edu)

Abstract

Phylogenetic analysis of Migadopinae Chaudoir, 1861, based on morphological characters analyzed using maximum parsimony and Bayesian inference, recognizes the tribal adelphotaxa Aquilicini Moret, 2005 and Migadopini. Amarotypini Erwin, 1985 (type genus *Amarotypus* Bates, 1872) is newly synonymized with Migadopini, as its taxonomic recognition renders Migadopini paraphyletic. Phylogenetic relationships within Migadopinae establish the Andean tropicomontane *Aquilex* Moret, 1989—type genus of the monogeneric Aquilicini—as sister group to the circum-Antarctic Migadopini. The earliest-diverging member taxa of Migadopini are distributed across southern South America and the subantarctic Falkland Islands. Subsequent divergence implicates Australia, New Zealand, and the Campbell Plateau. Internodes of the taxon-area cladogram are optimized using RASP (Reconstruct Ancestral State in Phylogenies), with nodal optimizations interpretable by both vicariance or dispersal. Campbell Plateau taxa are ambiguously derived from an ancestral node optimized to either South America, Australia, or the Campbell Plateau itself, a result most consistent with fragmentation of these Gondwanan terranes. Only the origin of the Tasmanian *Migadopiella* Baehr—taxonomically placed within a paraphyletic assemblage comprising the New Zealand genera *Amarotypus*, *Amaroxenus* Larochelle & Larivière, and *Amarophilus* Larochelle & Larivière—is interpreted unambiguously as dispersal based, in this instance via east to west trans-Tasman dispersal. Winged flight by migadopine carabid beetles, previously hypothesized as a vehicle for dispersal between Australia and South America, is dismissed based on restriction of macropterous taxa to two disparate and highly subordinate taxa; one comprising the Australian tropicomontane *Dendromigadops* Baehr and its temperate rainforest-occupying sister genus *Decogmus* Sloane, and the second, *Antarctonomus complanatus* of Valdivian and Magellanic *Nothofagus* forest in Chile and Argentina. Relevant fossil evidence supporting austral relationships of Migadopinae is briefly reviewed, including the mid-Cretaceous occurrence of Migadopinae in Kachin Burmese Amber, and the Miocene-aged fossil carabid beetle, *Antarctotrechus balli* Ashworth and Erwin (Trechini), described from the trans-Antarctic Mountains. The former supports a Cretaceous origin for Migadopinae consistent with Austral vicariance, the latter augurs the discovery of biogeographically homologous Antarctic fossil representatives that could corroborate an Austral vicariance hypothesis for the migadopine radiation.

Key Words

Antarctica, Austral disjunct pattern, biogeography, dispersal, Gondwana, vicariance

Introduction

No topic in historical biogeography has engendered more interest and controversy than the underlying bases for the biotic relationships of the southern continents. Extensive similarities among the floras of New Zealand, Australia, and South America were documented by Hooker (1867); by his estimation, of 303 genera he recognized for New Zealand, 252 also occurred in Australia, and 174 in South America. His explanation for such area relationships was founded on the hypothesis that "*many existing Orders and Genera of plants of the highest development may have flourished during the Eocene and Cretaceous periods, and have hence survived complete revolutions in the temperature and geography of the middle and temperate latitudes of the globe* (Hooker 1859, p. xvii)". Hooker himself immediately offered a counterargument to his hypothesis: "*Mr. Darwin has greatly extended in another direction these views of the antiquity of many European species, and their power of retaining their faces unchanged during most extensive migrations, by his theory of the simultaneous extension of the glacial temperature in both hemispheres, and its consequent effect in cooling the tropical zone* (Hooker 1859, xvii)". Thus, the conventionally-viewed dichotomy of vicariance of ancient biotas surviving revolutions in geography, versus dispersal mediated by climatic changes became established as competing hypotheses explaining the biotic relationships of life on the southern continents. These competing viewpoints are well illustrated by alternate hypotheses proposed to explain diversification of the carabid beetle subfamily Migadopinae Chaudoir, 1861.

Based on Wegener's (1924) hypotheses regarding the past spatial relationships of the continents and oceans, which formed the historical basis for interpreting the climatological observations of Köppen and Wegener (1924), Jeannel (1938) proposed that migadopines originated as early as the Cretaceous on Gondwanan terranes that subsequently became isolated to form present-day southern South America, Australia, New Zealand, and the subantarctic Auckland Islands. Jeannel supported his hypothesis using comparisons of congruent biogeographic patterns in other taxa including, among others, representatives of the carabid subfamilies Broscinae, Bembidiinae tribe Oopterini, and Trechinae tribe Homaloderini (Jeannel 1938: 52). Jeannel's approach accords with Hooker's (1859) view of biogeographic history as revolutionary, with significant changes in both geography and climate underlying historical patterns of diversification.

Darlington (1965), also chose migadopines to exemplify the austral disjunct biogeographic pattern wherein taxa occupy the southern reaches of Australia, New Zealand and South America. He posited that "All faunas are derived. Nowhere in the world is there an existing fauna that cannot be accounted for in terms of derivations from other parts (Darlington 1971: 216)." Moreover, "The history of dispersal of animals seems to be primarily the history of successions of dominant groups, which in turn evolve, spread over the world, compete with and destroy and replace older groups, and then differentiate in different places until overrun and replaced by succeeding groups (Darlington 1959: 488)." In explaining migadopine biogeographic history, he focused on migadopine taxa that occur in subtropical areas, and one—*Decogmus* from subtropical New South Wales, Australia (Baehr 2013)—that retains fully developed metathoracic flight wings in contradistinction to most other migadopine taxa that have reduced, nonfunctional wings. He also noted that Elaphrinae Latreille, 1802, proposed as the closest relatives to Migadopinae by Jeannel (1938), are of Holarctic distribution, necessitating long-distance dispersal from the Northern Hemisphere to account for a southern ancestral distribution for Migadopinae. Darlington also assumed that "the continents and climatic zones have been constant in position during the period under consideration, which is mainly the later Tertiary, Pleistocene, and Recent (Darlington 1959: 489)," thereby requiring migadopines to have dispersed across the Southern Ocean while colonizing Australia, New Zealand and South America.

More recent findings help illuminate the diversification history of Migadopinae. Moret (1989) discovered a remarkable, high-elevation migadopine on Chimborazo, Ecuador—*Aquilex diabolica* Moret—that he proposed as the sister group to all other migadopines. This finding fills in the biogeographic "gap" between migadopines and any Holarctic relatives. Roig-Juñent (2004) conducted a parsimony-based cladistic analysis of migadopines, corroborating Moret's (2005) placement of *Aquilex diabolica*. He also demonstrated the initial radiation of migadopines in South America, with subsequent diversification in Australia and New Zealand. Rogi-Juñent also placed *Amarotypus edwardsii* Bates—type genus of Amarotypini Erwin, 1985—within Migadopini, thereby undercutting cladistic support for tribal status of Amarotypini.

Subsequent advances in taxonomic understanding have been contributed by Johns' (2010) revision of the migadopines of New Zealand, and Baehr's (2009) description of the Tasmanian genus *Migadopiella* Baehr, 2009, followed by his revision of the tribe for Australia (Baehr 2013). Finally, Larochelle and Larivière (2022) revised the New Zealand taxa related to *Amarotypus* Bates, 1872, proposing two new genera—*Amarophilus* Larochelle & Larivière and *Amaroxenus* Larochelle & Larivière—while newly describing 13 species. Their work validates taxa related to those presented informally as "undescribed carabid genus (Johns 1969: 398)", and "New genus, new species A … new species B (Sweney 1980: 107)."

This contribution provides an updated phylogenetic analysis, built on Roig-Juñent (2004), that incorporates additional character information provided by the inclusion of additional outgroup taxa representing the tribe Cicindini Bänninger (Kavanaugh and Erwin 1991), as well as genera described by Baehr (2009, 2013) and Larochelle and Larivière (2022). The resultant cladogram is used to establish a natural classification of Migadopinae wherein monophyletic subtribes and genera are recognized. Multiple generic representatives are included to test the mono-

phyly of the various genera. The phylogenetic hypothesis provides the necessary foundation for historical biogeographic analysis testing whether Migadopinae diversified contemporaneous with fragmentation of Gondwana into its constituent present-day areas of South America, Australia, and New Zealand. Relationships among various subsidiary, and therefore more recently evolved migadopine taxa that occupy Tasmania, New Zealand's South Island, and the Auckland and Antipodes Islands, are interpreted in the context of geological hypotheses in order to ascertain whether vicariance or taxic dispersal better explains these trans-Tasman biogeographical distributions.

Material and methods

Taxonomic material

Specimens were taken on loan for study from the following institutions: Cornell University Insect Collection (**CUIC**), Ithaca, NY, US; Essig Museum of Entomology (**EMEC**), University of California, Berkeley, CA, US; Field Museum of Natural History (**FMNH**), Chicago, IL, US; Lincoln University Entomology Research Collection (**LUNZ**), Lincoln, NZ; Museum of Comparative Zoology (**MCZ**), Harvard University, Cambridge, MA, US; The Natural History Museum (**NHML**), London, UK; New Zealand arthropod Collection, Mt. Albert, NZ (**NZAC**); Tasmanian Museum and Art Gallery (**TMAG**), Hobart, AU; Zoological Museum, University of Copenhagen (**ZMUC**), Copenhagen, DK; Zoologisches Staatssammlung (**ZSM**), München, Bavaria, DE.

Taxonomic protocols

Specimens were examined using a Wild M5 microscope with halogen ring-light illumination at 6–100× magnification. Genitalic dissections were made after specimens were relaxed in hot deionized water containing a few drops of Kodak Photo-Flo® detergent, with the dissections accomplished using modified minutens and watchmakers' forceps. The dissected structures were cleared in 10% cold KOH overnight, then neutralized in dilute acetic acid, and subsequently held in glycerin for viewing and ultimate storage in polyethylene genitalia vials mounted on the specimen pin. Female reproductive tract structures were stained in Kodak Chlorazol Black® suspended in methyl cellosolve after the acetic acid neutralizing step, and then transferred after 15 minutes' staining time to glycerin for viewing. These structures were likewise stored in genitalia vials. Specimen localities were recorded using the area definitions of Crosby et al. (1976).

Body proportions and shapes were quantified using mensural characters determined using an ocular reticle. These include eye size as the ocular ratio MHW / mFW, with MHW being maximal head width across the compound eyes, and mFW is minimum frons width between the compound eyes. Pronotal shape is represented by several ratios—APW / BPW, MPW / BPW, and MPW / PL—where **APW** is apical pronotal width measured at the front angles, **MPW** is maximal pronotal width, **BPW** is basal pronotal width measured between the basal angles, and **PL** is pronotal length measured along the midline. Elytral shape is quantified using HuW / MEW, and MEW / EL; that is **HuW** = width across the humeral angles, **MEW** = maximal elytral width, and **EL** = elytral length measured from the base of the scutellum to the apex of the left elytron. Standardized body size is quantified as the sum of HL + PL + EL, where HL is the midline distance between the anterior margin of the labrum and the ridge demarking the juncture between the vertex and cervix, and PL and EL are as defined above. Migadopines also exhibit variously laterally expanded pro- and mesotarsomeres, that development quantified as the ratio of the maximal lateral breadth of tarsomere 2, divided by the median tarsomere length; w / l. Terminology used for describing male genitalia was based on Lindroth (1957), with Liebherr and Will (1998) followed for interpretation of the female gonocoxae and bursa copulatrix.

Phylogenetic analysis

Cladistic analysis was performed under the maximum parsimony criterion based on a data matrix (Suppl. material 1) comprising 74 characters for 42 taxa (Table 1), this matrix an amended expansion of the 57 character × 29 taxon matrix of Roig-Juñent (2004). The additional taxa principally include those from New Zealand and Australia phylogenetically allied with *Amarotypus edwardsii*. The twenty characters added to the matrix of Roig-Juñent are each indicated below by an asterisk following the character number, while character 43 of Roig-Juñent was deleted as it is autapomorphic. Characters numbered 56 and 57 of Roig-Juñent (2004) were also deleted: 56 because it incorrectly coded *Amarotypus edwardsii* to lack the setose sensillum of the apical gonocoxite, and 57 because a helminthoid sclerite as defined by Liebherr and Will (1998) is not present in migadopine taxa. The resultant matrix was originally edited and entered using Winclada ver. 1.00.08 (Nixon 2002) and subsequently imported into Mesquite ver. 3.81 (Maddison and Maddison 2023b). Using Mesquite, the matrix was submitted to TNT (Goloboff and Morales 2023) with the Zephyr ver. 3.31 (Maddison and Maddison 2023a) package for both parsimony tree and jackknife resampling searches. Tree search was done using Mesquite's default commands for TNT modified to as follows: "Hold" increased to 1000000, "replic" set to 1000, and tbr used "nofillonly". For jackknife analysis Mesquite's default commands for TNT were used and 1000 replications were done. Tree statistics- CI, RI, and length- are given as reported by Mesquite.

The newly amended matrix was also analyzed using Bayesian inference. Bayesian analysis was run under a symmetric model in which the frequen-

Table 1. Outgroup and ingroup taxa analyzed cladistically, with Migadopinae tribal classification consistent with results of this analysis. Generic authorship is provided for genera of Migadopinae.

Cicindinae	*Nebriosoma* Laporte de Castelnau
Archaecicindis spp.[1]	*Nebriosoma fallax* Laporte de Castelnau
Cicindis horni Bruch	*Decogmus* Sloane
Elaphrinae	*Decogmus chalybeus* Sloane
Blethisa multipunctata L.	*Calyptogonia* Sloane
Elaphrus clairvillei Kirby	*Calyptogonia atra* Sloane
Loricerinae	*Dendromigadops* Baehr
Loricera foveata LeConte	*Dendromigadops gloriosus* Baehr
Migadopinae	*Amarotypus* Bates
Aquilicini	*Amarotypus edwardsii* Bates
Aquilex Moret	*Amarotypus murchisonorum* Larochelle & Larivière
Aquilex diabolica Moret	*Amaroxenus* Larochelle & Larivière
Migadopini	*Amaroxenus embersoni* Liebherr & Will, sp. nov.
Migadops Waterhouse	*Amaroxenus marrisi* Liebherr & Will, sp. nov.
Migadops jeanneli Nègre	*Migadopiella* Baehr
Migadops latus (Guèrin-Méneville)	*Migadopiella convexipennis* Baehr
Rhytidognathus Chaudoir	*Migadopiella octoguttata* Baehr
Rhytidognathus ovalis (Dejean)	*Amarophilus* Larochelle & Larivière
Rhytidognathus platensis (Roig-Juñent & Rouaux)	*Amarophilus otagoensis* Larochelle & Larivière
Migadopidius Jeannel	*Amarophilus rotundicollis* Larochelle & Larivière
Migadopidius bimaculatus (Reed)	*Stichonotus* Sloane
Lissopterus Waterhouse	*Stichonotus piceus* Sloane
Lissopterus hyadesi Fairmaire	*Stichonotus decoloratus* Baehr
Lissopterus quadrinotatus Waterhouse	*Stichonotus limbatus* Sloane
Pseudomigadops Jeannel	*Stichonotus leai* Sloane
Pseudomigadops ater Straneo	*Calathosoma* Jeannel
Pseudomigadops darwini (Waterhouse)	*Calathosoma rubromarginatum* (Blanchard)
Pseudomigadops falklandicus (Waterhouse)	*Taenarthrus* Broun
Pseudomigadops nigrocoeruleus (Waterhouse)	*Taenarthrus capito* (Jeannel)
Pseudomigadops ovalis (Waterhouse)	*Loxomerus* Chaudoir
Antarctonomus Chaudoir	*Loxomerus brevis* Blanchard
Antarctonomus complanatus (Blanchard)	*Loxomerus huttoni* (Broun)
Monolobus Solier	*Loxomerus nebrioides* (Guèrin-Méneville)
Monolobus ovalipennis Straneo	
Monolobus testaceus Solier	

[1]*Archaecicindis* spp. coded as composite terminal of *A. johnbeckeri* (Bänninger) in Kavanaugh and Erwin (1991) and *A. hormozensis* Azadbakhsh (2020).

cy of each state is equal and all characters informative using MrBayes ver. 3.2.7, (Ronquist et al. 2012). To ensure that an average standard deviation of split frequencies (ASDSF) below 0.01 was achieved (Ronquist et al. 2009), and that likelihood scores and all parameter values reached a stable plateau, an initial analysis was run using the command "stoprule = yes" with "stopval = 0.009998." Tracer (Rambaut et al. 2018) was used to examine trace files resulting from this run and the effective sample size (ESS) of the parameters used to assess convergence and stationarity. The trees in a burn-in period of 25% of the generations were excluded. While the ASDSF went below 0.01 in only 1.2 million generation for the initial analysis, the ESS values for a few parameters were still below 200, the rule of thumb threshold (Nascimento et al. 2017). The stop value command was removed and a second analysis of 6 million generations for four runs of eight chains was conducted. This analysis reached an ASDSF of 0.0087 and all ESS values viewed in Tracer were > 630. The majority-rule consensus tree of post-burn-in trees was calculated to determine Bayesian posterior probabilities (PP) of clades.

Characters

Character states for the 75 characters are listed below. Character number is based on Roig-Juñent (2004), that sequence modified only by additions or deletions. Characters newly used in this analysis are indicated by an asterisk following the character number. Multistate characters are considered non-additive; i.e., the states are unordered.

Character 1: Seta of mandibular scrobe; absent (0), present (1).
Character 2*: Maxillary stipes setation; 1 (0); 2 at base (1); 3, 2 basally, 1 medially (2); 4, 3 basally, 1 medially (3); 5 along length (4); 9 along length (5).
Character 3: Galea of maxillary palps; 2 articles (0), 1 article (1).
Character 4*: Number of setae on mentum; 2 straddling midline near mentum tooth (0), 4, 2 near midline, 2 basolaterally (1), many bordering margins of mentum (2).
Character 5*: Number of setae on submentum; 2 (0), 4 (1), 6 (2), 8 or more (3).
Character 6: Submentum; separated from mentum (0), fused to mentum, at least in central region (1).

Character 7: Mentum tooth; simple, angulate (0), bilobed or blunt with median concavity (1), absent, no forward expansion medially (2).

Character 8: Paraglossae; long (0), distinct (1), undifferentiated (2).

Character 9: Setae of glossal sclerite; four (0), two (1), one (2).

Character 10: Setae of paraglossae; absent (0), present (1).

Character 11: Labial and maxillary palps; elongate (0) short and wide, subrounded (1).

Character 12: Antennae; short, reaching base of elytron (0), long, reaching the basal third of elytra (1), very long, reaching the middle third of elytra (2).

Character 13: First four antennal segments; pubescent from apex of fourth segment (0), glabrous (1).

Character 14: Supraorbital setae; 2 each side (0), only 1 each side (posterior) (1), only 1 each side (anterior) (2), absent (3).

Character 15*: Posterior supraorbital seta; between eyes, anteriad their hind margin (0), at or posteriad hind margin of eyes (1).

Character 16: Neck; present (0), absent (1).

Character 17: Depression bordering hind margin of eye; absent (0), present (1).

Character 18*: Protibial antennal cleaner; isochaetous, longitudinally sulcate, posterior spur subapical (0), anisochaetous, transverse, posterior spur displaced proximally (1).

Character 19: Fourth male protarsomere apex; truncate (0), bilobed, with both lobes equal (1), bilobed, with anterior lobe more developed than posterior (2).

Character 20: Fourth male mesotarsomere; truncate (0), bilobed with anterior lobe more developed than posterior (1).

Character 21: Fourth male metatarsomere; truncate (0), bilobed, with anterior lobe more developed than posterior (1).

Character 22: Male protarsomeres; normally dilated (0), more distinctly dilated (1).

Character 23: Male protarsomeres; 1–3 with adhesive setae (0), 1–4 or 2–4 with adhesive setae (1).

Character 24: Male mesotarsomeres; 1–4 dilated (0), 1–3 dilated (1), not dilated (2).

Character 25: Male mesotarsomeres; without adhesive setae (0), with adhesive setae (1).

Character 26*: Unguitractor plate of fifth tarsomere; with short projection (0), with elongate projection nearly 1/5 length of ungues (1; Fig. 1).

Character 27: Female protarsomeres; not dilated (0), dilated (1).

Character 28: Female protarsomeres; with only 2 rows ventral setae (0), with expansive field of ventral setae (1).

Character 29: Female mesotarsomeres; 1–4 not dilated (0), dilated (1).

Character 30: Female mesotarsomeres; with only 2 rows ventral setae (0), with expansive fields of ventral setae (1).

Character 31*: Protibial apex; moderately expanded (0); robust overall, very broad apically (1).

Character 32*: Anterior pronotal margin; lined with microsetae across breadth (0), microsetae present medially but absent near front angles (1), microsetae absent medially but present near front angles (2)

Character 33*: Posterior pronotal margin; lined with microsetae across breadth (0), microsetae present medially, absent near basal angles (1).

Character 34: Lateral border of pronotum; broad (0), narrow (1).

Character 35: Anterior and posterior breadths of pronotum; of equal or subequal breadth (0), posterior breadth markedly greater than anterior (1).

Character 36: Anterior marginal bead of pronotum; not marked, at least incomplete medially (0), marked, distinct across breadth (1).

Character 37: Form of pronotum; wider before middle with base constricted (0), sides subparallel (1), sides diverging toward the back, width maximal at basal margin (2).

Character 38: Basal pronotal setae; present (0), absent (1).

Character 39: Lateral pronotal setae; present (0), absent (1).

Character 40: Prosternal process; not extended beyond procoxae except as vertical carina (0), extended posteriad procoxae w/o contacting mesosterum (1), dorsally extended posteriad procoxae, overlapping mesosternum (2).

Character 41: Elytral humeri; rounded (0), angulate to right (1).

Character 42: Basal border of elytra; absent (0), present (1).

Character 43: Elytral striae 1–9; absent, reduced to be untraceable on surface (0), discontinuous (1), fine, continuous (2).

Character 44: Punctation of elytral striae 1–9; absent (0), fine (1), distinct (2).

Character 45: Parascutellar stria; short striole (0), extended to apex of elytra (1).

The nomenclature for elytral striae follows the interpretation of homology for the parascutellar striole and stria 1 given by Will (2020). When impressed, the parascutellar striole is directly adjacent to the scutellum on the elytra and typically continuous with the basal marginal border of the elytra. In many Migadopini, the parascutellar striole has the appearance of a stria that is nearly the length of the elytra and joined to stria 1 in the apical third. In such cases the first two apparent intervals have a homologous correspondence to the branches of the 2nd anal vein of the insect wing.

Character 46*: Parascutellar seta; present (0), absent (1).

Character 47: Bases of elytral striae 1 and 2; fused in a common trunk basally (0), not fused, no common trunk (1)

Character 48: Parascutellar stria and elytral stria 1; fused apically (0), not fused (1).

Character 49: Striae 5 and 6; separated at base (0), joined basally (1).

Character 50*: Stem of fused striae 5 and 6; short (0), long (1).

Character 51: Ninth elytral stria; not crimped on the base (0), bent inwards at the base and attached to the eighth (1).

Character 52*: Elytral marginal setae in interval 9; 6–7 (0); 10–14 (1); 16–22 (2).

Character 53: Elytral coloration; uniform, concolorous on disc (0), with subapical patch of reddish color (1).

Character 54: Elytral marginal coloration; margin concolorous to evenly paler apically (0), margin with irregularly undulated pale areas apically (1).

Character 55*: Metathoracic flight wings; present (0), brachypterous, apex extended more than half elytral length (1), reduced, beetles apterous (2).

Character 56: Male aedeagal median lobe base; open ventrally (0), closed ventrally (1).

Character 57: Male median lobe basal carina; absent (0), present (1).

Character 58: Dorsoventral width of median lobe; thin (0), broad (1).

Character 59*: Ostium position at male median lobe apex; on right (ventral) side of lobe (0), on left (dorsal) side of lobe (1); on medial surface of lobe, dorsal when everted (2).

Character 60*: Ostium opening; broad opening on dorsal aedeagal surface (0), constricted, a small opening on aedeagal surface (1).

Character 61: Ventral region of male median lobe apex; straight, narrow (0), expanded euventrally (1).

Character 62: Male left paramere; glabrous (0), with a few setae (1), with many setae (2).

Character 63: Male left paramere; elongate (0), shape more conchoid (1).

Character 64: Male left paramere apex; sclerotized (0), membranous (1).

Character 65 Male right paramere; with 2 apical setae (0), with a row of ventral setae (1), with 2 rows of ventral setae (2).

Character 66: Sclerites X and Y of male aedeagal internal sac; present (0), absent (1).

Character 67: Ramus associated with female gonocoxite 1; absent (0), present (1).

Character 68: Female gonocoxite IX; 2-segmented (0), unsegmented, basal and apical gonocoxite fused (1).

Character 69: Female basal gonocoxite 1 (or basal portion of fused gonocoxites); apparently glabrous, without elongate setae across ventral surface (0), ventral surface covered with setae (1); with apical border of microtrichia (2), with apical border of palmate microtrichia (3).

Character 70*: Female apical gonocoxite (or apical portion of fused gonocoxites); without medioventral ensiform macrotrichia (0), with 4 mediodorsal ensiform macrotrichia (1).

Character 71*: Ligular sclerite of female bursa copulatrix; present (0), absent (1). This sclerotized structure lies on the ventral surface of the common oviduct, and is not associated with the bursal wall.

Character 72*: Ligular sclerite configuration; elongate (0); longitudinal ridges (1); sclerotized plate (2); cockscomb configuration (3). This character coded only for taxa exhibiting state 1, character 71.

Character 73*: Bursa copulatrix tubular diverticulum; absent (0), present (1). This diverticulum is elongate without an apical expansion, and it joins the bursa copulatrix distad the bursal juncture with the common oviduct. It is not interpreted as a primary spermatheca as it does not expand at the distal end, lacks any taenidial coils often observed in a primary spermatheca, and lacks a gland (Liebherr and Will 1998, fig. 3).

Character 74*: Bursa copulatrix basal diverticulum; absent (0), present (1).

Biogeographic analysis

The phylogenetic hypothesis of migadopine taxa was used to establish a context within which historical biogeographic events could be interpreted by converting the taxon cladogram to a taxon-area cladogram wherein all terminals were represented by areas of endemism. The areas of endemism were defined broadly so that migadopine taxa were geographically restricted relative to the scale of the adopted areas of endemism, and thus all terminals could be coded as single areas. For purposes of this analysis, Tasmania was combined with mainland Australia into a single area of endemism (AU), and both South and North Islands of New Zealand were combined into a single area (NZ). The Auckland and Antipodes Islands represent the Campbell Plateau (CP), considered for this analysis to be an area of endemism distinct from New Zealand. South America is considered as three different areas, one located in the northern high Andes of Ecuador, above 4000 m altitude (ESA), a second, in southern South America including mainly subantarctic moorland and *Nothofagus* forest and Patagonian steppes (SSA), and a third Neotropical region (NEO) comprising tropical lowlands that house one ultimate outgroup taxa, *Cicindis horni* Bruch. The two cicindine genera *Cicindis* and *Archaecicindis* were included in the phylogenetic analysis to enhance character polarizations, but the Cicindini–*Archaecicindis johnbeckeri* Bänninger and *C. horni*–represent the Inabresian zoogeographic pattern (Jeannel 1942; Kavanaugh and Erwin 1991) that spans eastern tropical South America to the Persian Gulf east of Africa. The Inabresian Region was vicariated by the opening of the Atlantic Ocean during the Cretaceous, 119–105 Ma (McLoughlin 2001). This pattern is not analyzed further in the biogeographic analysis as the Holarctic outgroups Loricerinae and Elaphrinae, i.e. *Elaphrus* and *Blethisa*, are considered the successive, closest outgroups to Migadopinae.

Nodal optimizations on the taxon-area cladogram (Fig. 8) were calculated by RASP (Yu et al. 2015, 2019) using 1,000,000 cycles of the Bayesian MCMC BBM algorithm. Nodal optimizations were considered unambiguous (unitary) when the maximal probability of any particular optimization exceeded 0.95. When the maximal probability for any particular optimization was less than 0.95, values for all optimizations exceeding 0.01 are presented for interpretation.

Results

Phylogenetic analysis

Parsimony analysis resulted in 16 shortest trees of 276 step-length; CI of 38, RI of 75. Five nodes within the ingroup Migadopinae collapse in the 283-strep strict consensus tree: 1, four *Pseudomigadops* spp. are collapsed into a polytomy.; 2, *Calyptogonia atra* and *Nebriosoma fallax* and the sister taxa *Decogmus chalybeus* and *Dendromigadops gloriosus* are unresolved adelphotaxa to the clade subtended by *Monolobus* spp.; and 4 and 5, three species each of *Loxomerus* and *Stichonotus* comprise tritomies. The equally parsimonious trees also differ in proposed relationships of three outgroups—*Blethisa multipunctata*, *Elaphrus clairvillei*, and *Loricera foveata*—with the consensus tree collapsing the nodes subtending these taxa. Respective monophyly for the four focal genera—*Amarotypus*, *Amaroxenus*, *Migadopiella*, and *Amarophilus*—is supported.

Bayesian analysis resulted in a majority-rule consensus tree consistent with relationships of the parsimony analysis, though the Bayesian consensus tree is less resolved (Suppl. material 2). As parsimony analysis elucidates characters informing the various relationships, and produces a more resolved consensus cladogram, subsequent analysis and discussion is restricted to the parsimony-based hypothesis (Fig. 5)

The results of the cladistic analysis mirror those of Roig-Juñent (2004) in the placement of *Amarotypus*— plus affiliated taxa from Tasmania and the South Island of New Zealand recognized as Amarotypini by Johns (2010) and Larochelle and Larivière (2022)—as a subset of taxa nested within Migadopini. Were Amarotypini retained as a valid taxon, this result would render Migadopini paraphyletic. Therefore Amarotypini Erwin (1985) is synonymized under Migadopini. Erwin's (1985) proposal for Amarotypini was based on the presence in *Amarotypus* of an elongate unguitractor plate at the apex of the fifth tarsomere (character 21; Fig. 1). Though this synapomorphy is unique and distinctive, its occurrence within the heterobathmy of characters evolving during diversification of Migadopinae restricts its phylogenetic significance to the definition of a subsidiary clade within the tribe Migadopini we name the "*Amarotypus* clade."

Monophyly for the family-group names, Migadopinae, Aquilicini, and Migadopini is supported based on the following sets of characters.

Migadopinae. The subfamily is diagnosed by: 1, antennomeres 1–4 glabrous except for apical setae (character 13); 2, presence of a single supraorbital seta in the posterior setal position each side of head (character 14); 3, head without a posterior constriction, or neck (character 16, reversed to presence of a neck in *Monolobus*); 4, lateral and basal pronotal setae absent (characters 37, 38); 5, male aedeagal internal sac sclerites X and Y (as observed in outgroups and Broscini; e.g. Liebherr et al. 2011, fig. 3b) absent (character 66).

Within Migadopinae, *Aquilex diabolica* Moret is placed as the sister group to taxa constituting Tribe Migadopini,
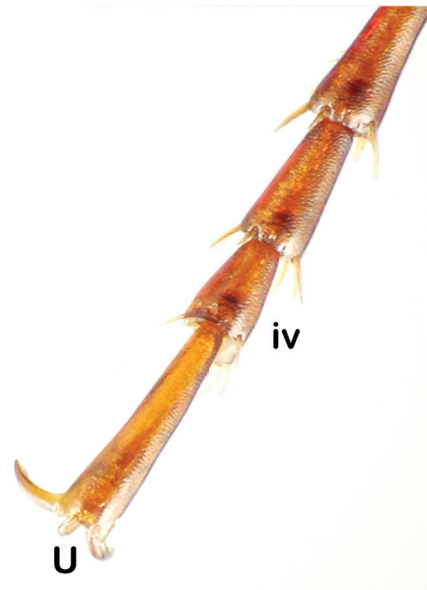

Figure 1. *Amaroxenus marrisi* right metaleg, apical four tarsomeres, showing asymmetrical lobe on anterior of tarsomere 4 (iv), and elongate, digitiform unguitractor plate of apical tarsomere (U).

and thus the status of Aquilicini Moret, 2005 is corroborated. *Aquilex* is excluded from its adelphotaxon Migadopini, as it lacks the elongate parascutellar stria extended beyond elytral mid-length of Migadopini (Moret 2005, fig. 1; character 45). *Aquilex* also shares elongate labial paraglossae (character 8) with the outgroups, whereas members of the Migadopini exhibit shortened paraglossae, most extremely when the paraglossae are not well differentiated from the glossa. The male protarsomeres of *Aquilex* have the basal three tarsomeres bearing squamose setae on the ventral surface as observed in the outgroups, whereas Migadopini have either the four basal tarsomeres with such setae, or tarsomeres 2–4 so clothed (character 23).

Cladistic analysis supports taxonomic recognition of the four genera comprising the *Amarotypus* clade—*Amarotypus*, *Amarophilus*, *Migadopiella* plus *Amaroxenus* (Fig. 5)—via three synapomorphic state changes: 1, presence of four glossal setae (character 9); 2, the uniquely synapomorphous presence of an elongate unguitractor plate of the fifth tarsomere (character 26, Fig. 1); and 3, distinctly punctate elytral striae (character 44), though such punctation is polymorphically present or absent in *Amarophilus murchisonorum* (Suppl. material 1).

Amarotypus stands as sister group to the other three genera, with its monophyly defined by highly derived female gonocoxal morphology, including large macrosetae spanning the juncture between the basal and apical gonocoxite (Fig. 3A), and the presence of four large ensiform medioodorsal setae on the apical gonocoxite (character 70; Fig. 3A). The submentum of *Amarotypus* also exhibits four setae versus the presence of six setae in the other three genera (Larochelle and Larivière 2022) plus *Stichonotus*.

Monophyly of the clade comprising the other three genera—*Amaroxenus*, *Amarophilus*, and *Migadopiella*—is unambiguously supported by: 1, posterior pronotal

margin without microsetae across breadth (character 33); 2, pronotum with subparallel lateral margins (character 35; though *Migadopiella octoguttata* shares a basally broader pronotum with species of *Amarotypus*); 3, female gonocoxite unipartite (character 68; though no female is known for *M. octoguttata*).

Both *Amaroxenus* spp. exhibit a cordate, basally constricted pronotum (character 37, Fig. 2B, C), though such a cordate pronotum also occurs in *Migadopiella convexipennis*. Tarsal characters parsimoniously overrule pronotal shape in this instance, as *Migadopiella* + *Amarophilus* synapomorphously possess a symmetrically bilobed protarsomere 4 (character 19), and a truncate metatarsomere 4 (character 21). Moreover, males of *Migadopiella* spp. synapomorphously exhibit truncate mesotarsomeres 4 (character 20). *Migadopiella* monophyly is also supported by the male aedeagal ostium opening on the left side of the median lobe (character 59; Baehr 2009, fig. 3).

And to conclude, *Amarophilus* monophyly is defined by: 1, the presence of foreshortened antennae that reach the base of the elytra (character 12); and 2, at least partially discontinuous elytral striae (character 43), though this condition is also observed in *Amarotypus edwardsii*. *Amarophilus* spp., in this analysis, are also distinguished by broadly dilated male protarsomeres (character 22, Larochelle and Larivière 2022, fig. 34). That said, the degree of protarsomere dilation in this clade is evolutionarily plastic, with both *Amarotypus murchisonorum* (Larochelle and Larivière 2022, fig. 26) and *Amaroxenus embersoni* (Fig. 2B) of this data set also possessing very broad male protarsomeres.

Taxonomic treatment

Subfamily Migadopinae [as Migadopidae] Chaudoir, 1861: 510 (type genus *Migadops* C. O. Waterhouse, 1842: 136)

Tribe Migadopini Chaudoir, 1861
Monolobina Jeannel, 1938: 13 (type genus *Mololobus* Solier, 1849: 189; synonymy Roig-Juñent, 2004: 12)
Amarotypini Erwin, 1985: 468 (type genus *Amarotypus* Bates, 1872: 50; New Synonymy)
Tribe Aquilicini Moret, 2005: 30 (type genus *Aquilex* Moret, 1989: 246; New Rank)

In order to phylogenetically test the monophyly of the migadopine genera proposed by Baehr (2009) and Larochelle and Larivière (2022), we describe below two species of *Amaroxenus* that complement the species pairs representing *Amarotypus*, *Amarophilus*, and *Migadopiella*.

Amaroxenus Larochelle & Larivière, 2022: 10.

Type species. *Amaroxenus kahurangiensis* Larochelle & Larivière, 2022: 10 (by original designation).

Diagnosis. Within Migadopini exhibiting an elongate parascutellar stria that extends beyond the elytral midlength; mentum medially bidentate, the mentum tooth notched medially; submentum with six setae; pronotum cordate, with basal width subequal to apical width, the lateral margin sinuate anteriad distinct hind angle; pronotal anterior marginal bead usually incomplete medially—in *A. embersoni* sp. nov. polymorphically complete or incomplete medially—always present laterally; metathoracic wings vestigial; pro- and mesothoracic legs with tarsomeres 1–4 laterally expanded in both sexes; female gonocoxite unipartite, the narrower apical portion indistinctly defined relative to the equally sclerotized, broader basal portion, no microtrichia—or a single small seta—situated along the inner margin of the gonocoxite at the point of apical narrowing (Fig. 3B, C).

Diversity. Four species were described by Larochelle and Larivière (2022), to which we add two new species, with the six species determinable using the following key.

Identification key to adults of *Amaroxenus* Larochelle & Larivière

1   Elytral stria 3 with indistinctly developed, fine setiferous punctures. Pronotum subcordate; side moderately rounded; laterobasal fovea not separated from lateral depression by an upraised ridge 2

–   Elytral stria 3 with well-developed, coarse setiferous punctures. Pronotum cordate, sides distinctly rounded before sinuate basolateral margins; laterobasal fovea separated from lateral depression by a distinct ridge 4

2(1) Dorsum of body glossy rufopiceous; microsculpture indistinct, a fine transverse mesh on elytra. Pronotal laterobasal foveae moderately broad, shallow, separated from lateral depressions by a pronounced convexity. Elytra distinctly convex; striae shallow, finely punctate, intervals moderately to distinctly convex 3

–   Dorsum of body matte brunneous; microsculpture well developed, granulate especially on elytra. Pronotal laterobasal foveae very broad, deep, extended to lateral margins. Elytra moderately convex; striae deep, coarsely punctate, intervals only slightly convex .... *Amaroxenus glacialis* Larochelle & Larivière

3(2) Pronotum moderately transverse, MPW / PL = 1.29; elytra narrowly ovate, MEW / EL = 0.71; elytra with 14–15 lateral setae in 9th interval bordering lateral marginal depression; standardized body length 6.5—6.6 mm ....
....*Amaroxenus arnaudensis* Larochelle & Larivière

–   Pronotum broadly transverse, MPW / PL = 1.42; elytra broadly ovate, MEW / EL = 0.76; elytra with 11–13 lateral setae in 9th interval bordering lateral marginal depression; standardized body length 7.8—8.1 mm ....
.... *Amaroxenus embersoni* Liebherr & Will, sp. nov.

4(1) Antennae brunneous to rufopiceous, apices of antennomeres 5–11 may be darker, but their constricted bases not con-trastedly darker than basal four antennomeres; pronotum moderately convex, sides moderately to distinctly sinuate posteriorly, basal angles slightly to distinctly acute, laterobasal foveae very deep; elytra glossy with silvery reflection, moderately to distinctly convex, striae continuous, distinctly punctate 5

–   Antennal segments 1–2 rufotestaceous, 3–11 rufopiceous; pronotum distinctly convex, sides not sinuate posteriorly, basal angles rectangular, laterobasal foveae shallow; elytra matte, distinctly convex, striae shallow, finely punctate .... *Amaroxenus huttensis* Larochelle & Larivière

5(4) Elytra moderately convex, disc flat near mid-length mesad stria 4 each side (note parascutellar stria extends between sutural and stria 2), sutural stria finely incised with rudimentary punctures along length on disc; two setae associated with stria 3, both anteriad elytral mid-length; eyes slightly convex, ocular ratio = 1.31 ....*Amaroxenus kahurangiensis* Larochelle & Larivière

–   Elytral distinctly and evenly convex, sutural stria deep and smooth on disc; three setae associated with stria 3, the posterior seta just posteriad elytral mid-length; eyes subdepressed, ocular ratio = 1.27 ..... *Amaroxenus marrisi* Liebherr & Will, sp. nov.

Amaroxenus embersoni Liebherr & Will, sp. nov.

https://zoobank.org/45DA3BFE-373C-47A0-B736-B8406053EDAD

Types. *Holotype* male (LUNZ) mislabeled: *Arthurs Pass Nat. / Pk, NC 1650 m / Mt. Philistine / 1-i-1988 P. Syrett / R. M. Emberson // under rock / in fine damp / gravel //* HOLOTYPE ♂ / Amaroxenus / embersoni / Liebherr and Will 2023 (black-bordered red label). Based on consultation with Emberson field notes (P. Syrett pers. comm.) the holotype was actually collected at: Arthur's Pass N. P., Mt. Aicken, 1750 m, 1-i-1988 (Fig. 7). *Paratypes*: same incorrect data label as holotype (LUNZ, 1 ♂); New Zealand: Arthur's Pass N. P., Mt. Aicken, 1750 m, 1-i-1988, R. M. Emberson and P. Syrett, under rock sparse fell field vegetation (LUNZ, 1 ♀) [as noted above, these data are appropriate for all three specimens of *A. embersoni*].

Diagnosis. A broad-bodied species, with transverse pronotum, MPW / PL = 1.42, and broadly ovate elytra, MEW / EL = 0.76 (Fig. 2B); elytra moderately convex but with disc flat; elytral striae punctate in basal ¾ of length, intervals moderately convex on disc; standardized body length 7.8–8.1 mm.

Description. *Head.* Frons broad, frontal grooves broad and shallow depressions isolated from clypeus, lined with shallow oblique wrinkles on mesal surface; eyes slightly convex, horizontal diameter intersecting ~20 ommatidia, ocular ratio = 1.28. *Prothorax* broadly convex dorsally, middle of disc flat, lateral margins distinctly sinuate anteriad slightly acute hind angles, MPW / BPW = 1.05; basal margin trisinuate, medial margin extended slightly posteriad line intersecting hind angles; base indistinctly, narrowly margined, marginal bead narrowest posteriad laterobasal depression; median base smooth, with shallow ovoid depression at midline; laterobasal depressions broad, defined mesally by irregular declivity, surface dimpled laterad declivity and depression curved upward to broadly meet the narrow lateral margin; median impression very fine, intersecting ~12 fine, transverse impressions that represent little more than irregularities in microsculpture; lateral marginal bead narrowly upraised, lateral marginal depression very narrow and immediately abutting convex disc; anterior margin with distinct, broad lateral bead laterally, but margin nearly smooth medially, margin traceable only in certain orientations of light source; front angles acute, inner margin adhering to lateral surface of head, APW / BPW = 0.74; prosternum smooth medially, lateral reaches slightly undulated; posterior margin of prosternal process extended as adze-like projection, its ventral surface bearing a deep longitudinal declivity; proepisternum / proepimeron juncture lined with ~7 rugose longitudinal depressions. *Elytra* narrow basally, HuW / MEW = 0.59, humeri evenly expanded posteriad narrowly rounded humeral angle defined by basal and lateral margins; elongate parascutellar stria joined basally to stria 2, the fused trunk curved laterally parallel to sutural stria; parascutellar stria free apically, terminated at 0.70× elytral length; elytral stria 2 extended nearly to apex, finely punctate even apically, striae 3–6 progressively shorter on apex, stria 7 fused both basally and apically to stria 8, both striae distinctly punctate anteriad posterior juncture, stria 8 irregularly punctate posteriad juncture; stria 9—i.e. lateral marginal depression—punctate nearly to juncture of striae 7 and 8; elytral interval 3 bearing two very fine setae in obscure depressions set at and posteriad elytral mid-length, the impressions situated just mesad stria and associated with slight deviations in the strial orientation; 11–13 lateral elytral setae situated just laterad stria 8. *Pterothorax* foreshortened, mesepisternum broadly punctate, with ~20 punctures in posterior 2/3 of length; mesosternum smooth, with fine median crest aligned with adze-like prosternal projection; mesepimeron a narrow longitudinal strap bordering posterior margin of mesepisternum, both sclerites reaching disjunct mesothoracic coxal cavity; metepisternum irregularly quadrate, anterior and posterior margins parallel, medial margin concave along juncture with mesosternum; lateral reaches of metasternum punctate, ~8 punctures over surface. *Abdomen* finely punctate basally on first visible ventrite; lateral reaches of ventrites 2–3 longitudinally wrinkled, ventrites 4–6 very finely punctulate over surface; apical ventrite of one male and the female specimen with one seta each side of midline, second male with two setae on right, and one on left side of the ventrite. *Legs* with expanded tarsomeres on pro- and mesothoracic legs; males with protarsomere 2 w / l = 1.33, mesotarsomere 2 w / l = 1.04, and females with protarsomere 2 w / l = 1.37,
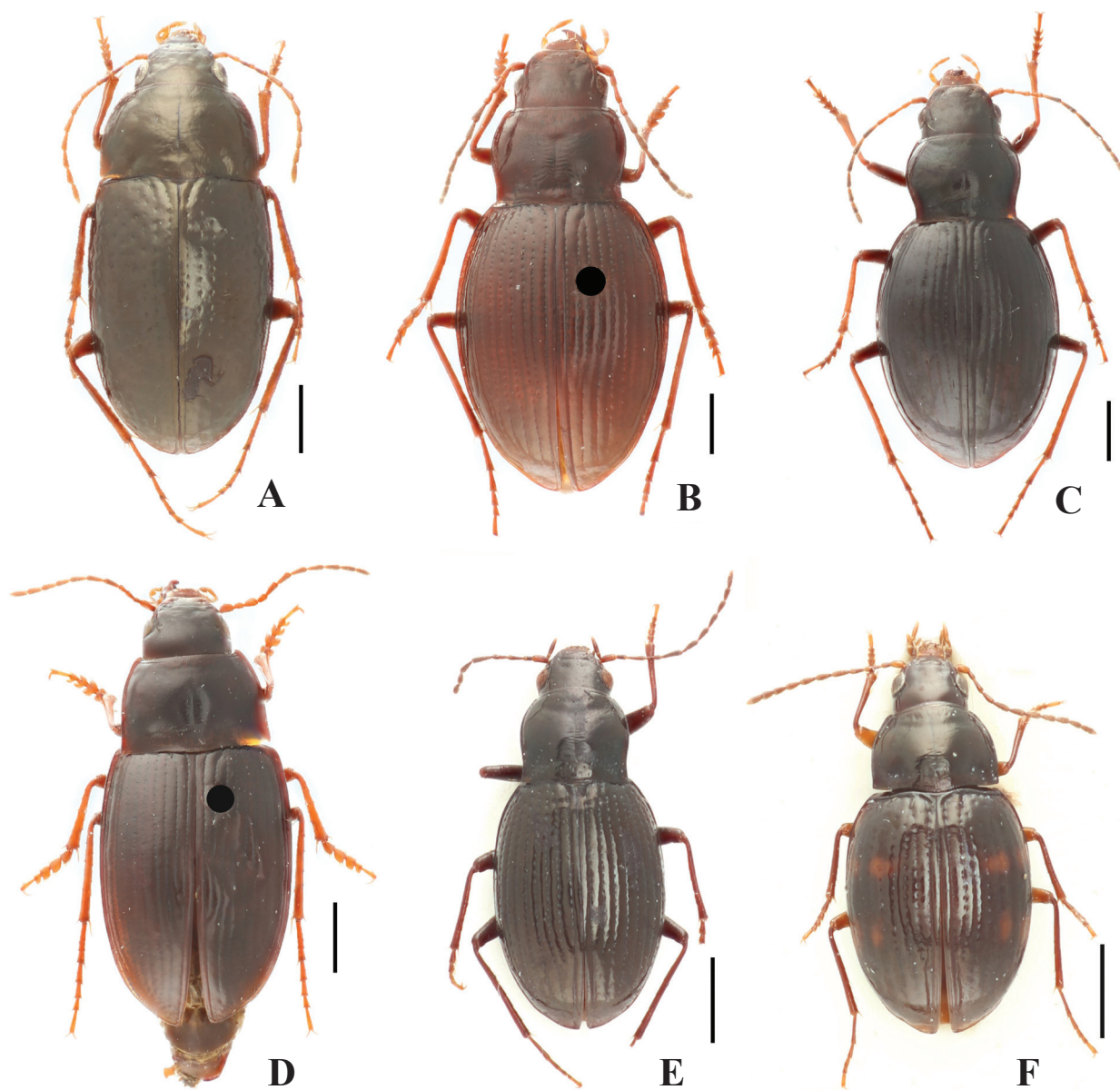
Figure 2. Representative taxa of the *Amarotypus* clade, dorsal view. **A.** *Amarotypus edwardsii*; **B.** *Amaroxenus embersoni*; **C.** *Amaroxenus marrisi*; **D.** *Amarophilus otagoensis*; **E.** *Migadopiella convexipennis*; **F.** *Migadopiella octoguttata*.

mesotarsomere 2 w / l = 0.81; male pro- and mesotarsomeres 1–4 both with ventral surfaces clothed with laterally expanded setae, those on protarsomeres 1–3 broadly expanded laterally, squamose; female protarsomeres 1–4 and mesotarsomeres 2–4 clothed with dense, apical fields of thick, silky, presumably flexible setae.

Male genitalia (Fig. 6A–C). Aedeagal median lobe robust, broad dorsoventrally and bilaterally from base to apically rounded apex (Fig. 6A, B), median lobe basal bulb closed, bearing an apically divergent sagittal crest; median lobe sclerotized basally, ostium opening apically on left side; right paramere broadly conchoid, parallel sided with narrowly rounded ventral apex, ventral margin lined with 3 dense rows of long setae; left paramere conchoid, parallel sided, glabrous, acuminate apicoventrally (Fig. 6B); aedeagal internal sac with heavily sclerotized fields including a dorsal flagellum and a dense ventral

spicular field (Fig. 6A); mediotergite VIII broadly rounded distally, sclerotized apex broadened relative to tubular lateral margin (Fig. 6C).

Female reproductive tract. Gonocoxite narrow, elongate, unipartite, articulated basally with heavily sclerotized median boss along anterior margin of laterotergite IX (Fig. 3B); two nematiform setae in apical sensorial pit; ventroapical surface of gonocoxite lined with campaniform sensoria, with several small trichoid sensilla in median half of coxite; bursa copulatrix circular (when compressed on microslide), with common oviduct-bursal juncture on ventral surface, and cristate "helminthoid sclerite" near juncture (Fig. 4B); ventroapical surface of bursa broadly, moderately sclerotized, resulting in a discrete plate just distad the bursal-oviduct juncture.

Etymology. We take great pleasure in naming this species for Professor Rowan M. Emberson (Fig. 7), late

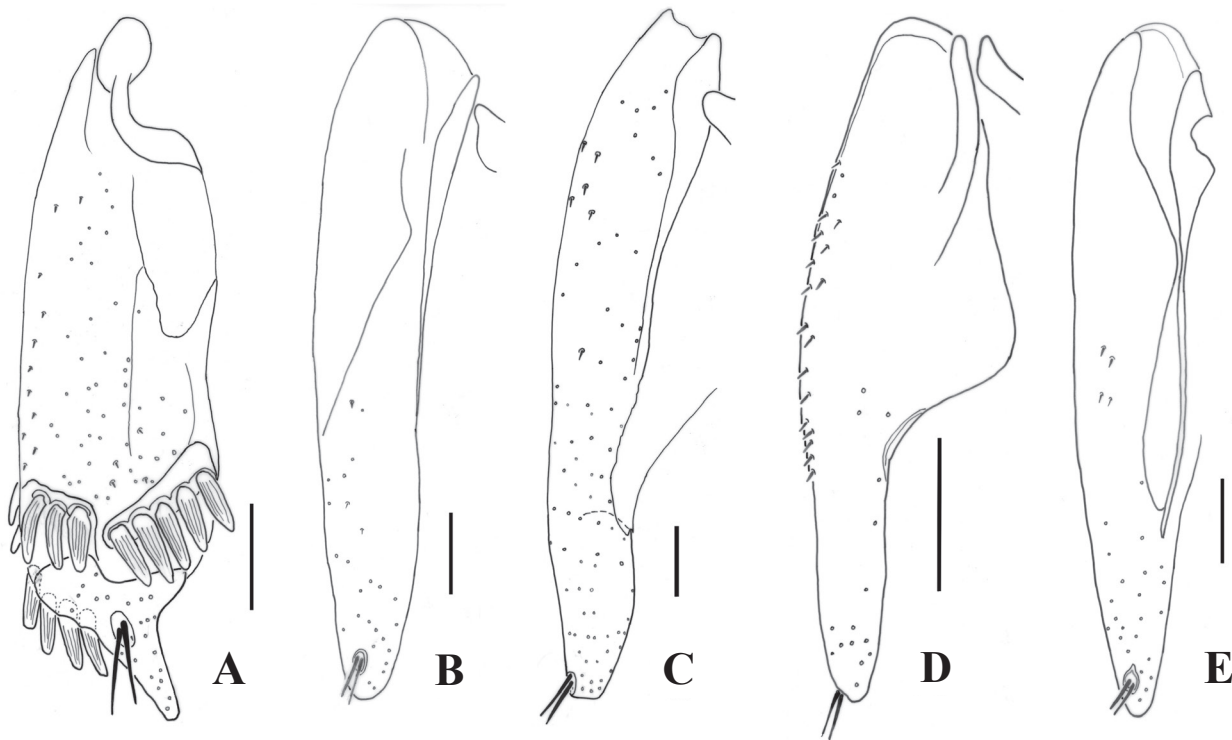Dtsch. Entomol. Z. 71 (2) 2024, 319–338

329

Figure 3. Female left gonocoxite, ventral view. **A.** *Amarotypus edwardsii*; **B.** *Amaroxenus embersoni*; **C.** *Amaroxenus marrisi*; **D.** *Migadopiella octoguttata*; **E.** *Amarophilus otagoensis*.

of Lincoln University. He collected the three type specimens during a hike, accompanied by Pauline Syrett, to the summit of Mt. Aicken in the Southern Alps of New Zealand, December, 1987. The species epithet recognizes Professor Emberson's dedication to the study of New Zealand's insects, including discovery of this high montane New Zealand insect species comprising animals that live in extreme situations far beyond the limits of most entomological exploration.

Distribution. Mt. Aicken is located at 42°55.85'S, 171°35.70′E, and has a summit elevation of 1859 m (https://climbnz.org.nz/nz/si/arthurs-pass/mt-aicken).

Habitat. This is a species of high montane grassland and exposed glacial till. At elevations of 1650–1750 m in the Southern Alps, these habitats are strictly alpine in character. The three specimens were collected under rocks at the edge of receding snowfields (Fig. 7)

Amaroxenus marrisi Liebherr & Will, sp. nov.

https://zoobank.org/38EA8D51-2C05-4BA5-AAD2-705A5FBAFA19

Types. *Holotype* male (LUNZ): New Zealand BR / Ridge above Mt. Cedric, 1695 m / GPS 41°53.380S, 172°43.520E / 13 Dec 2008, J. W. M. Marris / Under rock in outcrop // ♂ // HOLOTYPE ♂ / Amaroxenus / marrisi / Liebherr and Will 2023 (black-bordered red label). *Paratypic allotype* female (LUNZ): same data as holotype // ♀ // ALLOTYPE ♀ / Amaroxenus / marrisi / J.K. Liebherr 2023 (black-bordered red label). *Paratypes*: New Zealand, Buller, Nelson Lakes N. P., ridge ENE Mt. Ced-

ric, 1698 m, 41°53.36'S, 172°43.50'E, 13-xii-2008, J. K. Liebherr, under fractured graywacke on moist ground, snowmelt (CUIC, 2 ♂♂, 2 ♀♀; NZAC, 1 ♂, 1 ♀).

Diagnosis. Pronotum slightly transverse, MPW / PL = 1.27, narrower than prothorax of the similar *A. kahurangiensis* with MPW / PL = 1.39; eyes small, indistinctly convex, ocular ratio = 1.27, versus ocular ratio = 1.31 for *A. kahurangiensis*; parascutellar stria and stria 2 punctate, continuous on disc, versus shallower, finely incised with smaller, isolated punctures in *A. kahurangiensis*; three dorsal elytral setae set just mesad stria 3, the anterior two at 0.25× and 0.34× elytral length, the posterior seta posteriad mid-length, near 0.57× elytral length versus only two dorsal elytral setae set before elytral mid-length in *A. kahurangiensis*; standardized body length = 6.9–7.4 mm, tending larger in the extreme than *A. kahurangiensis* at 6.9–7.05 mm. [Note that this size range, based on a male and female (LUNZ) from the same series as the types (Larochelle and Larivière 2022: 13), were measured using the protocol described above. Even though the landmarks used in this study deviate little from those suggested for measuring body length in the works of Larochelle and Larivière (e.g., 2007, fig. 119), our body length measurements for *A. kahurangiensis* are significantly greater than the 5.3–6.6 mm value reported in Larochelle and Larivière 2022).

Description. *Head.* Frons broad, flat, with only very shallow frontal impressions traceable each side of midline, middle of frons narrowly flattened, with shallow wrinkles obliquely emanating from flat area approaching the shallow frontal impressions; eyes with horizontal diameter
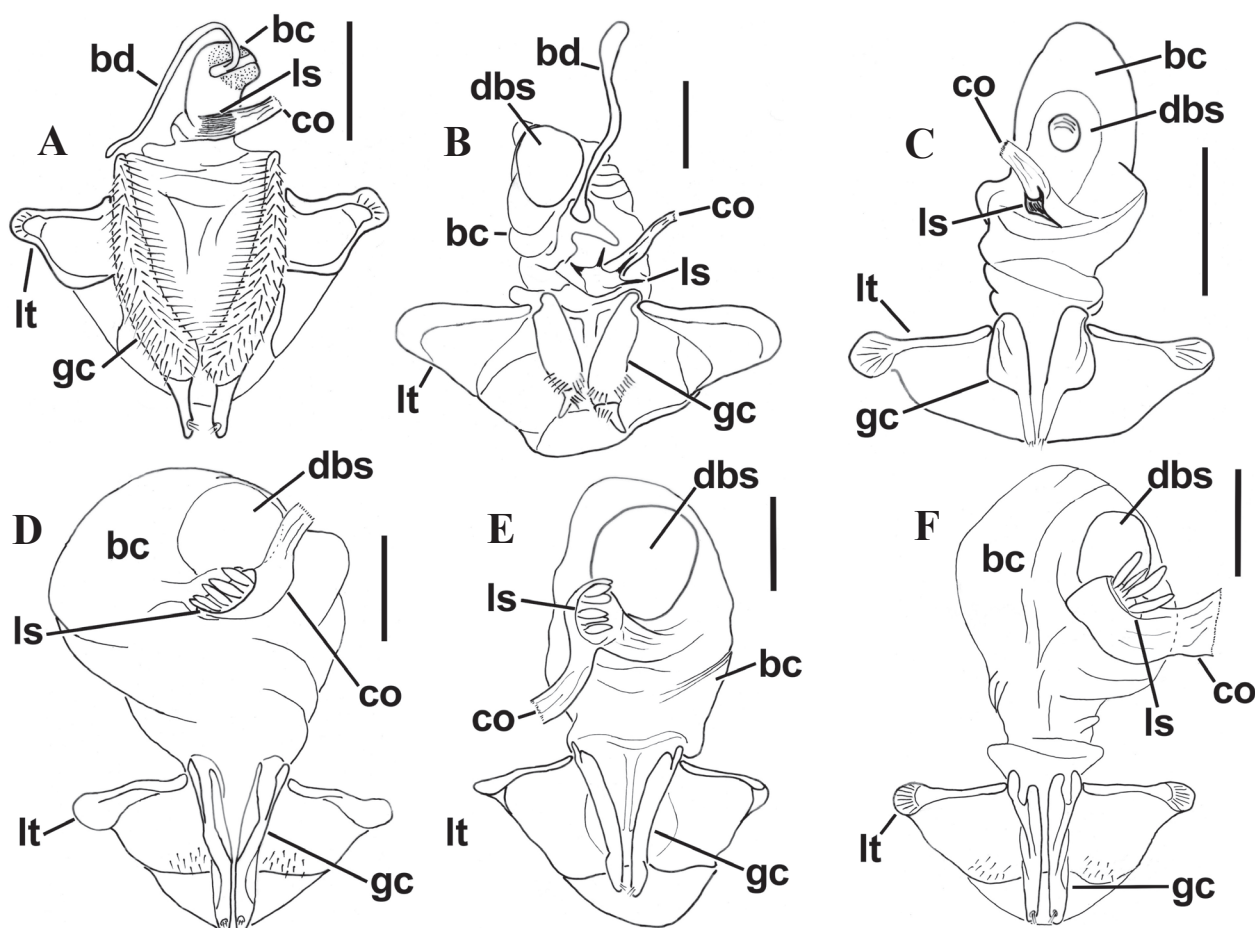
Figure 4. Female reproductive tract, ventral view, scale bar = 0.5 mm to right of each figure. **A.** *Stichonotus piceus*; **B.** *Amarotypus edwardsii*; **C.** *Migadopiella octoguttata*; **D.** *Amaroxenus embersoni*; **E.** *Amaroxenus marrisi*; **F.** *Amarophilus otagoensis*. Abbreviations for anatomical structures include: bc, bursa copulatrix; bd, bursal diverticulum; co, common oviduct; dbs, distal bursal sclerite; gc, gonocoxa; ls, ligular sclerite; lt, laterotergite.

intersecting ~20 ommatidia. **Prothorax** broadly convex dorsally, middle of disc flat, lateral margins moderately sinuate anteriad slightly obtuse hind angles, MPW / BPW = 1.11; basal margin trisinuate, medial margin extended slightly posteriad line intersecting hind angles; base with distinct, narrow marginal bead medially, bead less upraised and flatter laterally but continuous to hind angle; median base smooth, convex; laterobasal depressions ovoid, defined mesally by a smooth declivity, surface of depression smooth, only slightly dimpled, depression isolated from lateral margin by broad convexity; median impression very finely inscribed on elevated disc, intersecting ~5 broad transverse impressions between elevated disc and median base; lateral marginal bead very narrow, only slightly upraised, lateral marginal depression exceedingly narrow and immediately abutting convex disc; anterior margin with broad, irregularly flattened lateral bead in medial 4/5 of breadth, distinctly upraised only immediately mesad front angles; front angles acute, inner margin adhering to the lateral surface of the head, APW / BPW = 0.86; prosternum smooth medially, lateral reaches slightly depressed anteriad prosternal-proepisternal suture; posterior margin of prosternal process extended as adze-like projection, its ventral surface bearing a nar-row longitudinal declivity that deepens toward apex of projection; proepisternum / proepimeron juncture lined with ~5 rugose longitudinal depressions. **Elytra** narrowly ovate, MEW / EL = 0.74, narrow basally, HuW / HEW = 0.58, humeri narrowly expanded posteriad rounded humeral angle defined by basal and lateral margins; elongate parascutellar stria free from stria 2 at basal groove; parascutellar stria free apically, terminated at 0.73× elytral length; elytral stria 2 obsolete near elytral apex, impunctate and discontinuous apicad termination of parascutellar stria, striae 3–7 progressively reduced on apex, discontinuous to obsolete, stria 8 a discontinuous series of distant punctures near humerus, punctures more closely set near mid-length, stria shallow and impunctate in apical half of elytra; stria 9—i.e. lateral marginal depression—closely set with ~10 punctures posteriad humerus, minutely punctate at mid-length and smooth apically; 11–13 lateral elytral setae situated just laterad stria 8. **Pterothorax** foreshortened, mesepisternum broadly, shallowly punctate with ~16 punctures across surface; mesosternum smooth, with narrowly cristate median crest aligned with prosternal projection; mesepimeron a narrow parallel-sided strap bordering posterior margin of mesepisternum, both sclerites broadly reaching disjunct mesothoracic coxal
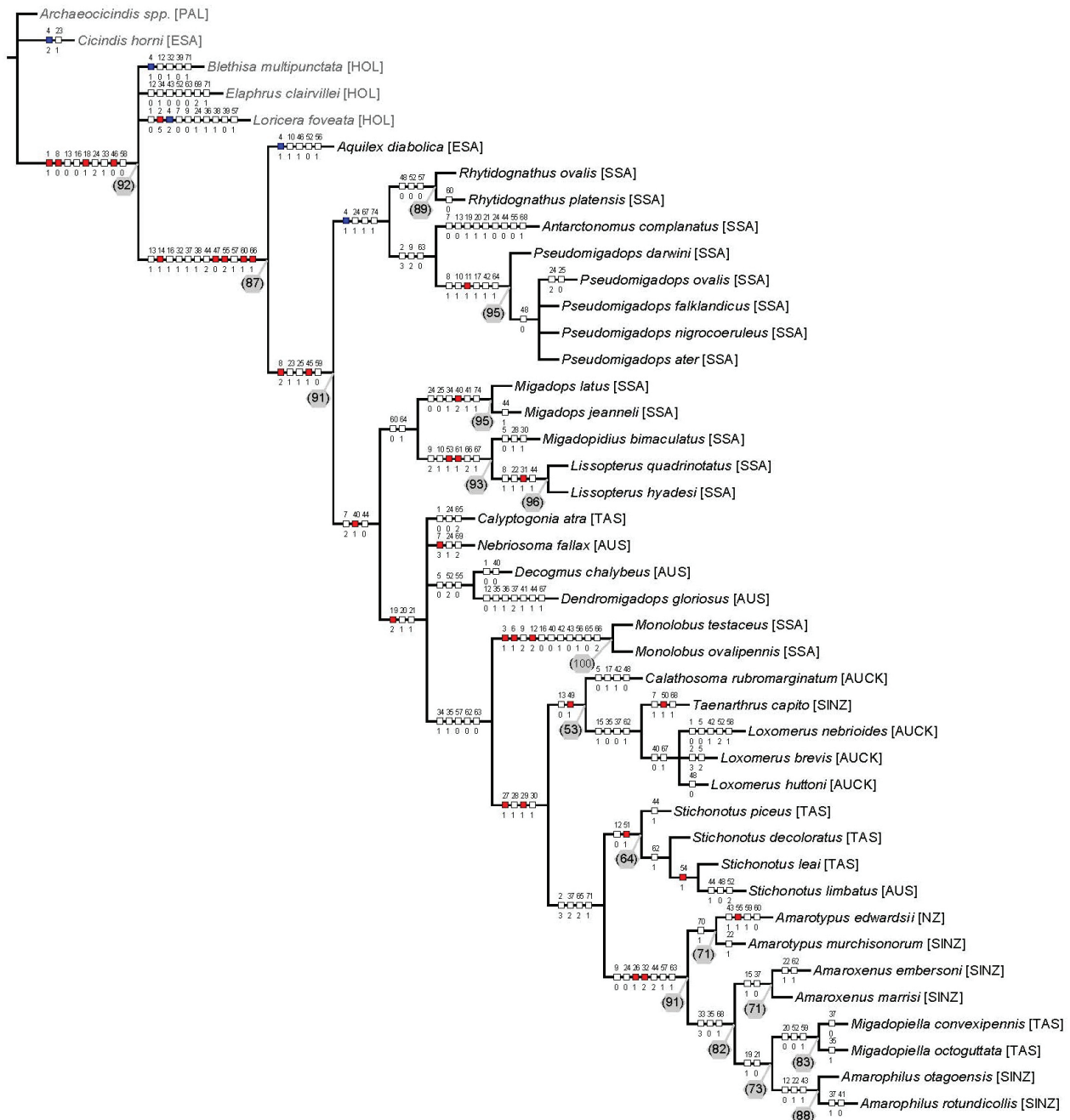
Figure 5. Strict consensus cladogram for Migadopinae plus five outgroup taxa representing Cicindinae, Elaphrinae, and Loricerinae; length 282 steps, CI = 37, RI = 74, with characters indicated under unambiguous optimization option; characters numbered starting with 1; grey spots with Jackknife numbers for nodes with scores ≥ 50; red = not homoplasious; white = homoplasious; blue = deltran character optimization. Areas of endemism occupied by the various taxa include: AUCK, Auckland and Antipodes Islands; AUS, mainland Australia; ESA, equatorial tropicomontane South America; HOL, Holarctic; NEO, Neotropics; NZ, North and South Islands, New Zealand; PAL, Palearctic; SINZ, South Island, New Zealand; SSA, southern South America; TAS, Tasmania.

cavity; metepisternum subquadrate, appearing slightly longer than broad due to concave medial margin along juncture with mesosternum, surface undulated with ~5 minute punctures near medial margin; lateral reaches of mesosternum irregularly undulated along metacoxal juncture. *Abdomen* with first visible ventrite smooth, slightly longitudinally wrinkled; lateral reaches of ventrites 2–3 longitudinally wrinkled; ventrites 4–6 smooth except for broad depression halfway between abdominal

articulatory setae and lateral margin; apical ventrite of both males and females with one seta each side of midline. *Legs* with expanded tarsomeres on pro- and mesothoracic legs; males with protarsomere 2 w / l = 1.2, mesotarsomere 2 w / l = 1.0, and females with protarsomere 2 w / l = 1.37, mesotarsomere 2 w / l = 0.81; male pro- and mesotarsomeres 1–4 both with ventral surfaces clothed with laterally expanded setae, those on protarsomeres 1–3 broadly expanded laterally, squamose, those on tarsomere
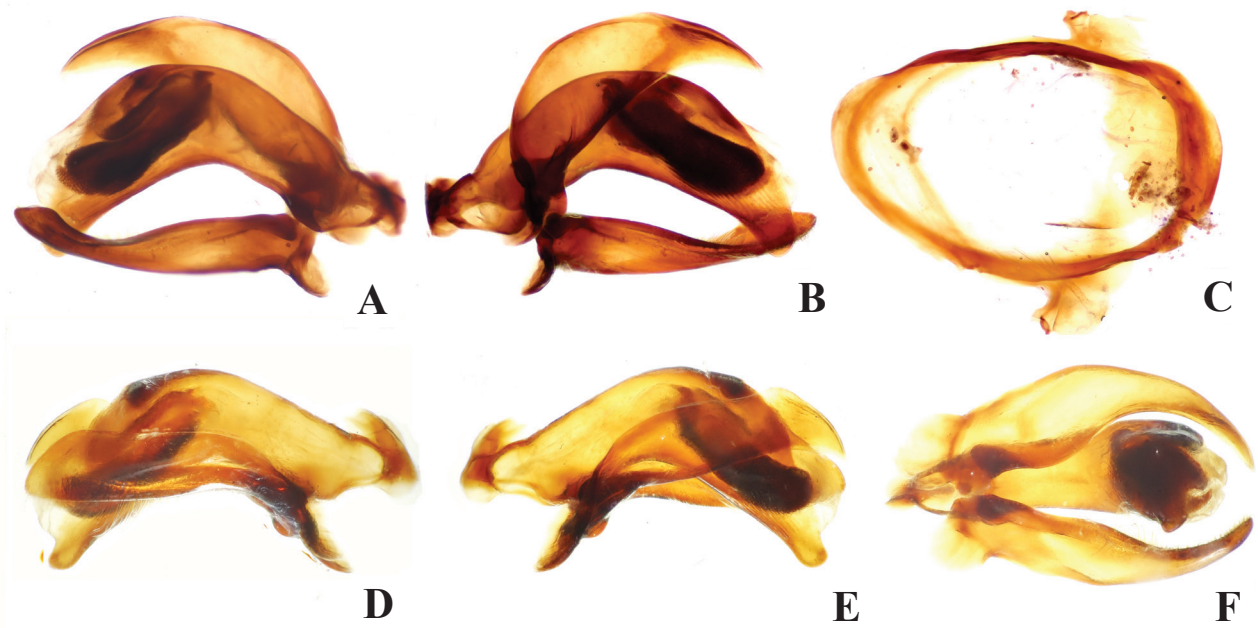
Figure 6. Male aedeagal complex. **A–C.** *Amaroxenus embersoni*. **A.** Median lobe and parameres, dextral view; **B.** Median lobe and parameres, sinistral view; **C.** Metatergite, ventral view. **D–F.** *Amaroxenus marrisi*: **D.** Median lobe and parameres, dextral view; **E.** Median lobe and parameres, sinistral view; **F.** Median lobe and parameres, ventral view.

Figure 7. Type locality of *Amaroxenus embersoni* showing Professor Rowan Emberson collecting the type series (photo courtesy Pol Syrett).

4 tightly packed, silky looking; female protarsomeres 1–4 and mesotarsomeres 2–4 clothed with dense, apical fields of thick, silky, presumably flexible setae.

Male genitalia. Aedeagal median lobe robust, broad dorsoventrally and bilaterally from base to narrow, parallel-sided and apically rounded apex (Fig. 6D–F), median lobe basal bulb closed, bearing an apically divergent sagittal crest (Fig. 6D, E); median lobe sclerotized basally, ostium opening apically on left side; right paramere broadly conchoid, parallel sided with narrowly rounded ventral apex, ventral margin lined with three dense rows of long setae (Fig. 6F); left paramere conchoid, parallel sided, glabrous, acuminate apicoventrally (Fig. 6E); aedeagal internal sac with heavily sclerotized fields including dorsal flagellum and a dense ventral spicular field (Fig. 6D).

Female reproductive tract. Gonocoxite narrow, elongate, apparently unipartite, articulated basally with heavily sclerotized median boss along anterior margin of laterotergite IX (Fig. 3B); two nematiform setae in apical sensorial pit; ventral surface of gonocoxite lined with campaniform sensoria, with a small number of trichoid sensilla along the median half of coxite; bursa copulatrix broadly ovoid (when compressed on microslide), with common oviduct-bursal juncture on ventral surface, and cristate "helminthoid sclerite" near juncture (Fig. 4C); ventroapical surface of bursa broadly, moderately

sclerotized, resulting in discrete plate just distad the bursal-oviduct juncture.

Etymology. This species is named to honor John W. M. Marris for his support of New Zealand entomology, including his efforts to document the high elevation alpine insects of New Zealand; among others the very interesting, lichenophilic *Protodendrophagus antipodes* Thomas (Coleoptera, Silvanidae; see Marris et al. 2019).

Distribution. This species is known only from type locality on the ridge above and ENE of Mt. Cedric, in Buller District. The collecting site is along the valley rim above the headwaters of Open Creek south branch, which flows southwest into the Sabine River.

Habitat. Adult beetles were found within cracks of exposed and crumbling blocks of graywacke in an area of recently melted snow, with the rocky substrate still moist. The rocks had been separated through frost action, with the cracks infiltrated by plant roots, thereby providing moist laminar spaces for insect habitation. The *Amaroxenus* beetles were cohabiting the rock crevices along with adults and larvae of *Protodendrophagus antipodes*.

Biogeographic analysis

Cladistic relationships for Migadopinae versus the closest outgroups included in the phylogenetic analysis (Fig. 5)—represented by *Loricera foveata*, *Blethisa multipunctata*, and *Elaphrus clairvillei*—define a biogeographic hypothesis (Fig. 8) that supports initial diversification of Migadopinae in South America (Fig. 8, node 72). This node ancestral to the Migadopinae is optimized at probability 0.93 to the Holarctic (A), interpreted as a South American origin of the Migadopinae with its sister group in Laurasia.

Within South America, *Aquilex* is placed as the adelphotaxon to all other Migadopinae (Fig. 8, node 71), supporting recognition of the two sister tribes Aquilicini and Migadopini. Node 71 is ambiguously optimized (Table 2)

as Holarctic (A, 0.29), equatorial montane South America (B, 0.39), or southern South America (C, 0.22).

Subsequently, diversification of the migadopine genera, *Rhytidognathus*, *Antarctonomus*, *Pseudomigadops*, *Migadops*, *Migadopidius*, and *Lissopterus* took place within South America (Fig. 8, subtending nodes 70, 69). The RASP analysis then posits that occupation of Australia by the grade of taxa including *Calyptogonia*, *Nebriosoma*, *Decogmus*, and *Dendromigadops* (Fig. 5) incorporated an ancestral area (Fig. 8, node 68) that can be variously optimized as South America (C, 0.56), Australia (D, 0.23), or the union of South America and Australia (C + D, 0.21) (Table 2).

Such geographic adjacency is reiterated by optimization of node 67 circumscribing the Antipodean areas, Australia, Campbell Plateau, and New Zealand, with ancestral area states including South America (C, 0.74), Australia (D, 0.12), or the union of the two (C + D, 0.10). The Campbell Plateau was isolated (node 66) prior to isolation of Tasmania and New Zealand (node 65), with optimization probabilities of an ancestral area calculated as either Australia (D, 0.61), New Zealand (0.24), or the union of those (D + E, 0.07) (Table 2).

The taxon-area cladogram posits an origin of the Campbell Plateau fauna as sister group to the Tasmanian *Stichonotus* clade and the amarotypine clade rooted in New Zealand. Node 66 subtending this area relationship is variously optimized to Australia (D, 0.29), New Zealand (E, 0.29), or the Campbell Plateau (F, 0.26) (Table 2), suggesting non-hierarchical area relationships of these terranes.

Subsequent optimization of node 65 supports isolation of Australia from New Zealand, with either Australia (D, 0.61), New Zealand (E, 0.24) or a both areas as ancestral (C + D, 0.7) (Table 2). Ancestral area optimizations for both nodes 66 and 65 strongly suggest an independent history for the Campbell Plateau versus New Zealand west of the Alpine Fault; i.e. North Island and western South Island. The New Zealand clade

Table 2. Ancestral state probabilities for nodes of taxon-area cladogram (Fig. 8) where maximal probability of any particular optimization is < 0.95. Areas include: Holarctic (A); equatorial montane South America (B); southern South America (C), Australia (D), New Zealand (E), and Campbell Plateau (F). Nodal-state probabilities are based on 1,000,000 cycles of the RASP Bayesian Binary MCMC (BBM) algorithm (Yu et al. 2019).

| Areas	Node No.									
	72	71	68	67	66	65	64	63	62	60
A	0.93	0.29	< 0.01	< 0.01	< 0.01	< 0.01	< 0.01	< 0.01	< 0.01	< 0.01
AB	0.01	0.03	< 0.01	< 0.01	< 0.01	< 0.01	< 0.01	< 0.01	< 0.01	< 0.01
AC	< 0.01	0.02	< 0.01	< 0.01	< 0.01	< 0.01	< 0.01	< 0.01	< 0.01	< 0.01
B	0.02	0.39	< 0.01	< 0.01	< 0.01	< 0.01	< 0.01	< 0.01	< 0.01	< 0.01
BC	< 0.01	0.03	< 0.01	< 0.01	< 0.01	< 0.01	< 0.01	< 0.01	< 0.01	< 0.01
C	0.02	0.22	0.56	0.74	0.29	0.03	< 0.01	< 0.01	< 0.01	< 0.01
CD	< 0.01	< 0.01	0.21	0.10	0.03	< 0.01	< 0.01	< 0.01	< 0.01	< 0.01
CF	< 0.01	< 0.01	< 0.01	< 0.01	0.02	< 0.01	< 0.01	< 0.01	< 0.01	< 0.01
D	< 0.01	< 0.01	0.23	0.12	0.29	0.61	0.02	< 0.01	0.02	0.93
DE	< 0.01	< 0.01	< 0.01	< 0.01	< 0.01	0.07	0.07	0.06	0.11	0.06
DF	< 0.01	< 0.01	< 0.01	< 0.01	0.02	< 0.01	< 0.01	< 0.01	< 0.01	< 0.01
E	< 0.01	< 0.01	< 0.01	< 0.01	0.06	0.24	0.91	0.94	0.86	0.01
EF	< 0.01	< 0.01	< 0.01	< 0.01	< 0.01	< 0.01	< 0.01	< 0.01	< 0.01	< 0.01
F	< 0.01	< 0.01	< 0.01	0.01	0.26	0.02	< 0.01	< 0.01	< 0.01	< 0.01
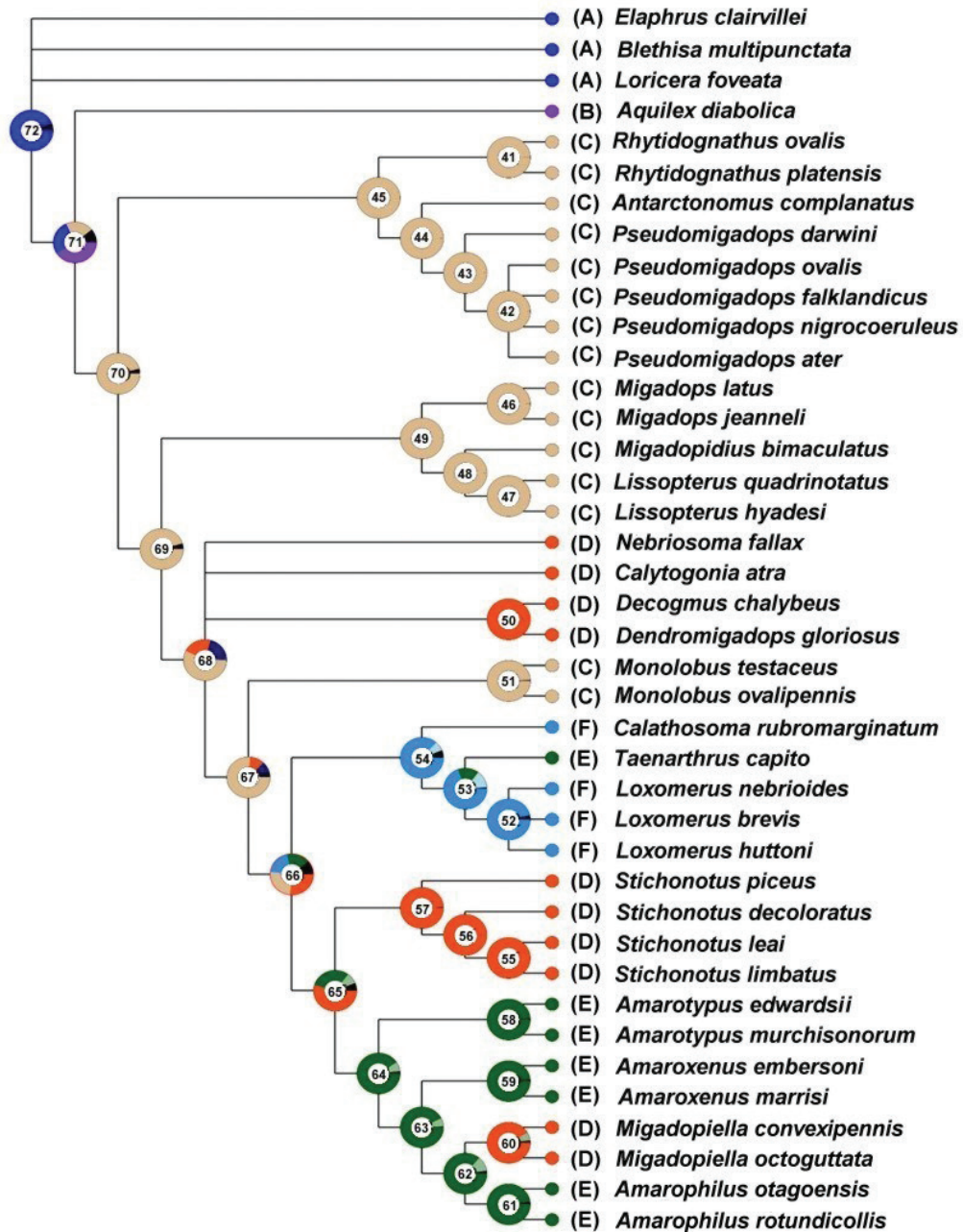
Figure 8. RASP-optimized taxon area cladogram for Migadopinae and closest outgroups in Elaphrinae and Loricerinae. Areas of endemism shown in Figure 5 simplified to allow elucidation of austral disjunct relationships. Areas analyzed include: Holarctic (**A**), equatorial tropicomontane South America (**B**), southern South America (**C**), Australia (**D**), New Zealand (**E**), and Campbell Plateau (**F**). Optimization probabilities for significantly polymorphic nodes—60, 62, 63, 64, 65, 66, 67, 68, 71, 72—in Table 2, other nodes have maximal probabilities of a particular node > 0.95 (optimizations determinable from figure).

rooted with *Amarotypus* sister to the *Stichonotus* lineage of Tasmania and southeast Australia stands as sister to the Campbell Plateau radiation of *Calathosoma*, *Loxomerus*, and *Taenarthrus*.

The most subordinate area relationship connecting New Zealand and Australia is defined by placement *Migadopiella* spp. within the New Zealandian *Amarotypus*, *Amaroxenus*, and *Amarophilus* (node 62, fig. 8). RASP optimizes this node to either New Zealand at probability 0.86, or a combined New Zealand plus Australia at a minority probability of 0.11.

Discussion

Biogeographic History. The closest outgroup Loricerini, represented by *Loricera foveata* LeConte (Fig. 5), is a tribe of Holarctic distribution with extensions southward to the Tibetan Plateau and the mountains of southern Mexico and Middle America (Ball and Erwin 1969). The group was hypothesized to have diversified initially in the Palearctic based on the sister group relationship of the Madeiran *Loricera wollastoni* Javet to the remainder of *Loricera*. The oldest rocks associated with the Tore-Ma-

deira Rise date to the Cretaceous, 80 Ma (Merle et al. 2018), setting a Cretaceous minimum age for loricerine diversification, and by extension the minimum age of the sister group, subfamily Migadopinae (Fig. 8, node 72) isolated by vicariance of Laurasia and Gondwana. Discovery of the Eocene Baltic Amber fossil *Loricera groeni* Cai, Liu and Huang (2017) significantly expanded the paleodistribution of the *Loricera obsoleta* Semenov Tian-Shanskii species group, known to Ball and Erwin (1969) only from the Tibetan Plateau. This recent discovery supports prehistorical sympatry between the *Loricera obsoleta* group currently geographically restricted to the Tibetan Plateau, and the widespread, Holarctic "pilicornis" group that extends southward into Middle America. Subsequent discovery of the fossilized larval stage of the loricerine, *Cretoloricera electra* Liu et al. (2023b), in mid-Cretaceous Kachin amber extends the time of origin of Loricerinae to 99 Ma, thereby setting the time of origin of its adelphotaxon, Migadopinae, to that date.

The sister group relationship between Aquilicini, represented by *Aquilex diabolica*, and Migadopini supports a New World vicariant relationship between the equatorial and southern temperate zones during initial diversification of subfamily Migadopinae (Fig. 8, node 71). The initial divergence of *Aquilex* in equatorial South America versus all other taxa occupying southern South America is represented herein by recognition of the sister tribes Aquilicini and Migadopini.

The biogeographic nexus between South American and Australian taxa (Figs 5, 8) included an initial diversification of the group in Australia—the mid-grade grouping of *Calyptogonia*, *Nebriosoma*, *Decogmus*, and *Dendromigadops* (Fig. 5)—followed by a second radiation of taxa of the Campbell Plateau, New Zealand, and southeastern Australia centered on Tasmania. The initial divergence of the *Calyptogonia* grade in Australia would have occurred with mid-Cretaceous opening of the Australia-east Antarctic rift (Michaux 2009, fig. 2A), allowing secondary dispersal between Australia and east Antarctica to reestablish a cosmopolitan Austral fauna (Fig. 8, node 68).

Monolobus, restricted to the Maule and Valdivian rain forest in Argentina and Chile, is the sister group to the second radiation of Australian and New Zealand taxa (Fig. 8, node 67); i.e., the Campbell Plateau taxa, plus *Stichonotus* of southeastern Australia, and the three New Zealand genera, *Amarotypus*, *Amaroxenus* and *Amarophilus*, plus *Migadopiella* of Tasmania (Fig. 5). The occurrence of a South American Valdivian rainforest taxon that is more closely related to New Zealand and Australian taxa than to other South American taxa was also reported for *Nothobroscus* Roig-Juñent and Ball (Carabidae: Broscinae) (Roig-Juñent 2000, fig. 14; Liebherr et al. 2011, fig. 2). This phylogenetic placement supports the diversification of taxa allied with *Nothobroscus* across a contiguous Gondwana comprising terranes now isolated as southern South America, Australia, the Campbell Plateau and New Zealand.

Isolation between the Campbell Plateau versus New Zealand plus Australia would have been accomplished by mid-Cretaceous along the Campbell Rift (Michaux 2009, fig. 2A), with opening of the Tasman Sea isolating western New Zealand from Australia by late Cretaceous. Although *Taenarthrus*, nested within the Campbell Plateau *Calathosoma* and *Loxomerus* (Fig. 8), comprises species currently occupying the southern portions of the South Island with highest diversity in Fjordland, this region is hypothesized to share a common history with the currently isolated Auckland Islands plus other islands of the Campbell Plateau (Michaux and Leschen 2005).

The area relationship between *Migadopiella* and the New Zealand genera *Amarotypus*, *Amaroxenus* and *Amarophilus* is best explained, within the context of all other biogeographic events, as east to west trans-Tasman dispersal from New Zealand's South Island to Tasmania (node 62; Table 2, Fig. 8). This interpretation is consistent with dispersal being the preferred explanation for the biogeographic origin of a subordinate taxon nested within a larger paraphyletic assemblage of taxa occupying a second area (Enghoff 1993). Such a dispersal event is hypothesized to have occurred in a clade predominantly comprising apterous taxa; the only exception being *Amarotypus edwardsii* which is characterized by brachyptery, with its reduced flight wings extended to 65–75% of elytral length (Larochelle and Larivière 2022: 5). East to west trans-Tasman dispersal hypothesized for *Migadopiella* conforms to findings of Sanmartín and Ronquist (2004, table 4, fig. 9), who reported no significant directionality to trans-Tasman dispersal among insect taxa.

Flightlessness, dispersal and colonization

Darlington (1965) proposed that flight-capable migadopine taxa such as the South American *Antarctonomus* plus the Queensland, Australian *Dendromigadops* represent the ancestral stock of the group, with such winged taxa dispersing between South America and Australia to establish a southern disjunct distribution. Although all three immediate outgroup representatives–*Blethisa multipunctata*, *Elaphrus clairvillei*, and *Loricera foveata* (Fig. 5)–are characterized by macroptery, only the phylogenetically subordinate ingroup taxa *Antarctonomus complanatus*, *Decogmus chalybeus*, and *Dendromigadops gloriosus* exhibit fully developed flight wings. Analogously, *Amarotypus edwardsii* exhibits brachypterous flight-wings—i.e. reduced in length by approximately half—while being placed within a clade otherwise characterized by totally reduced flight wings; aptery. These several instances may be explained by the demonstrably frequent evolution of flightlessness across Carabidae among taxa occupying montane and islandic habitats (Darlington 1943; Kavanaugh 1985), with that repeated evolution violating the principal of parsimony (Trueman et al. 2004). Conversely, re-evolution of fully developed flight wings from apterous ancestors has been argued for Phasmatodea (Whiting et al. 2003; Forni et al. 2022). Regardless, the earliest diverging lineages within Migadopinae are not characterized by macroptery, and so

Darlington's hypothesis of ancestral dispersal by migadopines across open southern oceans is not corroborated.

Darlington's (1965) proposal that ancestral colonizing migadopine taxa were flight capable conforms to an interpretation that dispersal to novel terranes occurs via winged beetles. Yet the trans-Tasman colonization of Tasmania by *Migadopiella* occurred from among a set of wingless taxa. Also, among the Campbell Plateau migadopine taxa, four species—*Loxomerus nebrioides*, *L. katote* Johns, *L. huttoni*, and *Calathosoma rubromarginatum* (Johns 2010)—occupy the Auckland Islands, with that archipelago comprising Miocene shield volcanoes overlying Cretaceous granite (Denison and Coombs 1977), yet the Pleistocene-aged Antipodes Islands (Scott et al. 2013) house the similarly flightless *Loxomerus brevis*. The occurrence of *L. brevis* on the Antipodes is thus best explained by overwater dispersal, with such an instance again occurring within a brachypterous clade.

Fossil corroboration

Based on phylogenetic analysis of extant taxa, we predict future discovery of fossil taxa representing tribe Migadopini from Antarctica. We already have the first example of an Antarctic carabid beetle corroborating a trans-Antarctic biogeographic relationship through the discovery of the fossil, *Antarctotrechus balli* Ashworth and Erwin (2016). In this instance, *Antarctotrechus* is a member of a clade within the tribe Trechini comprising *Trechisibus* Motschulsky of South America, the Falkland Islands and South Georgia, and *Tasmanorites* Jeannel of Tasmania, Australia. The fossil *Antarctotrechus* is dated 20–14 Ma, i.e., Early to Mid-Miocene, well after the Oligocene opening of the Southern Ocean, suggesting that it was part of a fauna already evolving in isolation from related taxa on opposite sides of the southern world. It was deposited in materials consistent with mixed forest and tundra vegetation, including *Nothofagus* (southern beech) and *Ranunculus* (buttercup), indicating a riparian habitat. The present phylogenetic hypothesis incorporating austral Migadopini (Fig. 5) lays out characters that may be evaluated should a fossil Antarctic migadopine become available.

Recently, a much older Cretaceous amber fossil from Myanmar—*Cretomigadops bidentatus* (Liu et al. 2023a)—has been described as a member of Migadopinae based on a first instar larva encased within Burmese Kachin amber dated to 99 Ma. The fossil exhibits synapomorphies characterizing Carabidae, though placement as Migadopinae is based solely on the presence of two retinacular teeth on the mandible; a larger tooth in a plesiomorphic position near mid-length on the mandible, and a second smaller tooth more basad along the medial mandibular margin. Such a second mandibular tooth is reported for third instar larvae of *Loxomerus brevis* and *L. nebrioides* (Johns 1974), as well as larvae of *Omophron* Latreille, Tribe Omophronini (Thompson 1979). The Cretaceous *Cretomigadops* larva differs from *Loxomerus* larvae in: 1, the second, basal mandibular tooth being much larger relative to the distal tooth; 2, the structure of the antennal sensorium; 2, the very long

legs; 3, the slender and very elongate urogomphi; and 4, paired ungual claws of equal length. The occurrence of *Cretamigadops* in Kachin amber necessitates additional assumptions concerning the historical biogeography based on extant taxa. Confirmation of a trans-Tethyan migadopine distribution can be corroborated through discovery of fossilized adult Migadopinae in Kachin Amber. Of course, more extensive taxonomic representation of known migadopine larval stages among extant taxa would also allow confirmation that the basal, larval retinacular tooth serves as a synapomorphy for Migadopinae. Given that the phylogenetic nexus between the Laurasian outgroups and Gondwanan Migadopinae occurred across what is now the Neotropics (Crowson 1980; McLoughlin 2001), the phylogenetic position of Burmese Migadopinae is predicted to be sister group to Aquilicini + Migadopini. The above-presented hypothesis for Gondwanan vicariance and trans-Tasman dispersal would remain unaffected, with the Aquilicini + Migadopini hypothesized to have evolved on a fragmenting Gondwana.

Acknowledgements

References

Ashworth AC, Erwin TL (2016) *Antarctotrechus balli* sp. nov. (Carabidae, Trechini): the first ground beetle from Antarctica. ZooKeys 635: 109–122. https://doi.org/10.3897/zookeys.635.10535

Azadbakhsh S (2020) A new species of *Archaeociocindis* Kavanaugh & Erwin, 1991 (Coleoptera: Carabidae: Cicindini) from the south of Iran. Zeitschrift der Arbeitsgemeinschaft Österreichischer Entomologen 72: 37–42.

Baehr M (2009) A new genus and two new species of the subfamily Migadopinae from Tasmania (Coleoptera: Carabidae). Folia Heyrovskyana (series A) 17: 95–103.

Baehr M (2013) [2012] A revision of the carabid tribe Migadopini in Australia (Insecta: Coleoptera: Carabidae: Migadopini). Memoirs of the Queensland Museum-Nature 65(2): 279–304.

Ball GE, Erwin TL (1969) A taxonomic synopsis of the tribe Loricerini (Coleoptera: Carabidae). Canadian Journal of Zoology 47: 877–907. https://doi.org/10.1139/z69-146

Cai C, Liu Y, Huang D (2017) A new species of *Loricera* Latreille from Eocene Baltic amber (Coleoptera: Carabidae: Loricerinae). Alcheringa: An Australasian Journal of Palaeontology 41(3): 315–320. https://doi.org/10.1080/03115518.2017.1283050

Dtsch. Entomol. Z. 71 (2) 2024, 319–338

337

Crosby TK, Dugdale JS, Watt JC (1976) Recording specimen localities in New Zealand: an arbitrary system of areas and codes defined. New Zealand Journal of Zoology 3: 69. https://doi.org/10.1080/03014223.1976.9517903

Crowson RA (1980) On amphipolar distribution patterns in some cool climate groups of Coleoptera. Entomologia Generalis 6(2/4): 281–292. https://doi.org/10.1127/entom.gen/6/1980/281

Darlington Jr PJ (1943) Carabidae of mountains and islands: data on the evolution of isolated faunas, and on atrophy of wings. Ecological Monographs 13: 37–61. https://doi.org/10.2307/1943589

Darlington Jr PJ (1959) Area, climate, and evolution. Evolution 13: 488–510. https://doi.org/10.2307/2406131

Darlington Jr PJ (1965) Biogeography of the Southern End of the World, Distribution and history of far southern life and land, with an assessment of continental drift. Harvard University Press, Cambridge, M, x + 236 pp. https://doi.org/10.4159/harvard.9780674492073

Darlington Jr PJ (1971) The carabid beetles of New Guinea. Part IV. General considerations: analysis and history of fauna: taxonomic supplement. Bulletin of the Museum of Comparative Zoology 142(2): 129–337.

Denison RE, Coombs DS (1977) Radiometric ages for some rocks from Snares and Auckland Islands, Campbell Plateau. Earth and Planetary Science Letters 34: 23–29. https://doi.org/10.1016/0012-821X(77)90101-7

Enghoff H (1993) Phylogenetic biogeography of a Holarctic group: the julidan millipedes. Cladistic subordinateness as an indicator of dispersal. Journal of Biogeography 20: 525–536. https://doi.org/10.2307/2845724

Erwin TL (1985) The taxon pulse: a general pattern of lineage radiation and extinction among carabid beetles. In: Ball GE (Ed.) Taxonomy, Phylogeny and Zoogeography of Beetles and Ants, Dr. W. Junk Publishers, Dordrecht, 437–472.

Forni G, Martelossi J, Valero P, Henneman FH, Conle O, Luchetti A, Mantovani B (2022) Macroevolutionary analyses provide new evidence of phasmid wings evolution as a reversible process. Systematic Biology 71: 1471–1486. https://doi.org/10.1093/sysbio/syac038

Goloboff PA, Morales ME (2023) TNT version 1.6, with a graphical interface for MacOS and Linux, including new routines in parallel. Cladistics 39: 144–153. https://doi.org/10.1111/cla.12524

Hooker JD (1859) On the flora of Australia, its origin, affinities, and distribution; being an Introductory essay to the flora of Tasmania (reprinted from the Botany of the Antarctic Expedition, Part III, Flora of Tasmania, Vol. I.). Lovell Reeve, London, cxxviii pp. https://doi.org/10.5962/bhl.title.60980

Hooker JD (1867) Handbook of the New Zealand flora: a systematic description of the native plants of New Zealand and the Chatham, Kermadec's, Lord Auckland's, Campbell's and Macquarrie's Islands. https://doi.org/10.5962/bhl.title.132966

Jeannel R (1938) Les Migadopides (Coleoptera Adephaga), une lignée subantarctique. Revue Française d'Entomologie 5: 1–55.

Jeannel R (1942) La Genèse des Faunes Terrestres, Éléments de Biogéographie. Bibliothèque de l'Institut Maritime et Colonial, Presses Universitaire de France, 513 pp. [+ 8 pls]

Johns PM (1969) The mountain invertebrate fauna. In: Knox GA (Ed.) The Natural History of Canterbury, AH Reed and AW Reed, Wellington, 392–399.

Johns PM (1974) Arthropoda of the subantarctic islands of New Zealand (1) (Coleoptera: Carabidae), southern New Zealand, Patagonian, and Falkland Islands insular Carabidae. Journal of the Royal Society of New Zealand 4: 283–302. https://doi.org/10.1080/03036758.1974.10419396

Johns PM (2010) Migadopini (Coleoptera: Carabidae: Migadopinae) of New Zealand. Records of the Canterbury Museum 24: 39–63.

Kavanaugh DH (1985) On wing atrophy in carabid beetles (Coleoptera: Carabidae), with special reference to Nearctic *Nebria*. In: Ball GE (Ed.) Taxonomy, Phylogeny and Zoogeography of Beetles and Ants, Dr. W. Junk Publishers, Dordrecht, 406–431.

Kavanaugh, DH, Erwin TL (1991) The tribe Cicindini Bänninger (Coleoptera: Carabidae): comparative morphology, classification, natural history, and evolution. Proceedings of the Entomological Society of Washington 93: 356–389.

Köppen W, Wegener A (1924) Die Klimate der geologischen Vorzeit. Gebrüder Borntrager, Berlin, 275 pp. https://doi.org/10.1515/9783111491530

Larochelle A, Larivière M-C (2022) Synopsis of the tribe Amarotypini in New Zealand (Coleoptera: Carabidae). Insecta Mundi 0942: 1–30. https://doi.org/10.5281/zenodo.7300590

Liebherr JK, Will KW (1998) Inferring phylogenetic relationships within Carabidae (Insecta, Coleoptera) from characters of the female reproductive tract. In: Ball GE, Casale A, Vigna Taglianti A (eds.); Phylogeny and classification of Caraboidea (Coleoptera: Adephaga). Atti Museo Regionale de Scienze Naturali 5: 107–170.

Liebherr JK, Marris JWM, Emberson RM, Syrett P, Roig-Juñent S (2011) *Orthoglymma wangapeka*, gen. n., sp. nov. (Coleoptera: Carabidae): a newly discovered relict from the Buller Terrane, northwestern South Island, New Zealand, corroborates a general pattern of Gondwanan endemism. Systematic Entomology 36: 395–414. [3 suppl. appendices]. https://doi.org/10.1111/j.1365-3113.2011.00569.x

Lindroth C (1957) The principal terms used for male and female genitalia in Coleoptera. Opuscula Entomologica 22(2/3): 241–256.

Liu H, Beutel RG, Makarov KV, Jarzembowski EA, Xiao C, Luo C (2023a) The first larval record of Migadopinae (Coleoptera: Adephaga: Carabidae) from mid-Cretaceous Kachin amber, northern Myanmar. Cretaceous Research 142: 105413. [12 pp.] https://doi.org/10.1016/j.cretres.2022.105413

Liu H, Makarov KV, Jarzembowski A, Xiao C, Luo C (2023b) *Cretoloricera electra* gen. et sp. nov., the oldest record of Loricerini (Coleoptera: Adephaga: Carabidae: Loricerinae) from mid-Cretaceous Kachin Amber. Cretaceous Research 148: 105540. [8 pp.] https://doi.org/10.1016/j.cretres.2023.105540

Maddison DR, Maddison WP (2023a) Zephyr: a Mesquite package for interacting with external phylogeny inference programs. Version 3.31. http://zephyr.mesquiteproject.org

Maddison WP, Maddison DR (2023b) Mesquite: a modular system for evolutionary analysis. Version 3.81. http://www.mesquiteproject.org

Marris J, Hawke D, Glenny D (2019) Eating at high elevation: an herbivorous beetle from alpine rock outcrops relies on ammonia-absorbing lichens. Ecology 100(5): e02598. https://doi.org/10.1002/ecy.2598

McLoughlin S (2001) The breakup history of Gondwana and its impact on pre-Cenozoic floristic provincialism. Australian Journal of Botany 49: 271–300. https://doi.org/10.1071/BT00023

Merle R, Jourdan F, Goirardeau J (2018) Geochronology of the Tore-Madeira Rise seamounts and surrounding areas: a review, Australian Journal of Earth Sciences 65(5): 591–605. https://doi.org/10.1080/08120099.2018.1471005

Michaux B (2009) Reciprocality between biology and geology: Reconstructing polar Gondwana. Gondwana Research 16: 655–668. https://doi.org/10.1016/j.gr.2009.06.002

Michaux B, Leschen R (2005) East meets west: biogeology of the Campbell Plateau. Biological Journal of the Linnean Society 86: 95–115. https://doi.org/10.1111/j.1095-8312.2005.00511.x

Moret P (1989) Un Migadopidae sans stria surnuméraire des Andes de l'Équateur: *Aquilex diabolica* gen. nov., sp. nov. (Coleoptera: Caraboidea). Nouvelle Revue d'Entomologie (N.S.) 6(3): 245–257.

Moret P (2005) Los coléopteros Carabidae del páramo en los Andes del Ecuador: Sistemática, ecología y biogeografía. Monografía 2: 306 pp. [Museo de Zoología, Pontifica Universidad Católica del Ecuador, Quito, Ecuador]

Nascimento FF, Reis MD, Yang Z (2017) A biologist's guide to Bayesian phylogenetic analysis. Nature Ecology & Evolution 1: 1446–1454. https://doi.org/10.1038/s41559-017-0280-x

Nixon KC (2002) WinClada (a computer program for manipulating cladistic data and examining trees). Ithaca, NY. http://www.cladistics.com

Rambaut A, Drummond AJ, Xie D, Baele, Suchard MA (2018) Posterior summarisation in Bayesian phylogenetics using Tracer 1.7. Systematic Biology 67: 901–904. https://doi.org/10.1093/sysbio/syy032

Roig-Juñent S (2000) The subtribes and genera of the tribe Broscini (Coleoptera: Carabidae): cladistic analysis, taxonomic treatment, and biogeographical implications. Bulletin of the American Museum of Natural History 255: 1–90. https://doi.org/10.1206/0003-0090(2000)255<0001:TSAGOT>2.0.CO;2

Roig-Juñent S (2004) Los Migadopini (Coleoptera: Carabidae) de América del Sur: descripcíon de las estructuras genitales masculinas y femininas y consideraciones filogenéticas biogeográficas. Acta Entomologia Chilena 28: 7–29.

Ronquist F, Van Der Mark P, Huelsenbeck JP (2009) Bayesian phylogenetic analysis using MRBAYES. In: The Phylogenetic Handbook: A Practical Approach to Phylogenetic Analysis and Hypothesis Testing (eds P Lemey, M Salemi & A-M Vandamme). Cambridge University Press, Cambridge, 210–266. https://doi.org/10.1017/CBO9780511819049.009

Ronquist F, Teslenko M, van der Mark P, Ayres DL, Darling A, Höhna S, Larget B, Liu L, Suchard MA, Huelsenbeck JP (2012) MrBayes 3.2: efficient Bayesian phylogenetic inference and model choice across a large model space. Systematic Biology 61: 539–542. https://doi.org/10.1093/sysbio/sys029

Sanmartín I, Ronquist F (2004) Southern hemisphere biogeography inferred by event-based models: plant versus animal patterns. Systematic Biology 53: 206–243. https://doi.org/10.1080/10635150490423430

Scott JM, Turnbull IM, Auer A, Palin JM (2013) The sub-Antarctic Antipodes Volcano: a <0.5 Ma HIMU-like Surtseyan volcanic outpost on the edge of the Campbell Plateau, New Zealand. New Zealand Journal of Geology and Geophysics 56: 134–153 https://doi.org/10.1080/00288306.2013.802246

Sweney WJ (1980) Insects of Mount Cook National Park. M.S. thesis, University of Canterbury, Lincoln College, 328 pp. https://hdl.handle.net/10182/4038

Thompson RG (1979) Larvae of North American Carabidae with a key to the tribes. In: Erwin TL, Ball GE, Whitehead DR, Halpern AL (Eds) Carabid Beetles: Their Evolution, Natural History, and Classification, Dr W Junk Publishers, The Hague, The Netherlands, 209–291. https://doi.org/10.1007/978-94-009-9628-1_11

Trueman JWH, Pfeil BF, Kelchner SA, Yeates DK (2004) Did stick insects really regain their wings? Systematic Entomology 20: 138–139. https://doi.org/10.1111/j.0307-6970.2004.00251.x

Wegener A (1924) The Origins of Continents and Oceans (translated from the third German edition by Skerl JGA). EP Dutton and Company Publishers, New York, xx + 212 pp.

Whiting MF, Bradler S, Maxwell T (2003) Loss and recovery of wings in stick insects. Nature 421 (16 January 2003): 264–267. https://doi.org/10.1038/nature01313

Will KW (2020) Phylogeny and classification of the genus-group taxa of Loxandrina (Coleoptera, Carabidae, Abacetini). Deutsche Entomologische Zeitschrift 67(2): 151–182. https://doi.org/10.3897/dez.67.55985

Yu Y, Harris AJ, Blair C, He X (2015) RASP (Reconstruct Ancestral State in Phylogenies): a tool for historical biogeography. Molecular Phylogenetics and Evolution 87: 46–49. https://doi.org/10.1016/j.ympev.2015.03.008

Yu Y, Blair C, He X (2019) RASP 4: Ancestral State Reconstruction too for multiples genes and characters. Molecular Biology and Evolution 37(2): 604–606. https://doi.org/10.1093/molbev/msz257

Supplementary material 1

Data matrix exported as an SS file from Winclada (Nixon 2002) data file used for cladistic analysis

Authors: James K. Liebherr, Sergio Roig-Juñent, Kipling W. Will

Data type: pdf

Link: https://doi.org/10.3897/dez.71.134268.suppl1

Supplementary material 2

Majority-rule consensus of post-burn-in trees showing Bayesian posterior probabilities (PP) of all clades

Authors: James K. Liebherr, Sergio Roig-Juñent, Kipling W. Will

Data type: pdf

Explanation note: Resolution of this tree should be compared to Fig. 5 (see text).

Link: https://doi.org/10.3897/dez.71.134268.suppl2